SUPRAMOLECULAR SYSTEMS

CHEMISTRY USING PEPTIDES

By

Charalampos Pappas

A thesis submitted to the Department of Pure and Applied Chemistry, University of Strathclyde, in fulfilment of the requirements for the degree of Doctor of Philosophy

2015

Declaration

‘This thesis is the result of the author’s original research. It has been composed by the author and has not been previously submitted for examination which has led to the award of a degree.’

Copyright

‘The copyright of this thesis belongs to the author under the terms of the United Kingdom Copyright Acts as qualified by University of Strathclyde Regulation 3.50. Due acknowledgement must always be made of the use of any material contained in, or derived from, this thesis.’

Signed:

Date:

Contents

1. Introduction 14
1.1 Introduction to thesis 15
1.2 Thesis outline 17

2. Literature Review: Peptide self-assembly, sound directed assembly and supramolecular systems chemistry 20
2.1 Introduction 21
2.2 Building blocks 23
2.2.1 Aromatic peptide amphiphiles 23
2.2.3 Non-covalent interactions driving self-assembly 26
2.2.4 Purely peptidic systems 26
2.2.5 Predicting dipeptide aggregation 29
2.2.6 Tripeptide self-assembly 30
2.2.7 Morphology of the hydrogels across the lengths scales 34
2.3 (Ultra)-sound responsive supramolecular systems 36
2.4 Supramolecular Systems Chemistry 46
2.4.1 Biocatalytic self-assembly: achieving thermodynamic, kinetic and away-from-equilibrium control 48
2.4.2 Kinetically controlled chemical systems 55
2.4.2.1 Kinetic control over supramolecular gel formation using catalysis 56
2.4.2.2 Kinetically controlled systems using biocatalytic self-assembly 58
2.4.2.3 Replication 61
2.5 Away-from-equilibrium assemblies 63
2.6 Conclusions and Outlook 68

3. Alignment of nanostructured tripeptide gels by directional ultrasonication* 70
3.1 Introduction 72
3.2 Materials and Methods 75
3.2.1 Synthesis and characterization of the tripeptides 75
3.2.2 Ultrasonic Setup 76
3.2.3 Sample preparation 77
3.2.4 Transmission electron microscopy (TEM) 77
3.2.5. Scanning electron microscopy (SEM) 77
3.2.6 Two-photon fluorescence excitation microscopy (TPM) 78
3.2.7 Mass and NMR Spectroscopy 78
3.2.8 Circular (CD) and Linear (LD) Dichroism Spectroscopy 78
3.2.9. FTIR spectroscopy 79
3.3 Results and Discussion 80
3.3.1 Nanostructure reconfiguration 80
3.3.2 Supramolecular interactions 81
3.3.3 Ultrasonic effect on a different peptide sequence and solvent environment 83
3.3.4 Ultrasound assisted formation of larger aggregates. 85
3.3.5 Supramolecular chirality and structural orientation 86
3.4 Conclusion 90

4. Transient Supramolecular Reconfiguration of Peptide Nanostructures using Ultrasound* 91
4.1 Introduction 93
4.2 Materials and Methods 96
4.2.1 Synthesis of Fmoc-Tyr-Leu-OH (Fmoc-YL) 96
4.2.2 Ultrasonic Setup 98
4.2.3 Hydrogel formation 98
4.2.4 Fluorescence Spectroscopy 98
4.2.5 Circular Dichroism (CD) 99
4.2.6 FTIR spectroscopy 99
4.2.7 TEM Microscopy 99
4.4 Results and Discussion 100
4.4.1 Selection of the dipeptides 100
4.4.2 Acoustic and thermal behaviour of the sound responsive systems 101
4.4.3 Transient ultrasonic effect on supramolecular chirality 106
4.4.4 Microscopic visualization of sound induced transient supramolecular reconfiguration 108
4.5 Conclusion 110

5. Tuneable Fmoc-Phe(4-X)-Phe-NH_2 nanostructures by variable electronic substitution* 111
5.1 Introduction 113
5.2 Materials and Methods 116
5.2.1 Transition electron microscopy (TEM) 116
5.2.2 Fluorescence spectroscopy 116
5.2.3 FTIR spectroscopy 116
5.2.4 High-performance liquid chromatography (HPLC) 116
5.2.5 Circular Dichroism (CD) 117
5.3 Results and Discussion 118
5.3.1 Effect of electronic substitution on the formation and yield of Fmoc-Phe(4-X)-Phe-NH_2 118
5.3.2 Effect of electronic substitution on supramolecular interactions 119
5.3.3 Effect of electronic substitution on nanoscale organisation 122
5.4 Conclusion 125

6. Searchable Dynamic Peptide Libraries (DPLs) for Materials Discovery. 126
6.1 Introduction 128
6.2 Materials and Methods 132
6.2.1 Sample preparation 132
6.2.2 HPLC 132
6.2.3 Infrared Spectroscopy 132
6.2.5 Transmission Electron Microscopy (TEM) 133
6.2.6 Atomic force microscopy (AFM) 133
6.2.7 Cryo-Transmission Electron Microscopy (Cryo-TEM) 133
6.3 Results and Discussion 134
6.3.1 Dipeptide oligomerisation *via* biocatalytic self-assembly 134

6.3.2 Leucine libraries 134
6.3.2 Phenylalanine libraries 137
6.3.3 Tryptophan Libraries 140
6.3.4 Effect of salts on library distribution 142
6.3.5 Effect of solvent on library distribution 144
6.3.6 Dynamic Peptide Libraries (DPLs). 147
6.3.7 Environmental response of Dynamic Peptide Libraries (DPLs). 148
6.3.8 Supramolecular interactions in the searchable DPLs. 152
6.3.9 Three-component mixture on dynamic peptide libraries (F_2, L_2, W_2) 154
6.3.10 Shape control comparing biocatalytic and chemical synthesized assemblies 157
6.4 Conclusion 160

7. Biocatalytic pathway selection in transient tripeptide nanostructures* 161
7.1 Introduction 163
7.2 Materials and Methods 165
7.2.1 Sample preparation 165
7.2.2 HPLC 165
7.2.3 Infrared Spectroscopy 165
7.2.4 TEM 166
7.2.5 Diffusion Ordered NMR Spectroscopy (DOSY) 166
7.3 Results and Discussion 167
7.3.1 Design of the transient supramolecular system 167
7.3.2 Chemical design dictates the kinetics of the reaction and consequent lifetime of the nanostructures formed. 169
7.3.3 Transient supramolecular interactions 173
7.3.4 Competitive transient biocatalytic self-assembly 175
7.4 Conclusion 179

8. Directing peptide self-assembly using sound waves 180
8.1 Introduction 182
8.2 Materials and Methods 184
8.2.2 Atomic force microscopy (AFM) 184
8.2.3 Transmission Electron Microscopy (TEM) 184
8.2.4 Dynamic light scattering (DLS) 184
8.2.5 Diffusion Ordered NMR Spectroscopy (DOSY) 184
8.3 Results 185
8.3.1 Spectroscopic evidence of the effect of sound on molecular self-assembly 185
8.3.2 Microscopic visualization of sound induced bigger in size aggregates 189
8.3.3 Unlocking the supramolecular aggregation using temperature 190
8.4 Conclusion 192

9. Conclusion and Future research 193
9.1 Conclusion 194
9.2 Future Research 196
Appendix 199
References 217

Acknowledgments

I would like to thank my supervisor, Prof. Rein Ulijn, for the patient guidance, encouragement and advice he has provided throughout my time as his student. I have been extremely lucky to have a supervisor who cared so much about my work, and who responded to my questions and queries so promptly.

Special thanks go to my colleagues and friends at the Ulijn group for their useful discussion and advice and for the nice time I spent with them in and out of the lab. Special thanks also go to Prof. Cachagan's lab, in the Department of Ultrasonic Engineering, in the university of Strathclyde for our collaboration with the ultrasonic responsive supramolecular systems (**Chapter 3, 4**) and to Stuart Reid from University West of Scotland, and his phD student, Peter Childs for our collaboration on the audible sound project (**Chapter 8**).

I would like to thank Dr. Sisir Debnath for his advice in synthesis, Dr. Nadeem Javid for his help in light scattering measurements, Dr. Pim Frederix for FTIR measurements, Dr. Margaret Mullin from University of Glasgow for TEM imaging, Craig Irving and Patricia Keating for the help with the NMR and Mass experiments and finally Dr Daniela Kalafatovic, Maria Paola Conte, Ines Moreira, Gary Scott, Dr. Jugal Sahoo, Krystyna Duncan, Ivan Ramos Sasselli and Dr. Yousef M. Abul-Haija, for always being there.

I must express my gratitude to Eirini, my girlfriend, for her continued support and encouragement. I was continually amazed by her patience to all of the ups and downs of my research. I have no words to thank my father, my mother and my brother for

their continuous moral support and in general I owed them everything that I have achieved in my life.

I would like also to acknowledge Ivor Sigmund Tiefenbrun, Director of Linn Products for funding.

Abstract

Living systems possess overwhelming molecular complexity that largely results from combinations of just twenty amino acids that are found across all life forms (the building blocks of life). Complexity of proteins arises from combinations of hundreds amino acid building blocks, where self-assembly dictates structure and functionality. Apart from their vital role on building living processes, short peptide sequences (minimalistic version of more complex biological machinery, consisted of 2-6 amino acids), appear to be ideal structural candidates for the fabrication of soft nanomaterials, with potential applications in food, cosmetics and nanomedicine.

Supramolecular systems can be classified into three distinct types of self-assembly, based on the way that precursors and self-assembling building blocks relate in the free energy diagram. *Thermodynamically* driven supramolecular systems, resulting in the formation of permanent supramolecular assemblies, where the self-assembly pathway and the final supramolecular state is irrelevant. The self-assembly pathway becomes a crucial factor for *kinetically* controlled supramolecular systems, with the structures formed, representing *local* minima in the free energy landscapes. Finally, *away-from-equilibrium* chemical systems, systems that transiently exist only under the influence of constant chemical energy (fuel) and when the energy runs out, the system relaxes back to the initial unassembled state.

In the first part of the thesis, we demonstrate the use of mechanical energy (high oscillating pressure waves-ultrasonic frequencies of 80.000 Hz) to trigger anisotropy and the formation of highly ordered supramolecular architectures. This is achieved by using tripeptide sequences with D-stereoisomer in the N-terminus of the

sequence, where the use of ultrasound gives rise to the formation of *gels* with enhanced supramolecular properties, as evidenced using spectroscopic (FT-IR, CD, LD) and microscopic techniques (TEM, SEM). Subsequently, ultrasound was used to transiently affect supramolecular systems. In this case, the mechanical energy was used to trigger temporary supramolecular reconfiguration of aromatic dipeptide amphiphiles. The supramolecular transitions observed were due to an alter balance of hydrophobic and H-bonding type interactions that drive the assembly of aromatic peptide amphiphiles. Notably, a direct comparison between thermal heating and mechanical energy is also demonstrated, which relates the directional and oscillating characteristics of ultrasound, when it is used to locally deliver heat into a system.

Responsiveness, functionality and adaptability are further demonstrated using different stimuli. Biocatalytic self-assembly has been utilised to direct supramolecular systems. Thermodynamically driven biocatalytic self-assembly is used to achieve morphological control (fibres, sheets and tubes) on aromatic dipeptide amphiphiles, *via* minimal stereo-electronic substitution on the *para* position of the phenylalaline amino acid residue. The control of the resultant supramolecular nanostructures and properties arises from the relative importance of stacking interactions among the aromatics and H-bonding between the dipeptide backbones.

The concept of thermodynamically driven biocatalytic self-assembly is further utilised to direct the formation of Dynamic Peptide Libraries (DPLs). The amino acids within a dipeptide sequence are exchanged dynamically using *in situ* catalytic synthesis and hydrolysis of amide bonds, where the free energy involved in self-assembly of the nanostructure provides the driving force for its formation. The use of

searchable dynamic peptide libraries gives rise to the ability to explore the structural sequences space of short peptides. Selective catalytic amplification is achieved through an interplay with environmental triggers. Differential formation of peptide subunits (library members), accompanied with structural reconfiguration is favored in the presence of different environment, such as solvents and salts. Additionally, a direct comparison between biocatalytically driven formation of different molecular species and chemically synthesized assemblies is used to show that shape control may be achieved.

Biocatalytic self-assembly is also used to trigger the formation of *non-equilibrium transient* supramolecular systems. In this case, structural adaption is achieved based on biocatalytic formation and hydrolysis of self-assembling tripeptides, which catalyzed by chymotrypsin, starting from a simple dipeptide methyl ester, the well-known sweetener, aspartame. The chemical design dictates the kinetics and the consequent lifetime of the nanostructures formed, which can be refueled several times by the addition of the fuel (aspartame), where the fibres are continuously forming and shortening, indicating a dynamically unstable system.

This thesis ends with a small chapter, where we demonstrate the use of audible sound frequencies (<1000 Hz) to direct supramolecular reorganization on an aromatic dipeptide amphiphile. We sought to achieve the formation of larger aggregates as a result of aqueous vibrations, using a variety of spectroscopic (FT-IR, fluorescence, DLS, DOSY NMR) and microscopic techniques (AFM, TEM), investigating the effect of pressure waves on molecular self-assembly.

The Author

Academic training

MSc degree in Applied Chemistry, University of Ioannina, Greece. Thesis title: "Stereoelectronic control of selective binding of synthetic analogue of Angiotensin II hormone in G-protein receptors AT2/AT1: Structural studies and development of bioactive molecules".

BSc degree in Applied Chemistry, University of Ioannina, Greece

Publications during candidature

1. C. G. Pappas, I. S. Sasselli, R. V. Ulijn, Biocatalytic Pathway in Transient Tripeptide Nanostructures. *Angewandte Chemie international Edition*, **2015**, 127, 8237-8241.

2. C. G. Pappas, T. Mutasa, P. W. J. M.; Frederix, S. Fleming, S. Debnath, S. Bai, S. M. Kelly, A. Gachagan, R. V. Ulijn, Transient supramolecular reconfiguration of peptide nanostructures using ultrasound. *Materials Horizons,* **2015**, 2, 198-202, (Inside front cover).

3. C. G. Pappas, Y. M. Abul-Haija, A. Flack, P. W. J. M. Frederix, R. V. Ulijn, Tuneable Fmoc-Phe-(4-X)-Phe–NH_2 Nanostructures by Variable Electronic Substitution. *Chemical Communications*, **2014**, 50, 10630-10633.

4. C. G. Pappas, P. W. J. M.; T. Mutasa, S. Fleming, Y. M. Abul-Haija, S. Kelly, A. Gachagan, D. Kalafatovic, J. Trevino, R. V. Ulijn, S. Bai, Alignment of

Nanostructured Tripeptide Gels by Directional Ultrasonication. *Chemical Communications*, **2015**, 51, 8465-8468.

5. S. Bai,[#] **C. G. Pappas**,[#] S. Debnath, P. W. J. M.; Frederix, J. Leckie, S. Fleming, R. V. Ulijn, Stable emulsions formed by self-assembly of interfacial networks of dipeptide derivatives, ACS Nano, **2014**, 7, 7005-7013 ([#]equally contributed authors).

6. P. W. J. M. Frederix, G. Scott, Y. M. Abul-Haija, D. Kalafatovic, **C. G. Pappas**, N. Javid, N. Hunt, R. V. Ulijn, Exploring The Sequence Space for (tri-) peptide Self-Assembly to Design and Discover New Hydrogels. *Nature Chemistry*, **2015**, 7, 30-37. Front cover.

7. S. Bai, S. Debnath, N. Javid, P. W. J. M.; Frederix, S. Fleming, **C. G. Pappas**, R. V. Ulijn, Differential Self-Assembly and Tunable Emission of Aromatic Peptide Bola-Amphiphiles Containing Perylene Bisimide in Polar Solvents Including Water, *Langmuir*, **2014**, 30, 7576-7584.

Conferences and workshops

- Super Cluster meeting, 2015, City University of New York, Centre of Discovery and Innovation, 20th of November: **oral presentation**.
- Active and Adaptive Symposium, 2015, City university of New York, Advanced Research Science Centre, 22-23rd of October: **oral presentation**.
- Nanopeptide 2015, University of Strathclyde, 2-4th of March: **oral presentation**.
- Biodesign Megameeting, Rutgers University, 20th January: **oral presentation.**
- WestChem Research Day, University of Strathclyde, August 2014: **oral presentation**.
- Peptide Materials for Biomedicine and Nanotechnology, October 2013: **poster presentation**, **poster prize**.
- RSC Macrocyclic and Supramolecular Chemistry Meeting 2013, University of Glasgow, UK. 16-17th December 2013: **poster presentation**.

1. Introduction

1.1 Introduction to thesis

Most of the existing laboratory based self-assembly processes are governed by thermodynamics. However, thermodynamic response is not always sufficient to achieve supramolecular functionality. Living systems are remarkably capable of altering their structures and properties in response to changing situations, largely through molecular assembly and dis-assembly via competing supramolecular pathways. There is tremendous interest in developing man-made analogues of such systems, which provides insights into the workings of biology's remarkable ability to adapt to changing environments.[1-7] The rapid responses required for biological survival are achieved through catalytic amplification, which enables dynamic change under otherwise constant conditions.

Self-assembly (or supramolecular polymerization) can be controlled using a variety of stimuli, including chemical and mechanical triggers, where the formation and breaking of non-covalent interactions is key to control this process. More specifically, (ultra)-sound (high oscillating pressure waves) has been used as an alternative to modulate supramolecular interactions, by mainly overcoming kinetic barriers.[8] Moreover, biocatalytic control over self-assembly has been proposed as an alternative paradigm for the design and fabrication of nano-and biomaterials.[9,10] Supramolecular self-assembled nanostructures produced *via* biocatalytic self-assembly that are defect-free and easily reproducible are of potential interesting in a wide range of applications, as function is a direct consequence of supramolecular order.

Peptides and peptide derivatives are emergent tools for “bottom up” fabrication of functional nanostructures. Sequence dependent function, adaptability and reversibility may be found even in very short peptide sequences.[11-14]

The biological world consists of a variety of supramolecular structures. The complexity of these structures arises from a balance between thermodynamic and kinetic aspects. Supramolecular aggregation in nature is directed from an interplay between self-assembly and dis-assembly rates (kinetics) and the self-assembly propensity of the final supramolecular nanostructures (thermodynamics). Biological systems rely on chemical energy stored in molecular fuels (such as adenosine triphosphate, ATP) to achieve the assembly of active nanostructures. For example, catalytic formation and degradation of actin filaments and microtubules under the influence of chemical fuels are critical to transport and movement in biological systems. The ultimate goal of this research is to design simple mimics of more complex biological assemblies that may be directed *via* thermodynamic, kinetic or transient self-assembly pathways under the influence of different type of energy (chemical or mechanical), using mainly biocatalytic self-assembly and mechanical forces. The fabrication of these systems may give rise to a better understanding of responsive, reconfigurable, active and adaptive supramolecular self-assembly.

1.2 Thesis outline

This thesis is divided into nine chapters. The thesis starts with the literature review (**Chapter 2**), which discusses briefly the building blocks used to study self-assembly (aromatic peptide amphiphiles and purely peptidic systems), (ultra)-sound responsive systems and supramolecular chemical systems, which can be directed through thermodynamics, kinetic and transient triggers. The following six chapters (**chapters 3, 4, 5, 6, 7, 8**) are structured in such a way that each chapter covers one area of the overall research presented in publication format. Each chapter defines its own objectives and carries an abstract and an introduction before presenting the materials and methods, results and discussion and finally conclusion and list of references.

Supramolecular reconfiguration using ultrasound is described in **Chapter 3**. For this project the ultrasonic devices were fabricated in the Centre of Ultrasonic Engineering, in the University of Strathclyde, in Prof. A. Gachagan's lab. The system is based on tripeptide *gels* with D-stereoisomer in the N-terminus of the sequence. The use of ultrasonic waves as an *in situ* approach to induce the self-assembly and alignment of tripeptides, forming highly ordered micro-fibrous structures in both organic and aqueous media is demonstrated. Two different peptides are studied, ^{D}FFD and ^{D}FFI with the former forming an anisotropic organogel in methanol, while the latter forms an anisotropic hydrogel, showing enhancement of supramolecular interactions, chirality and structural orientation. The concept of using ultrasound to direct supramolecular systems is further demonstrated in **Chapter 4**. In this case, the ultrasonic energy is used to achieve transient reorganization of supramolecular nanostructures, which revert back to the original state when sound is switched off. Aromatic peptide amphiphiles, Fmoc-FL and –YL

are used to study the transient acoustic response. These systems show temporary supramolecular transitions that were sequence dependent. The changes observed were due to an altered balance between H-bonding and π-stacking, giving rise to changes in the chiral organisation of peptide building blocks. Thermodynamically driven supramolecular transitions using biocatalytic self-assembly is described in the following two **Chapters** (**5**, **6**). Different supramolecular nanostructures (fibres, sheets, tubes) are produced by regulating the electronic properties of phenylalanine (in the *para* position) with electron donating or withdrawing groups on Fmoc-based dipeptides (Fmoc-Phe-(4-X)-Phe-NH_2) (**Chapter 5**). According to the nature of the electronic substituent, different supramolecular interactions are favoured (aromatic stacking or H-bonding type interactions), showing that minimal changes may have a dramatic effect on the resultant nanoscale architectures and self-assembly. The use of fully reversible amide bond formation and hydrolysis under thermodynamic control (using a non-specific endoprotease-thermolysin) is also used to trigger the formation of peptide oligomers from simple dipeptide sequences (F_2, L_2, W_2) (**Chapter 6**). As a result of continuous formation and breaking of amide bonds, different molecular species are observed. Dynamic peptide libraries (DPLs) are also demonstrated by changing the environmental conditions. Differential component selection and amplification is identified upon mixing dipeptides in the presence of thermolysin, by operating the DPL experiments in different conditions such as salts, solvents or a combination of them. A remarkable enhancement of the conversions of the species formed is observed, resulting in the discovery of novel adaptive peptide nanostructures. Biocatalytic self-assembly is furthermore used to achieve transience, sequence dependent formation of supramolecular nanostructures based on formation

and hydrolysis of self-assembling tripeptides (kinetically driven supramolecular reconfiguration). The systems are catalyzed by α-chymotrypsin and driven by hydrolysis of dipeptide aspartyl-phenylalanine-methyl ester (the sweetener aspartame, DF-OMe). We observed switch-like pathway selection, with the kinetics and consequent lifetime of transient nanostructures controlled by peptide sequence (**Chapter 7)**. The last chapter of this thesis (**Chapter 8**) reports on the effect of low energy frequencies (audible sound, <1,000 Hz) on molecular self-assembly, highlighting the use of pressure waves to trigger supramolecular aggregation on aromatic dipeptide amphiphiles. Finally, **Chapter 9** summarizes the key findings from the previous chapters, discusses the study limitations and provides directions for future research.

2. Literature Review: Peptide self-assembly, sound directed assembly and supramolecular systems chemistry

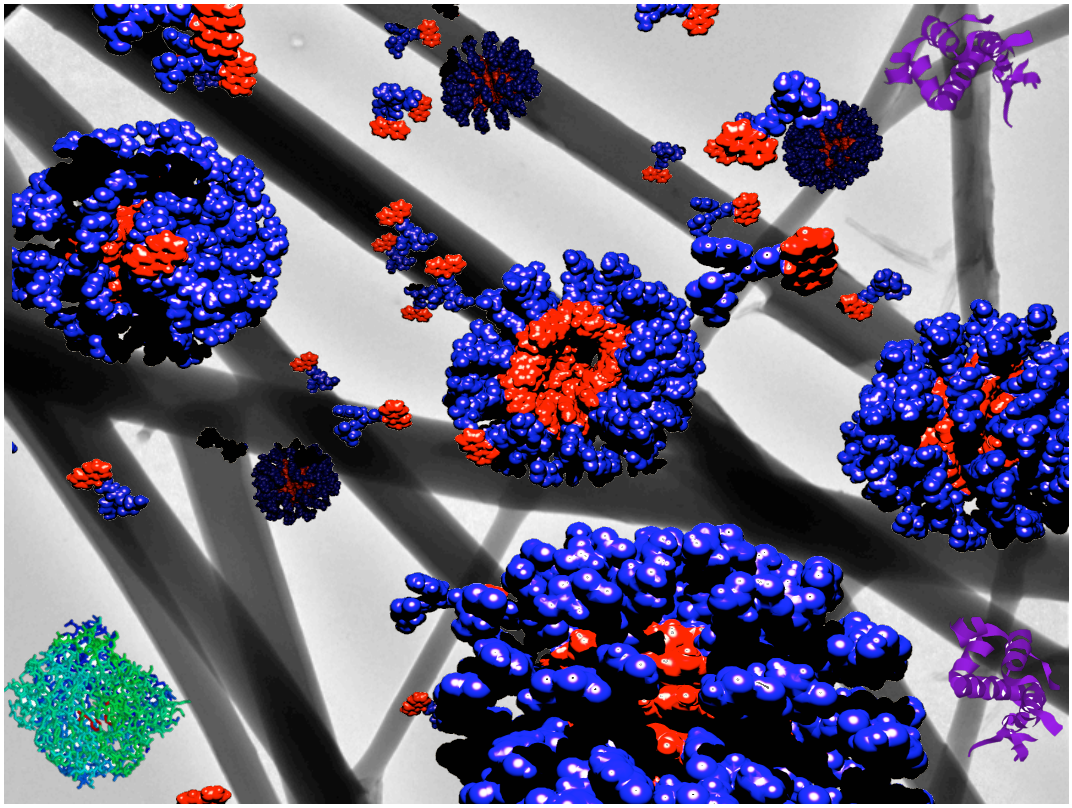

2.1 Introduction

This literature review is divided in three parts. In the first part, there is a brief description of the building blocks used in this thesis to study directed self-assembly (aromatic peptide amphiphiles and purely minimalistic peptide sequences). The second part is devoted to the use of (ultra)-sound to direct molecular self-assembly and the last part, covers the field of supramolecular systems chemistry, highlighting self-assembling peptide systems under thermodynamic, kinetic and away-from-equilibrium control, mainly through biocatalytic self-assembly, as relevant to the thesis.

Supramolecular self-assembly offers a route for "bottom up" fabrication of nanostructures, with supramolecular properties emerging through the assembly of simple building blocks.[15-19] These systems are dynamic, reversible, tunable and they have various potential applications in catalysis, food, cosmetics, drug delivery and tissue engineering. Peptides and peptide derivatives are versatile building blocks for the design and fabrication of nanoscale materials, as they are constituted of the 20 gene encoded amino acids - the expression of biology's language (**Figure 2.1**). They provide both structural and functional motifs, as peptides and proteins play a key role in catalysis, adaption, molecular recognition, reconfiguration and compartmentalization in their biological roles. Structure and function may also be found in minimalistic versions of biological architectures. Due to their chemical richness (variety of side chains) minimalistic peptide-based nanomaterials are increasingly used for the construction of tuneable, highly ordered supramolecular architectures, that are potentially more versatile compared to synthetic polymeric materials.[20-24]

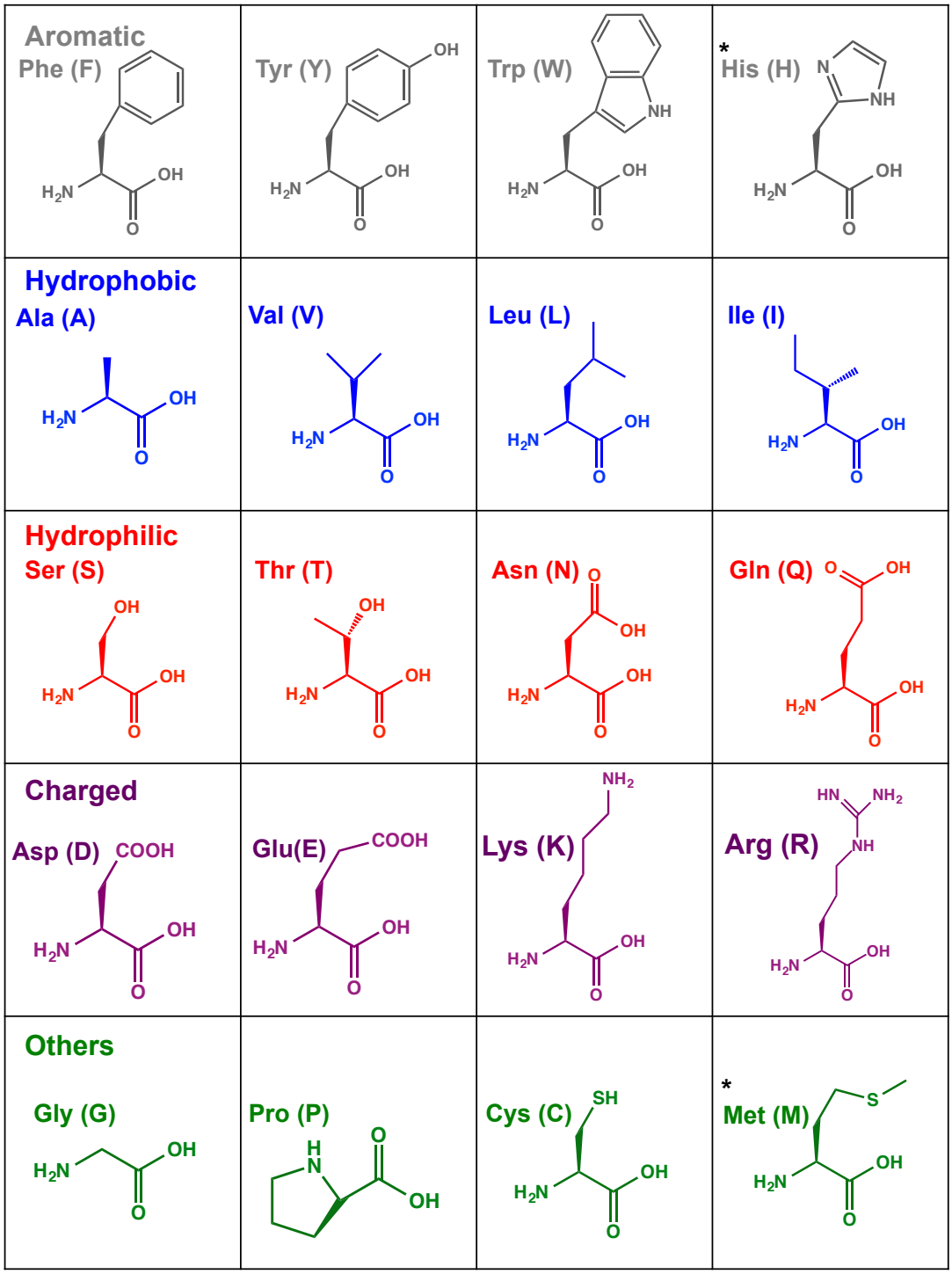

Figure 2.1 Twenty-gene encoded amino acids. * Histidine (His) is also considered as both charged and aromatic amino acid, while Methionine (Met) is also a hydrophobic amino acid.

2.2 Building blocks

2.2.1 Aromatic peptide amphiphiles.

Aromatic peptide amphiphiles are a subclass of self-assembling peptides. They consist of four distinct components.[25] The peptide component is usually composed of two or three amino acids, while the N-terminus is capped with an aromatic moiety (**Figure 2.2a**). The linker segment between N-terminal aromatic and peptide sequence is also an important structural parameter.[26] The C-terminus of the peptide sequence, which is either free or capped, is another crucial structural factor, mainly through a balance of electrostatic forces.[25] There is significant effort from supramolecular chemists to design and control the self-assembly properties of these chemical moieties, mostly through modifications on the aromatic ligand or the amino acid sequence. The first reported and still most commonly used aromatic synthetic moiety to drive peptide self-assembly is Fmoc (9-fluorenylmethoxycarbonyl), mainly due to the fact that the majority of the commercially available amino acids are Fmoc-protected in the N-terminus for solid phase peptide synthesis (Fmoc-tBu strategy). The first aromatic dipeptide amphiphile, which self-assembled into a hydrogel, capped with the Fmoc-group in the N-terminus and with the amino acids leucine (L) and aspartic acid (D) in the peptide sequence (Fmoc-LD) was reported in 1995.[27] Since then, the number of Fmoc-peptide-based amphiphiles and hydrogels reported steadily increased.[25, 28-30] Taking into consideration the importance of the aromatic ligand as structural motif, a variety of aromatic synthetic moieties has been used including naphthalene, pyrene, azobenzene, phenyl, perylene and others.[25] Additionally, by taking advantage of their functionality, energy or charge transfer interactions (perylene, naphthalene)[31,32] and isomerization of chemical bonds (azobenzene)[33] has been reported (**Figure 2.2a**).

As mentioned earlier, the peptide sequence is undoubtedly a crucial aspect for the design of supramolecular structures from aromatic peptide amphiphiles. It should be noted that a direct correlation between self-assembly behaviour (for example hydro- and organogelation capacity) with the amino acid sequence is not trivial. In addition to chemical composition, the route of self-assembly is critical. Indeed, there are a number of thermodynamically, kinetically or non-equilibrium (transient) route dependent supramolecular pathways, possibly resulting in different supramolecular states, as discussed later in the literature review (see Section **2.4**). In terms of chemical structure, it is generally accepted that hydrophobic and more specifically aromatic amino acid residues (F, Y, W) have higher aggregation propensity. There are also literature instances of effective supramolecular hydrogel formation, using hydrophilic and charged amino acids (S, T, Q, N, E, K) in combination with aromatic amino acid residues (F, Y), showing the that the whole sequence space may potentially be utilized to fabricate nanostructures, from aromatic peptide amphiphiles.[34] Furthermore, minimal changes in the peptide sequence by simply replacing phenyl to phenol (H to OH) found to have a dramatic impact on self-assembly properties.[35] Differential nanostructure organisation could be observed using Transmission Electron Microscopy (TEM), which can probably be attributed to the difference in the electron density of the benzene group (H- neutral and OH- electron donating) and the hydrogen bonding capacity of the tyrosine derivative due to the additional OH group[36] (**see Chapter 5**). Differential self-assembly organisation was also revealed on Fmoc-dipeptides containing hydrophilic amino acids on the C or N-terminus (S to T and N to Q).[37,38] A schematic representation of differential self-assembly showing a fibrillar, a twisted fibrillar, a micellar and a tape

like assembly is shown in **Figure 2.2b,** highlighting the supramolecular configuration of the fluorophores (red arrows) and the peptide component (blue tail).

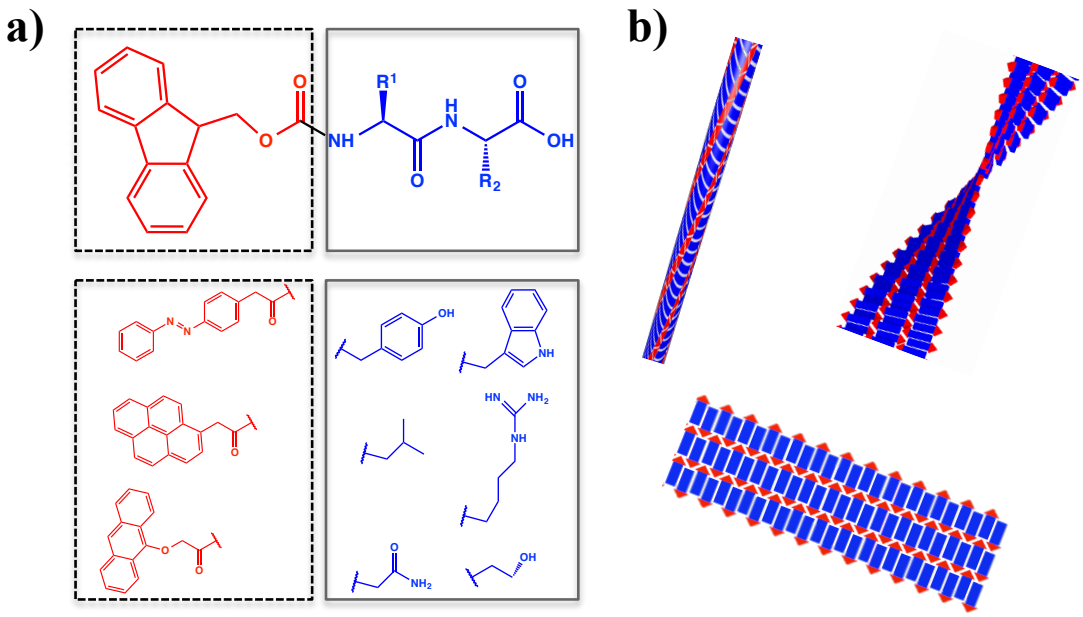

Figure 2.2 a) Chemical structure of an aromatic dipeptide amphiphile, highlighting examples of different structural motifs for the aromatic and the peptidic part and **b)** Schematic representation of different supramolecular organisation, which arised from the balance of π-stacking, H-bonding and steric factors.

Transmission Electron Microscopy (TEM) images of differential supramolecular nanostructure formation, including tubes, fibres, sheets and spherical aggregates are available in **Figure 2.3**.

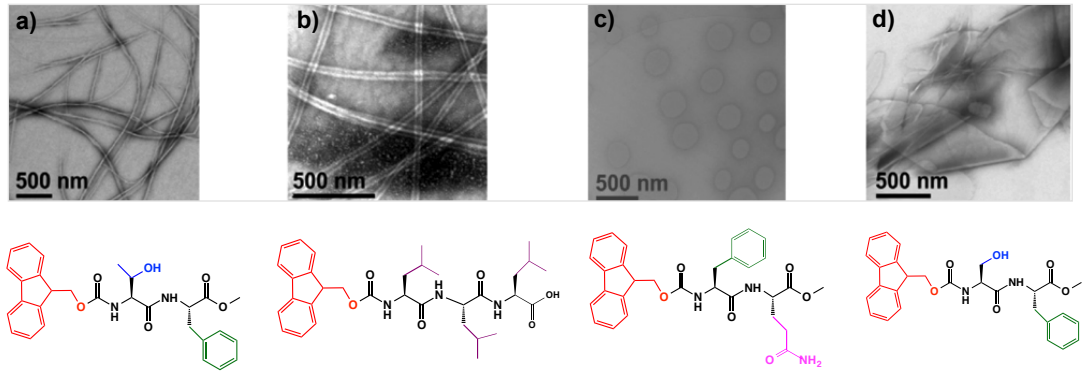

Figure 2.3 TEM images of differential self-assembly organisation of **a)** Fmoc-TF-OMe, **b)** Fmoc-L_3, **c)** Fmoc-FQ-OMe and d) Fmoc-SF-OMe, scale bar 500 nm. Adapted from ref. 37, 38.

2.2.3 Non-covalent interactions driving self-assembly

The self-assembly behaviour of these systems is governed mainly through a delicate balance between hydrophobic, stacking interactions among the aromatic moieties and hydrogen bonding type interactions between the peptide backbones.[25] The balance between these two structural components has a dramatic impact on the supramolecular properties and resultant nanoscale architectures and will be further discussed in **Chapters 4, 5.** Electrostatic interaction between opposite charged amino acid residues and van der Waals forces have also been found to influence self-assembly and supramolecular properties.

2.2.4 Purely peptidic systems

As described in the previous section a common methodology to tune the self-assembly behaviour of short peptide sequences (di-or tripeptide sequences) is to modify them with aromatic groups in the N-terminus of the sequence. The use of *purely peptidic systems* in supramolecular self-assembly has gained significant attraction the last decade, as they represent minimalistic versions of more complex biological structures. Robustness, scalability and reduced cost compared for example

to proteins are also considered as important factors, with these self-assembling units to exhibit potential applications in food, cosmetics and biomedicine. [12]

The potential of peptides as self-assembling building blocks for nanostructured materials was first recognized in the early 1990s by pioneers such as Zhang[39] and Ghadiri.[40] The use of very short peptide derivatives pioneered by Gazit in 2003, who showed that diphenylalanine (F_2), the core motif of amyloid polypeptide could undergo supramolecular organisation to form tubular like structures after dilution with hexafluoropropanol in water (**Figure 2.4**).[13] Differential supramolecular organization was identified in other organic solvents.[41] A variety of properties have been reported using dipehenylalanine as structural motif, by taking advantage of the tubular nanoscale assembly, which is driven by aromatics interactions, such as thermal and chemical rigidity, metal like stability as well as piezoelectric, semiconductive and optical properties.[42] Vesicular structures have also been found for FF in low pH.[43]

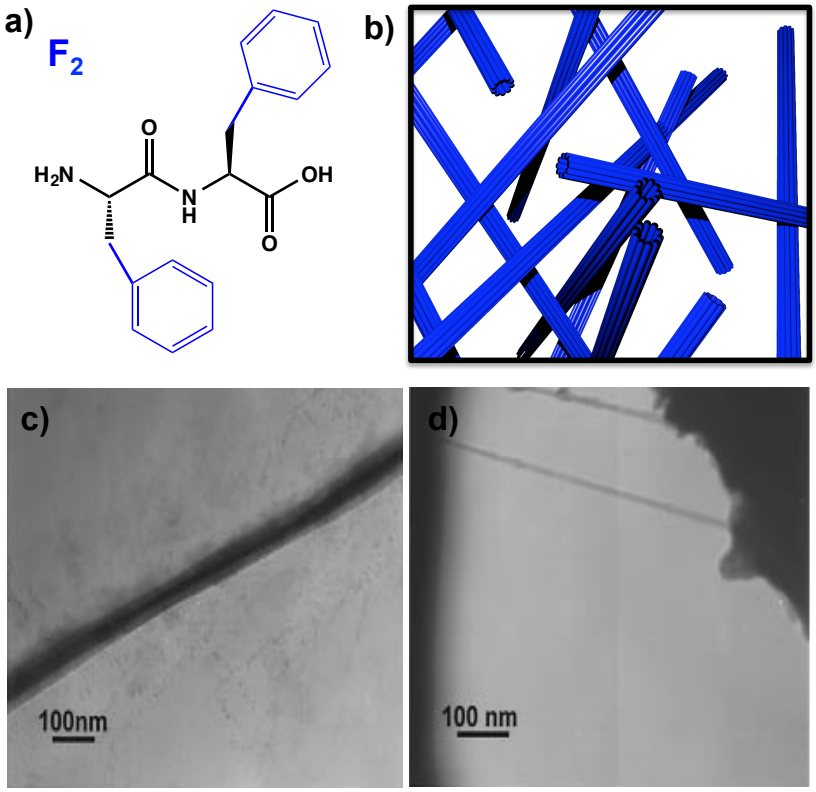

Figure 2.4 a) Chemical structure of F_2 **b)** Schematic representation of tubular assemblies formed by F_2, **c)** TEM images of peptide tubes filled with silver nanowires and **d)** after addition of proteinase K enzyme to the nanotube solution. Adapted from ref. 13.

Additionally, FW was also found to form tubular architectures.[44] Other dipeptide sequences consisting of aromatic amino acids found to have self-assembly propensity were W_2 and WY (forming disordered aggregates) as evidenced by Transmission Electron Microscopy (TEM).[13] Notably, the first example of a simple dipeptide that self-assembled into nanofibrous hydrogels was reported in 2007.[45] The dipeptide sequence consisting of isoleucine and phenylalanine (IF) formed hydrogels at physiological pH, while a mutation of isoleucine with valine (VF) did not result in supramolecular organisation, highlighting the importance of the peptide sequence with structure and function.

2.2.5 Predicting dipeptide aggregation

In order to explore the entire dipeptide sequence space of 20^2 examples, a coarse grained computational approach was developed to discover and rationalize possible dipeptide sequences that have potentially supramolecular aggregation.[46] In this work, coarse-grained molecular dynamics were applied to screen the whole sequence space of 400 different dipeptide sequences and predict their ability to aggregate. It was revealed that most of the aromatic dipeptide sequences and especially F_2 and FW have the tendency to aggregate (**Figure 2.5**). The introduction of charged amino acid residues (D, E, K, R) reduced the self-assembly propensity, most likely due to the reduction of the hydrophobic effect and the introduction of electrostatic forces. Furthermore, the combination of aromatic (F, Y, W) with hydrophobic-aliphatic amino acids (L, V, I) seemed to be an effective combination for self-assembly. Notably, hydrophilic amino acids such as serine (S) and threonine (T) with aromatic amino acids (FS, FT) showed aggregation ability, suggesting that a balance of hydrophobic and hydrophilic interactions can be applied to identify different supramolecular architectures. Finally, a remarkably high aggregation propensity was identified for the dipeptide SH, which was earlier also found to participate in catalysis.[47] Trans-acylation reactions were observed between acetylated amino acid esters (Ac-Phe-OEt) with amino acid amides (Phe-NH_2, Leu-NH_2) in the presence of the catalytic dipeptide, however, it is currently not clear whether a link exists between self-assembly propensity of the dipeptide and catalytic capability.[47]

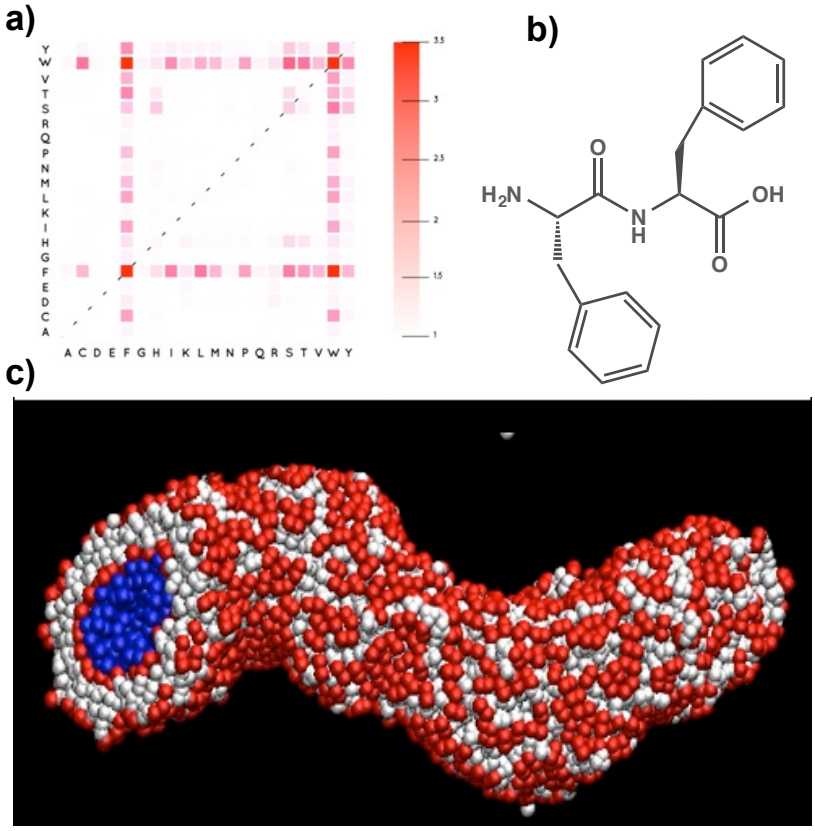

Figure 2.5 a) Two-dimensional screening of aggregation propensity of dipeptides **b)** Chemical structure of diphenylalanine (F_2) and **c)** Coarse grained representation of the tubular arrangement. Adapted from ref. 46.

2.2.6 Tripeptide self-assembly

There are a few examples reported to date using tripeptides (3 amino acids) that form supramolecular organisations in aqueous media. One early example was a cysteine containing tripeptide sequence (CFF), which was found to self-assemble into spherical aggregates, suggesting that aromatic interactions govern the assembly, however the role of cysteine (C) is not clear on supramolecular interactions.[48] Triphenylalanine peptide sequences (FFF) were found to self-assemble into fibrillar[49] or plate like structures[50] depending on the experimental conditions used. A more hydrophilic peptide sequence (KFG) was recently discovered, showing pH responsiveness, resulting in supramolecular reconfiguration from vesicular to tubular

like assemblies, showing also potential biological applications.[51] Furthermore, an interesting manipulation on the tripeptide sequence to drive gelation and self-assembly organisation was reported from Marchesan *et al*. They reported that a change in the configuration in the N-terminal of the tripeptide sequence from L to D is sufficient to tune supramolecular self-assembly, resulting in the formation of hydrogels at physiological pH.[52] More specifically, it was shown that the tripeptide sequences (FFV, VFF) did not form distinct supramolecular assemblies, whereas, the D-containing amino acid (^{D}FFV, ^{D}VFF) were found to form self-supporting hydrogels at physiological pH. The authors used Cryo-TEM and Atomic Force Microscopy (AFM) to visualize the fibrillar networks formed by the tripeptides in combination with a variety of spectroscopic techniques to get insights into the supramolecular interactions.

It is clear from the above examples that most of the tripeptide sequences that have aggregation propensity have been discovered through serendipity or by mapping onto known sequences from biological systems, mainly through the core amyloid motif (F_2). Thus, a rational approach on the self-assembly of (tri)-peptide-based materials through mapping the whole sequence space would be of a great interest.

Recently, a rational design of the self-assembly and gelation properties of tripeptides was reported by Frederix *et al.* In this work, the authors used computational filters by screening all possible combinations of amino acids in tripeptides (8,000 different sequences) to discover tripeptide sequences that show a tendency to aggregate.[12] After detecting the "best" tripeptide candidates, an experimental investigation has been carried out to validate and further support the computational findings using a variety of microscopic and spectroscopic techniques. The self-assembly of

tripeptides was predicted using the aggregation propensity of the clustered systems. This was achieved by measuring the ratio of the solvent accessible surface area (SASA) at the initial and final stage of assembly. The logP (total hydrophobicity) factor was introduced to favourably bias toward tripeptides with high self-assembly propensity but also relatively low hydrophobicity. As a result of the simulations, a number of useful design rules for tripeptide assembly emerged. In particular, both the chemical nature and position within sequence are critical. As probably expected, aromatic amino acids (F, Y and to a lesser extend W) found to play the most important role on self-assembly. Interestingly, their position is more favourable in the middle or at the C-terminus of the sequence rather the N-terminus. Additionally, the C-terminus seemed to be preferred for negatively charged amino acids (E, D), while positively charged (K, R) and H-bonding donating amino acids (S, T, Q, N) are favoured in the N-terminus of the sequence. An interesting observation was that proline is preferentially located at the N-terminus due to possible steric effects of the pyrrolidine ring (**Figure 2.6**). The experimental validation of the simulation evidence, led to the discovery of the first, unprotected, all L tripeptide hydrogel reported. KYF was found to self-assemble into hydrogels at physiological pH, forming a three-dimensional fibrillar network, as evidenced by TEM. Similar peptide sequences have also been found to from hydrogels at physiological pH (KFF, KYY, KYW), through a combination of aromatic stacking interactions among the aromatic amino acid residues and hydrogen bonding type interactions between the tripeptide backbones. A cationic-pi interaction between lysine and aromatic amino acid residues is also possible to assist self-assembly. Diffusion Ordered NMR (DOSY) and FT-IR experiments were used to identify the aggregation size and H-bonding

type interactions in the tripeptides. Interesting nanostructures were also discovered adopting other tripeptide sequences. PFF was found to form crystalline like structures, while KLL self-assembled into tubular like architectures.

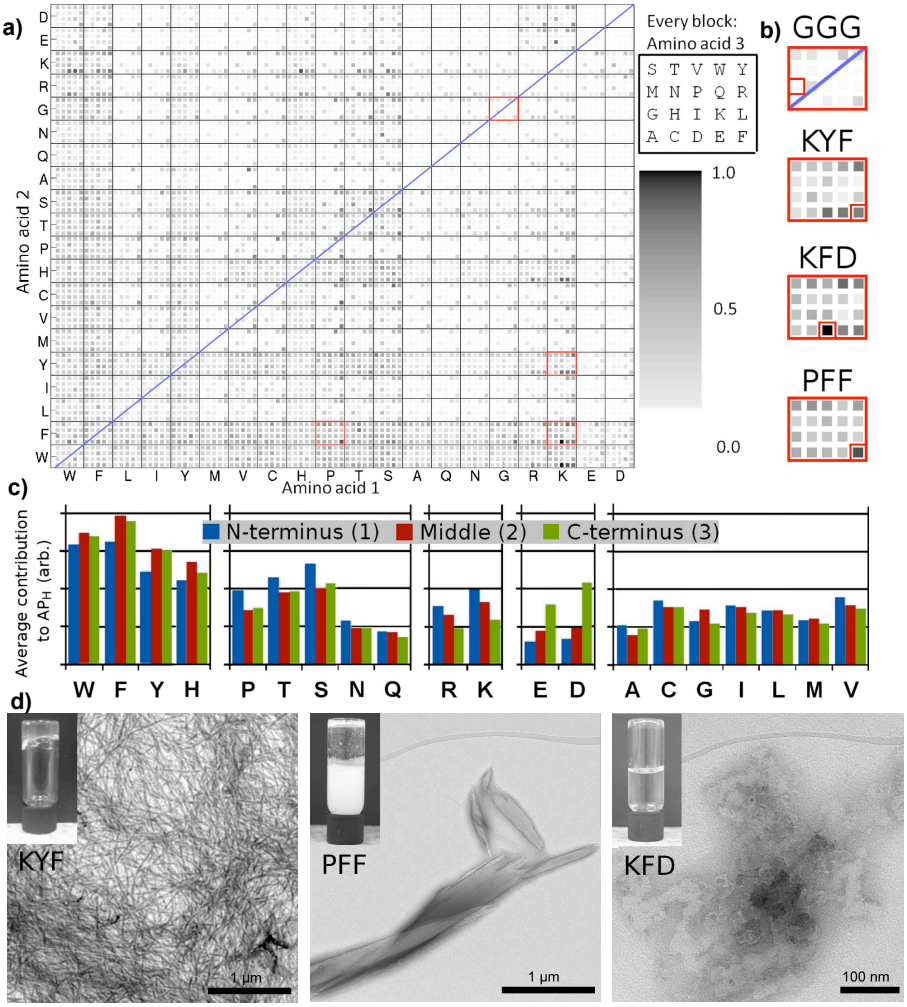

Figure 2.6 a) Normalized score for all 8,000 combinations of three amino acids after a 50 ns simulation, **b)** Expansion of the highlighted areas showing in **a**, **c)** Average AP_H scores of tripeptides with the specific amino acid on the x-axis in the N-terminal (blue), middle (red) and C-terminal (green) positions and **d)** TEM images of KYF, PFF and KFD. Adapted from ref. 12.

2.2.7 Morphology of the hydrogels across the lengths scales

One unique aspect of supramolecular self-assemblies and hydrogels is that their molecular properties translate across the lengthscales to dictate materials properties. Typically, building blocks will be of nanometer lengthscale, with self-assembled objects spanning tens of nanomaterials to microns. In turn, these may assemble to form higher order fibrillar structures, which entrap water, resulting in the hydrogel state. Different characterisation techniques are used to interrogate systems at different lengthscales. XRD[38] and computational tools[12] on peptide derivatives gave a better understanding on the lengthscales of these self-assembling units, highlighting the role of supramolecular interactions with hydrogel fromation. It is worth mentioning that is challenging to link these techniques together to come up with a full picture of the self-assembling systems as a whole, across the nanometer to macroscales. This has been recognized for some time, and has been discussed by Zhang.[39] He pioneered the design of peptide self-assembling units (ionic self-complementary 8 to 16 amino acid residue peptides) with altering polar and non-polar amino acids of approximately 5 nm in size. On the charged sides, both positive and negative charges are packed together through intermolecular ionic interactions.[39] In general, these self-assembling peptides form stable β-sheet structures in water, leading to the formation of a supramolecular hydrogel, consisting of interconnected nanofibres. Since these hydrogel scaffolds contain 5-200 nm pores and have high water content (99%), they have been used as 3-D cell culture media, inspiring supramolecular scientists for designing peptides with potential biological applications (**Figure 2.7**).[39] Another class of self-assembling peptide building blocks belongs to a lipid-like molecular structure of approximately 2 nm in size, similar to that of biological phospholipids. In this case, the design differs from the above, as

the latter consist of a hydrophilic head (either positively or negatively charged amino acid residues) and a hydrophobic tail, consisting of 6 amino acid residues. Their hydrophilic heads are exposed to water, while their hydrophobic tail is hidden inside of a micellar, tubular or vesicular like structure with a diameter of 30-50 nm (**Figure 2.7**). Significant insights have been given on the structure and size of these peptide-based nanomaterials using microscopy techniques (SEM, TEM, AFM), giving rise to visualise individual nanofibres ranging from a few hundred nanometers to a few microns.

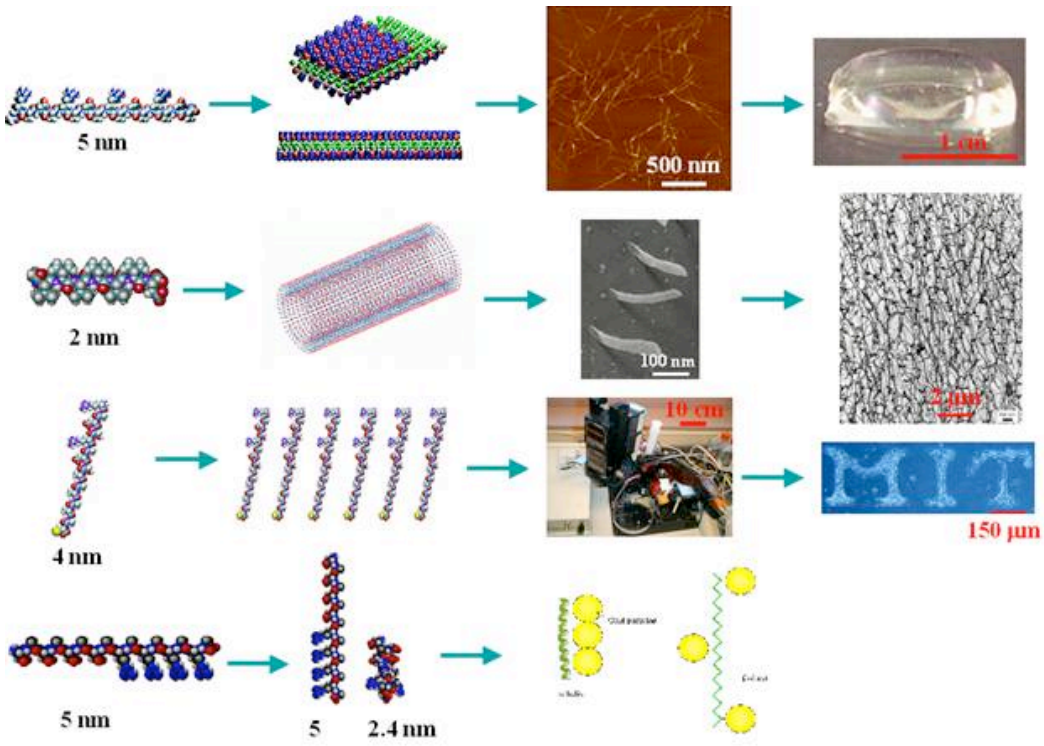

Figure 2.7 Design of peptide based nanomaterials. Ionic self-complementary 16 amino acid residues peptides (5 nm in size), froming a β-sheet like structure, where the nanofibres are interconnected to form a supramolecular hydrogel (top panel). Peptide surfactants (2 nm in size), consisting of a hydrophilic head and a hydrophobic tail, which can undergo self-assembly to form a micellar, vesicular (middle panel) or a nanotubular structure (bottom panel). Adapted from ref. 39.

2.3 (Ultra)-sound responsive supramolecular systems

(Ultra)-sound waves and mechanical forces have recently been reported as important stimuli to influence supramolecular properties of soft nanomaterials.[8] Ultrasonic waves (>20,000 Hz) may be used to dissolve molecules and disperse particles, by disrupting (nonspecific) intermolecular interactions. Recent reports have shown that ultrasound may be used to control self-assembly and gelation process. These studies generally involve high ultrasound frequencies (>20,000 Hz) and control gelation, resulting in dramatic effects on nanoscale morphology and material properties. In supramolecular chemistry ultrasound and mechanical forces have been used as an alternative for tuning the physical properties of gels.[8] The majority of literature examples focus on the effect of (ultra)-sound in organic media, where the use of sound waves resulted in stable supramolecular (re)-organizations.

The first example of ultrasound induced gelation and supramolecular organization was reported by Naota and coworkers in 2005.[53] They reported that brief ultrasound exposure (40 KHz, 0.45 Wcm^{-2} for 0-15 sec) on a dinuclear palladium complex, led to gelation in a variety of organic solvents. It is proposed that sonication directed the molecular self-assembly, affecting mainly the intermolecular stacking interactions among the aromatic moieties. The supramolecular reconfiguration was monitored using UV-VIS, NMR Spectroscopy and SEM Microscopy (**Figure 2.8**). The sound responsive organogels were stable for several months and reversibility was only observed after heating the samples.

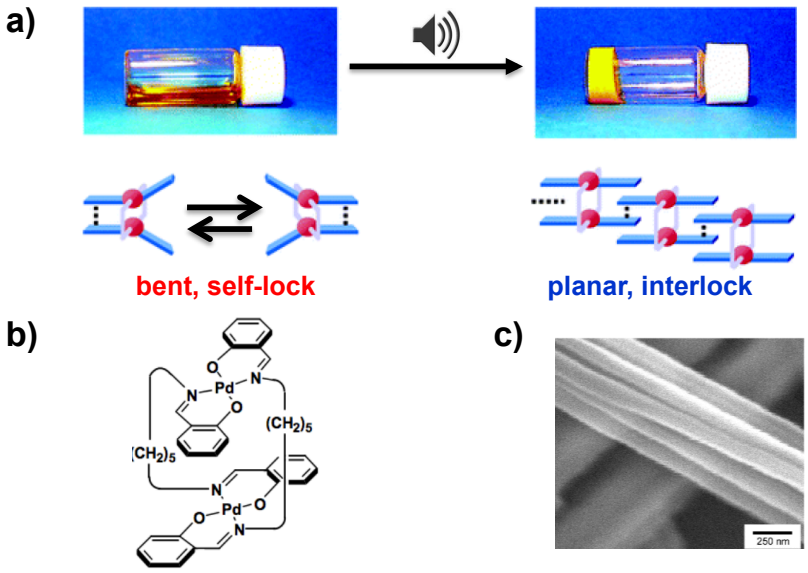

Figure 2.8 a) Digital photos of the supramolecular transitions observed after ultrasound exposure **b)** Chemical structures of the palladium based complex and **c)** SEM picture of the xerogel in cyclohexane after ultrasound exposure. Adapted from ref. 53.

Moreover, Naota and coworkers reported on a rapid gelation upon ultrasound exposure (60 s, 40 KHz, 0.45 Wcm^{-2}) on a palladium bound peptide, capped at the N-terminus with the Fmoc group.[54] In this case, the mechanism of gelation in a variety of organic solvents is triggered by reorganization of intermolecular hydrogen bonding. Ultrasound exposure released the self-lock arrangement and induced the formation of assembly by supramolecular reorganization of the initial domain to form β-sheet like aggregates. The increase of sonication time led to accelerated gelation rates and furthermore formation of higher-order nanostructures with heat-resistant properties. The presence of intermolecular hydrogen bonding interactions was determined using NMR Spectroscopy. Temperature dependent ^{1}H NMR studies revealed the involvement of the amide protons in the formation of intermolecular

hydrogen bonding. Ultrasound exposure led to the formation of lamellar structure of β-sheet monolayers (**Figure 2.9**).

Ultrasound has moreover been used to influence nanoscale morphology and the mechanical properties of aromatic peptide amphiphiles. Using the delicate balance of aromatic and H-bonding combination, ultrasonic waves may disrupt or enhance hydrophobic interactions among the aromatics and hydrogen bonding between the peptides. Specifically, an Fmoc-dipeptide containing two amino acid residues of leucine and a benzoyl group in the C-terminus (Fmoc-LL-OBz) could undergo supramolecular organisation into a three-dimensional fibrillar network upon ultrasound exposure.[55]

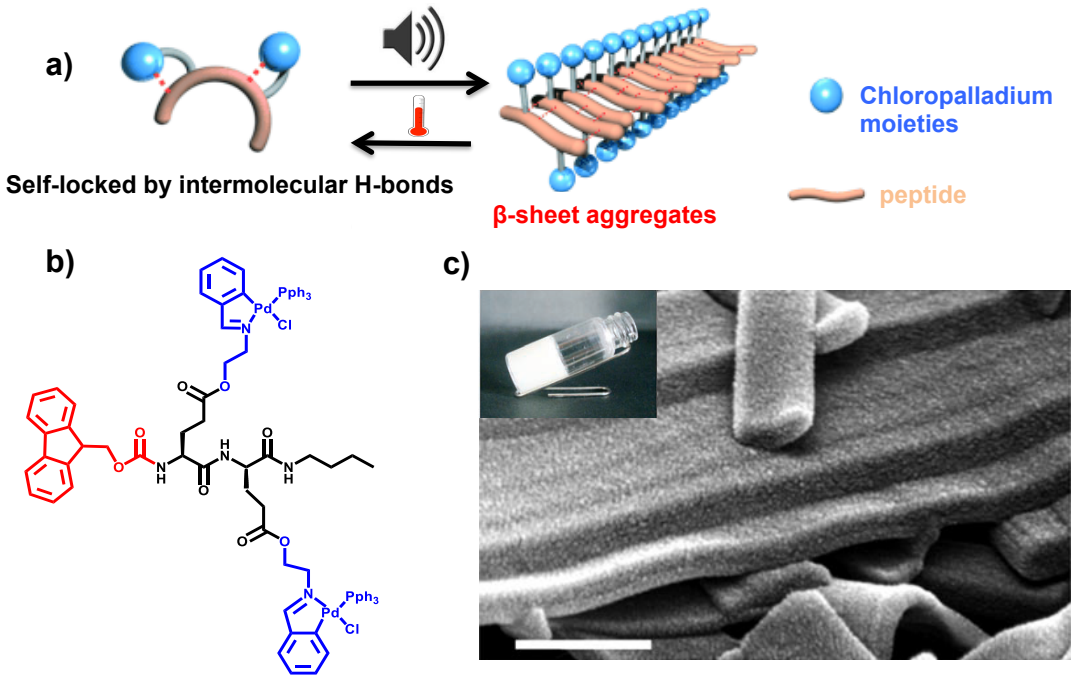

Figure 2.9 a) Schematic representation of supramolecular reorganization induced by ultrasound **b)** chemical structure of the palladium bound peptide and **c)** SEM image of xerogel showing lamellar aggregates of β-sheet monolayers (scale bar: 200 nm). The inset photo represents organogel formation. Adapted from ref. 54.

Dispersion of the dipeptide in a variety of organic solvents, followed by sonication (4 minutes), resulted in the formation of stable organogels. The formation of ultrasound responsive organogels was highly dependent on the molecular interactions, mainly on the stacking interactions among the aromatic groups. Removing or replacing the benzoyl or the Fmoc group from the peptide sequence, further confirmed this observation. Ultrasound exposure of the uncapped dipeptide (removing the Fmoc group) did not undergo supramolecular organization. In this study, the authors highlighted also the importance of the exposure time, indicating that variation of sonication time could result in the formation of different type of supramolecular structures. More specifically, ultrasound exposure (40 kHz, 0.28 W cm^{-2}) for 10 sec led to the formation of particles, whereas an increase of sonication time from 20-60 sec, revealed the formation of an entangled fibrillar network. The final architecture of nanoribbons was obtained after 10 minutes of sound exposure. Solid state NMR Spectroscopy revealed the formation of β-sheet like structures (**Figure 2.10**).

Yao et al. reported another example of ultrasound induced gelation and supramolecular organization on an Fmoc peptide derivative.[56] In this case the authors investigated the differences on supramolecular organization and interactions between ultrasound and heat. Remarkably, significant differences were observed when compared to thermal heating, which depended on the oscillating and directional characteristics of ultrasound when is used to locally deliver heat into a system. Gelation was exclusively observed by ultrasound exposure (0.40 W/cm^{-2}, 40 KHz, <10 s) on a N-Fmoc-Octyl-glycine (Fmoc-Octyl-Gly) peptide derivative in cyclohexane, while a precipitation was observed as the sample was left to cool down to room temperature without ultrasonic exposure.

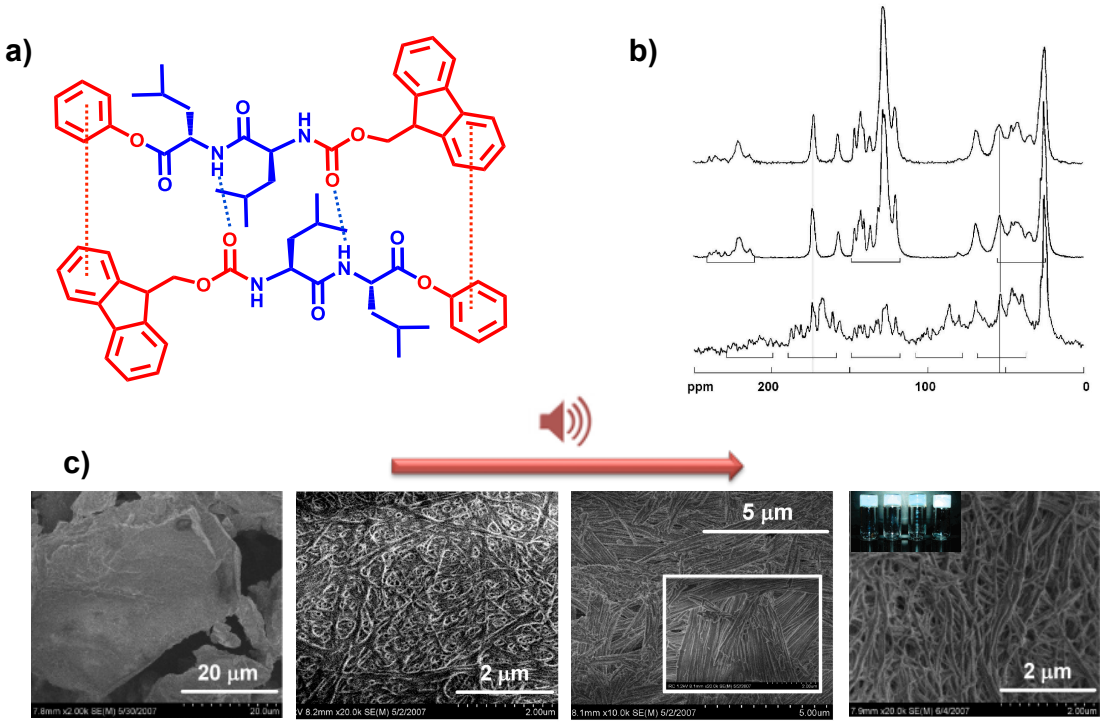

Figure 2.10 a) Schematic representation of supramolecular interactions using ultrasound on aromatic dipeptide amphiphile, **b)** Solid state NMR before and after ultrasound exposure and **c)** SEM images of the organogel at different exposure time, showing supramolecular transition from particles to ribbon like structures. Adapted from ref. 55.

Ultrasound facilitated a switch from intra to inter-molecular interactions. Analysis by SEM (Scanning Electron Microscopy) revealed that the gel was made by interconnected nanofibres, while the precipitated state consisted of unbranched nanowires. Fluorescence experiments revealed red-shifted structures upon gel formation, while no shift was observed for the arrangement of the aromatics without ultrasonic exposure. Additionally, FT-IR and Circular Dichroism experiments suggested that ultrasound facilitated the formation of hydrogen bonding type interactions and enhancement of supramolecular chirality (**Figure 2.11**).

Furthermore, Ke and coworkers reported on an amphiphilic tripeptide (KFA)-bipyridine conjugate, which could undergo supramolecular organization in 1:1 mixture of water: tetrahydrofuran from nanovesicles to fibres upon ultrasonic exposure.[57] Ultrasound exposure (40 kHz, 0.28 Wcm^{-2}) led to the collapse of the vesicular nanostructure and subsequent formation of nanoribbons, which further twisted due to chirality of the peptide segments and elongated into short nanofibers. Using a variety of spectroscopic techniques (FT-IR, fluorescence, XRD and NMR) it was revealed that the supramolecular transition and switch of intermolecular interactions were triggered by ultrasonic energy (**Figure 2.11**).

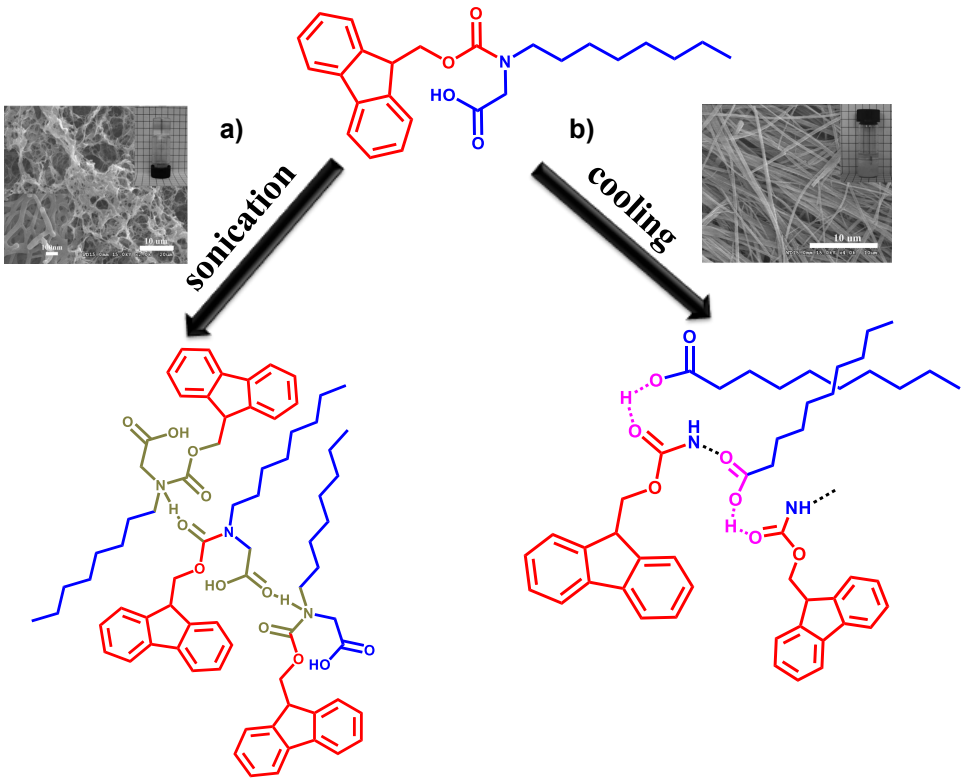

Figure 2.11 a) Schematic representation of the effect of **a)** ultrasound and **b)** temperature on nanoscale morphologies and supramolecular interactions (switch from intra to intermolecular interactions) on Fmoc-Octyl-Gly in cyclohexane. Adapted from ref. 56.

Most examples published to date focus on the effect of ultrasound in organic media, while there are few reports focusing on aqueous systems. Recently, it was reported that ultrasound may induce hydrogelation and the formation of entangled fibrillar network on a peptide based derivative consisted of lysine, which acted as a linker to connect 7-carboxyl methoxycoumarin and hydrazine.[58] Fluorescence and ^{1}H NMR spectroscopy were used to investigate the interactions within or between the hydrogelators. Temperature dependent ^{1}H NMR studies revealed that the amide protons are involved in the formation of intermolecular hydrogen bonding, while no shift was observed for the aromatic protons of the coumarin moiety (**Figure 2.12**).

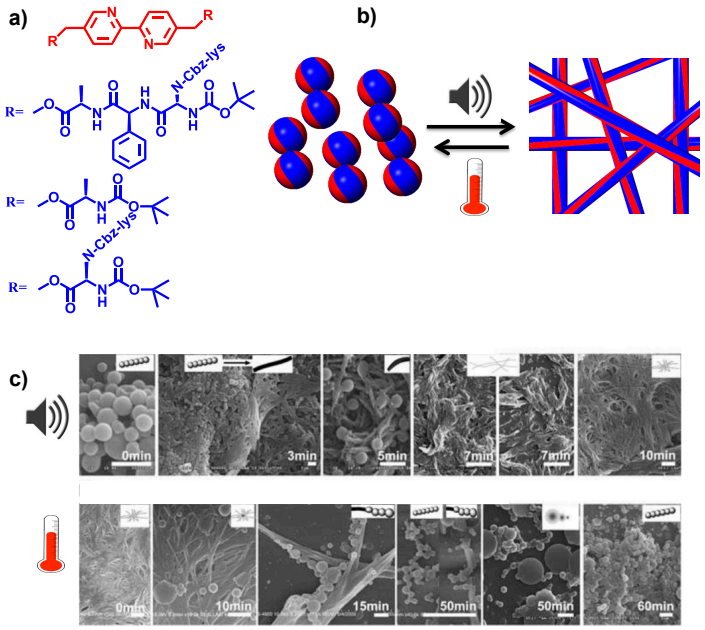

Figure 2.12 a) Chemical structures of the peptide derivatives, **b)** Schematic representation of the supramolecular transition induced by ultrasound and temperature and c) TEM images of the transitions induced by ultrasound and temperature respectively. Adapted from ref. 57.

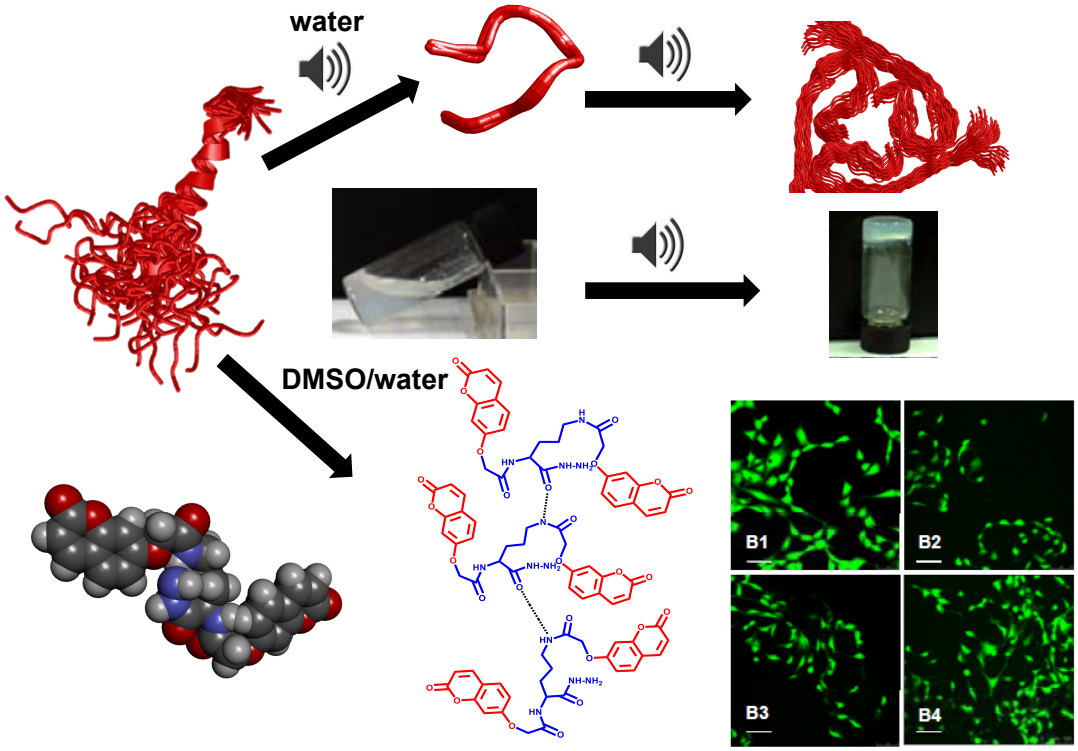

Figure 2.13 Supramolecular organization induced by ultrasound in a different (co-) solvent environment, highlighting the importance of hydrogen bonding interactions in self-assembly. The picture on the bottom right shows hydrogel biocompatibility with NIH 3T3 fibroblasts cells at different time points. Adapted from ref. 58.

Audible sound frequencies have also been used to trigger supramolecular reorganization. The frequency range of audible sound (20-20,000 Hz) is lower than the ultrasound. The question of whether audible sound vibrations can influence molecular or macromolecular interactions is a long-standing scientific argument.[59] In 2010, Tsuda and coworkers reported on the effect of audible sound on molecular self-assembly.[59] They demonstrated that a zinc-porphyrin molecule in chloroform solution could respond to audible sound waves in specific range frequencies (100-500 Hz). In the absence of sound, the molecule can self-assemble into a fibrillar network. The orientation of the nanofibres in solution can be characterised using linear dichroism spectroscopy (LD). No LD signal was obtained without audible

sound exposure. However, the molecule showed a strong negative LD signal upon audible sound exposure. This observation indicated that the nanofibres could be vertically aligned, parallel to the propagation direction of the audible sound. It is worth mentioning that the acoustic response was highly dependent on the frequency and the amplitude of the sound. Specifically, no response was detected upon sound exposure with frequencies in the range 320-1,000 Hz (**Figure 2.14**). The authors proposed that low frequency sound waves have a slow directional change in the liquid vibrations, resulting in large fluctuations in the solvent, where alignment of the supramolecular nanofibres may be observed.

More recently, dynamic acoustic alignment of anthracene based supramolecular nanofibres upon audible sound exposure was reported using Linear Dichroism Spectroscopy (LD.)[60] In the previous example, the zinc-porphyrin molecule could respond to a limited range of frequencies (below 300 Hz). However, Tsuda and associates showed that the anthracene-based molecule might respond to higher frequencies (up to 1,000 Hz). The authors proposed a plausible mechanism for the acoustic alignment, suggesting that there is no direct physical interaction between the molecule and the audible sound waves but the nanofibres interacted mainly with the acoustic flowing, which is due to sound vibrations. It should be noted that the mechanism of the effect of acoustic vibrations on supramolecular self-assembly and on structural orientation is not completely clear.

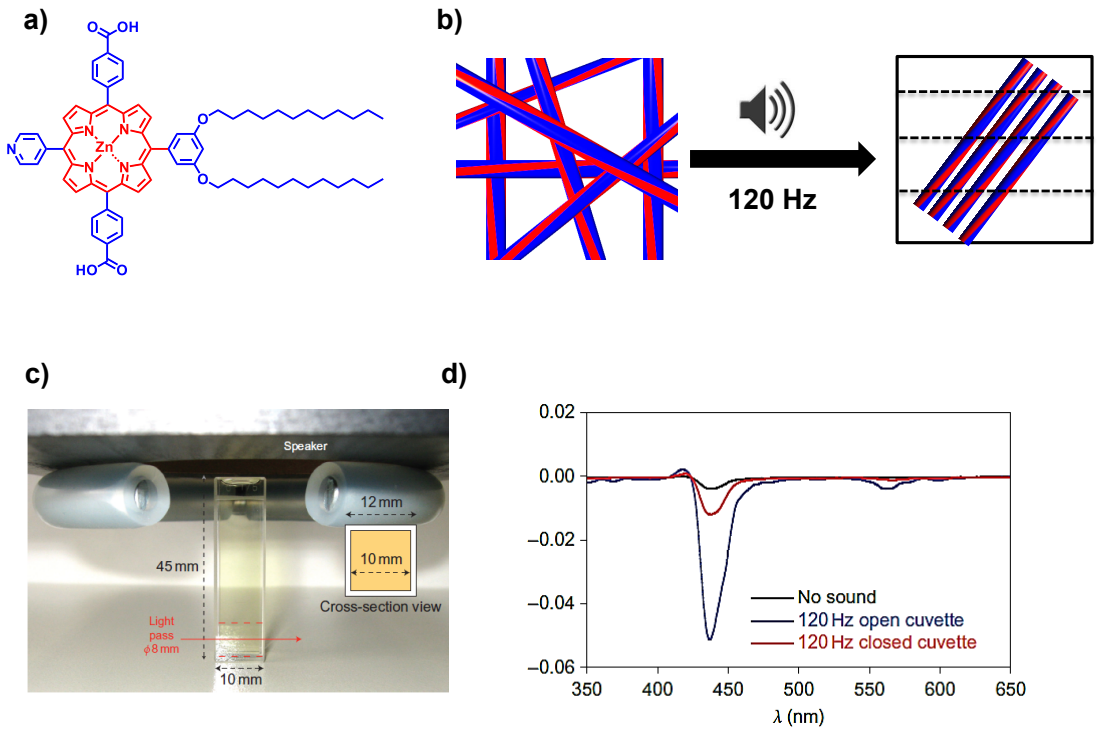

Figure 2.14 a) Chemical structure of zinc-porphyrin molecule bearing 4-pyridyl and 4-carboxyphenyl groups, **b)** Schematic representation of fibrillar alignment upon sound exposure, **c)** Experimental set-up and **d)** Linear Dichroism spectrum with and without sound exposure. Adapted from ref. 59.

Table 2.1 Summary of frequency**,** exposure time and (re)-organisation in (ultra)-sound responsive systems.

Frequency (Hz)	Sonication time (s)	Nanostructure	Reference
40,000	0-15	nanofibres	53
40,000	0-60	nanofibres	54
40,000	0-6,000	nanoribbons	55
40,000	<10	nanowires	56
40,000	0-6,000	nanovesicles	57
40,000	<20	chiral nanofibres	58
100-500	<10	fibrillar alignment	59
100-1,000	<10	fibrillar alignment	60

2.4 Supramolecular Systems Chemistry

Supramolecular chemistry is a powerful approach to create, direct and influence chemical systems.[61] The formation and breaking of non-covalent interactions is key to control the self-assembly processes. Traditional supramolecular systems are designed with **thermodynamics** in mind,[62] resulting in formation of permanent supramolecular structures, where the pathway to reach the final assembled state is irrelevant. Notably, in the last decade there is a tremendous effort from supramolecular chemists to create systems where the assembled state is dictated by **kinetics**,[63] with the self-assembly pathway becoming a crucial factor. Kinetically controlled self-assembly systems may be classified into two categories, in the systems that exist in a kinetic trapped state and to those that their existence is transiently observed, **away-from-equlibrium,**[64] under the influence of a constant supply of energy.

The biological world consists of a variety of supramolecular structures. Protein folding, formation of liposomes from phosphatidyl surfactants, nucleic acids transcription and assembly of proteins are processes that are mainly governed through thermodynamics aspects in nature. Nonetheless, for a significant number of biological functions thermodynamic assembly is insufficient, as it precludes active responsiveness. Continuous free energy dissipation activates complex biological supramolecular systems and thereby chemical reactions may occur, giving rise to cell function. Therefore, life is far-from equlibrium.[61]

The following classification can be proposed in order to summarize various pathways to control and direct supramolecular self-assembly (**Figure 2.15**).

i) Self-assembly under **thermodynamic control** (final self-assembled state irrelevant to supramolecular pathway) with a negative free energy change.

ii) Self-assembly under **kinetic control** (supramolecular pathway is crucial for supramolecular order), structures formed represent *local minima* in the free energy landscapes.

iii) **Away-from-equilibrium** supramolecular systems, systems that only exist under the supply of constant energy and when the energy runs out, the system relaxes back to the initial unassembled thermodynamically or kinetically trapped state.

As mentioned earlier, most of the existing laboratory-based self-assembly processes are triggered by changes in environmental conditions, where a change in concentration, pH, ionic strength or solvent results in self-assembly.[65] Nowadays, there is a tremendous effort from supramolecular chemists to move into systems that can transiently use a specific type of energy (chemical, mechanical, thermal) to activate their functions.

Nonetheless, there are only few experimental and computational examples in the literature that represent away-from-equilibrium chemical systems, showing temporary response to an external or internal stimuli to activate assembly. Herein, we

aim to highlight a few examples of systems under thermodynamic, kinetic or away-from-equilibrium control, involving peptides.

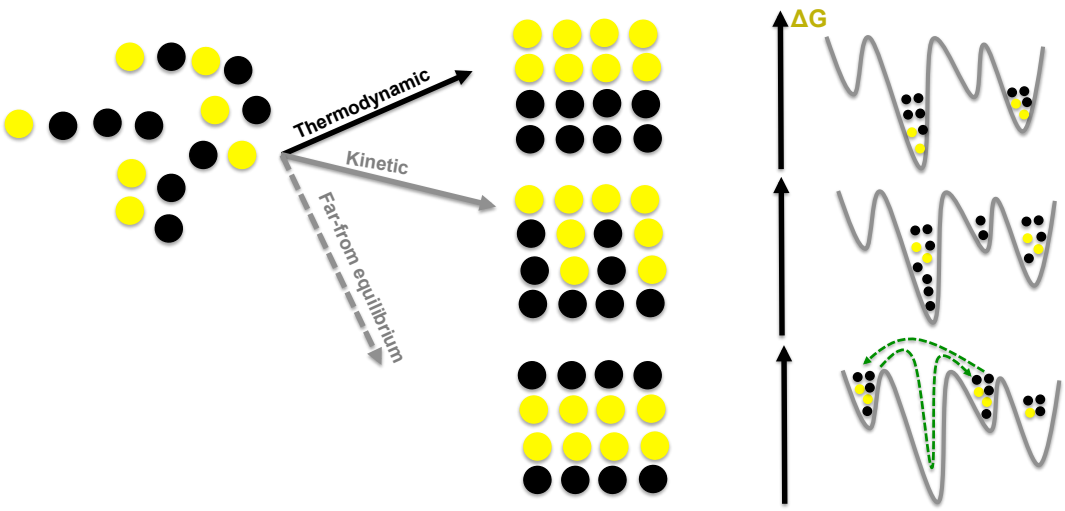

Figure 2.15 a) Thermodynamic, kinetic and away-from-equilibrium representation of chemical systems with their free energy landscapes.

2.4.1 Biocatalytic self-assembly: achieving thermodynamic, kinetic and away-from-equilibrium control

Biocatalytic self-assembly is a versatile approach to control assembly.[62] There are three distinct types of biocatalytic self-assembly based on how precursors and self-assembling building blocks relate in the free energy diagram: i) Equilibrium self-assembly. These systems are the most stable ones and reach a thermodynamic (global) minimum in the free energy landscape, ii) non-equilibrium biocatalytic self-assembly. These systems are kinetically controlled, trapped in a local minimum in the free energy diagram and are driven by enzyme kinetics, iii) non-equilibrium biocatalytic system, based on continuous consumption of *fuels* (**Figure 2.16**).

Thermodynamically controlled supramolecular systems *via* biocatalytic self-assembly provide an effective route for a direct correlation of supramolecular order and function (**Figure 2.16a**). Traditional approaches to direct molecular self-assembly lead to the formation of (meta-stable) kinetically trapped states, as these are highly dependent on experimental conditions (solvent, pH, ionic strength etc.)[64] A highly ordered supramolecular organization (thermodynamically driven self-assembly), produced *via* enzymatic condensation/hydrolysis can shift the thermodynamic equilibrium towards amide bond formation, as it is known that the backward reaction (amide hydrolysis) is relatively close to equilibrium ($\Delta G^0_{amide\ hydrolysis}$=-4KJ/mol).[62]

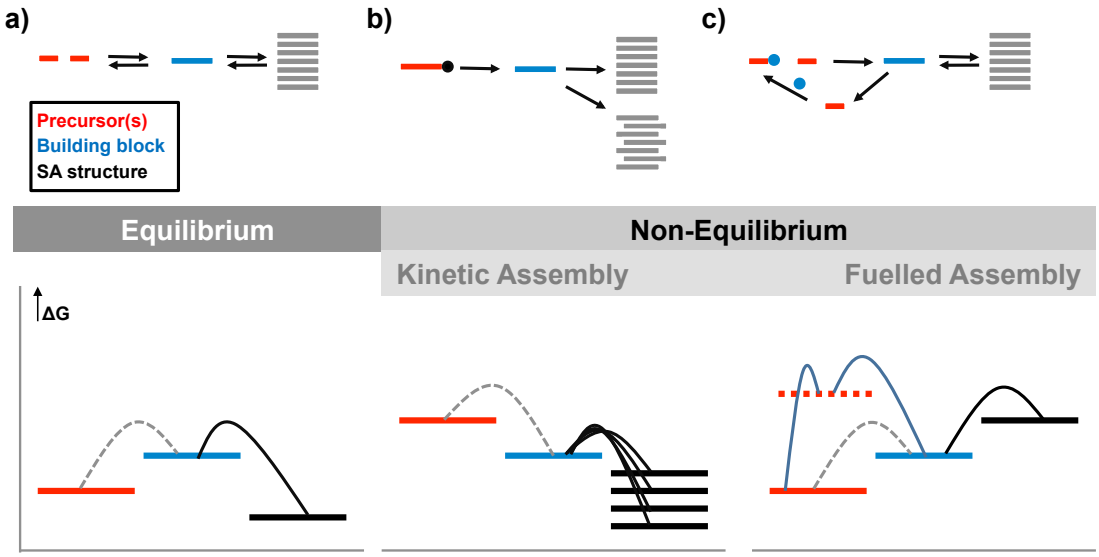

Figure 2.16 Free energy diagram associated with all three different types of self-assembly under **a)** thermodynamic, **b)** kinetic and **c)** away-from-equilibrium control.

The first example of thermodynamically driven biocatalytic self-assembly was reported in 2006 by our group.[66] A non-specific endoprotease (thermolysin from *Bacillus Thermoproteolyticus rokko*) was used to catalyse amide bond formation and hydrolysis between non-assembling precursors and Fmoc-peptide building blocks.

The precursors were Fmoc-protected amino acids with dipeptides (F_2 and L_2) to form the corresponding tripeptide derivatives, which self-assembled into fibrillar organizations, as a combination of aromatic/stacking interactions among the aromatics and hydrogen bonding type interactions between the peptide backbones (see Section **2.2.3**). The authors used a variety of Fmoc-amino acids precursors (G, L, V, A, P, F), where it was demonstrated that the self-assembly propensity dictates the yield (higher for F and L). Non-assembling peptides (G, P) lack the thermodynamic driving force and do not give rise to high yielding conditions (**Figure 2.17**).

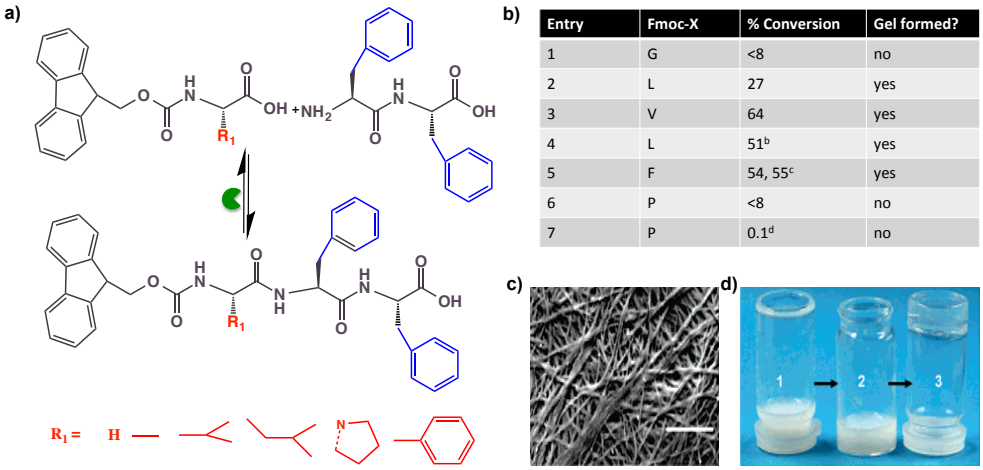

Entry	Fmoc-X	% Conversion	Gel formed?
1	G	<8	no
2	L	27	yes
3	V	64	yes
4	L	51[b]	yes
5	F	54, 55[c]	yes
6	P	<8	no
7	P	0.1[d]	no

Figure 2.17 a) Biocatalytic self-assembly between Fmoc-protected amino acids and F_2, **b)** Table of conversion yields with macroscopically observed transitions of different precursors (b: Fmoc-pentapeptide also formed, c: 60 mmol starting material, d:chymotrypsin instead of thermolysin), **c)** Cryo-SEM image and **d)** Digital photos of Fmoc-F_3. Adapted from ref. 66.

The biocatalytic amide condensation and assembly concept was furthermore investigated for the production of different peptide nanostructures. Amide bond formation using thermolysin for coupling of Fmoc-protected hydrophilic amino acids (Fmoc-S/T) with amino acid esters (F, L-OMe), led to the formation of different supramolecular organisation (sheets, fibers, twisted fibers and tape like structures), with the corresponding peptide nanomaterials showing different supramolecular properties (mechanical and fluorescence properties), highlighting sequence/structure relationship assisted *via* biocatalytic self-assembly. The authors used spectroscopic techniques (fluorescence and FT-IR) to investigate the effect of the minimalistic change of the amino acid side chain on the relative importance of hydrophobic and H-bonding interactions (**Figure 2.18**).[37]

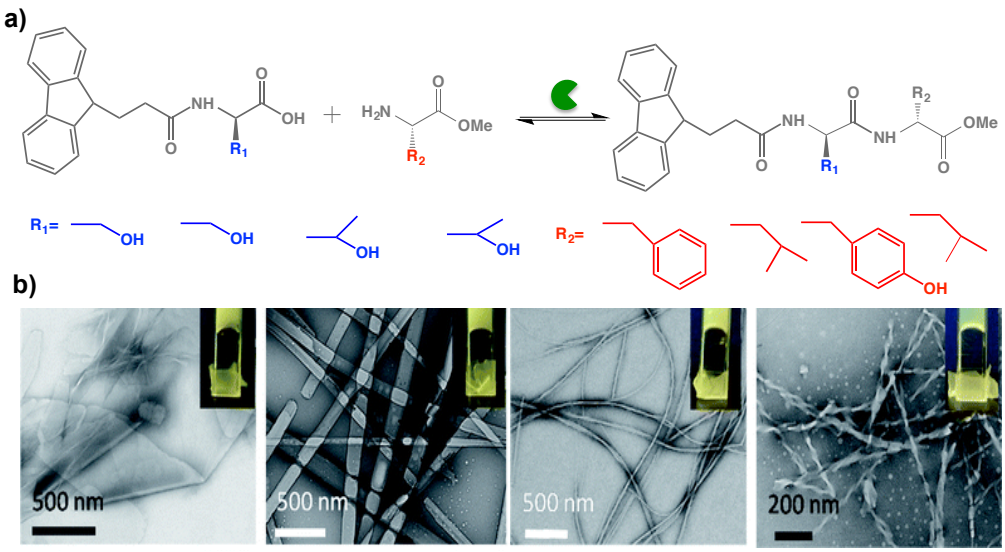

Figure 2.18 a) Chemical structures **b)** TEM images of the corresponding Fmoc-dipeptide esters (Fmoc-SF-OMe, -TF-OMe, -SL-OMe, -TL-OMe), highlighting the formation of different nanostructures. Adapted from ref. 37.

A thorough study of the use of biocatalytic self-assembly for thermodynamically driven supramolecular reconfiguration on aromatic peptide amphiphiles was reported

in 2009 by Williams et *al*.[62] The authors sought to achieve self-correction avoiding the kinetically trapped assembled states by using fully reversible condensation and hydrolysis. Additionally, self-selection of the most thermodynamically stable supramolecular component in a Dynamic Combinatorial Library (DCL) was demonstrated, with this representing the first example of using biocatalytic self-assembly to trigger dynamic component amplification and reduction in a DCL concept. To produce such a system a condensation reaction between Fmoc-protected amino acids (Fmoc-G, L, T, F) with a variety of nucleophile dipeptide amides (G_2, F_2, L_2) was investigated. Interestingly, it was demonstrated that different supramolecular organization might be observed over time as a result of dynamic reversible exchange of covalent bonds between the components of the library. More specifically, Fmoc-L_3 was identified as the major product in first 100h. However, the distribution was significantly changed, which eventually reached a constant distribution to form Fmoc-L_5 as the major product. These time-dependent changes in the distribution coincide with nanostructure reconfiguration, from nanofibers (Fmoc-L_3) to nanosheets (Fmoc-L_5), accompanied with continuous enhancement of supramolecular chirality and fluorophores arrangement, as evidenced using Circular Dichroism (CD) and fluorescence spectroscopy respectively (**Figure 2.19**).

Furthermore, biocatalytic self-assembly was used in order to produce thermodynamically stable supramolecular charge transfer nanostructures. More specifically, an NDI-appended tyrosine with phenylalanine amide in the presence of donor/acceptor complexes was used.[67] Thermodynamically driven biocatalytic self-assembly gave rise to the formation of free-energy optimized functional aqueous electronic nanostructures, avoiding kinetically trapped route dependant aggregates, associated with the poor solubility of these hydrophobic peptides in aqueous media. (**Figure 2.19**).

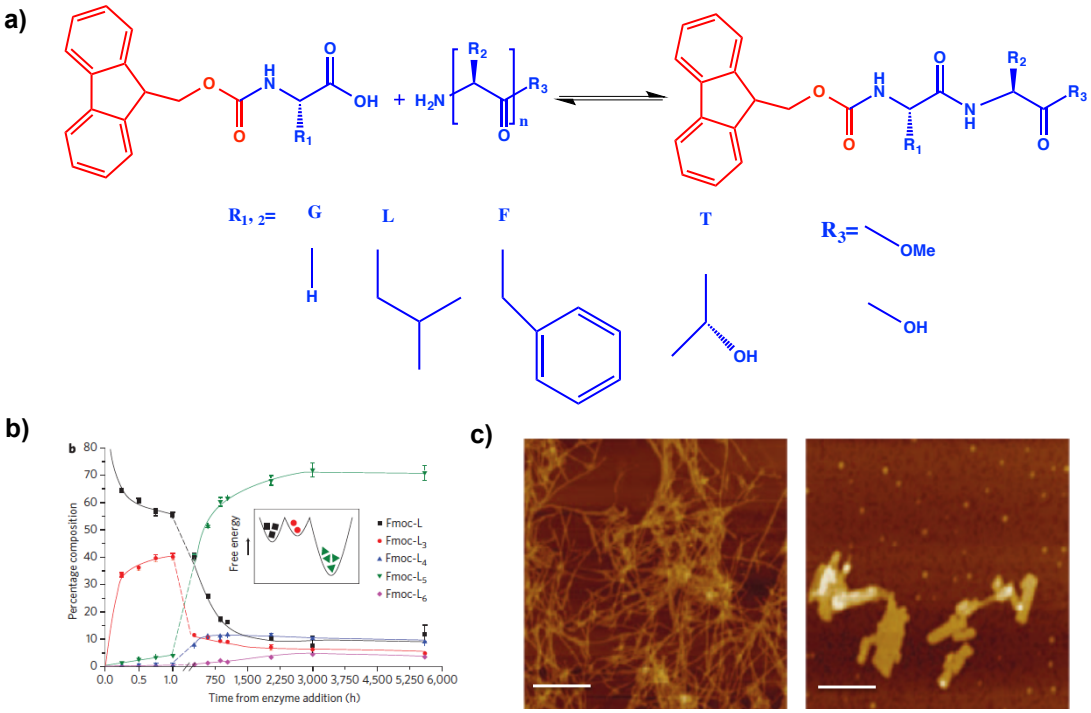

Figure 2.19 a) Chemical structures, **b)** Energy diagram of thermodynamically driven self-assembly with HPLC profile over time **c)** AFM images of supramolecular transition *via* biocatalytic self-assembly over time for Fmoc-L_3 to Fmoc-L_5. Adapted from ref. 62.

An interesting study using biocatalytic self-assembly within the Dynamic Combinatorial Library (DCL) context has been demonstrated in 2010 by Miller and

coworkers.[68] In this case, thermolysin was used to drive the synthesis and gelation of ionic-complementary peptides from non-assembling tetrapeptide precursors (FEFK). Initially, the protease partially hydrolyzed the tetrapeptide into dipeptides (FE+FK). Subsequently, longer peptide sequences were found to form through reverse-hydrolysis. The formation of different peptide components in the library was dependent on the supramolecular properties and their thermodynamic stability was highly associated with the formation of antiparallel beta-sheet structures, as demonstrated using FT-IR spectroscopy. Finally, the main product of the library was an octapeptide, which suggests that it represents the thermodynamically stable supramolecular component (**Figure 2.20**). The authors investigated the effect of enzyme concentration on the morphology and supramolecular properties.[69] Biomedical applications were also shown using biocatalytic self-assembly.[70]

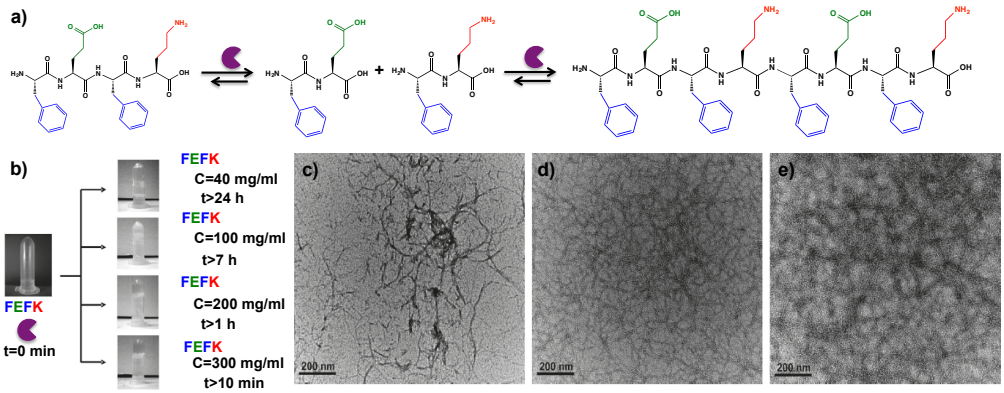

Figure 2.20 a) Thermodynamically driven biocatalytic self-assembly of FEFK to form the corresponding octapeptide, **b)** Optical photographs of different concentration samples before and after thermolysin addition and TEM images of **c)** undiluted, **d)** diluted 100 times and **e)** diluted (200 mg ml^{-1}) samples after 24 h incubation. Adapted from ref. 68.

2.4.2 Kinetically controlled chemical systems

A number of thermodynamically controlled fully reversible self-assembled systems have been described in the previous section, highlighting the importance of final self-organization and function. However, there are many supramolecular systems in which self-organization resulting from kinetic aspects, where the product is not the most stable, but it exists in a kinetically trapped state. In contrast to the thermodynamically driven supramolecular reorganizations, the self-assembly pathway is crucial for structure and function. Consequently, the control of different kinetic states may open up new opportunities for fabrication of nanomaterials with different supramolecular properties. In biology, kinetic control is sometimes linked to function. For example, folding of insulin is not directed through thermodynamics but is indeed a kinetically trapped state, as this arises from a biocatalytic product of a protein cleavage.[71] Complex pathways, with different functions and self-assembly routes, orchestrate kinetic aspects of supramolecular systems, until they finally reached or converted into thermodynamically stable states.

2.4.2.1 Kinetic control over supramolecular gel formation using catalysis

Catalytic control over the formation of supramolecular structures drives a variety of biological processes, such as cell motility and muscle contraction. There is a significant effort from supramolecular chemists to design synthetic mimics of these systems, where chemical catalysis may control their properties, providing access to alternative self-assembly pathways. In 2013, Boekhoven *et al.* demonstrated that the rate of gel formation and the resultant supramolecular properties may be controlled by *in situ* catalysis of the formation of gelator molecules.[72] Interestingly, an addition of an acid or a base (nucleophilic aniline), may dramatically enhance the rate of the formation and the mechanical properties of the gels. The gelator can be formed *in situ* by the reaction of the cyclohexane trishydrazide (1) (**Figure 2.21**) and three-time excess of an aldehyde (2). The formation of the hydrazine gelator (3) is governed mainly through hydrogen bonding interactions. The authors observed that mixing (1) and (2) at pH 7 in a concentration of 8 mM for (1), resulted in the formation of turbid solutions, while at pH 5 opaque gels were formed. An increase of the concentration to 20 mM (1), led to the formation of weak crystalline gels, suggesting significantly higher crtitical gelation concentration (CGC). These observations suggest a strong relationship between the rates of formation (macroscopically observed turbidity increased) with structure formation of the resulting material, as furthermore evidenced using TEM. Stronger gels, formed under catalytic control, consisted of branched fibrillar network, while unbranched bundles are observed for uncatalysed samples (**Figure 2.20**).

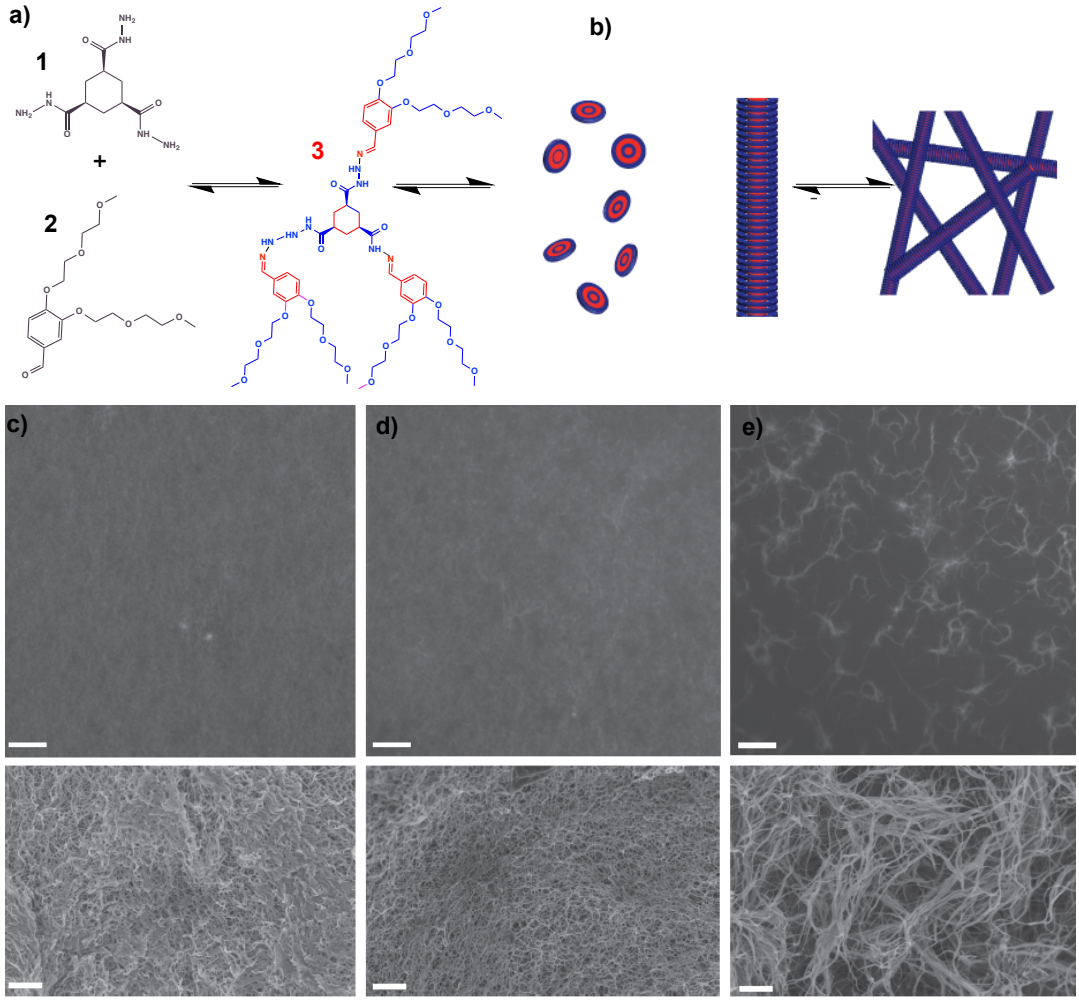

Figure 2.21 a) Catalytic formation of trishydrazone hydrogelator from soluble building blocks **b)** Fibre formation, which eventually crosslink to form a network that traps the surrounding solvent, leading to gelation and Confocal laser scanning fluorescence micrographs (top) with scanning electron micrographs (bottom) show differences in network morphology and fibre thickness that depend on catalyst loading at **c)** pH 5.0 **d)** pH 7.0 with 10 mM aniline and **e)** uncatalysed samples at pH 7.0. Adapted from ref. 72.

2.4.2.2 Kinetically controlled systems using biocatalytic self-assembly

Biocatalytic self-assembly has also been used to produce kinetically trapped assemblies with functionality.[73] Enzymatic catalysis give rise to the possibility to quickly access more ordered supramolecular states. Varying the enzyme concentration, a significant enhancement of supramolecular order was observed, while critical gelation concentrations remain similar. The system focused on Fmoc-dipeptide methyl esters (Fmoc-FF-OMe, -FY-OMe, YL-OMe, VL-OMe, FL-OMe) with molecular self-assembly to be initiated by the enzyme subtilisin, which hydrolyses the methyl ester to form a peptide derivative that self-assembled (**Figure 2.22a,b**).[73] Control of enzyme concentration in the case of Fmoc-YL (changing rate of hydrolysis), gave rise to tune the physical and chemical properties of the corresponding dipeptides. Heat-cool cycles gave insights on the nanostructure differences of the same structures formed (inset photo of the fluorescence spectrum- **Figure 2.22c**). After melting and regelation of the samples, the differences in organisation where no longer present, clearly showing that the biocatalytic self-assembly formed, represented local minima. Structural evidence of supramolecular order with the formation of catalytic clusters was visualised using Atomic Force Microscopy (AFM), demonstrating that supramolecular organisation of the Fmoc-dipeptide hydrogel network was dictated by substilisin concentration, where entangled fibrillar architectures may be obtained at higher enzyme concentrations (**Figure 2.22f-h**). A variety of spectroscopic techniques (Fluorescence, FT-IR, CD) revealed that a more ordered environment for the arrangement of the fluorophores, for the conformation of amide backbones and supramolecular chirality of the building blocks might be achieved as the enzyme concentration was increased. (**Figure 2.22**).[73]

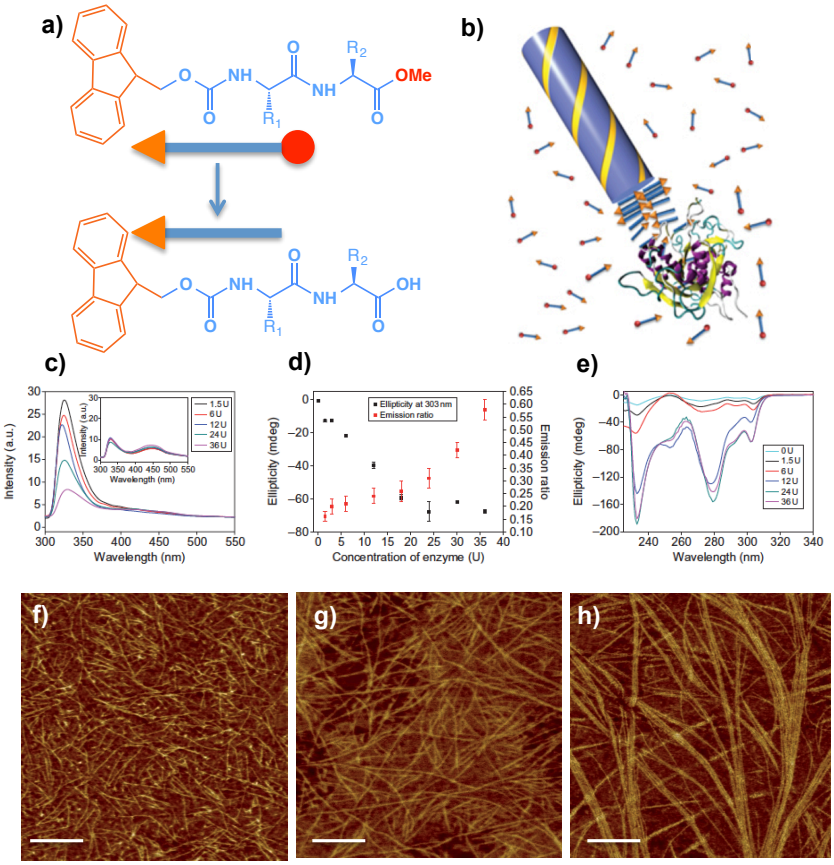

Figure 2.22 a) Chemical structure of Fmoc-dipeptide methyl esters where subtilisin catalyses hydrolysis to form the corresponding Fmoc-peptide gelators. **b)** Schematic representation of nucleation and growth mechanism of self-assembly controlled by subtilisin, **c)** Emission spectrum (excitation at 280 nm) of Fmoc-YL gel obtained at different enzyme concentrations. Inset: Emission spectrum of the gels after a heat-cool cycle, **d)** Correlation of the increase in ellipticity at 303 nm with emission ratio, **e)** CD spectrum of Fmoc-YL with increasing enzyme concentrations and **f-h)** AFM analysis of the fibrillar formation at different enzyme concentrations (1,5, 6, 12, 24, 36U). Adapted from ref. 73.

Furthermore kinetically locked peptide oligomerisation using chymotrypsin and papain was reported by Gross *et al.*[74] In this case, the addition of chymotrypsin or papain to an aqueous dipeptide-ethyl ester solution, consisting of lysine and leucine (KL-OEt), led instantly to peptide oligomerisation forming alternating or random oligopeptides of mixed chain length $(KL)_n$. As a result of rapid sol-gel supramolecular transition (10s), the formation of fibrillar supramolecular architectures was observed using Atomic force Microscopy (AFM). The biocatalytic peptide oligomerisation and assembly resulted in enhancement of hydrogen bonding type interactions and supramolecular chirality of the building blocks (**Figure 2.23**).

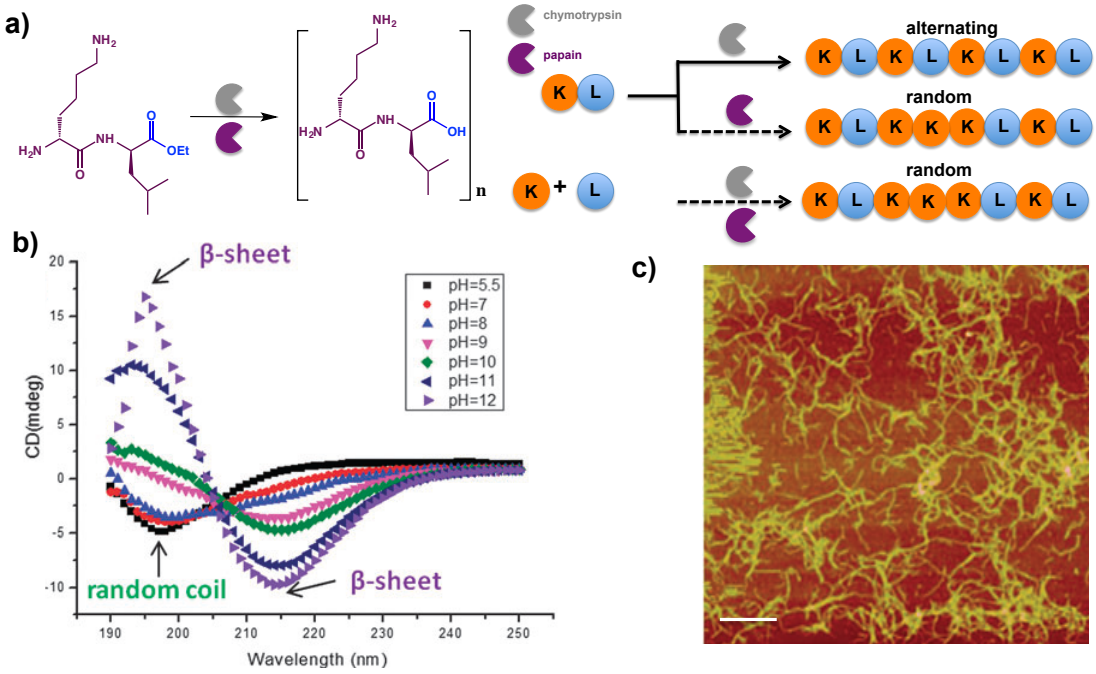

Figure 2.23 a) Schematic representation of altering or random peptide oligomerisation using chymotrypsin or papain of the dipeptide ethyl ester KL-OEt**, b)** CD spectrum after peptide oligomerisation at different pH and C) AFM image of the corresponding peptide oligomers. Adapted from ref. 74.

2.4.2.3 Replication

Replication of supramolecular systems *via* self-assembly is another important aspect of kinetically driven nanostructure reconfigurations that results from autocatalysis. In this case, the approach of dynamic combinatorial libraries is used to develop molecules capable of promoting their own formation, while forming extended assemblies at the same time. An interesting kinetically controlled replicating system was reported in 2010 by Otto's lab.[75] The authors used peptide sequences consisting of altering hydrophobic (leucine) and hydrophilic (lysine) amino acids, due to their propensity to non-covalently assemble into beta-sheet structures. Oxidative disulphide reactions, gives rise to the formation of different disulphide macrocycles, with tuneable size and shape (**Figure 2.24a**). Initially, they observed the formation of cyclic trimers and tetramers in the library after 15 days. However, after that period an unexpected change in library composition occurred, with the cyclic heptamer rapidly became the dominant product. The reconfiguration observed was depending on the mode of agitation. Remarkably, the formation of cyclic hexameric product was observed after stirring the sample instead of agitation, suggesting that mechanical energy may have a dramatic impact on the outcome of the competition in the library. The authors proposed that the fibrillar formation (hexa-heptamer) might explain the mechano-responsiveness, where three phases can be observed: i) initial nucleation phase, ii) a growth phase in which the concentration of these macrocycles increases exponentially, due to mechanical breaking of fibres and creating new network ends iii) phase in which the rate of growth depends on the consumption of the starting material, resulting in a constant rate of formation of hexamer or heptamer (linear growth). This may be achieved by the breaking of fibres through mechanical energy (**Figure 2.24b,c**).

Notably, the solvent environment was found to have a significant impact on the existence and outcome of the competition in the library. In this case, similar peptide sequences were preselected to ensure formation of beta-sheet structures, replacing leucine (L) at the C-terminus with phenylalnine (F), serine (S) and alanine (A). A co-solvent system of water and 2,2,2-trifluoroethanol (TFE) with varying ratios (0-30%) was used to tune the composition of the library, by interplaying with hydrophobic and hydrogen bonding interactions, which may favour the formation of different macrocycles.[64] Interestingly, it was demonstrated that the hexameric macrocycle may be favoured in a percentage of 20-30% of TFE, while an octameric product may be observed in the presence of lower TFE percentages.[76]

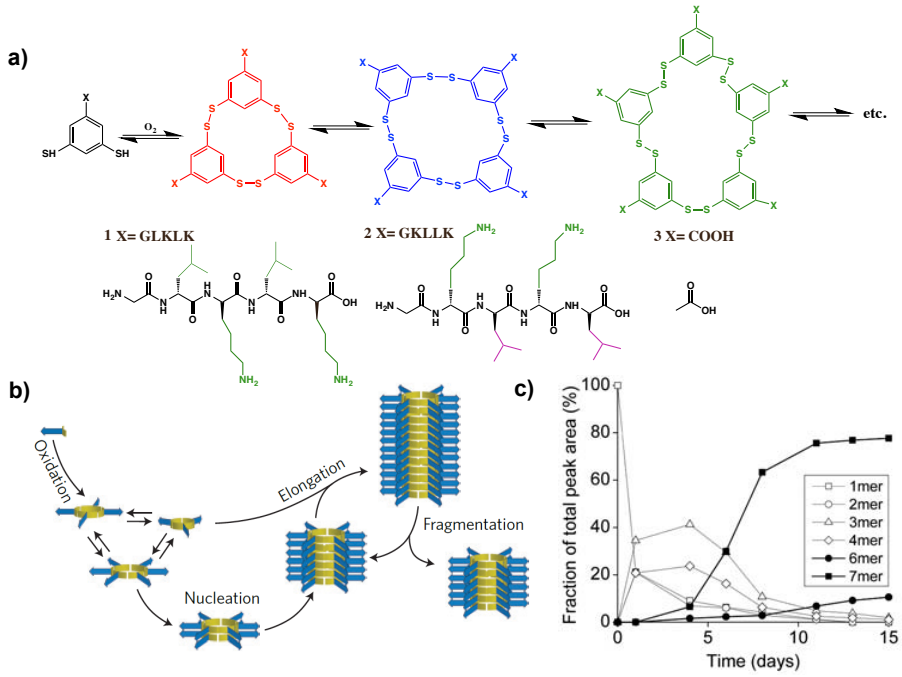

Figure 2.24 a) Peptide sequence that undergo air oxidation to form disulphide macrocyles, **b)** Schematic representation of fibre elongation and fragmentation through self-replication and **c)** HPLC profiles of different macrocycle formation over time. Adapted from ref. 75.

2.5 Away-from-equilibrium assemblies

In contrast to thermodynamically and kinetically driven supramolecular reconfigurations, away-from-equilibrium supramolecular systems owe their transient existence on the energy that is supplied into the system. Supramolecular organization and function may only be found in the transient state and, when the energy is switched off, the system relaxes back to the initial unassembled thermodynamically stable state. Biological systems rely on chemical energy stored in molecular fuels (such as adenosine triphosphate, ATP) to achieve assembly of active nanostructures. For example, catalytic formation and degradation of actin filaments and microtubules under the influence of chemical fuels are critical to transport and movement in biological systems. These active nanostructures are essential for vital cellular functions such as migration, division and differentiation. These biological assemblies have been studied in vitro to gain insight into the mechanisms and molecular interactions that underpin their remarkable dynamic behaviour.

The first example of a chemically fuelled, non-equilibrium supramolecular system was demonstrated by Boekhoven *et al*.,[77] who showed that transient hydrogelation may be achieved by catalytic esterification (to form a gelator) and competing, thermodynamically favoured hydrolysis of an ester group. More specifically, a non-assembling diacid consisted of dibenzoyl-cystine is fully converted into the diester using methyl iodide (MeI), resulting in transient formation of a fibrillar network. Ester hydrolysis leads to energy dissipation and breaking of the fibres (**Figure 2.25**).

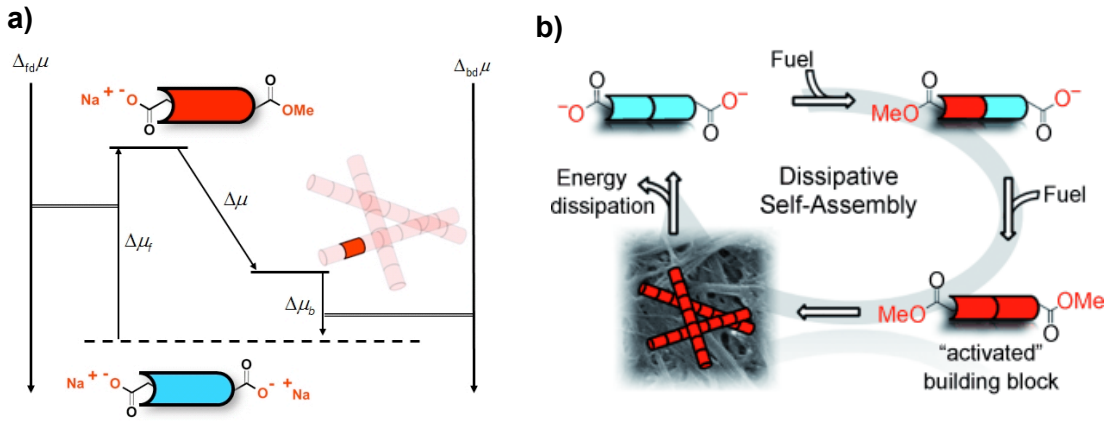

Figure 2.25 a) Energy diagram of Dissipative Self-Assembly (DSA) and **b)** Net reaction of dissipative self-assembly cycle with ester formation and hydrolysis using chemical fuel. Adapted from ref. 77.

Furthermore, away-from-equilibrium chemical systems have also been reported using biocatalytic self-assembly. Debnath and coworkers reported the first example of biocatalytically triggered transient supramolecular response.[78] The authors demonstrated chemically fuelled biocatalytic formation of peptide nanofibers, which display dynamic instability based on transient formation (fuelled by ester hydrolysis) and degradation of an aromatic dipeptide amphiphile (**Figure 2.26)**. A naphthalene appended aromatic amino acid methyl ester (Nap-Y-OMe) was converted into an amidated aromatic dipeptide amphiphile (Nap-YF-NH_2, Nap-YY-NH_2, Nap-YL-NH_2) using chymotrypsin as the catalyst in the presence of amino acid nucleophile amides as acceptors. Gradually the dipeptide was hydrolysed to form the non-assembling amino acid derivative (Nap-Y-OH). The authors demonstrated that the final supramolecular state (macroscopically observed gel-like material or solution) is dictated by the chemical design. More specifically, Nap-YF-NH_2 remained in the gel state after hydrolysis, while replacing F with Y (Nap-YY-NH_2) gave rise to a transition to the solution state. Atomic Force Microscopy studies revealed the

formation and breaking of peptide fibres as the hydrolysis reaction dominated in the system. Circular Dichroism (CD) and fluorescence spectroscopy revealed the transient supramolecular chirality and arrangement of the fluorophores respectively. Changing the pH of the solution, the lifetime of the gels could be regulated. The system could be refuelled several times by the addition of the precursor.

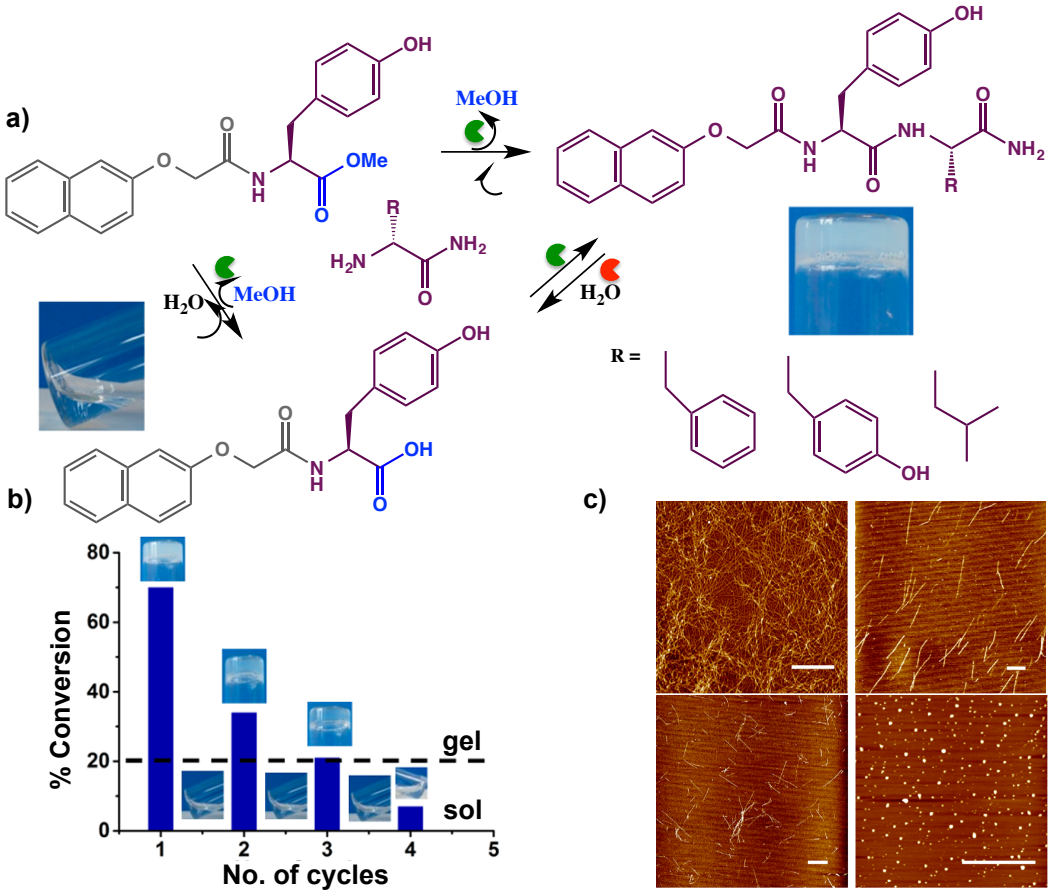

Figure 2.26 a) Chemical structures of non-equilibrium biocatalytic self-assembly **b)** Refuelling of the system highlighting repeated sol-gel processes and **c)** AFM images at different time points, highlighting the formation (gel) and breaking of the fibres (sol) Adapted from ref. 78.

Recently, Heuser *et al*., demonstrated catalytic control of the time domain existence of a self-assembling system - a pH responsive aromatic peptide amphiphile appended

to the N-terminus with the Fmoc group and leucine and glycine in the peptide sequence (Fmoc-LG).[79] The authors sought to achieve precisely programmable acidic pH profiles, where the feedback is driven by the slow release in a slightly basic environment using urease. More specifically, kinetic balances may be achieved by providing acidic conditions using buffer solutions and basic environment, by the urease-catalysed conversion of urea into CO_2 and NH_3, giving rise to highly controlled time dependent acid-based reactions. The Fmoc-dipeptide (Fmoc-LG) self-assembled into twisted ribbon-like architectures at low pH values, with supramolecular reconfiguration to form fibrillar assemblies to be observed at higher pH values (≈6). The pH of the system changes when the dipeptide coupled to the acidic/basic environment. Notably, the urease concentration gave rise to control the lifetime of the gels, as evidenced by both vial inversion and the mechanical properties of the gels using rheology (**Figure 2.27**). Additionally, the authors designed transient barriers in microfluidic devices, in the presence of the aromatic dipeptide amphiphile, showing continuous gel-sol transitions as a result of pH responsiveness. The approach of biocatalytic feedback-driven transient programming of self-regulating peptide hydrogels can be considered as an important step forward with respect to classical stimuli-responsive supramolecular systems, as it provides access to dynamic, self-repairing nanomaterials based on internal triggers.

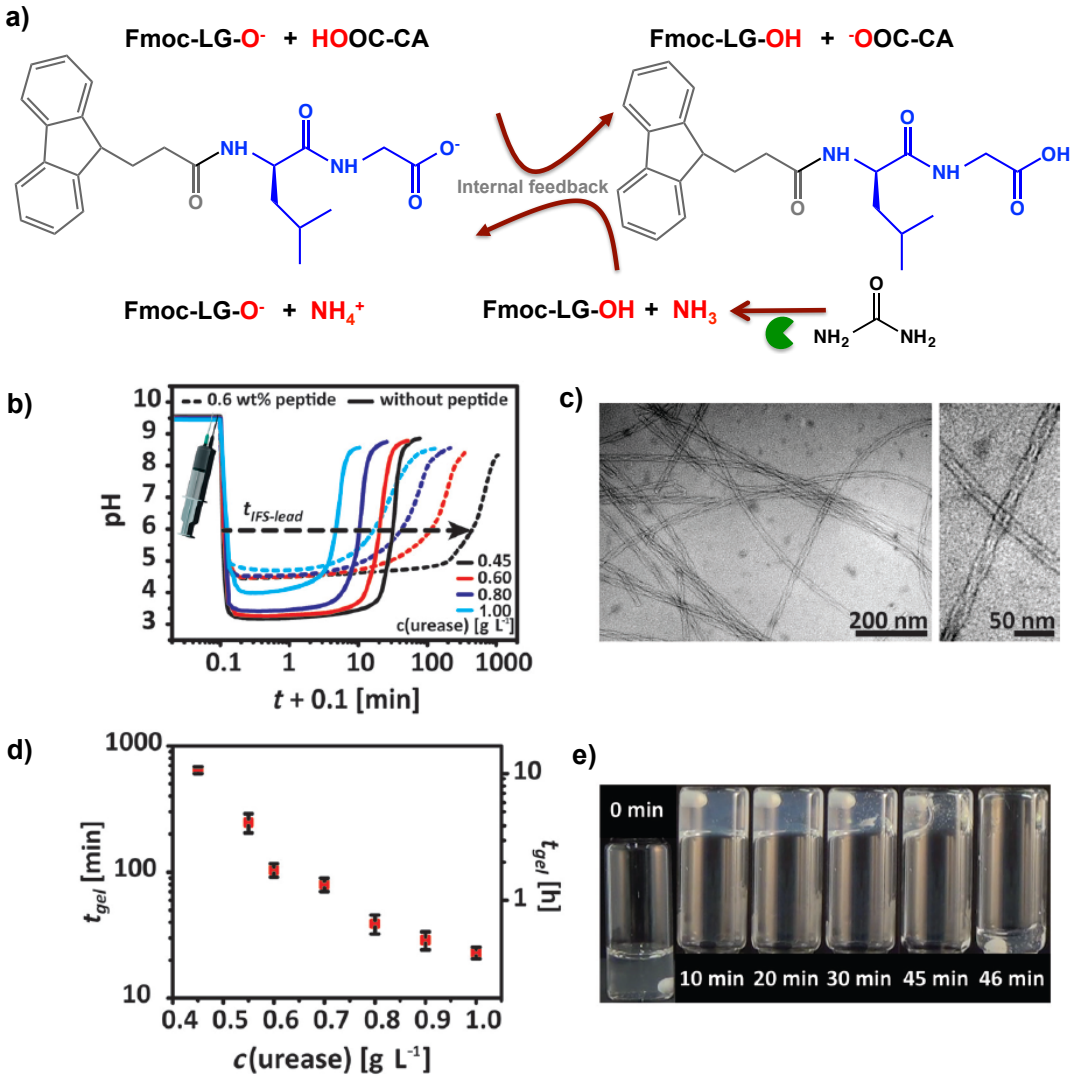

Figure 2.27 a) Coupling of the dipeptide with the acidic/basic environment. **b)** pH-time profiles at different urease concentrations, **c)** Cryo-TEM of the hydrogels, **d)** Gel lifetimes as determined by tube-inversion tests and **e)** Digital photos of programmable peptide hydrogels. Adapted from ref. 79.

Light has also been used to design away-from-equilibrium systems. Ragazzon *et al.*, recently reported an example of light responsive dissipative assemblies, where solar energy is used to perform directed molecular movements in a repetitive fashion out of equilibrium.[80] The system is based on an azobenzene macrocycle derivative, which can undergo E-Z photoisomerisation.

2.6 Conclusions and Outlook

Minimalistic peptides as structural motifs, are fascinating building blocks for "bottom up" construction of nanoscale assemblies, as they are constituted of the 20 gene encoded amino acids - the expression of biology's language (**Figure 2.1**). They are potentially ideal structural and functional candidates as they play a key role in catalysis, adaption, molecular recognition, reconfiguration and compartmentalization in living systems.

Most of the existing laboratory self-assembly processes are governed with **thermodynamics**, resulting in permanent supramolecular self-assembled states, where the pathway is irrelevant to the final assembled state. There is a significant effort from supramolecular chemists to move into systems where the existence and the outcome of competition are dictated by **kinetics**, where the self-assembly pathway becoming a crucial factor and more specifically, moving into chemical systems that only exist **away-from-equlibrium** under the influence of constant chemical energy. **Away-from-equlibrium** laboratory based processes are probably the most representative mimics of more complex biological machinery that requires continuous energy dissipation for biological response and cells function. There are only few literature examples that represent away-from-equilibrium chemical systems, showing temporary response to an external or internal stimulus to activate function and properties. It is clear that these kind of chemical systems have rich potential, thus the real challenge for supramolecular chemists for the next years is to discover keys to unlock this potential. The dynamic optimization of nanostructures through changes in molecular make-up under energy dissipating conditions - with simple bio-derived molecules will give rise to a better understanding to the degree of

supramolecular complexity and the emergent properties of such systems. The development of adaptive materials of this type may play a role in new, rapid-response active materials, soft robotics and ultimately evolvable materials that autonomously adapt to their environment and are not restricted by thermodynamics or predefined molecular composition.

3. Alignment of nanostructured tripeptide gels by directional ultrasonication*

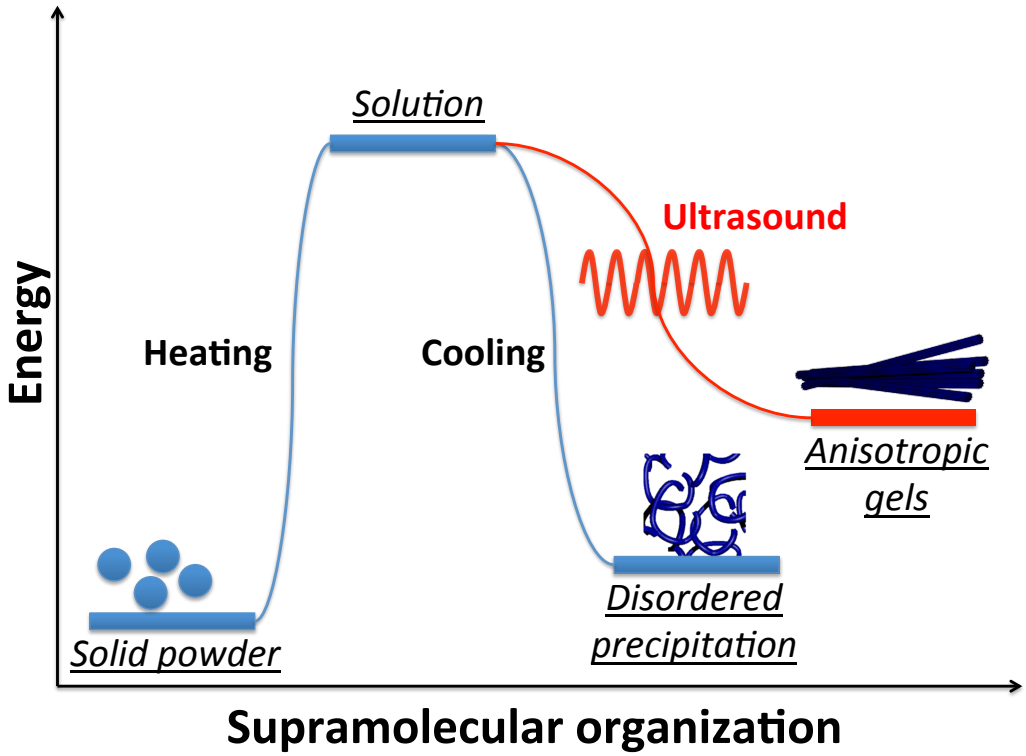

Objectives

The key research objectives of this chapter are to:

i. Demonstrate an *in situ* ultrasonic approach to influence peptide self-assembly.

ii. Investigate the effect of ultrasonic waves on supramolecular interactions (hydrophobic and hydrogen bonding type interactions).

iii. Investigate the effect of peptide sequence used and solvent environment on nanostructure reconfiguration using ultrasound.

* This work was published in part as: C. G. Pappas, P. W. J. M. Frederix, T. Mutasa, S. Fleming, Y. M. Abul-Haija, S. M. Kelly, A. Gachagan, D. Kalafatovic, J. Trevino, R. V. Ulijn and S. Bai*, Chem. Commun*., **2015**, 51, 8465-8468.

C.G.P. and R.V.U. conceived, designed the experiments, analysed the data and wrote the paper. C.G.P. synthesized the tripeptides, performed the CD, LD and rheological experiments. T.M. and A.C. were responsible for the fabrication of the ultrasonic transducer. P.W.J.M.F. performed the FT-IR experiments. S.F. and Y.M.A. helped with the cartons. S.M.K. helped with analysing the CD and LD experiments. S.B. D.K. and J.T. helped with the imaging.

3.1 Introduction

Peptides are versatile building blocks for the formation of structured materials for a range of applications in biomedicine and bionanotechnology.[16, 20, 81] However, while they may be highly organized at the supramolecular (nanoscale) level, most self-assembling materials are disordered at the macro-scale. The ability to control their orientation across the length scales may open up ways to better control mechanical, optical and electronic properties.[82-86]

A number of approaches have been used to align both inorganic and organic materials. These include Langmuir-Blodgett techniques, lithography, chemical vapour deposition, magnetic and electric fields.[87-93] Several successful examples have been reported to generate anisotropic gels but few methods allow for *in situ* alignment in solution or in gel-phase. Stupp's group demonstrated a thermal pathway to process self-assembling peptide amphiphiles into highly aligned macrostructures.[94] Yan and coworkers used heating to trigger covalent crosslinking of cyclo-dipeptides, leading to highly ordered peptide crystals.[95,96] Xu and coworkers reported on the use of biocatalytic self-assembly to trigger anisotropic changes in fibrillar architectures on aromatic peptide amphiphiles, highlighting the importance of aromatic-aromatic interactions on structural alignnment.[97] Shear-flow and magnetic field were also used to align macroscopic domains within peptide hydrogels.[98,99] Gazit and coworkers reported on the formation of vertically aligned peptide nanotubes of F_2, after exposure to a magnetic field.[100]

Ultrasound, i.e. high oscillating pressure waves (>20,000 Hz), is commonly used in supramolecular chemistry to overcome energy barriers and disrupt intermolecular interactions, which has been routinely used to control self-assembly and gelation

processes,[101-107] including most recently the demonstration of dynamic and transient reconfiguration of peptide nanostructures,[107] as will be discussed in details on the next chapter (**Chapter 4**). Short peptide sequences[12,108] have gained significant attraction as building blocks to trigger self-assembly and gelation, (see Section **2.2.4-2.2.6**) with their supramolecular properties to be regulated *via* a variety of environmental triggers.

Herein, we demonstrate the use of ultrasound to trigger the self-assembly and alignment of tripeptide nanostructures resulting in stable anisotropic organo- and hydrogels (**Scheme 3.1**). We reasoned that the directionality of sound waves-longitudinal pressure waves that lead to oscillating compression of the solvent volume in the same direction as the wave itself - may provide opportunities to introduce anisotropy in gel-phase.

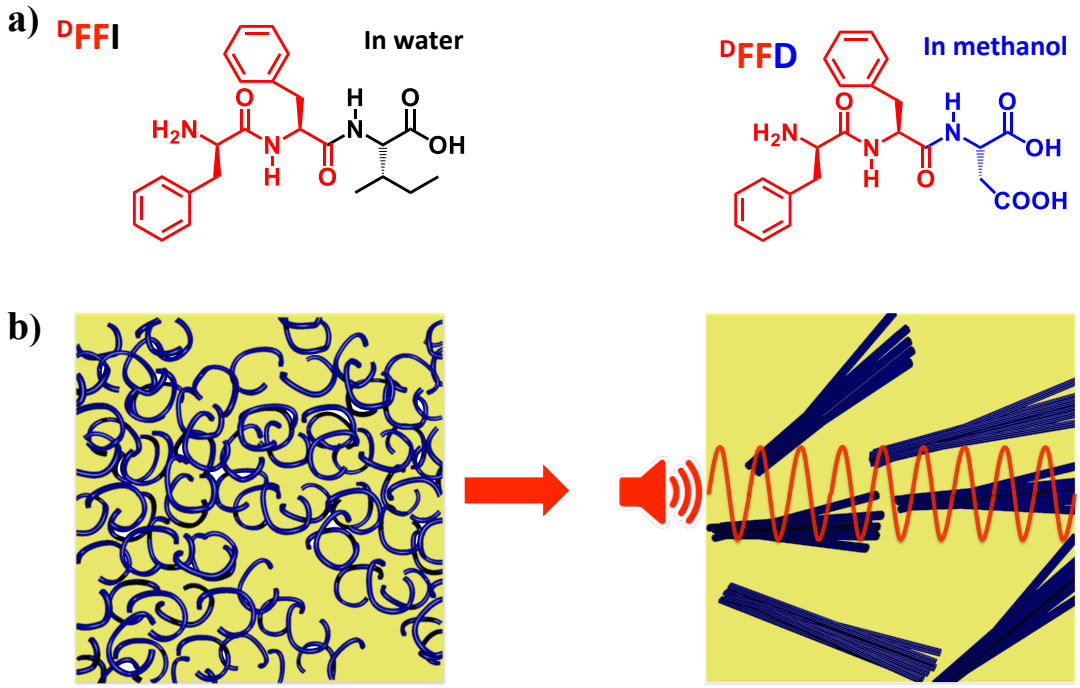

Scheme 3.1 a) Chemical structures of tripeptide derivatives of ^{D}FFI and ^{D}FFD, **b)** Schematic representation of self-assembly of ^{D}FFD and ^{D}FFI altering from disordered short fibers to highly oriented fibrous clusters after ultrasound exposure in methanol (^{D}FFD) and buffer solution (pH 8, ^{D}FFI).

3.2 Materials and Methods

Fmoc-Ile and Fmoc-Asp(otBu)-Wang resin were purchased from Novabiochem UK. 2-(1H-Benzotriazole-1-yl)-1,1,3,3-tetramethyluroniumhexafluorophosphate (HBTU), Fmoc-Phe-OH, Fmoc-^{D}Phe-OH, Piperidine, trifluoroacetic acid (TFA), diisopropyl ethyl amine (DIPEA), triisopropyl silane (TIPS) were purchased from Sigma Aldrich and used as received. Phosphate buffer solution (pH 8) was prepared by dissolving 94 mg $NaH_2PO_4 \bullet H_2O$ and 2.5 g $Na_2HPO4 \bullet 7H_2O$ in 100 ml water.

3.2.1 Synthesis and characterization of the tripeptides

The tripeptides were synthesized by using the Fmoc-strategy. Coupling reactions of the Fmoc amino acids were carried out by using a molar ratio of Fmoc-amino acid/HBTU /DIEA/resin (3:3:6:1) in anhydrous DMF. Removal of the Fmoc group was achieved by using 25% piperidine in DMF. The cleavage of the peptide from the resin was performed by using a mixture of TFA/TIPS/water in a molar ratio of 95/2.5/2.5.

^{D}FFD

Purity by HPLC (214 nm) 97.5% 1H-NMR (400 MHz, DMSO, TMS): δ 8.8 (d, 1H, NH), 8.49 (1H, NH), 7.20 (m, 10H, Ar), 4.76 (m, 1H, αCH), 4.41 (m, 1H, αCH), 3.92 (m, 1H, αCH), 3.2 (2H, CH_2 Asp), 2.9-2.618 (4H, 2xβCH_2 phenylalanine) MS (ES+): m/z 428.1 [M + H].

^{D}FFI

Purity by HPLC (214 nm) 97.7% 1H-NMR (400 MHz, DMSO, TMS): δ 8.85 (d, 1H, NH), 8.42 (1H, NH), 7.23 (m, 10H, Ar), 4.86 (m, 1H, αCH), 4.20 (m, 1H, αCH), 4.01 (m, 1H, αCH), 3.094-2.692 (m, 4H, 2xβCH_2 phenylalanine), 1.47-1.22 (3H Isoleucine) and 0.9 (6H Isoleucine). MS (ES+): m/z 426.2 [M + H].

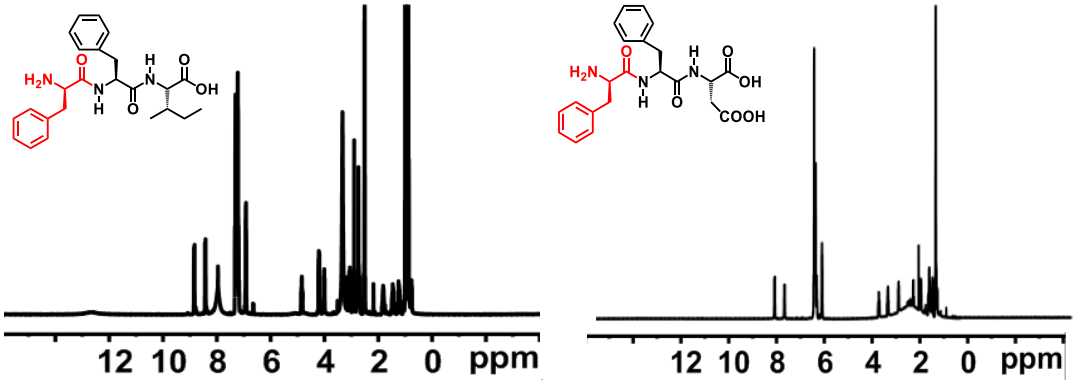

^{1}H NMR spectra of the tripeptides ^{D}FFI and ^{D}FFD in dmso-d_6 at 298K.

3.2.2 Ultrasonic Setup

The ultrasonic set up was developed in the Centre of Ultrasonic Engineering in the University of Strathclyde, in Prof. A. Gachagan's lab. An ultrasonic cell was fabricated, which was controlled by standard ultrasonic laboratory equipment to provide control of the operating parameters. An 80,000 Hz Tonpilz transducer (Morgan Electroceramic Ltd, UK) was bonded to the base of a 50 ml glass beaker. A Tektronix AFG 3102 signal generator was used to generate a 78,000 Hz continuous wave signal that was subsequently amplified through a 100W Kalmus 155CLR amplifier and used to drive the Tonpilz transducer. To improve the electrical energy transfer from the Kalmus amplifier to the transducer, the signal from the amplifier was fed into a bespoke impedance matching network that matched the amplifier output impedance to the impedance of the transducer for power efficiency. The network comprised a 1:6 transformer and reduced the electrical impedance of the transducer from ~500Ω to ~10Ω, at the operating frequency. This matching network was then connected to the transducer that generated ultrasound.

3.2.3 Sample preparation

Samples prepared without ultrasound: 12.5 mg of ^{D}FFI were dissolved in 1 ml sodium phosphate buffer (100 mM, pH 8). The sample was heated up to 80 °C for 4 minutes to enhance the solubility. After cooling down, a precipitate was observed. For ^{D}FFD, 10 mg were dissolved in 1 ml methanol. The sample was heated up to 50 °C for 3 minutes. After cooling down, a precipitation was observed.

Samples prepared with ultrasound: 12.5 mg of ^{D}FFI were dissolved in 1 ml sodium phosphate buffer (100 mM, pH 8). The sample was heated up to 80 °C for 4 minutes. Then the sample was treated with ultrasound for 30 sec and a gel-phase material was obtained. In the case of ^{D}FFD 10 mg were dissolved in 1 ml methanol. The sample was heated up to 50 °C for 3 minutes. Then the sample was treated with ultrasound for 60 s and a gel-phase material was obtained.

3.2.4 Transmission electron microscopy (TEM)

Carbon-coated copper grids (200 mesh) were glow discharged in air for 30 s. The support film was touched onto the gel surface for 3 s and blotted down using filter paper. Negative stain (20 ml, 1% aqueous methylamine vanadate obtained from Nanovan; Nanoprobes) was applied and the mixture blotted again using filter paper to remove excess. The dried specimens were then imaged using a LEO 912 energy filtering transmission electron microscope operating at 120kV fitted with 14 bit/2 K Proscan CCD camera.

3.2.5. Scanning electron microscopy (SEM)

The self-assembled structures of tripeptides were visualized by Hitachi S800 field emission scanning electron microscope (SEM) at an accelerating voltage of 10 keV.

3.2.6 Two-photon fluorescence excitation microscopy (TPM)

The formation of tripeptide fibers and gels labeled by ThT were characterized by Two-photon fluorescence excitation microscopy (TPM). The TPM system consisted of a (multiphoton) scanning system (1024 MP; Bio-Rad, Hemel Hempstead, UK) coupled to the upright, fixed stage of a microscope (Eclipse E600FN; Nikon Tokyo, Japan).

3.2.7 Mass and NMR Spectroscopy

Mass spectra were recorded on a Thermo Electron Exactive. 400.1 (1H) NMR spectra were recorded on Brucker Avance 400 spectrometer at room temperature using perdeuterated solvents as internal standards. Diffusion ordered spectroscopy (DOSY) spectra were acquired at 600 MHz using a Bruker Avance 600 spectrometer at 298 K. The eddy current delay (Te) was set to 5 ms. The diffusion time was adjusted to 100 ms. The duration of the pulse field gradient, δg, was optimized in order to obtain 5% residual signal with the maximum gradient strength with the resulting δ value of 3.6 ms. The pulse gradient was increased from 2 to 95% of the maximum gradient strength using a linear ramp 16k data points in the F2 dimension (20 ppm) and 16 data points in the F1 dimension were collected. Final data sizes were 16k×128.

3.2.8 Circular (CD) and Linear (LD) Dichroism Spectroscopy

Circular (CD) and Linear (LD) Dichroism spectra were measured on a Jasco J-815 spectropolarimeter with 1s integrations with a step size of 3 nm and a single acquisition with a slit width of 1 nm. Demountable cells of 0.01 cm path length were used for the measurement. The measuring wavelength was covering the region from 190-400 nm.

3.2.9. FTIR spectroscopy

Infrared absorption spectra were recorded on a Bruker Vertex 70 spectrometer, averaging 25 scans per sample at a resolution of 1 cm^{-1}. Samples were sandwiched between two 2 mm CaF_2 windows separated with a 50 μm polytetrafluoroethylene (PTFE) spacer. For the samples without ultrasound treatment, a sample was taken in the form of the suspended precipitate. Spectra were corrected for background absorptions from phosphate buffer, TFA and atmospheric water where necessary.

3.3 Results and Discussion

3.3.1 Nanostructure reconfiguration

Tripeptides were synthesized by using the standard Fmoc (Fluorenylmethyloxycarbonyl)-tBu strategy. Initially, starting from the L-containing tripeptide (FFI), nanostructure organization and gelation was not observed in phosphate buffer pH 8 (the sample appeared to be a suspension). However, the formation of hydrogels was observed after a change in the stereochemistry of the phenylalanine amino acid residue on the N-terminus of the sequence (^{D}F), where ultrasound may be used to fabricate anisotropic hydrogels, indicating that the anisotropic arrangement of nanostructures is highly related to the peptide configuration (L or D). More specifically, 12.5 mg of ^{D}FFI were dissolved in 1 ml phosphate buffer solution (pH 8). Heating up to 80 °C enhanced the solubility.

After cooling down to room temperature, a precipitate was obtained, while exposure to ultrasound for 30 seconds during the cooling process, resulted in the formation of a hydrogel. We used a variety of microscopic techniques to compare the nanostructure organization on the precipitation and on the gel state. TEM images revealed that short nanofibers (50-150 nm) might be formed prior to ultrasound exposure, giving rise to a precipitate like structure (**Figure 3.1a**). Interestingly, ultrasonic waves gave rise to macroscopically observed supramolecular reorganisation from precipitate to hydrogel structures, accompanied with the formation of bundles of highly oriented fibrillar assemblies, with the fibres increasing both in length (50 μm) and density until an entangled fibrillar arrangement was formed (**Figure 3.1b**). SEM images revealed macroscopic alignment of peptide fibers up to 1 μm of thickness (**Figure 3.1c**). These microscopic

observations (size and diameter of supramolecular structures) are in a good aggrement with previous reports from Marchesan *et al.* on the formation of hydrogels with D-stereoisomer (^{D}FFL and ^{D}FFV) in the N-terminus.[108]

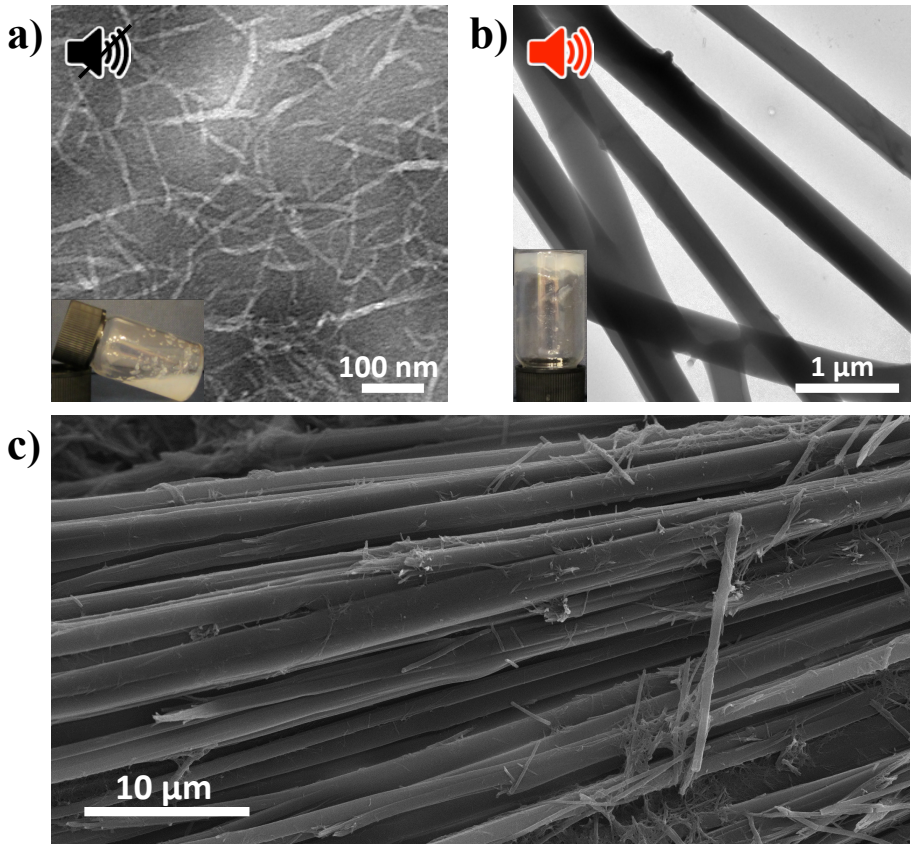

Figure 3.1 TEM images of ^{D}FFI in phosphate buffer (pH 8) **a)** before and **b)** after ultrasound exposure, inset photographs are ^{D}FFI forming solution or gel without or with ultrasound in buffer and **c)** SEM image of the ultrasonicated ^{D}FFI peptide gels. The scale bars are **a)** 100 nm, **b)** 1 µm, **c)** 10 µm. The concentration is 30 mM.

3.3.2 Supramolecular interactions

To acquire more insights at the supramolecular level in the aqueous media, the samples were characterized by spectroscopic methods. Significant enhancement of CD and LD signal at 215 nm revealed the presence of chiral centres within β-sheet type conformation and anisotropic arrangement of phenyl moieties in self-assembled

structures after ultrasonic exposure, leading to the formation of a supramolecular hydrogel, as evidenced using Circular and Linear Dichroism spectroscopy (**Figure 3.2a,b**).[109] IR absorption spectrum were taken by using deuterated phosphate buffer at pD 8, showing a broad band from 1635 to 1650 cm^{-1} (**Figure 3.2c**), indicating a less ordered H-bonding pattern between the peptide backbones.[110] **Figure 3.2d** shows the linear viscoelastic responses of the ^{D}FFI hydrogels. The storage modulus (G') exceeds the loss modulus (G") by factor of 22 demonstrating that the tripeptides formed viscoelastic gels. It is worth to mention that change of solvent from water to methanol and other alcohols did not result in the formation of gel phase materials, with ultrasonic treatment found to have no effect on the self-assembly in this environment.

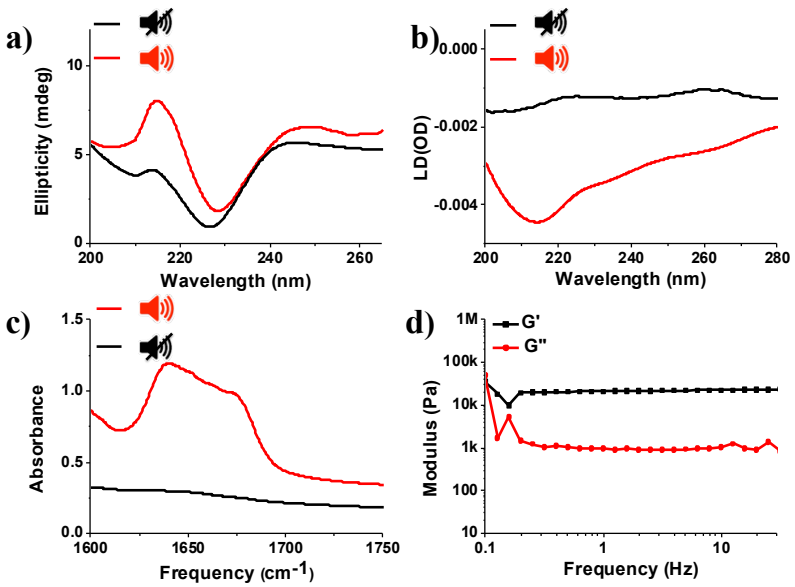

Figure 3.2 a) CD (Circular Dichroism), **b)** LD (Linear Dichroism), **c)** FT-IR spectra of ^{D}FFI in phosphate buffer (pH 8) before and after ultrasound exposure and **d)** Rheology of the elastic modulus (G') and viscous modulus (G") of ^{D}FFI hydrogel after ultrasound exposure. The concentration is 30 mM.

3.3.3 Ultrasonic effect on a different peptide sequence and solvent environment

In order to further investigate the effect of ultrasonic waves on self-assembly and aggregation of tripeptides, an alteration on the peptide sequence was introduced. While keeping the same stereochemistry for the N-terminus of the sequence (^{D}F), which gave rise to nanostructure reconfiguration, in the C-terminus isoleucine (I) was replaced by aspartic acid (D). Gelation was not observed for ^{D}FFD in phosphate buffer, most likely due to the hydrophilicity of charged aspartic acid. However, rapid gelation was detected in methanol. Additionally, the L-containing tripeptide (^{L}FFD) appeared to be a transparent solution in both aqueous and organic media (methanol), without any further macroscopic change after ultrasound exposure.

In this case, 10 mg of ^{D}FFD were fully dissolved in 1 ml methanol by heating up to 50 °C. After cooling down to room temperature, a precipitate was observed. TEM images prior to ultrasound exposure showed that the precipitate consists of random, short and curved nanofibres of approximately 50 nm in size (**Figure 3.3a**). Upon ultrasound exposure of the peptide solution for 60 seconds, a gel-phase material may be observed (**Figure 3.3b**). Scanning and transmission electron microscopy (SEM and TEM) showed formation of aligned peptide structures consisting of tube-like nanostructures of approximately 15 nm in diameter that, in turn, organize into bundles of microtubes (approximately 1 μm in diameter) of tens of μm in length (**Figure 3.3c and 3.3d**). Two-photon microscopy of structures labelled with thioflavin T (ThT) (dissolved with ^{D}FFD in methanol) further supported formation of micro-structures in the gel-phase, verifying that structures observed by electron microscopy were not drying induced artefacts during sample preparation (**Figure 3.3e**). Overall, molecular modelling and XRD experiments[108] would be of a great

importance in order to futhermore understand the ultrasonic responsive supramolecular transitions and relate this information with the microscopic findings at the nanoscale. It has been previously demonstrated that hydrogels containing D-stereoisomer (^{D}FFL, ^{D}FFV) in the N-terminus exhibited an extended 3D structure with a molecular length of 19.5 Å.[108]

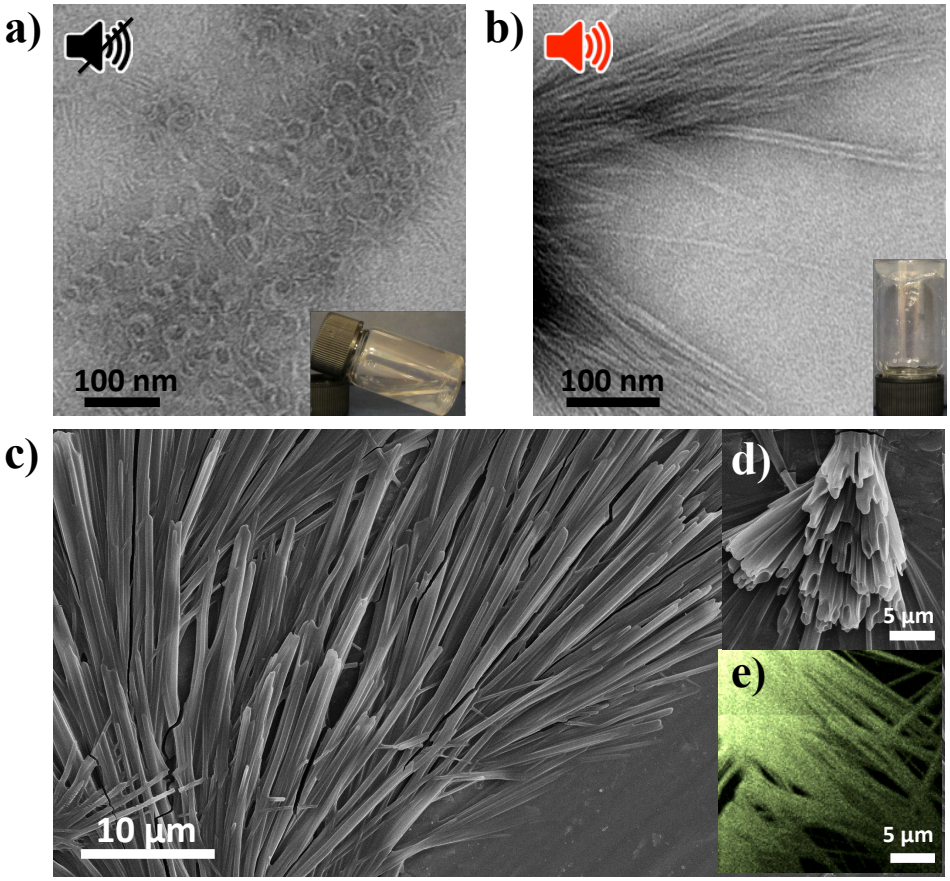

Figure 3.3 TEM images of ^{D}FFD in methanol **a)** before and **b)** after ultrasound exposure, inset photographs are ^{D}FFD forming precipitation or gel without or with ultrasound in methanol, **c, d)** SEM and **e)** Two-photon microscopy images of the ultrasonicated ^{D}FFD peptide gels. The scale bars are **a)** 100 nm, **b)** 100 nm, **c)** 10 µm, **d)** 5 µm and **e)** 5 µm. The concentration is 25 mM.

3.3.4 Ultrasound assisted formation of larger aggregates.

We used nuclear magnetic resonance (NMR) Spectroscopy to obtain insights into the supramolecular transitions induced by ultrasound.[12] As **Figure 3.4a** shows, after exposure of ^{D}FFD to ultrasound, a downfield shift for all the protons of the tripeptide was observed (0.05-0.2 ppm), suggesting change in the chemical environment with enhanced supramolecular interactions. We further investigated these observations using diffusion-ordered spectroscopy (**DOSY**), where the presence and size of aggregates may be determined. The diffusion constant (D) for the Hα protons of the tripeptide (4.55-4.80 ppm) after cooling down to room temperature was found to be around $6x10^{-10}$ m^2s^{-1}. The diffusion constant (D) was decreased ($5x10^{-10}$ m^2s^{-1}), after exposure to ultrasound, suggesting supramolecular reorganization towards formation of larger structures (α) (**Figure 3.4b)**, according to the Stokes-Einstein equation (3.1).

$$D = \frac{KT}{6\pi\eta\alpha} \qquad (3.1)$$

D: Diffussion constant

K: Boltzmann consant

T: Temperature

π: 3.14

η: Viscocity

α: Hydrodynamic radius

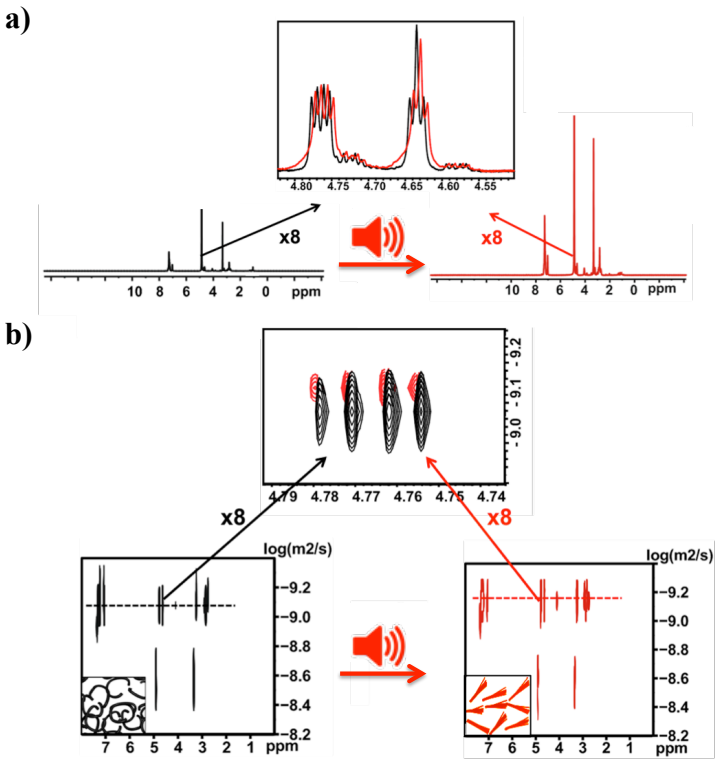

Figure 3.4 a) ^{1}H NMR spectra of ^{D}FFD in deuterated methanol (CD_3OH) prior to (black peaks) and after (red peaks) ultrasound exposure, with the inset spectrum to represent an overlay of the chiral protons (zoomed $x8$). **b)** DOSY NMR spectra of ^{D}FFD in CD_3OH before and after ultrasound exposure with the inset DOSY spectrum to represent an overlay of the chiral protons (zoomed $x8$).

3.3.5 Supramolecular chirality and structural orientation

To gain insights into the chiral organization of the peptide structures and the presence of chirally organized and oriented phenyl moieties of self-assembled structures within the tripeptide before and after ultrasound, Circular (CD) and Linear Dichroism (LD) spectroscopy were used. As **Figure 3.5a** shows, a CD and LD silent spectrum may be observed for ^{D}FFD prior to ultrasound exposure for the precipitate state. Remarkably, sound waves induced supramolecular chirality, by significantly enhancing the peaks at 240 and 270 nm in the organogel, which may be attributed to

the supramolecular organization of chiral centers within π-π stacking of phenylalanines.[52] LD spectra show a minimum at 205 nm and a maximum at 255 nm respectively, which indicates anisotropic arrangement of phenyl moieties in self-assembled structures (**Figure 3.5b**).[108]

Infrared spectroscopy in the amide I region of the spectrum (1600-1700 cm^{-1}) was used to determine the hydrogen bonding networks within the fibrous structures. Spectra of the samples with and without ultrasound exposure are available in **Figure 3.5c**. Prior to ultrasound exposure ^{D}FFD exhibits a weak, broad peak around 1680 cm^{-1}, suggesting the presence of a less hydrogen-bonding pattern. Notably, a strong redshift of the amide absorption around 1650 cm^{-1} was observed upon ultrasound exposure, together with a second peak around 1694 cm^{-1}. These observations suggest a more ordered H-bonding conformation for the amide backbones. **Figure 3.5d** shows the linear viscoelastic responses of the ^{D}FFD organogels. The storage modulus (G') exceeds the loss modulus (G") by factor of 12 demonstrating that the tripeptides formed viscoelastic gels. In both cases of the tripeptide gel formation (^{D}FFI and ^{D}FFD), ultrasonic waves promote a more favourable environment for supramolecular interactions with the solvent, resulting in the formation of highly ordered fibrillar structures in the micrometer range, whereas, prior to ultrasonic exposure precipitate like structures were observed in the nanometer range, arising from a less ordered supramolecular network. This was furthermore demonstrated by investigating the effect of ultrasonic waves on different tripeptide sequences (^{D}FFI and ^{D}FFD) and different solvent environment (phosphate buffer and methanol), resulting in the formation of different macroscopically observed supramolecular states (gelation, precipitation, solution).

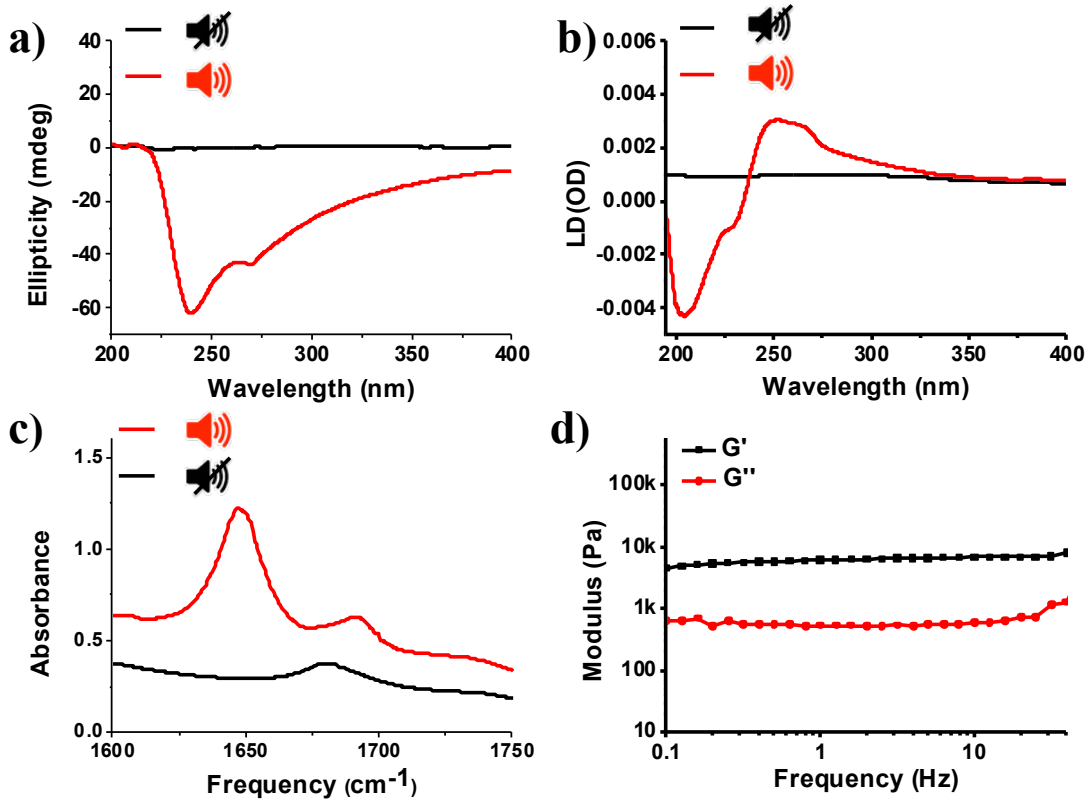

Figure 3.5 a) CD, **b)** LD, **c)** FT-IR spectra of ^{D}FFD in methanol before and after ultrasound exposure and **d)** Rheology of the elastic modulus (G') and viscous modulus (G") of ^{D}FFD organogel after ultrasound irradiation. The concentration is 25 mM.

Following the same experimental procedure as mentioned above, we used a commercially available sonication bath (the frequency is around 40,000 Hz with varied acoustic pressure and amplitude) instead of our ultrasonic setup as a control experiment. **Figure 3.6** shows that ultrasound using a common sonication bath can also trigger the gelation of ^{D}FFD in methanol and ^{D}FFI in buffer solution. However, disordered fibrous structures are observed by SEM, giving insights into the oscillating and directional characteristics of ultrasound, resulting in the formation of highly oriented peptide nanostructures.

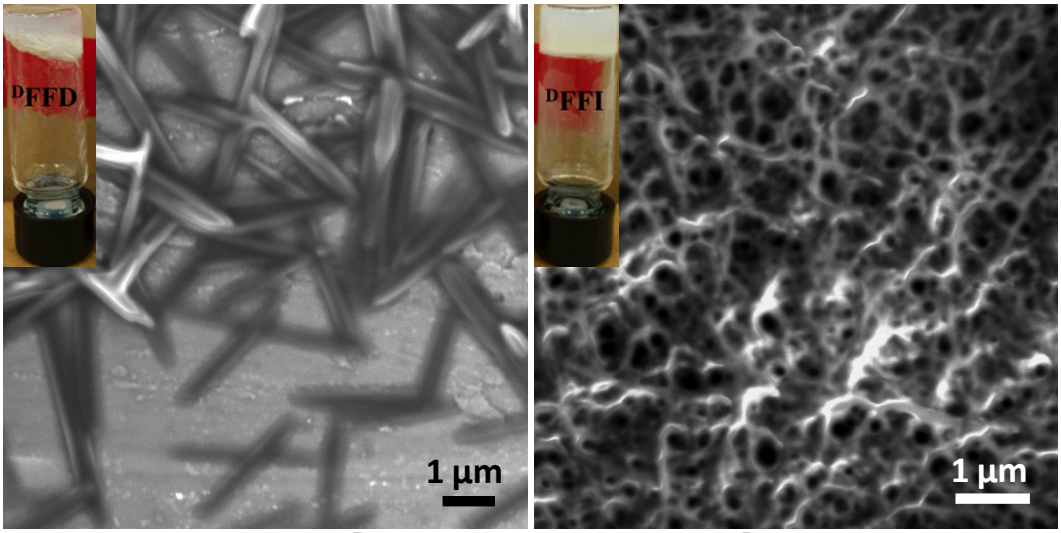

Figure 3.6 SEM images of ^{D}FFD in methanol (left) and ^{D}FFI in phosphate buffer (pH 8) (right) prepared by using commercially available sonication bath. Inset photographs are ^{D}FFD and ^{D}FFI forming gels in methanol and buffer, respectively. The scale bars are 1 µm. The concentrations are 25 and 30 mM, respectively.

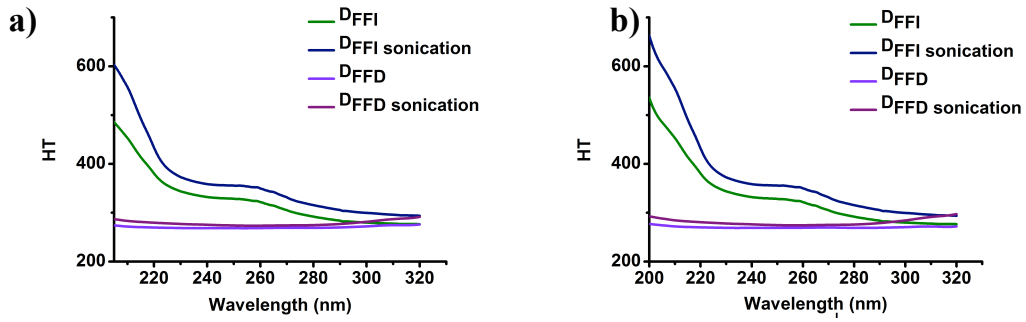

Figure 3.7 HT values of the a) CD and b) LD spectra.

3.4 Conclusion

In conclusion, we demonstrate the use of ultrasonic waves as an *in situ* approach to induce the self-assembly and alignment of tripeptides, forming highly ordered micro-fibrous structures in both organic and aqueous media. Two different peptides were studied, ^{D}FFD and ^{D}FFI with the former forming an anisotropic organogel in methanol, while the latter forms a hydrogel, showing that anisotropic arrangement of supramolecular interactions is highly related to the peptide sequence and solvent environment. These results indicate that the influence of ultrasound transcends the molecular to nano- and micron length scales. The ultrasonic approach may give rise to facilitate amelioration of organization and mechanical properties in supramolecular systems.

4. Transient Supramolecular Reconfiguration of Peptide Nanostructures using Ultrasound*

Objectives

The key research objectives of this chapter are to:

i. Demonstrate the ability of ultrasound to achieve transient changes in materials properties of aromatic peptide amphiphiles.
ii. Investigate the effect of ultrasound on the relative impact of aromatic stacking and H-bonding interactions, by studying two closely related aromatic dipeptide amphiphiles with different electron densities.
iii. Compare acoustic response with thermal heating in transient supramolecular reorganisation.

* This work was highlighted in the inside front cover of Materials Horizons and was published in part as: C. G. Pappas, T. Mutasa, P. W. J. M. Frederix, S. Fleming, S. Bai, S. Debnath, S. M. Kelly, A. Gachagan, and R. V. Ulijn*, Mater. Horiz*., **2015**, 2, 198-202.

C.G.P. and R.V.U. conceived and designed the experiments, analysed the data and wrote the paper. C.G.P. synthesized Fmoc-YL and performed the fluorescence and CD experiments. T.M. and A.C. were responsible for the fabrication of the ultrasonic transducer. P.W.J.M.F. performed the FT-IR experiments. S.F. and S.B. helped with the cartons. S.M.K. helped with the analysis of the CD experiemnts. S.D. helped with imaging.

4.1 Introduction

Molecular self-assembly plays a key role in biological systems and also provides a versatile approach for materials fabrication.[15-18] Molecular self-assembly can be controlled using a variety of stimuli including chemical[11,112] and mechanical triggers.[75,81] By definition, self-assembly systems operate in the direction that lowers their free energy. Non-equilibrium, transient nanostructures, that only exist away from thermodynamic equilibrium are increasingly of interest. Such systems require energy input to maintain a certain assembled state, which relaxes back to the initial state when energy supply is run out.[77,78] (Ultra-) sound, i.e., oscillating pressure waves of varying frequency provides substantial and largely unexplored opportunities to provide mechanical energy to direct transient nanostructure formation.

The ability of pressure waves to overcome energy barriers is well known - e.g., to dissolve molecules or disperse particles by disrupting (non-specific) intermolecular interactions. For example, using low frequencies (manual shaking at approximately 2 Hz) may result in reversible sol-gel transitions.[113] Audible sound frequencies (<1,000 Hz) have been used to trigger anisotropy changes (fibre alignment).[60] Ultrasound (>20,000 Hz) may also be used to control self-assembly and gelation processes, resulting in dramatic changes in nanoscale morphology and material properties.[8] Recently, reversible sol-gel transitions using sonication of supramolecular metallopolymers was reported (see Section **2.3**).[114]

Peptides are versatile building blocks in molecular self-assembly[115-117] with recent reports revealing that ultrasound energy may be used to trigger supramolecular transitions, resulting from changes in supramolecular interactions. Mostly these

studies used organic solvents,[55-57] with some reports using aqueous media.[103] Yokoi *et al.* reported the dynamic (re)-assembly of a 16 amino-acid residue peptide in water using sonication. They demonstrated that upon sonication the peptide nanostructure broke up into smaller fragments that recombine into nanofibers when sonication is switched off.[118] Very recently, non-equilibrium dynamic simulations were used to investigate the effect of ultrasonic cavitation on amyloid fibre nucleation and disruption.[119]

Clearly, ultrasound may be used to influence nanostructure assembly and dis-assembly mechanisms. Herein, we investigate whether sound waves may be used to trigger temporary supramolecular reconfiguration, and consequently change nanostructure morphology, which will relax back to thermodynamic equilibrium when sound is switched off. We use aromatic peptide amphiphiles as model systems.[25] These systems assemble as a result of a combination of aromatic stacking interactions and H-bonding, the balance between these two components has a dramatic impact on the nanoscale morphology observed. H-bonding and aromatic stacking/hydrophobic interactions have different thermal dependencies and therefore it seems reasonable that ultrasound - as a directional means to supply heat - may influence their reorganization.

The objectives of this study are therefore (i) to demonstrate the ability of ultrasound to achieve transient changes in materials' properties of aromatic peptide amphiphiles (schematically shown in **Scheme 4.1a**,**b**); (ii) to investigate the effect of ultrasound on the relative impact of aromatic stacking and H-bonding interactions, by studying two closely related aromatic dipeptide amphiphiles with different electron densities;

(iii) to compare acoustic response with thermal heating in transient supramolecular reorganisation.

In our system, an ultrasonic transducer provides high-energy frequencies (80,000 Hz) of precisely defined wavelength and amplitude. The acoustic pressure was measured to be in a range of 0-120 KPa for 0-100mV amplitude values. In this work, an acoustic pressure of 120 kPa was constantly used.

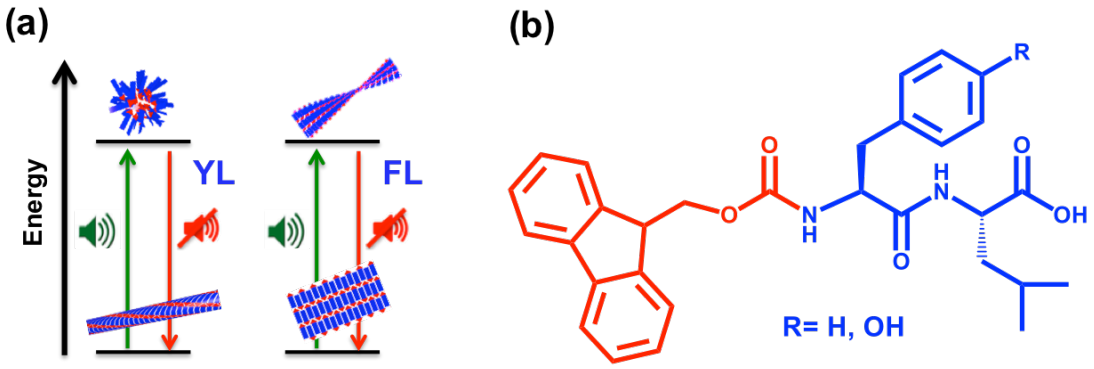

Scheme 4.1 (a) Energy diagram of supramolecular transitions induced by ultrasound, highlighting temporary transition from fibres or tapes to spherical aggregates and twisted fibres respectively and **(b)** Chemical structures of aromatic dipeptide amphiphiles used in this Chapter (Fmoc-FL, R=H and Fmoc-YL, R=OH).

4.2 Materials and Methods

Fmoc-Tyrosine, Leu-Otbu HCl, Diisopropylethylamine (DIPEA) (>99.5%) were purchased from Sigma-Aldrich and used as received. 2-(1H-Benzotriazole-1-yl)-1,1,4,4-tetramethyluronium hexafluorophosphate (HBTU) was purchased from Novabiochem. All other reagents and materials from commercial sources were used without further purification. Silica gel used in chromatographic separations was obtained VWR (Silica Gel, ultrapure, 40-60 mm).

4.2.1 Synthesis of Fmoc-Tyr-Leu-OH (Fmoc-YL)

Fmoc-Tyr-OH, H-Leu-OtBu.HCl and HBTU were dissolved in anhydrous dimethylformamide (~15 ml) and DIPEA (2 ml) was added. The reaction mixture was left to stir for 24 hours. Product was precipitated out by addition of saturated sodium bicarbonate solution (~40 mL) and extracted into ethyl acetate (~50 mL). The mixture was washed with equal volumes of saturated brine, 1M hydrochloric acid and brine again. The resulting organic layer was dried by anhydrous magnesium sulphate and the ethyl acetate was removed by evaporation *in vacuo*. The resulting solid was then purified by column chromatography using 2.5 % methanol in dichloromethane as eluent. Fractions were tested by TLC using UV (254 nm) light to visualise spots. Fractions containing the compound were combined and solvent removed *in vacuo*. The removal of the t-Bu group was carried out by dissolving the sample in dichloromethane and adding 10 mL of trifluoroacetic acid. The reaction mixture was stirred for four hours. The dichloromethane was removed by evaporation *in vacuo*. The TFA was removed with the addition of toluene (~10 mL) and solvent removed by evaporation *in vacuo* (carried out in triplicate). The resulting solid was washed 6 times with cold diethyl ether and the product dried under

vacuum. The final Fmoc-protected dipeptide was identified using ^{1}H NMR and Mass Spectroscopy.

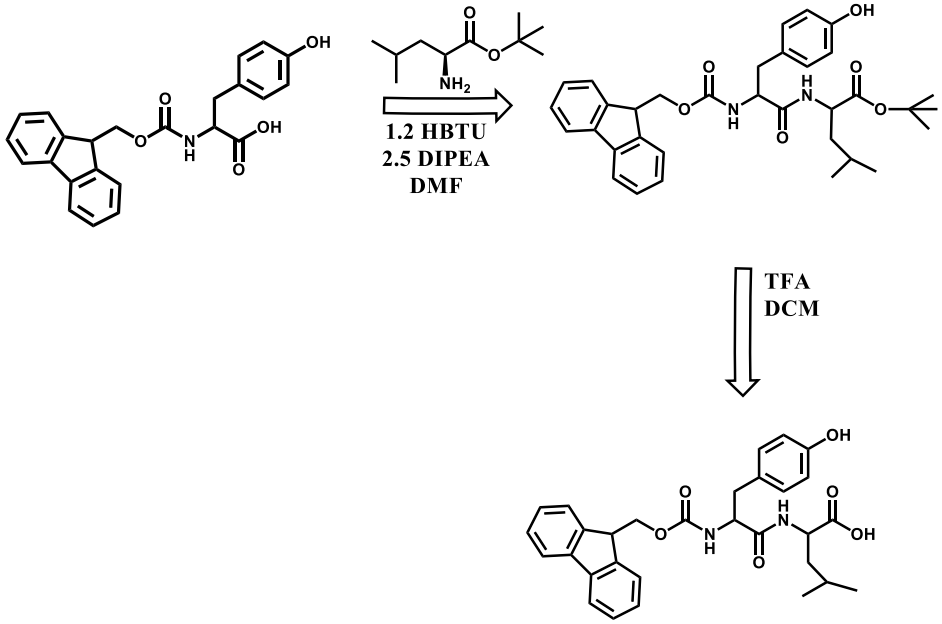

Strategy for the synthesis of Fmoc-YL

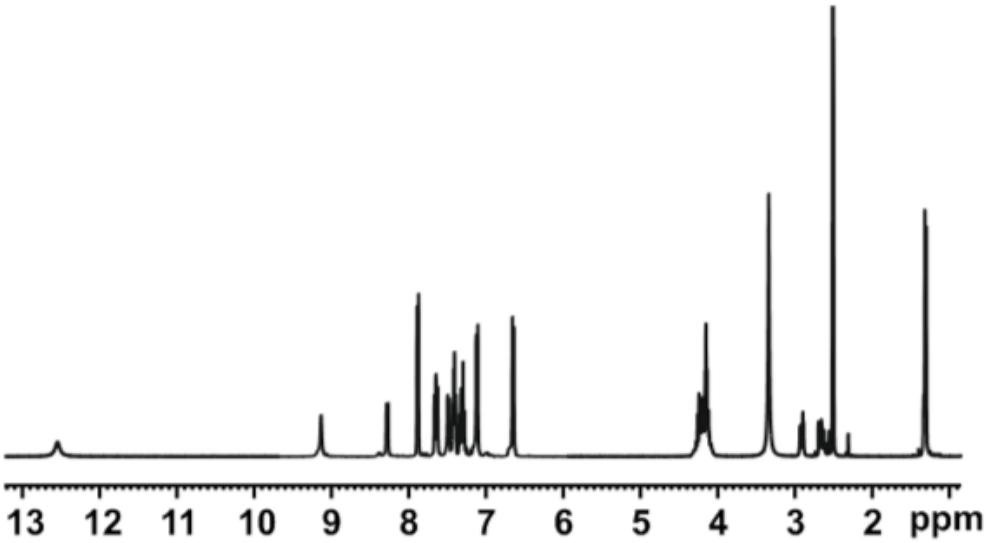

^{1}H NMR spectra of Fmoc-YL in dmso-d_6 at 298K.

Purity by HPLC (400 nm) = 97.00 % ^{1}H NMR spectrum of Fmoc-YL in DMSO-d_6 at 298K: 12.6 (1H, s, OH), 9.2 (1H, s, Tyr OH), 8.44 – 8.42 (1H, NH d, J = 8 Hz), 7.89 – 7.87 (2H, d, J = 7.5 Hz, 2 fluorenyl Ar-CH), 7.66 – 7.62 (2H, m, 2 fluorenyl Ar-CH), 7.55 – 7.54 (1H, d, J = 9 Hz, NH), 7.44 – 7.49 (2H, m, 2 fluorenyl Ar-CH), 7.44 – 7.27 (2H, m, 2 fluorenyl Ar-CH), 7.10 – 7.09 (2H, d, j = 8.4 Hz, 2 Tyr Ar-CH), 6.64 – 6.62 (2H, d, J = 8.45 Hz, 2 Tyr Ar-CH), 4.25 – 4.10 (5H, m, fluorenyl CH, fluorenyl CH_2 and CαH), 2.92 – 2.91 (1H, m, Tyr CH), 2.74 – 2.71 (1H, m, Tyr CH), 1.68 -1.62 (1H, m, Leu CH) 1.55-1.52 (2H, m Leu CH_2), 0.9-0.84 (6H, m Leu $2CH_4$) MS (ES+): m/z 517.2

Fmoc-Phe-Leu (Fmoc-FL) was purchased and used without any further purification from CS Bio Co (code: CS4005). Purity (214 nm) 97%. The Fmoc-dipeptide was used as the TFA salt.

4.2.2 Ultrasonic Setup

For the ultrasonic set up see Section **3.2.2**.

4.2.3 Hydrogel formation

20 mM of Fmoc-YL was dissolved in 1 ml of 100 mM sodium phosphate buffer pH 8. Then the Fmoc-dipeptide was heated up to 363K for two minutes until it fully dissolved. A translucent gel like material was obtained after 20 minutes as evidenced by vial inversion. The concentration used for Fmoc-FL was 20 mM at pH 6. An opaque gel like material was obtained after 5 minutes. The ultrasound exposure for both the Fmoc-dipeptides was 5 minutes.

4.2.4 Fluorescence Spectroscopy

Fluorescence emission spectra were measured on a Jasco FP-6500 spectrofluorometer with light measured orthogonally to the excitation light, at a

scanning speed of 500 nm min^{-1}. For both the aromatic dipeptide amphiphiles the concentration was 20 mM. The excitation wavelength was 280 nm, and emission data were recorded in the range between 300 and 600 nm. The spectra were measured with a bandwidth of 4 nm with a medium response and a 3 nm data pitch.

4.2.5 Circular Dichroism (CD)

For CD experiments see Section **3.2.8**.

4.2.6 FTIR spectroscopy

For FTIR experiments see Section **3.2.9**.

4.2.7 TEM Microscopy

For TEM experiments see Section **3.2.4**.

4.4 Results and Discussion

4.4.1 Selection of the dipeptides

Two aromatic dipeptide amphiphiles with different sequences (fluorenyl-methoxycarbonyl-phenylalanine-leucine, Fmoc-FL and the equivalent tyrosine derivative, Fmoc-YL, **Scheme 4.1b**) were used. These are well suited for the current study because Fmoc-FL/-YL are clearly similar in structure, but have different electron density on the aromatic side chain residue (phenyl/phenol), giving rise to an altered relative contribution of aromatic and hydrogen bonding type interactions (see **Chapter 5**).[36] The resulting changes in supramolecular interactions upon thermal heating were investigated using temperature dependent ^{1}H NMR Spectroscopy. NMR in the aromatic region shows increase in the multiplicity for Fmoc-YL upon thermal heating, with peaks become cleared and sharper (solution state) compared to room temperature (gel state, broader peaks), indicating increased disorder at 338K (**Figure 4.1a)**. By contrast, for Fmoc-FL the peaks become broader upon increasing temperature (gel state), suggesting increased order and stronger supramolecular interactions (**Figure 4.1b**). Thus, fluorophores are overlapping in a more ordered environment upon heating for Fmoc-FL, resulting in retention of gel state, in line with previous observations for other aromatic dipeptide amphiphiles, Fmoc-FG[120] and Fmoc-LG.[121] By contrast, heating disrupts aromatic interactions for Fmoc-YL, resulting in gel dissolution. These observations show that upon altering the electron density of the aromatic side chain residue (in this case, replacing phenyl by phenol in F and Y) the relative contribution of aromatic and hydrogen bonding type interactions, and therefore the thermal effects on molecular self-assembly can be regulated. Temperature dependent solid-state multidimensional NMR experiments would be of a great importance in orde to investigate supramolecular interactions.

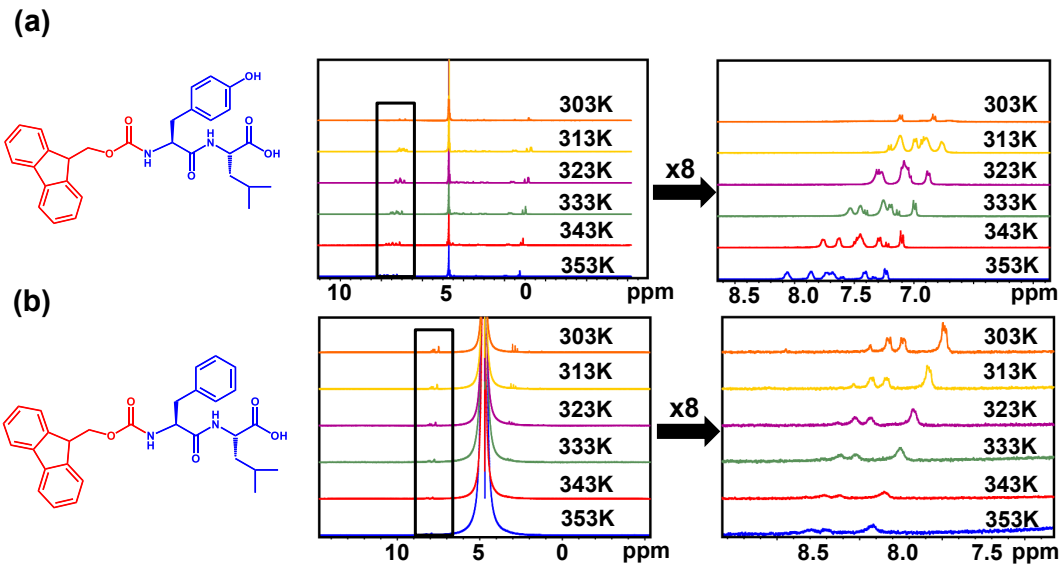

Figure 4.1 (**a**) Temperature dependent ^{1}H NMR spectra of 20 mM of Fmoc-YL in D_2O pH 8 from 303-353K and (**b**) Fmoc-FL in D_2O pH 6 highlighting their differential aggregation behaviour upon heating. Full spectra on the left side show a water peak at 4.7 ppm just adjacent to the aromatic region. A zoomed in (8 times) image of the aromatic region is shown on the right.

4.4.2 Acoustic and thermal behaviour of the sound responsive systems

For the ultrasound experiments, 20 mmol of Fmoc-YL was dissolved in 1 ml sodium phosphate buffer (100 mM) pH 8 and heated up to 363K for two minutes until fully dissolved. The sample was then left to cool to room temperature for 20 minutes. A translucent gel was obtained as evidenced by vial inversion and visual inspection. The Fmoc-dipeptide was then exposed to ultrasound during five minutes. Gradually, the gel converted to a solution and when the ultrasound was switched off, the gel reformed after 10 minutes. We noticed that during ultrasonication the temperature of water in the glass beaker rose to 320K, which is considerably below the melting temperature of the gel (338K), as discussed in more details below. For Fmoc-FL 20 mmol was dissolved in 1 ml sodium phosphate buffer (100 mM) pH 6. An opaque gel was observed after 10 minutes at this pH, while a viscous suspension was

observed at pH 8. In this case, ultrasound exposure during five minutes did not reveal noticeable macroscopic difference as the Fmoc-dipeptide was maintained in the gel phase. Therefore, macroscopically the effect of ultrasound is qualitatively comparable to that of heating for both peptides.

In order to acquire insights into the supramolecular transitions induced by ultrasound we firstly used fluorescence spectroscopy, focusing on the hydrophobic-stacking interactions among the fluorenyl moieties.[122] Specifically, for Fmoc-YL in the (pre-sonication) gel state, two characteristic peaks were observed, a narrow band at 331 nm corresponds to the monomeric state and a broad red shifted band at 420-450 nm. After exposure to ultrasound (five minutes) and immediate transfer to the fluorimeter (<5 sec), a 7 nm blue shift is observed for the main peak at 331 nm. This result demonstrates that there is a disruption of the stacking interactions during sonication. After 10 minutes in the absence of sonication, the emission intensity at 331 nm reverts back to the initial value (**Figure 4.2a**), suggesting stacking interactions among the aromatics are reformed (**Figure 4.2b**). In the case of Fmoc-FL a peak appears at 348 nm, while the excimer peak covers the region from 415-450 nm. After ultrasound exposure during five minutes, a red shift is observed and a significant quenching of the emission for the peak at 348 nm, providing an indication that sound waves promote formation of extended stacking interactions among the fluorenyl moieties, that can be interpreted as a more ordered supramolecular structure. **Figure 4.2c** highlights the fluorescence response of the monomeric peak upon exposure to ultrasound, with Fmoc-YL showing increased emission (unquenching), and Fmoc-FL showing enhanced quenching. The effects are reversed as sound is switched off.

To establish whether the observed effects can also be obtained by thermal heating, we compared the results with those obtained by thermal heating to the same temperature. Short exposure times of five minutes gave rise to heating of the sample from 298 to 320K. While ultrasound induced a significant emission enhancement for the main peak at 331 nm, temperature dependent fluorescence experiments revealed quenching at the same temperature (320K) and no blue-shifted structure was observed for Fmoc-YL. Temperature dependent fluorescence experiments for Fmoc-FL revealed that the emission at 348 nm also decreased but to a smaller extent (**Figure 4.2d**). Clearly, the observed effects on supramolecular structures for ultrasound are different from those achieved using thermal heating.

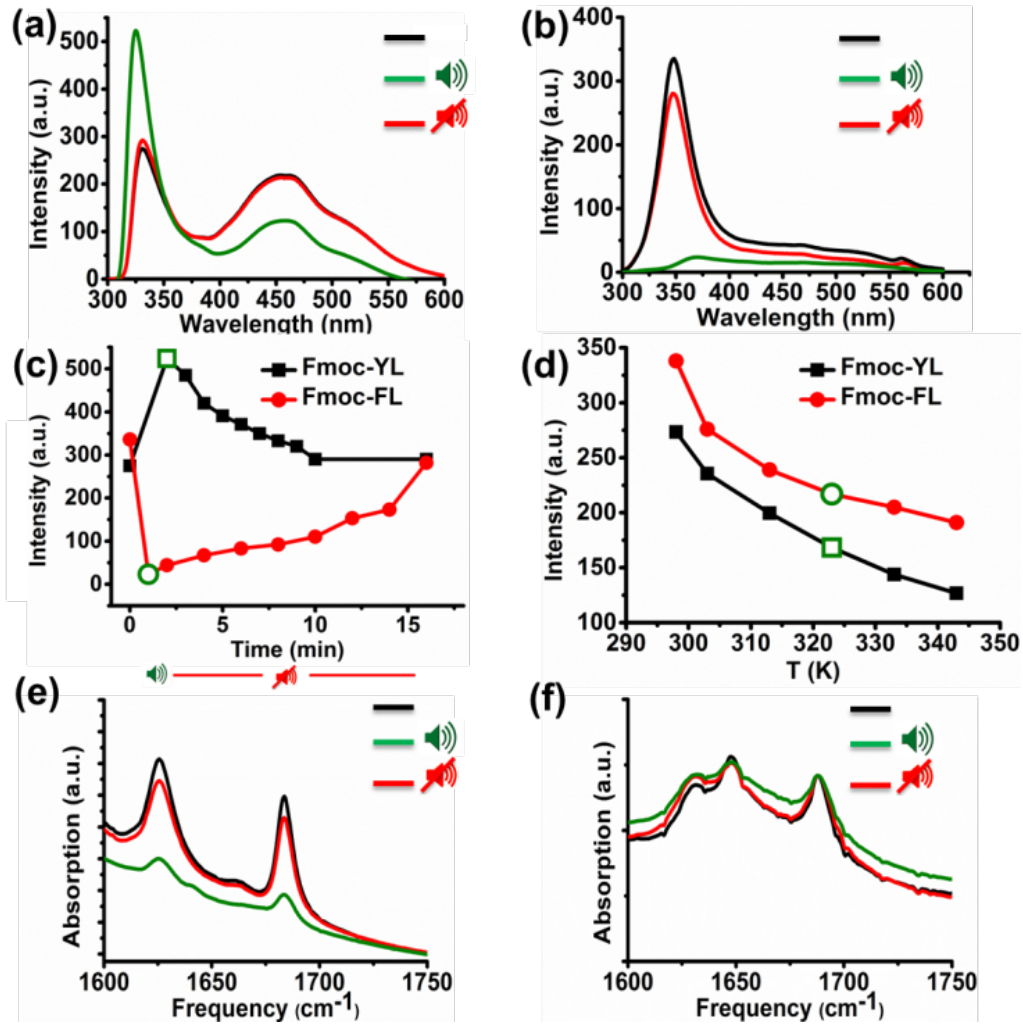

Figure 4.2 Fluorescence emission spectra (excitation at 280 nm) of (**a**) 20 mM Fmoc-YL in phosphate buffer pH 8 and (**b**) 20 mM of Fmoc-FL in phosphate buffer pH 6 before, after 5 minutes ultrasound exposure and when the sound is switched off, (**c**) Plot of the fluorescence intensity of on/off ultrasound experiments (323-331 nm for Fmoc-YL) and (348-360 nm for Fmoc-FL). Green symbols indicate values immediately after sound exposure, (**d**) Plot of fluorescence intensity for Fmoc-YL and Fmoc-FL (monomeric state) respectively upon thermal heating from 298-350K. Green symbol represent the temperature observed upon sonication, for comparison and FT-IR of (**e**) Fmoc-YL in D_2O pH 8 and (**f**) Fmoc-FL pH 6 before, after 5 minutes ultrasound exposure and when the sound is switched off.

Next, we investigated ultrasound-induced changes in hydrogen bonding type interactions *via* the amide groups of the backbone. Analysis by Fourier transform infrared spectroscopy (FT-IR) in D_2O of 20 mM of Fmoc-YL pH 8 prior to ultrasound exposure revealed two characteristic peaks in the amide I region. The peak at 1624 cm^{-1} shows formation of H-bonded type interactions via amide, while 1682 cm^{-1} corresponds to the stacked carbamate.[110] After ultrasound exposure during five minutes, both of the peaks transiently showed a reduction in intensity, indicating that ultrasound energy disrupts the H-bonds. When the ultrasound was switched off, there is reappearance of the H-bonding network and the intensity of the β-sheet like peak was close to the initial values (**Figure 4.2e**). FT-IR spectra of 20 mM of Fmoc-FL in D_2O pH 6 prior to sonication revealed 3 characteristic peaks. Peaks at 1624 cm^{-1} and 1682 cm^{-1} as previously observed for Fmoc-YL, but also one peak at 1648 cm^{-1} suggesting a less ordered hydrogen-bonding conformation for the peptide backbones.[12] Notably, sound exposure for five minutes in this case did not have a dramatic impact on H-bonding interactions (**Figure 4.2f**).

Notably, when the ultrasound was switched off, the transitions were fully reversible, reverting back to the initial supramolecular organisation prior to ultrasonication. This was further investigated using fluorescence spectroscopy showing that the emission reverts back to the initial level (**Figure 4.3**).

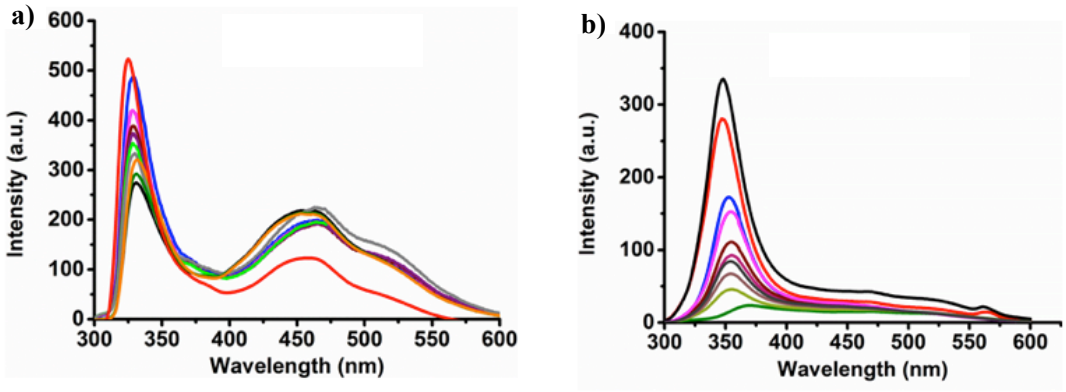

Figure 4.3 (a) Fluorescence emission spectrum of 20 mM of Fmoc-YL pH 8 before ultrasound exposure (black line), after 5 minutes ultrasound exposure (red line) and when the ultrasound is off (spectra recorded every minute after switching the sound off), (**b)** Fluorescence emission spectra of 20 mM of Fmoc-FL pH 6 before ultrasound exposure (black line), after 5 minutes ultrasound exposure (green line) and when the ultrasound is off (spectra recorded every two minutes after switching the sound off).

4.4.3 Transient ultrasonic effect on supramolecular chirality

Having established the relative importance of aromatic interactions (enhanced in Fmoc-FL, reduced in Fmoc-YL) and hydrogen bonding (reduced in Fmoc-YL) we used Circular Dichroism spectroscopy (CD) to investigate the ultrasound effect on the chiral organization of the supramolecular self-assembly. On self-assembly of aromatic dipeptide amphiphiles, CD signals derive from the supramolecular chirality, induced by the stacking of chromophores rather than the molecular chirality of the chromophores themselves.[73] For Fmoc-YL, a negative signal was observed for the Fmoc peak (304 nm). After ultrasound exposure for five minutes no CD signal was observed as previously observed for micellar aggregates.[123] The chiral organization was restored when the ultrasound was switched off (**Figure 4.4a**). For Fmoc-FL initially a weak negative peak was observed at 307 nm. After 5 minutes ultrasound

exposure a stronger negative peak was noticed, indicating that supramolecular chirality can be induced by ultrasound. The temporary enhanced CD signal of the supramolecular organization was reduced when the sound was switched off (**Figure 4.4b**). Temperature dependent CD experiments for both of the aromatic dipeptide amphiphiles show that similar disruption or enhancement of the chirality can be achieved thermally, but at significantly higher temperatures (**Figure 4.5a,b**).

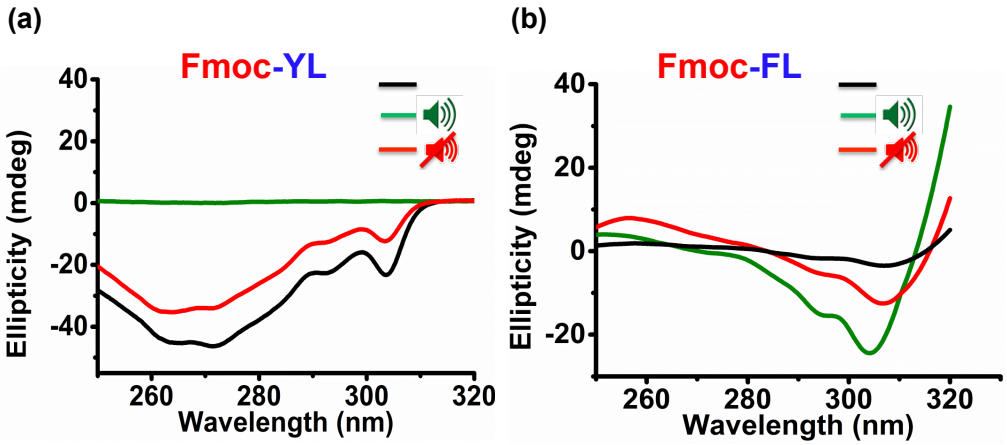

Figure 4.4 Circular dichroism spectra of (**a**) 20 mM Fmoc-YL in phosphate buffer pH 8 and (**b**) 20 mM of Fmoc-FL in phosphate buffer pH 6 before, after 5 minutes ultrasound exposure and when the sound is switched off after 10 minutes for Fmoc-YL and 16 minutes for Fmoc-FL.

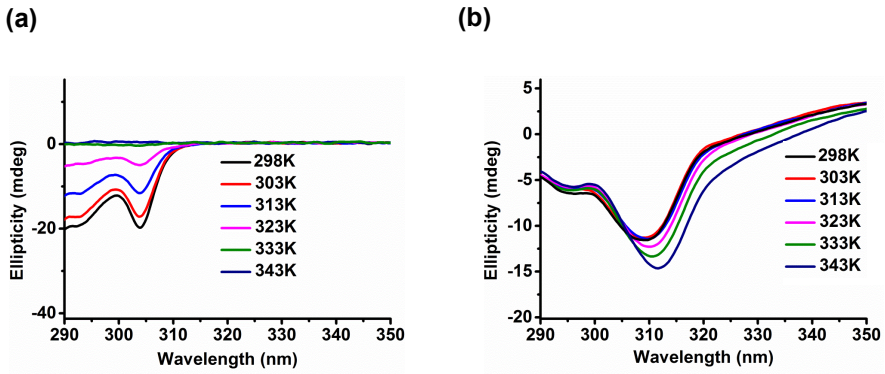

Figure 4.5 Temperature dependent CD spectra of 20 mM of (**a**) Fmoc-YL pH 8 from 298-343K and (**b**) 20 mM of Fmoc-FL pH 6 from 298-343K.

4.4.4 Microscopic visualization of sound induced transient supramolecular reconfiguration

The ultrasound induced transient supramolecular reconfiguration was further investigated by TEM (Transmission Electron Microscopy). As reported previously, Fmoc-YL assembled into fibers (gel, pre-sonicated state) of approximately 10 μm in length (**Figure 4.6a**).[73] Upon ultrasound exposure during five minutes, where an increase in temperature was observed, the mechanical energy gave rise to a transient fibrillar disruption, showing the formation of spherical aggregates of approximately 400 nm hydrodynamic radius (solution state) (**Figure 4.6b**). For the ultrasonic experiments three drops of the solution was drop casted immediately onto the carbon-coated copper grid and allowed to dry for few minutes at RT before imaging. When the ultrasound was switched off, accompanied with a decrease of temperature (room temperature) the Fmoc-YL reassembled into a fibrillar network (reformation of the gel state), similar in size with the presonicated state (**Figure 4.6c**). The results appear to be in agreement with a reconfiguration schematically shown in **Scheme 4.1a**: ultrasound exposure results in disruption of the H-bonded chiral nanofiber structure to form achiral spherical aggregates. In the case of Fmoc-FL prior to ultrasonication, tape-like structures were observed of approximately 5 μm in length (**Figure 4.6d**). After 5 minutes of ultrasound exposure the Fmoc-dipeptide adopted a twisted fibrillar architecture (**Figure 4.6e**), where an enhancement of the solubility of the sample was also observed. When the ultrasound was switched off the initial organization state was reformed (**Figure 4.6f**). In this case the dominance of the directional aromatic stacking interactions retains fibrillar morphology, with the reduced H-bonding upon sonication favoring a more twisted orientation. The same

temporary supramolecular reconfiguration may be achieved by a second ultrasonication cycle for both of the aromatic dipeptide amphiphiles (**Figure 4.7a-d**).

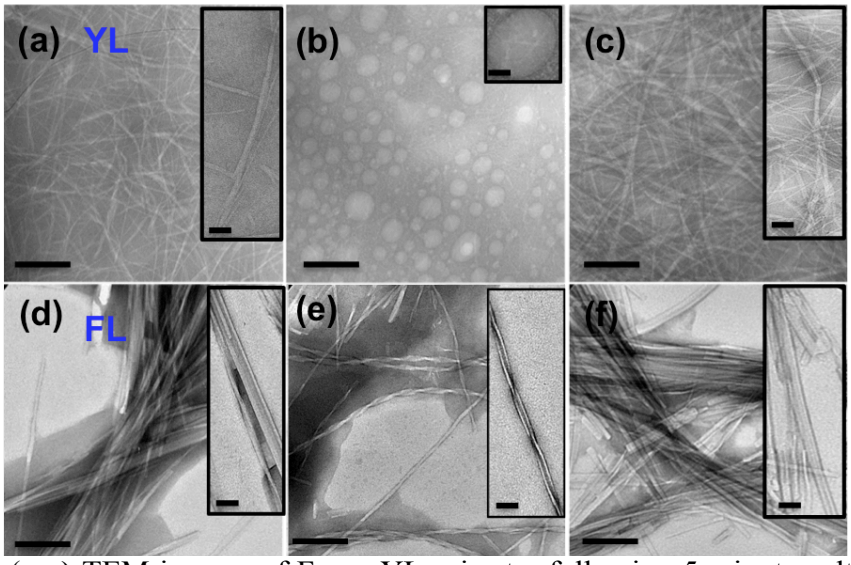

Figure 4.6 (**a-c)** TEM images of Fmoc-YL prior to, following 5 minutes ultrasound exposure and when the ultrasound is off and (**d-h)** TEM images of Fmoc-FL prior to, following five minutes ultrasound exposure and when the ultrasound is off. Scale bar 200 nm. Inset images represent single fibrillar, spherical and tape like structures.

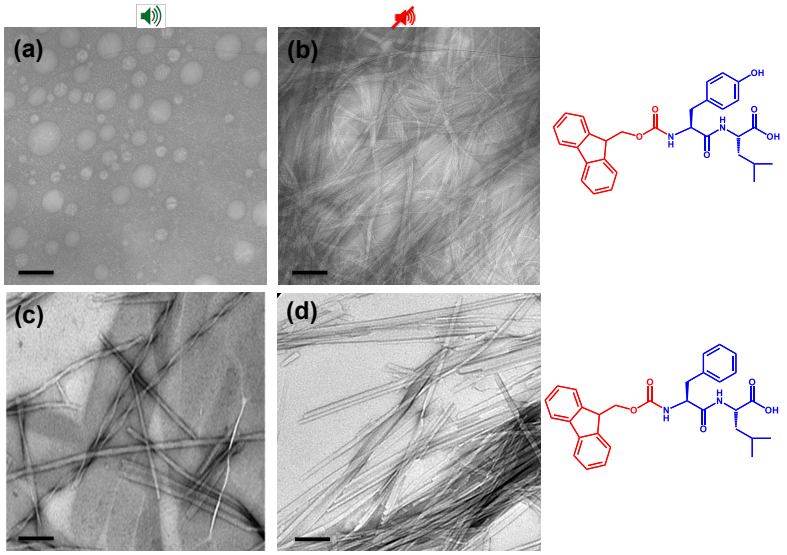

Figure 4.7 TEM images of a second sonication cycle after 5 minutes ultrasound exposure and when the sound is off for Fmoc-YL (**a-b)** and for Fmoc-FL (**c-d)** respectively.

4.5 Conclusion

In summary, we have demonstrated that in aqueous buffer solution ultrasound energy may have a temporary effect on supramolecular self-assembly of aromatic dipeptide amphiphiles, showing supramolecular reconfiguration from tapes to coiled fibers (Fmoc-FL) and straight fibers to spherical aggregates (Fmoc-YL) respectively, reverting back to the initial organization state as the sound is switched off. In the case of Fmoc-YL ultrasound energy disrupts the fibrillar network, giving rise to the formation of spherical aggregates, where the Fmoc-dipeptide adopted a less ordered organized structure accompanied with a reduction of fluorenyl order and H-bonding. For Fmoc-FL, sound waves enhance the stacking interactions among the fluorophores, while having a less effect on hydrogen bonding interactions. The work shows that ultrasound energy may be used to temporarily modulate the interplay between hydrophobic/H-bonding interactions. These insights provide a step towards a rational use of ultrasound to fuel transient, energy dissipating supramolecular systems. For future work, time dependent rheological experiments prior to and after ultrasonic exposure, will be important in order to furthermore investigate how the mechanical properties of the hydrogels changing upon ultrasound exposure in order to furthermore validate the spectroscopic and microscopic findings.

5. Tuneable Fmoc-Phe(4-X)-Phe-NH_2 nanostructures by variable electronic substitution*

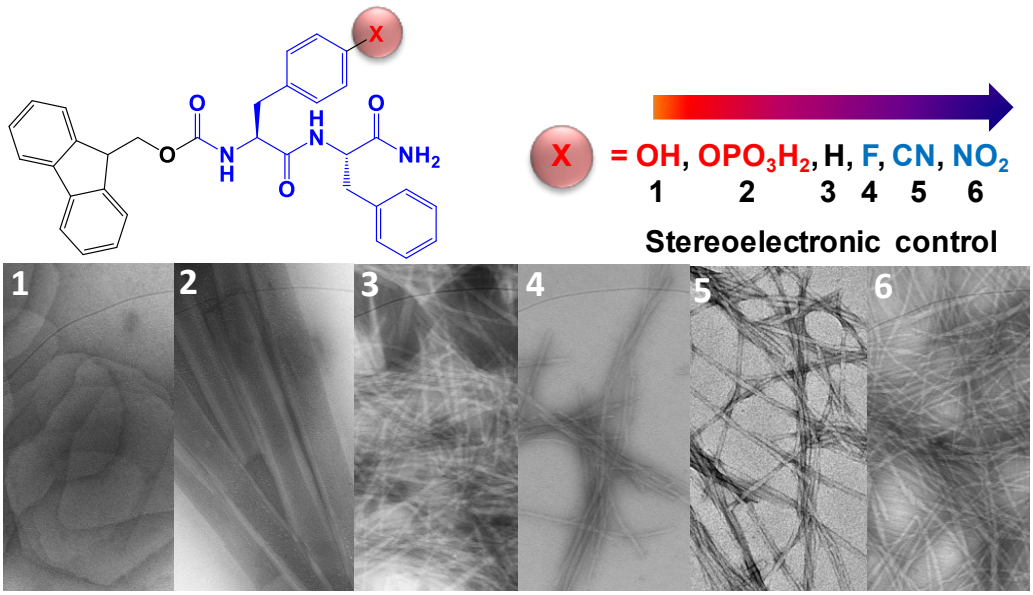

Objectives

The key research objectives of this chapter are to:

i. Demonstrate the effect of electronic substitution on the interplay of aromatic stacking and H-bonding type interactions, which drive the self-assembly of aromatic dipeptide amphiphiles.

ii. Investigate the effect of electronic substitution on morphological control of supramolecular nanostructures.

iii. Investigate the enzyme activity on non-natural amino acids containing electron-donating or -withdrawing groups on the *para* position of phenylalanine amino acid residue.

* This work was published in part as: C. G. Pappas, Y. M. Abul-Haija, A. Flack, P. W. J. M. Frederix and R. V. Ulijn *Chem. Commun*., **2014**, 73, 10630-10633.

C.G.P., Y.M.A. and R.V.U. conceived, designed the experiments, analysed the data and wrote the paper. P.W.J.M.F. performed the FT-IR experiments. A.F. helped with the preparation of the samples.

5.1 Introduction

Supramolecular self-assembly provides a route to fabrication of nanomaterials potentially useful in both high-tech and every-day life applications.[15,124-126] Peptide-based materials are of particular interest due to chemical diversity, biocompatibility and ease of synthesis.[127] In particular, aromatic peptide amphiphiles, short peptides appended with aromatic ligands, are of interest due to its ability to self-assemble to a remarkable range of nanostructures with minimal molecular complexity[128] (see Section **2.2.1**)

Biocatalysis is increasingly used for the *in situ* regulation of materials properties.[129-133] Proteases (and more recently lipases)[134] provide a route for *in situ* formation of peptide nanostructures from amino acid precursors, by fully reversible condensation reactions[62] which are driven by the energy contributions of molecular self-assembly, thereby overcoming the preference for hydrolysis rather than condensation in aqueous media. This approach avoids the formation of kinetic aggregates in favour of thermodynamically preferred structures, thus allowing for reproducible self-assembly of hydrophobic peptide derivatives.[67] Because these reactions operate under thermodynamic control, the approach allows for direct correlation of condensation yield with thermodynamic stability of peptide structure formed, as previously shown in dynamic combinatorial libraries[135] (see Section **2.4.1**).

It is clear that there are options for controlling the morphology of self-assembling peptide nanostructures. There are two main approaches to achieve control over morphology, either by changing the self-assembly pathway (kinetic control[73,136]) or by changing the peptide sequence.[38] The self-assembly of these structures is dictated both by H-bonding interactions and aromatic stacking contributions[25,137] and it

appears that the relative contributions of each of these can control nanoscale morphology. Indeed, systematic variation of the side chain of amino acids has a remarkable effect on the resultant structures (spheres, tubes, fibres, tapes and sheets).[37]

Nilsson's group recognised that the relative contributions of aromatic stacking interactions may be manipulated by using substituents on aromatic (Phe) side chains. Indeed, they demonstrated that atomic substitution on amino acid side chains have a significant effect on self-assembly and subsequent hydrogelation.[138,139] Gazit and Reches studied the effect of diphenylalanine modification on self-assembled nanostructures diluted from organic solvents.[140] Changing the electronic properties of benzyl group on Fmoc protected phenylalanine (Fmoc-Phe) with different halogens (F, Cl, Br) and at different positions (*ortho*, *meta*, *para*) could control the rate of self-assembly and mechanical properties of the gels formed.[139] Electronic modification on phenylalanine containing peptides has also been used to study peptide/carbon nanotubes interactions[141] and to investigate the effect of aromatic interactions on the formation of amyloid-like structures.[142]

In this work we study electronic modification *via* atomic substitution and combine this with enzymatic self-assembly under thermodynamic control to allow for direct comparison of structures formed. Specifically, we investigate (i) the effect of electronic substitution on the interplay of aromatic stacking and H-bonding (ii) the ability to exploit effects of electronic substitution for morphological control of supramolecular nanostructures.

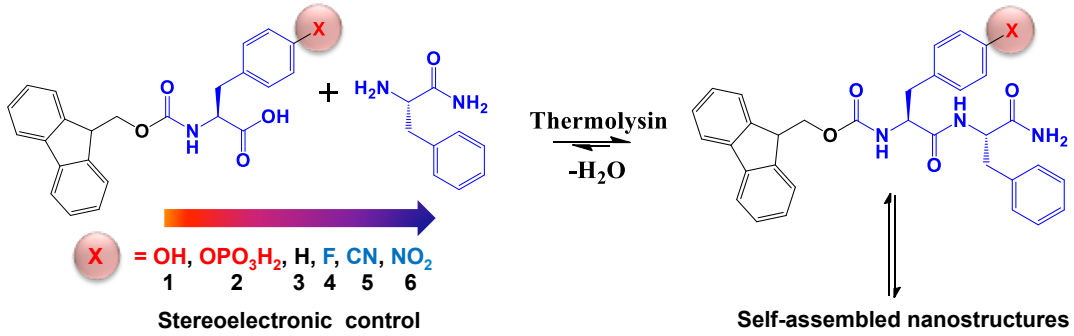

Scheme 5.1 Thermolysin catalyzed amide bond formation of Fmoc-dipeptide derivatives containing groups with different electronic density.

5.2 Materials and Methods

All compounds were purchased from Sigma Aldrich UK.

5.2.1 Transition electron microscopy (TEM)

Carbon-coated copper grids (200 mesh) were glow discharged in air for 30 s. The support film was touched onto the gel surface for 3 s and blotted down using filter paper. Negative stain (20 ml, 1% aqueous methylamine vanadate obtained from Nanovan; Nanoprobes) was applied and the mixture blotted again using filter paper to remove excess. The dried specimens were then imaged using a LEO 912 energy filtering transmission electron microscope operating at 120kV fitted with 14 bit/2 K Proscan CCD camera.

5.2.2 Fluorescence spectroscopy

Fluorescence emission spectra were measured on a Jasco FP-6500 spectrofluorometer at a scanning speed of 200 $nm.min^{-1}$. The emission spectra were recorded between 300 and 600 nm resulting from excitation at 280 nm, using a bandwidth of 3 nm with a medium response and a 1 nm data pitch.

5.2.3 FTIR spectroscopy

For FTIR experiments see Section **3.2.9**.

5.2.4 High-performance liquid chromatography (HPLC)

A Dionex P680 high-performance liquid chromatography pump was used to quantify conversions of the enzymatic reaction. A 20µl sample was injected onto a Macherey-Nagel C18 column with a length of 250 mm and an internal diameter of 4.6 mm and 5-mm fused silica particles at a flow rate of 1 ml.min-1. The eluting solvent system had a linear gradient of 20% (v/v) acetonitrile in water for 4 min, gradually rising to 80% (v/v) acetonitrile in water at 35 min. This concentration was kept constant until 40 min when the gradient was decreased to 20% (v/v) acetonitrile in water at 42 min.

Sample preparation involved mixing 50 µl of gel with acetonitrile-water (1 ml, 70:30 mixture) containing 0.1% trifluoroacetic acid. The purity of each identified peak was determined by UV detection at 280 nm.

5.2.5 Circular Dichroism (CD)

For CD experiments see Section **3.2.8**.

5.3 Results and Discussion

5.3.1 Effect of electronic substitution on the formation and yield of Fmoc-Phe(4-X)-Phe-NH_2

We studied the supramolecular assembly of an amidated aromatic dipeptide amphiphile, Fmoc-Phe-(4-X)-Phe-NH_2, produced by thermolysin catalysed amide condensation (**Scheme 5.1**). X represents a range of substituents on the *para*-position of the first amino acid (OH, OPO_3H_2, H, F, CN or NO_2). Substituents were chosen on the basis of Hammet-σp values,[143] as a measure of electronegativity. In order to drive amide bond formation we used 20 mM of the modified amino acid Fmoc-Phe-(4X)-OH and 4 times excess (80 mM) of the nucleophile H-Phe-NH_2 in the presence of 1 mg/ml thermolysin (from *Bacillus thermoproteolyticus Rokko*) in 100 mM sodium phosphate buffer at pH 8 based on the previously reported procedure.[33] Amide bond formation expressed as a percentage of conversion was determined by reverse-phase high performance liquid chromatography (HPLC), **Figure 5.1a**. Dipeptide derivatives show variable yield conversion after 24 hours of enzyme addition as summarized in **Table 5.1**. Compared with the unsubstituted Fmoc-Phe-Phe-NH_2 (82% conversion), higher conversions were observed when using electron-donating groups (OH, 100%), followed by the phosphorylated derivative (OPO_3H_2, 87%), both reaching their final conversions within 30 minutes. When using electron-withdrawing groups, lower conversion yields were observed (59-77%). Histograms in the Appendix (**Figure 1**) showing the conversion yield for three repeating experiments for different stereoelectronic substituents, suggesting small variations for the conversions observed after 1 day of the enzyme addition (≈3-5%). Therefore, there is a clear trend between the electron density on the benzyl group and the conversion yields, implying that aromatic interactions provide an important driving

force for self-assembly. It should be noted that there is also a correlation with macroscopic change, with the electron-donating substituents giving rise to suspensions, while electron-withdrawing groups giving gels.

Table 1. Summary of % Conversion values after 24 hours of enzyme addition and the corresponding appearance change.

Entry	Precursor	%Con.	Transition (if any)
1	Fmoc-Tyr	100	gel to suspension
2	Fmoc-Phe-(4-OPO_3H_2)	87	solution to suspension
3	Fmoc-Phe	82	suspension to gel
4	Fmoc-Phe-(4-F)	59	suspension to weak gel
5	Fmoc-Phe-(4-CN)	77	transparent gel to translucent gel
6	Fmoc-Phe-(4-NO_2)	60	translucent gel (no change)

5.3.2 Effect of electronic substitution on supramolecular interactions

In order to acquire insights into the changing supramolecular interactions, we used fluorescence spectroscopy to measure changes in fluorenyl group environment. [123,144] Some of the materials studied here are highly scattering (Appendix, **Figure 2**) and care should therefore be taken with interpretation of the results. With this in mind, we focus on spectral shape (changes in emission wavelength **Figure 5.1b)** rather than intensity.

The fluorescence emission of the precursors **1** and **2**, exhibit a similar main peak at 319 nm and an excimer peak at 360 nm (clearer for **1**), which was previously observed for Fmoc-amino acid precursors which form micellar aggregates.[145,146] After the addition of thermolysin and upon condensation and assembly, 8 nm red shift was observed for **1** and 14 nm for **2** for the main peak, while the excimer peak disappeared (**Figure 5.1b**), with these observations suggesting supramolecular

reorganisation[62], which was further investigated below. For **3** the main emission peak was detected at 322 nm. In this case, *in situ* condensation by thermolysin and consequent self-assembly induces a red-shifted structure to 330 nm and an excimer peak appears covering the region from 355-380 nm (**Figure 5.1b**), accompanied by a substantial decrease in the relative emission, due to the formation of extended stacking interactions among the aromatics. The fluorinated phenylalanine derivative **4** shows an emission peak at 327 nm. Condensation reaction led to a small red-shift (329 nm), with the emission peak significantly quenched. A remarkable quenching in the main peak emission was also observed for **5** (**Figure 5.1b**). Biocatalytic assembly of **6** did not show significant differences (1 nm) in the fluorescence spectrum, indicating minimal change on the fluorophores arrangement. From the hydrophobic contributions we can notice that the introduction of a donor (OH) or bulky phosphorylated group (OPO_3H_2) reorganised the structure, as the micellar peak disappeared, and a significant red-shifted structure is observed, promoting a more ordered supramolecular arrangement for the aromatics. As the electron density of the benzyl group reduced *via* the electron-withdrawing groups, a much smaller red-shifted structure was observed, while no difference was noticed for the strong electron-withdrawing group (NO_2). The fluorescence emission spectra of all the Fmoc-dipeptides are available in Appendix (**Figure 3**).

Next, we investigated the propensity of the substituted dipeptide derivatives to form hydrogen bonding type arrangements using FTIR spectroscopy, **Figure 5.1c**. For **1** and **2**, a weak peak observed at the region 1625-1638 cm^{-1} corresponds to formation of H-bonding type interactions and another peak at 1684 cm^{-1} for the stacked carbamate.[110]As the π- cloud of the benzyl group was reduced by the acceptor groups

(**4**, **5**, **6**), stronger conformation for amide backbones was identified, as a peak appeared at at 1638 cm^{-1}. These observations suggest an inverse correlation between the contributions of H-bonding and aromatic stacking, which is dictated by the electron density distribution of the aromatic side chain.

Having established the relative importance between stacking interactions and hydrogen bonding, we used Circular Dichroism (CD) spectroscopy to investigate the effect on supramolecular chirality, resulting from the altered balance between aromatic stacking and H-bonding (**Figure 5.1d**). For **1** and **2**, a strong positive CD signal for the Fmoc group (307 nm) was detected. Supramolecular chirality was reduced when peptides were modified with less electron density groups (**3**, **4**). Introduction of electron-withdrawing groups (**5**, **6**) showed opposite behaviour, giving rise to a negative signal for the Fmoc group (303 nm and 310 nm respectively). HT values for the CD experiments are available in Appendix (**Figure 4**).

Regarding the effect of electronic modification on hydrophobic contributions and hydrogen bonding interactions, we can conclude that the rich electron density group (OH) as well as the bulky phosphate group (OPO_3H_2) give rise to enhanced stacking interactions among the aromatics with less hydrogen bonding capacity. An opposite observation was revealed by the introduction of electron-withdrawing groups. From the above observations, it is clear that atomic substitution with electron-donating or withdrawing groups, may enhance or disrupt the delicate balance between aromatic interactions and hydrogen bonding which drive the molecular self-assembly.

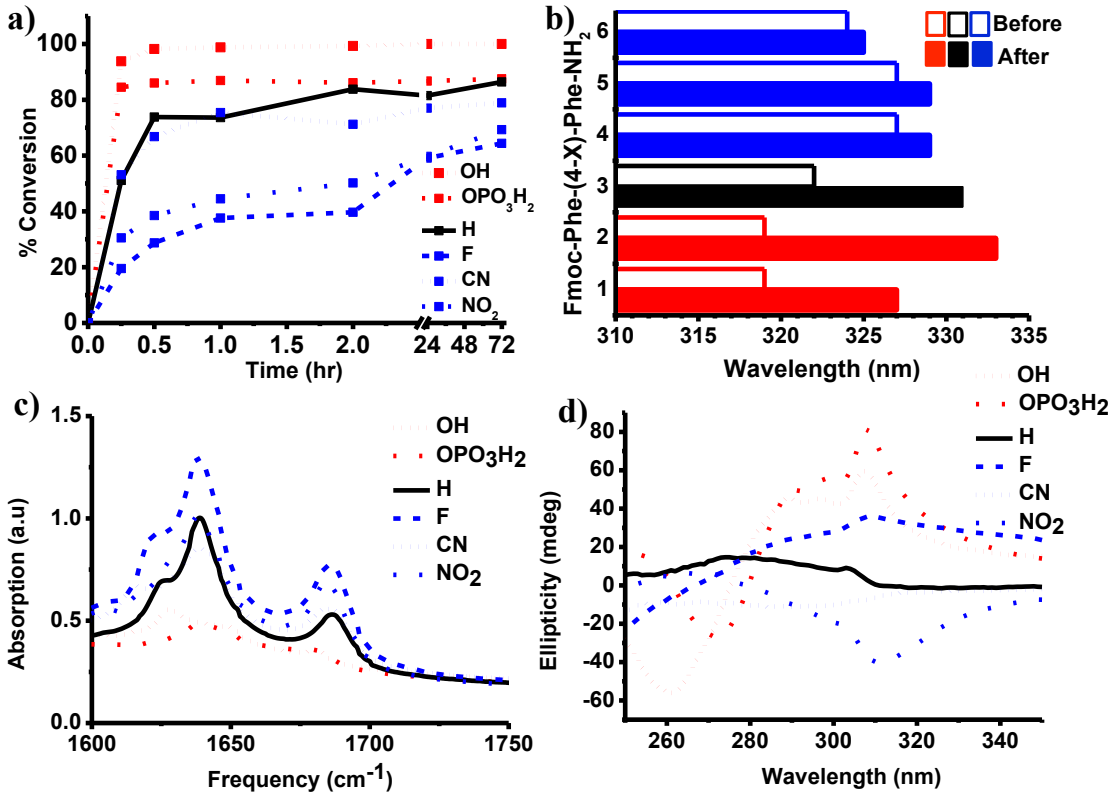

Figure 5.1 **a**) HPLC data, illustrating the percentage of peptide conversion of different Fmoc-diphenylalanine derivatives over time (λ=280), **b)** Histogram illustrating the difference of wavelength shifting before and after *in situ* condensation reaction and assembly, **c)** FT-IR amide region of Fmoc-diphenylalanine derivatives in D_2O and **d)** CD spectrum of the diphenylalanine derivatives.

5.3.3 Effect of electronic substitution on nanoscale organisation

Nanoscale morphology was then observed using TEM. Remarkably, different supramolecular architectures were obtained by altering the electron density of the phenylalanine amino acid residue (**Figure 5.2**). The base material, Fmoc-Phe-Phe-NH_2 self-assembled into a fibrillar network similar to that observed for Fmoc-Phe-Phe.[147,148] Upon substitution with OH, nanosheet-like structures were obtained[37], while tubular morphology was identified for the OPO_3H_2 derivative, possibly due to the bulky nature of the side chain which cannot be incorporated in a two dimensional sheet. The introduction of strong electron-withdrawing groups (CN, NO_2) did not

affect the nanoscale morphology. Fibrillar formation was observed with similar length and density. Hydrogel formation is observed upon introduction with electron-withdrawing groups (enchancement of hydrogen bonding interactions as evidence from FT-IR), while precipitate like structures are observed in the case of electron-donating groups (enchancement of the arrangement of the aromatics as evidenced using fluorescence spectroscopy). However, there are not significant differences regarding the size and the density of the fibrillar nnaostructures that are formed upon biocatalytic self-assembly in the case of electron-withdrwaing groups. Additional spectroscopy and microscopy techiques are required to further inverstigate their organisation at the nanoscale. More specifically, XRD and solid-state NMR experiments on the formation of different aromatic dipeptide amphimphiles upon electronic substitution would be furthermore informative. The molecular packing of these materials and possible differences on stacking and hydrogen bonding interactions upon regulating the electron density of the phenylalanine amino acid residue, will give rise to a better understanding in the relationship between the transitions observed and the supramolecular interactions at the nanoscale.

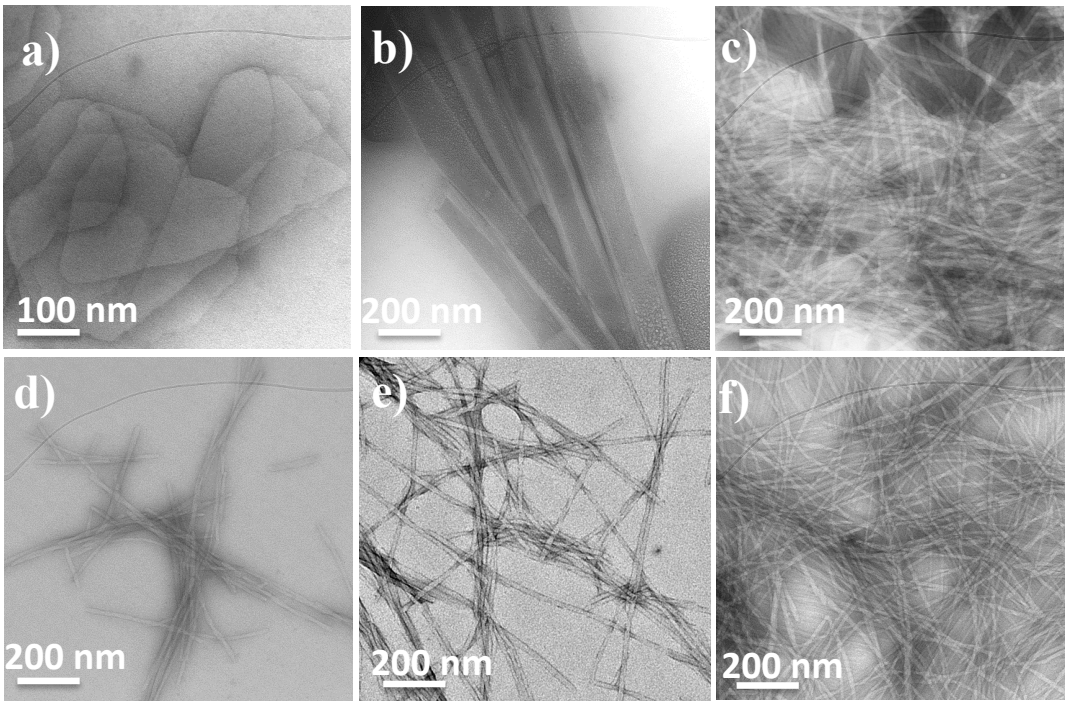

Fiure 5.2 TEM images of aromatic diphenylalanine derivatives after 48 hours of thermolysin addition. (**a-f** corresponds to **1-6**, respectively).

5.4 Conclusion

In conclusion, we have demonstrated that different supramolecular structures can be produced by changing the electronic properties of phenylalanine on Fmoc-Phe-(4-X)-Phe-NH_2, where X is electron donating or withdrawing group (OH, OPO_3H_2, F, CN, NO_2). Fibrillar nanostructures can be obtained in case of electron-withdrawing groups and the neutral phenylalanine (H), while sheet-like structure for the tyrosine derivative and tubular assemblies for the phosphorylated dipeptide. The electronic change of the phenylalanine amino acid residue gave rise to tune the stacking interactions among the aromatics and the hydrogen bonding between the dipeptides, which might be useful in developing biocompatible electronics, and sensing technology.

6. Searchable Dynamic Peptide Libraries (DPLs) for Materials Discovery.

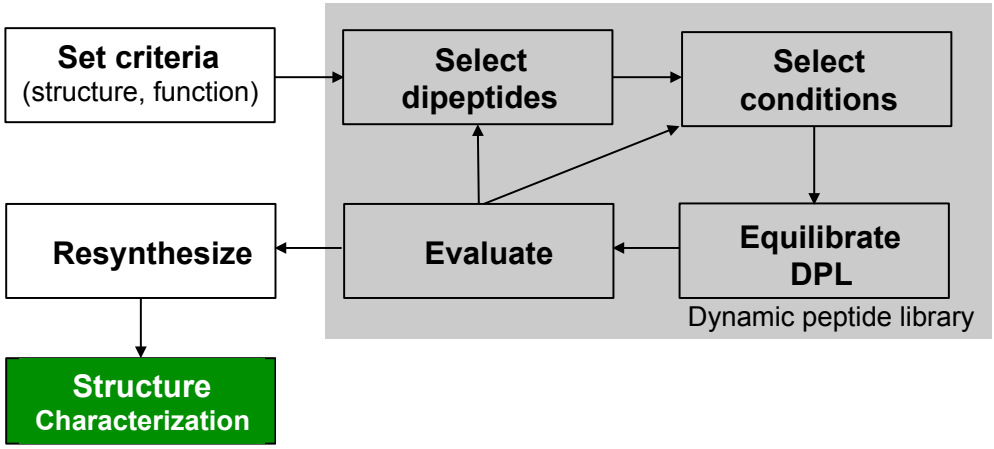

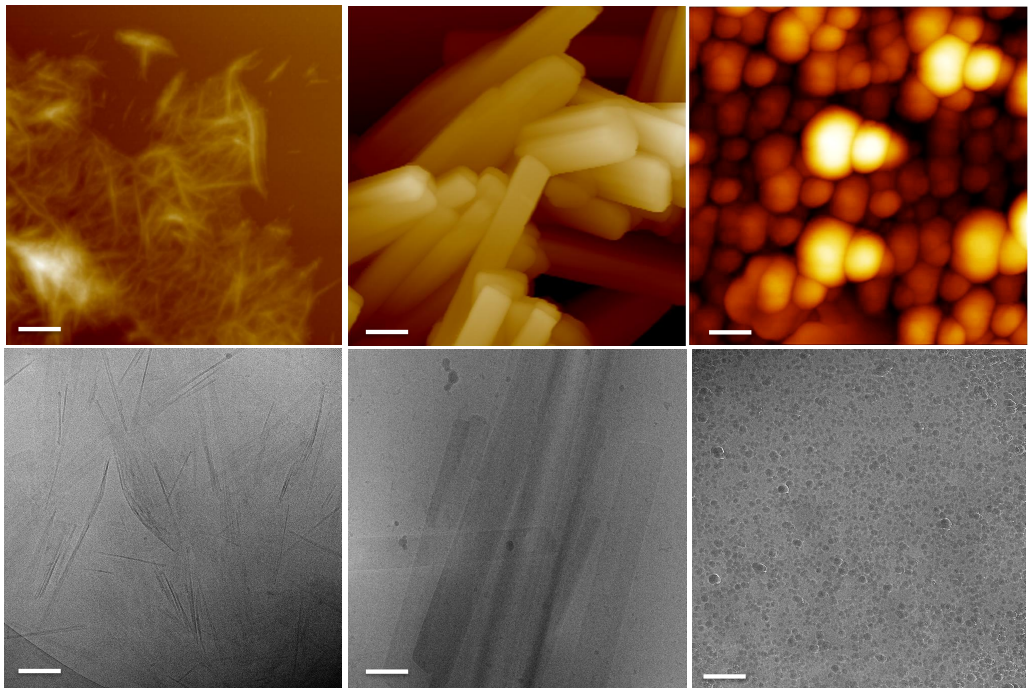

Objectives

The key research objectives of this chapter are to:

i. Demonstrate reversible peptide oligomerisation and hydrolysis from simple dipeptide building blocks through thermodynamically driven biocatalytic self-assembly, identifying the most stable self-assembling peptides.

ii. Investigate the effect of environmental conditions (salts, solvents) on dynamic peptide libraries, showing differential component selection and amplification accompanied with structural reconfiguration.

iii. Directly compare nanostructures from DPL with chemically synthesized assemblies for shape control and supramolecular properties.

6.1 Introduction

Structure and functionality of proteins arises from the combination of twenty gene-encoded amino acids - the building blocks of life.[38,117] These proteins form complex dynamic networks giving rise to processes such as evolving molecular complexity, adaptability and (re)-configuration.[149-151] Simpler versions of this complex biological machinery, short peptides (consist of 2-6 amino acid residues) represent interesting candidates for the fabrication of soft nanomaterials, with potential applications in food, cosmetics and biomedicine (see Section **2.2.4-2.2.6**). Notably, the majority of short peptide-based nanostructures have been discovered through serendipity, or by mapping onto known sequences (such as motifs from amyloid protein). In 2003, Gazit pioneered the use of the shortest possible aromatic peptide sequences, dyads of phenylalanine (F_2), which self-assembled into tubular assemblies.[13] Despite the discovery of F_2 peptide nanotubes and its tremendous popularity, there are only a small number of additional sequences that found to have potential to aggregate.[49-51]

Computational modelling has recently emerged as a useful screening tool to expand the sequence space of self-assembling peptides and potentially discover interesting structural and functional peptide candidates. More specifically, in collaboration with Dr. Tell Tuttle, we recently reported on the aggregation behaviour of tripeptides (8,000 candidates), identifying design rules, leading to the formation of the first tripeptide hydrogels **(**see Section **2.2.6)**.[12]

Despite the undoubted computational progress for the discovery of new peptide nanostructures, it is increasingly clear that there is a need to systematically investigate structure and function in short peptide sequences, using experimental approaches. Such experimental discovery of stable supramolecular nanostructures,

will allow for direct information regarding specific material properties, such as responsiveness, adaptability and reconfiguration.

Dynamic combinatorial libraries (DCLs),[152-156] are mixtures of building blocks that can interact through the exchange of reversible covalent bonds. They have been used to investigate chemical complexity and discover "unexpected" supramolecular systems with functionality. Environmental conditions may alter the relative stability of the library members, e.g., by differentially impacting on non-covalent interactions and thereby alter the molecular recognition of the library.[157]

Most of the existing literature reports on dynamic peptide libraries involve disulphide exchange, where in the presence of oxygen from the air, a number of thiol-based macrocycles may form of varying sizes. Solvents,[76] salts[158] and mechanical triggers[75] have been used to alter the library composition, giving rise to the formation of different molecular species.

The efficacy of this project (DPL approach) has been demonstrated by our group in 2009, using biocatalytic self-assembly. A non specific endoprotease was used to reversibly catalyze amide bond formation and breaking, thus enabling thermodynamic selection of short peptides with self-assembly capacity.[62] The DPL concept has been further exploited for the evolution of free energy optimized gel phase functional (rather than just structural) nanostructures from component mixtures of napthalene-appended peptide derivatives, identifying optimized peptide sequences for fabrication of energy transfer assemblies.[67] Additionally, Miller and coworkers reported on the use of DPL in purely tetrapeptide sequences (FEFK)[68]. In this case, the authors deliberately focused on the formation of β-sheet structures from

the precursors, where gradually the formation of an octapeptide (FEFKFEFK) was observed, after an initial hydrolysis into dipeptides (FE, FK) (see Section **2.6.1**), thus the library was intentionally based to favour formation of β-sheet-forming hydrogels.

Herein, we aim to develop an experimental methodology and especially "*searchable dynamic peptide libraries*" to investigate structural sequence spaces of short peptides and identifying pathways to discover functional nanomaterials.

We stress that the approach used in this chapter builds on previous work but gives much further insights on thermodynamically driven biocatalytic self-assembly due to the fact that exploits three following features **i)** Peptide oligomerisation from simple *unprotected* dipeptide building blocks through thermodynamically driven biocatalytic self-assembly, identifying the most stable supramolecular component, **ii)** Differential component selection and amplification accompanied with structural reconfiguration, by interplaying with environmental conditions (salts, solvent,) thus making the library *searchable* and **iii)** Nanostructure shape selection and control through a direct comparison between chemically and biocatalytically driven formation of different peptides (**Scheme 6.1**).

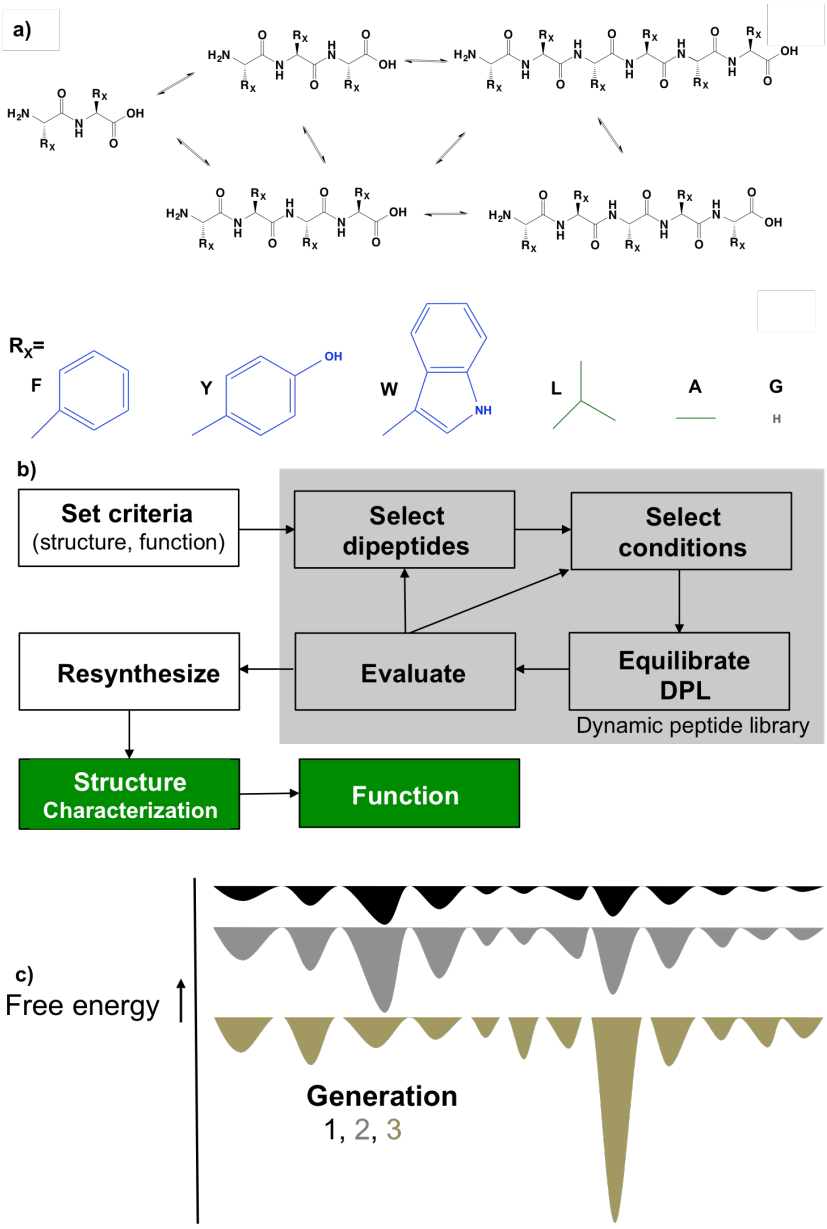

Scheme 6.1 a) Peptide oligomerisation through biocatalytic self-assembly with varying the amino acid side chain, **b**) Schematic representation of the pathway resulting in the discovery of functional nanostructures and **c)** Free energy landscape of the formation of different peptide generations at different environmental conditions.

6.2 Materials and Methods

Dipeptides (**F_2**, **L_2**, **W_2**, **Y_2, G_2 and A_2**) were purchased from Bachem, Switzerland. **F_6**, **W_4** and **F_2L_2** were purchased from CS bio. Thermolysin and organic solvents were purchased from Sigma Aldrich and Novabiochem.

6.2.1 Sample preparation

The total concentration used for the dipeptides (**F_2**, **L_2**, **W_2**, **Y_2, G_2 and A_2**) used in this study was 30 mM. For the mixture experiments (**F_2/L_2**) the concentration of each dipeptide was 15 mM and for the three-component mixture (**$F_2/L_2/W_2$**) was 10 mM each. For the aqueous and co-solvent experiments, the dipeptides were dissolved in (0-1 ml, according to the relative ratio of organic and aqueous media) of 100 mM sodium phosphate buffer pH 8 in the presence of 1 mg of thermolysin (thermolysin from *Bacillus Thermoproteolyticus rokko*).

6.2.2 HPLC

A Dionex P780 HPLC system equipped with a Macherey-Nagel C18 column of 270 mm length, 4.7 mm internal diameter and 7 mm particle size was used to quantify conversions to peptide derivatives. For the preparation of the HPLC samples 20 µl of the sample (gel, precipitation or suspension) was diluted to 1 ml mixture of acetonitrile:water (50:50) in the presence of 0.01% trifluoroacetic acid. All the chromatographs were monitored at 214, 225 and 254 nm and 280 nm.

6.2.3 Infrared Spectroscopy

For the FTIR experiments see Section **3.2.9**.

6.2.4 Circular Dichroism Spectroscopy

For the CD experiments see Section **3.2.8**.

6.2.5 Transmission Electron Microscopy (TEM)

For the TEM experiments see Section **3.2.4**. Images were taken in University of Glasgow and in the Advanced Science Research Centre, City University of New york.

6.2.6 Atomic force microscopy (AFM)

Samples were prepared by taking 20 µl of sample and diluted to a total volume of 100 µl solution in deionized water or the co-solvent system for each system. Then it was pipetted on a freshly cleaved mica sheet (G250-2 Mica sheets 1" x 1" x 0.006"; Agar Scientific Ltd, Essex, UK) attached to an AFM support stub and left to air-dry overnight in a dust-free environment, prior to imaging. The images were obtained by scanning the mica surface in air under ambient conditions using a Veeco diINNOVA Scanning Probe Microscope (VEECO/BRUKER, Santa Barbara, CA, USA) operated in tapping mode. The AFM scans were taken at 512 x 512 pixels resolution. The images were analyzed using NanoScope Analysis software Version 1.40.

6.2.7 Cryo-Transmission Electron Microscopy (Cryo-TEM)

Cryo-EM grids were prepared in an FEI Vitrobot at 21 °C with the relative humidity set to 100% and the blotting force set to 0. 3 µl of sample was pipetted onto a freshly glow-discharged lacey carbon grid. The sample solution was incubated on EM grid for 15 s, blotted for 4.5 s before being plunged into liquid ethane that was pre-cooled by liquid nitrogen. The cryo-EM grids were then transferred to and stored in liquid nitrogen. The cryo-EM grids were transferred in liquid nitrogen into a Gatan 626 cryo-specimen holder and then inserted into the microscope. The specimen temperature was maintained at -170 °C during data collection. Cryo-EM imaging was performed in an FEI TITAN Halo TEM operating at 80 or 300 kV.

6.3 Results and Discussion

6.3.1 Dipeptide oligomerisation *via* biocatalytic self-assembly

The self-assembly precursors consisted of homo dipeptides (**Leucine, L; Phenylalanine, F; Tryptophan, W; Tyrosine, Y; Glycine, G; Alanine, A**). A non-specific endoprotease (thermolysin) was used to catalyze amide bond formation and hydrolysis in sodium phosphate buffer at pH 8. The hydrophobic dipeptide building blocks (**L_2, F_2, W_2**) are generally poorly soluble, resulting in the formation of aggregates, in the starting mixtures. The use of enzymatic condensation and hydrolysis to reversibly control the oligomerisation of the dipeptides, overcomes the formation of route dependent aggregates. Additionally, the formation of by-products such as diketopiperazines (DKP),[159] where the dipeptide cyclisation is favoured in aqueous conditions at pH 8, is not observed, at these conditions (is mainly observed starting from dipeptide esters and not acids).[159] It is anticipated that some of the peptide oligomers formed (trimers, tetramers, pentamers, hexamers, etc.) may self-assemble through a combination of H-bonding and/or hydrophobic, stacking interactions among the aromatic side chains, which may vary according to the peptide sequence used.

6.3.2 Leucine libraries

Starting from dileucine (**L_2**), the system initially appears as an opaque free flowing suspension. Over time, the opacity of the sample was increasing, resulting after 48 hours in the formation of an opaque self-supporting hydrogel. Time dependent formation of leucine oligomers was monitored using high-pressure liquid chromatography (HPLC). Over the first 3 hours of the reaction, a distribution of peptide oligomers had formed, with the percentage of the dipeptide precursor (**L_2**) reduced to 74% with formation of the tetramer (**L_4**) (13%), pentamer (**L_5**) (3%) and

hexamer ($\mathbf{L_6}$) (10%). Notably, after 13 days the percentage of $\mathbf{L_4}$ and $\mathbf{L_6}$ increased and eventually reached 30 and 25% respectively. The relative distribution of the peptide oligomers then remained unchanged up to 28 days, suggesting that an equilibrium distribution had been reached (**Figure 6.1**). Time dependent HPLC chromatographs and mass spectra of the leucine libraries are available in the Appendix (**Figure 5, 6)**. The macroscopic (free flowing suspension to gel) and HPLC observations correlated with nanostructure reorganization as evidence by Transmission Electron Microscopy (TEM). Interestingly, the starting material ($\mathbf{L_2}$) self-assembled into chiral fibrillar structures. After oligomerisation and assembly, ($\mathbf{L_4}$ and $\mathbf{L_6}$) well-defined belt-like nanostructures were observed **(Figure 6.2)**. Aditional TEM images are available in the Appendix (**Figure 7).**

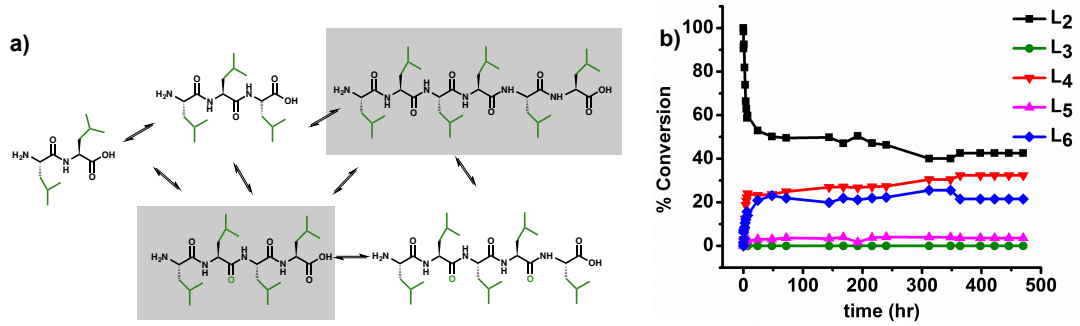

Figure 6.1 a) Schematic representation of biocatalytic self-assembly of $\mathbf{L_2}$ and corresponding oligomers, highlighting the formation of $\mathbf{L_4}$ and $\mathbf{L_6}$ **b**) HPLC profile of $\mathbf{L_2}$ oligomer distribution over time.

The morphological transitions coincide with significant spectroscopic changes. We used FT-IR spectroscopy to monitor the formation of H-bonded structures between peptide backbones upon biocatalytic oligomersation.[12] The FT-IR spectrum of $\mathbf{L_2}$ contained a peak at 1588 cm^{-1}, which can be assigned to the carboxylate group of the C-terminus. A broad peak at 1660 cm^{-1}, revealed the presence of a relatively less

ordered hydrogen-bonding pattern.[12] Upon oligomerisation and assembly, a new sharp peak developed at 1618 cm^{-1}, indicating the transition to a more ordered H-bonding network (**Figure 6.3a**), accompanied with a reduction in ionization (through protonation) of the carboxylic acid.[12] Additionally, Circular Dichroism spectroscopy (CD) was used to identify the role of supramolecular chirality on the transitions observed. A random coiled structure was observed for $\mathbf{L_2}$, as a peak was assigned at 206 nm. Upon the formation of tetra and hexamer peptide derivatives ($\mathbf{L_4}$, $\mathbf{L_6}$), a structural transition was identified with a peak appearing at 222 nm, suggesting formation of β-sheet structures (**Figure 6.3b**).

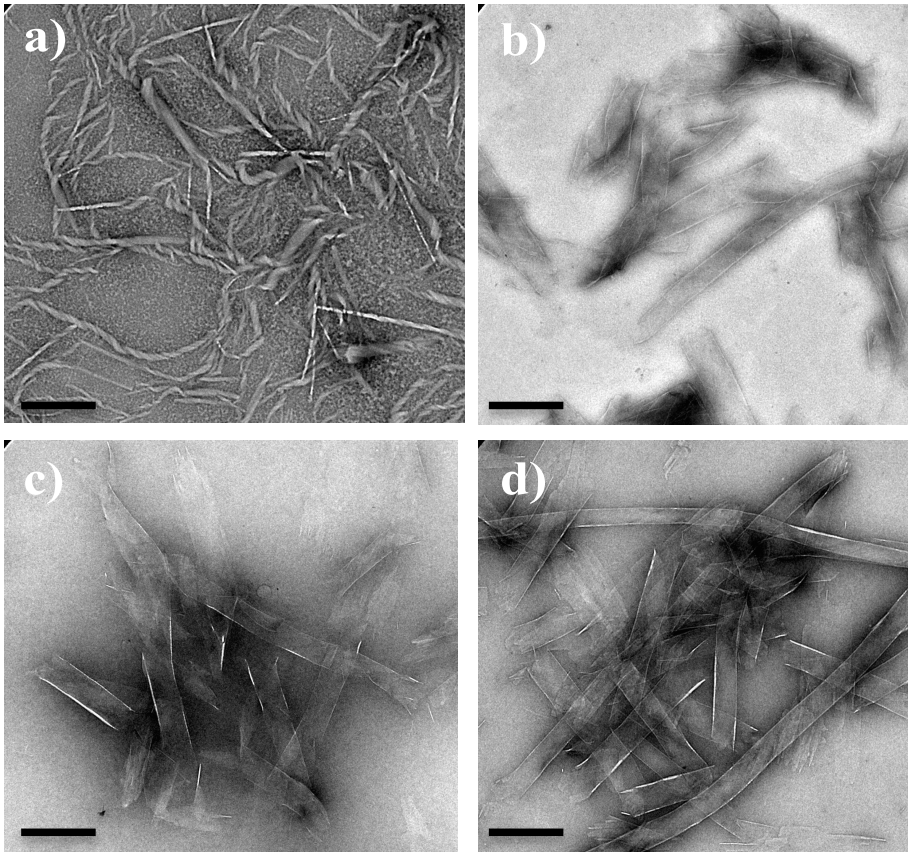

Figure 6.2 TEM images of $\mathbf{L_2}$ **a)** prior to and after thermolysin adition at **b)** 24, **c)** 96 and **d)** 400 hours of the reaction, showing fibrillar to belt-like transition, scale bar 500 nm.

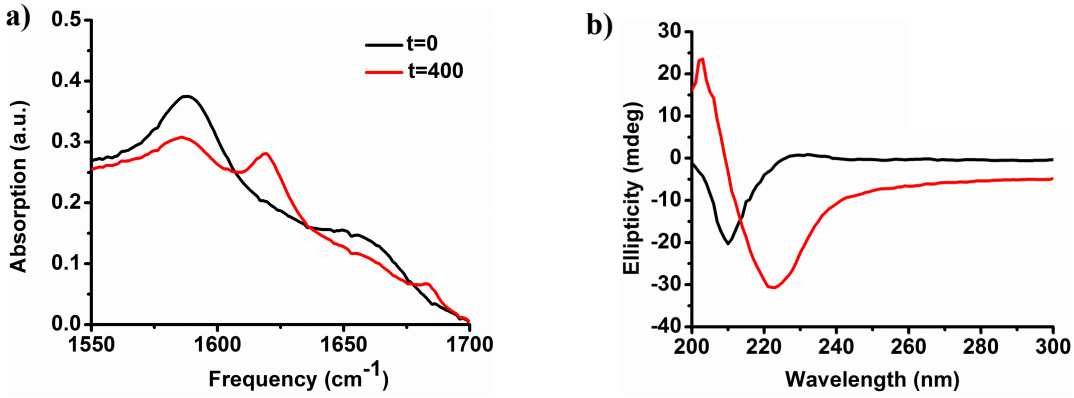

Figure 6.3 a) FT-IR and **b**) CD spectra before and after 400 hours of thermolysin addition for $\mathbf{L_2}$ library.

6.3.2 Phenylalanine libraries

The peptide oligomerisation through thermodynamically driven self-assembly was further demonstrated by studying another dipeptide sequence. In this case, the dipeptide precursor consisted of the well-known $\mathbf{F_2}$, investigating the role of aromatic stacking interactions on self-assembly and distribution of the peptide oligomers. Diphenylalanine ($\mathbf{F_2}$), was the first dipeptide sequence identified to self-assemble by Gazit into tubular assemblies, after dilution of hexafluoropropanol (HFIP) in water, at a final μM range concentartion.[13]

We use 30 mM of the dipeptide, which initially appeared to be a milky suspension and after oligomerisation and assembly, the viscosity of the sample increased without a further noticeable macroscopic change.

Using HPLC it was revealed that during the first day of the reaction, the major peptide product, which formed, was the hexamer ($\mathbf{F_6}$) in a percentage of 25%, with 70% of the dipeptide ($\mathbf{F_2}$) still present in the system. Traces of trimer ($\mathbf{F_3}$), tetramer ($\mathbf{F_4}$) and pentamer ($\mathbf{F_5}$) were also observed. After 12 days of the reaction, the dipeptide precursor reduced to less than 20%, giving rise to the formation of the

hexamer in high yield (80%) (**Figure 6.4**). Time dependent HPLC chromatographs and mass spectra of the phenylalanine libraries are available in the Appendix (**Figure 8, 9)**.

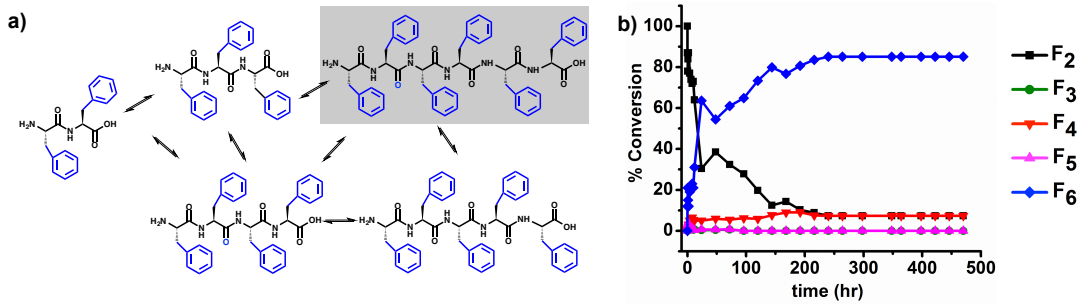

Figure 6.4 a) Schematic representation of biocatalytic self-assembly of $\mathbf{F_2}$ and corresponding oligomers, highlighting the formation of $\mathbf{F_6}$ **b**) HPLC profile of $\mathbf{F_2}$ oligomer distribution over time.

These observations show that the preferred length of the oligomerisation is dictated by the chemical nature of the amino acid ($\mathbf{L_2}$, $\mathbf{L_4}$ and $\mathbf{L_6}$ vs $\mathbf{F_6}$) in the peptide sequence, where supramolecular interactions dramatically affect the selection of the most stable supramolecular component.

Nanostructure reconfiguration was visualized by Transmission Electron Microscopy (TEM). Initially, $\mathbf{F_2}$ self assembled into tubular like nanostructures, confirming earlier reports.[13] Nanoscale fibres formed over time, increasing both in length and density until an entangled network was observed after the formation of $\mathbf{F_6}$ (**Figure 6.5**). Aditional TEM images are available in the Appendix (**Figure 10).**

In order to test whether this system evolves towards an equilibrium state that operates under thermodynamic control $\mathbf{F_6}$ was chemically synthesized and further exposed to hydrolysis/oligomerisation in the presence of thermolysin. Notably, there

was no product observed after 10 days of the reaction, suggesting that $\mathbf{F_6}$ represents a thermodynamically favourable component in the library (Appendix, **Figure 11**).

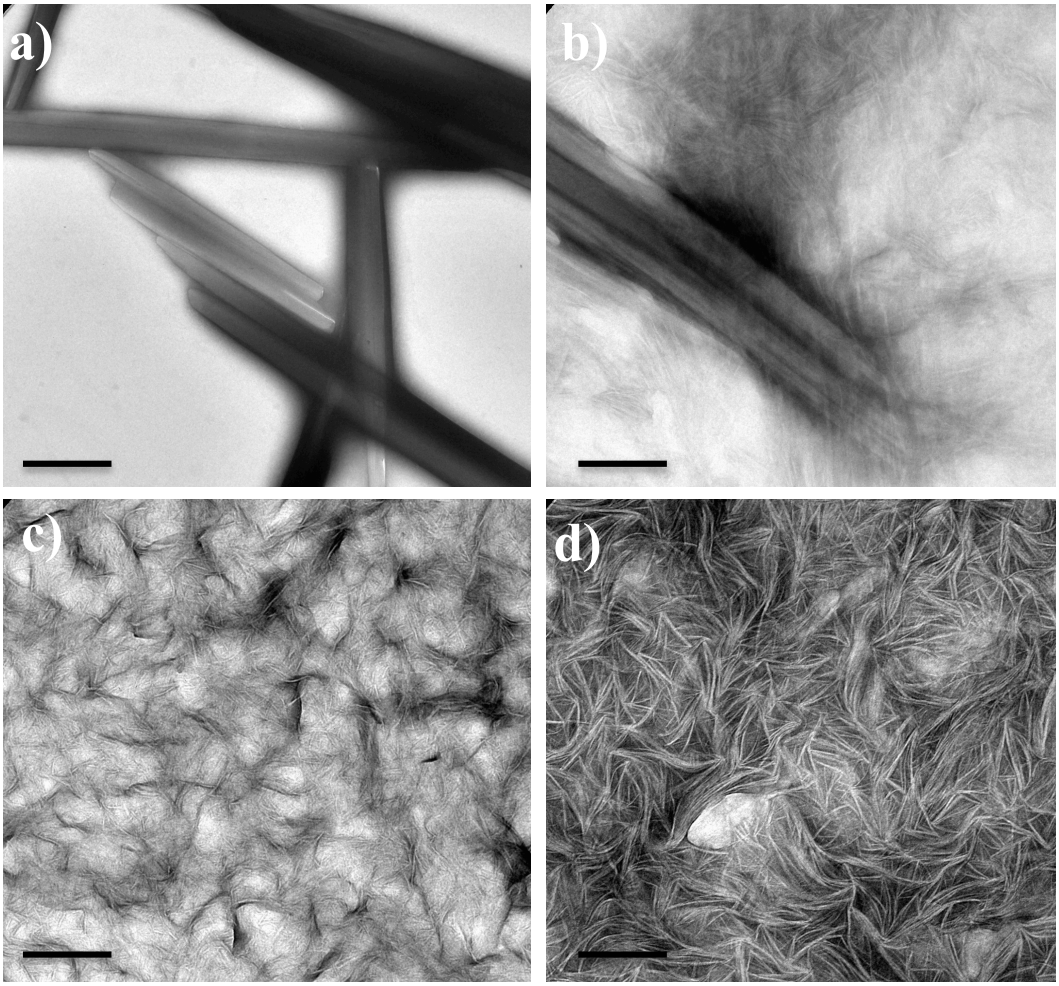

Figure 6.5 TEM images of $\mathbf{F_2}$ **a)** prior to and after thermolysin adition at **b)** 24, **c)** 96 and **d)** 400 hours of the reaction, highlighting tubular to fibrillar transition, scale bar 500 nm.

Supramolecular interactions were monitored using FT-IR and CD spectroscopy. The FT-IR spectrum prior to oligomerisation showed a peak at 1674 cm^{-1}. A remarkable shift was identified after the hexamer formation ($\mathbf{F_6}$) (1625 cm^{-1}), indicating strong intramolecular hydrogen bonding between amide modes, accompanied with significant reduction for the carboxylate peak (**Figure 6.6a**). A dramatic

enhancement of the supramolecular order of the building blocks was revealed upon formation of $\mathbf{F_6}$, showing enhancement of the CD signal at 230 nm, indicating an increase in chiral ordering of the phenylalanine amino acid residues (**Figure 6.6b**).

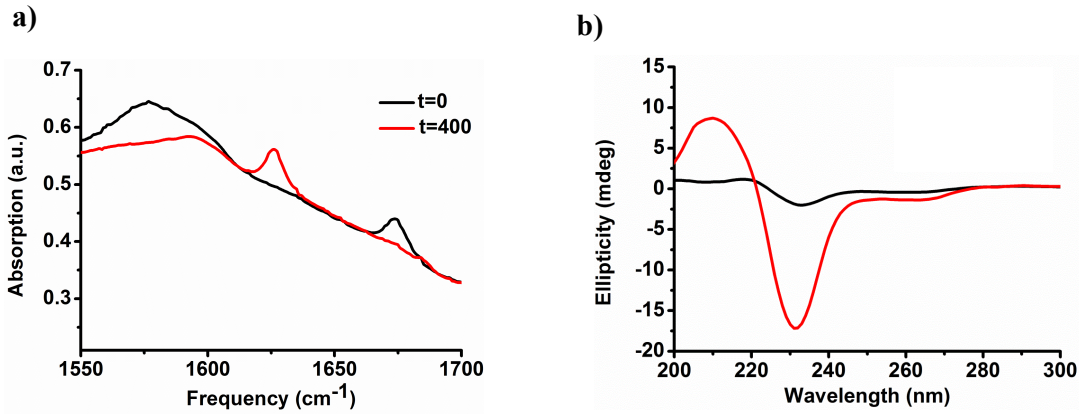

Figure 6.6 a) FT-IR and **b)** CD spectra before and after 400 hours of thermolysin addition for $\mathbf{F_2}$ library.

6.3.3 Tryptophan Libraries

Peptide oligomerisation and assembly was further exploited using another dipeptide sequence consisted of dyads of tryptophan ($\mathbf{W_2}$), which were previously observed to have high aggregation propensity.[46] After oligomerisation and assembly, there were two distinct peptide products presented in the DPL. Following the reaction for 7 days, $\mathbf{W_4}$ was found to be in a percentage of 16%, where $\mathbf{W_6}$ was formed at 6%. The yield of tryptophan peptide-based oligomers did not change over time (**Figure 6.7a**). Time dependent HPLC chromatographs and mass spectra of the tryptophan libraries are available in the Appendix (**Figure 12, 13)**. FT-IR spectroscopy in this case, revealed hydrogen-bonding interactions for $\mathbf{W_2}$, with a peak found at 1660 cm^{-1}. A strong peak at 1580 cm^{-1} was also observed for the carboxylate C-terminus. Notably after oligomerisation and assembly, the peak at 1660 cm^{-1} was lost, suggesting structural disruption for amide conformation, significantly different from the $\mathbf{F_2/L_2}$

library, where biocatalytic oligomerisation led to enhanced conformation for the amide backbones (**Figure 6.7b).**

It is worth mentioning that no oligomers were identified for diglycine ($\mathbf{G_2}$) and dialanine ($\mathbf{A_2}$), while for dityrosine ($\mathbf{Y_2}$), a very low $\mathbf{Y_4}$ (<3%) conversion was observed after 10 days, reflecting the poor self-assembly propensity of these dipeptide sequences, which were found to have low aggregation propensity using computational methods (see Section **2.2.5).**[46]

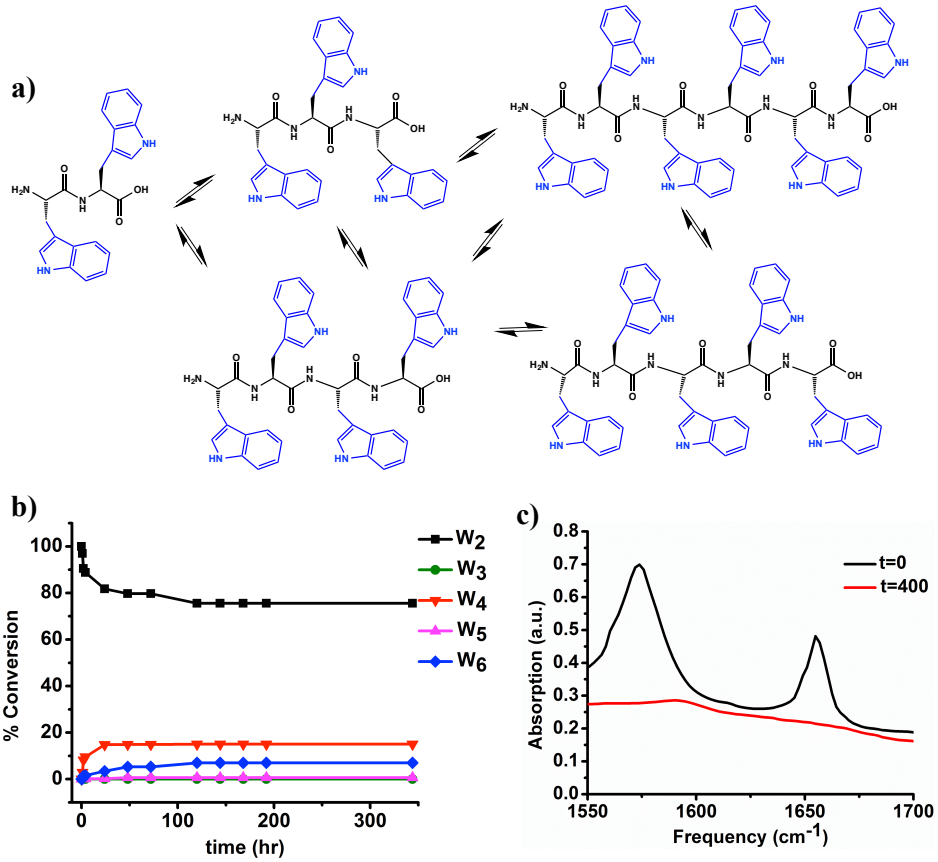

Figure 6.7 a) Formation of tryptophan oligomers through biocatalytic self-assembly, **b)** HPLC profile of $\mathbf{W_2}$ with oligomer distribution over time and **c)** FT-IR spectrum before and after enzyme addition at 400 hours of the reaction.

6.3.4 Effect of salts on library distribution

A number of approaches have been discussed earlier to direct peptide self-assembly, including examples where supramolecular organization is driven by changes in environmental conditions (pH, temperature, solvent polarity), or in the use of locally or directionally applied stimuli (light, enzymes) and (ultra)-sound. Ionic strength has also been reported as important chemical stimuli to tune the physical properties of gels by enhancing nanostructure formation. More specifically, the use of ions is recognized to impact self-assembly, by affecting the structure of water. Hofmeister first reported on the specific-ion effect, mainly in the folding of proteins and other large biomolecules.[160] Despite the fact that the molecular mechanism of the effect of Hofmeister salts in self-assembly remains a question in the scientific community, it is accepted that their addition affects the hydrophobic effect, which plays a key role on self-assembly. The presence of so-called kosmotropes, enhances water structure and thus promotes the hydrophobic effect in the self-assembled sate, whereas the presence of chaotropes reduces the hydrophobic effect in the less structured aqueous environment (**Figure 6.8a**). We have previously reported on the effect of salts on the resultant supramolecular properties of aromatic dipeptide amphiphiles following the Hofmeister trend of anions. It was demonstrated that the anions affect the relative importance off stacking among the aromatics and H-bonding interactions between the dipeptides, which in turn impacts nanoscale morphology and mechanical properties of the structures formed.[161]

Taking this into consideration and given the proposed substantial contribution of the hydrophobic effect in the $\mathbf{W_2}$ library, a number of salts were added in a concentration of 1M. Interestingly, the yield of $\mathbf{W_4}$ enhanced to approximately 22% in the presence

of sodium acetate ($C_2H_3NaO_2$) or sodium Chloride (NaCl). Notably, the ions that have a strong "salting in" effect (I^-, SCN^-) led to a significant increase of the hexameric product ($\mathbf{W_6} \approx 26\%$), where in an environment with weaker hydrophobic contributions, longer peptide sequences may be favoured (**Figure 6.8b)**. In order to furthermore understand the effect of salts on library distribution, concentration dependent salt experiments would be of a great importance, giving rise to the possibility to investigate the hydrophobic effect on the enchancement of different peptide species.

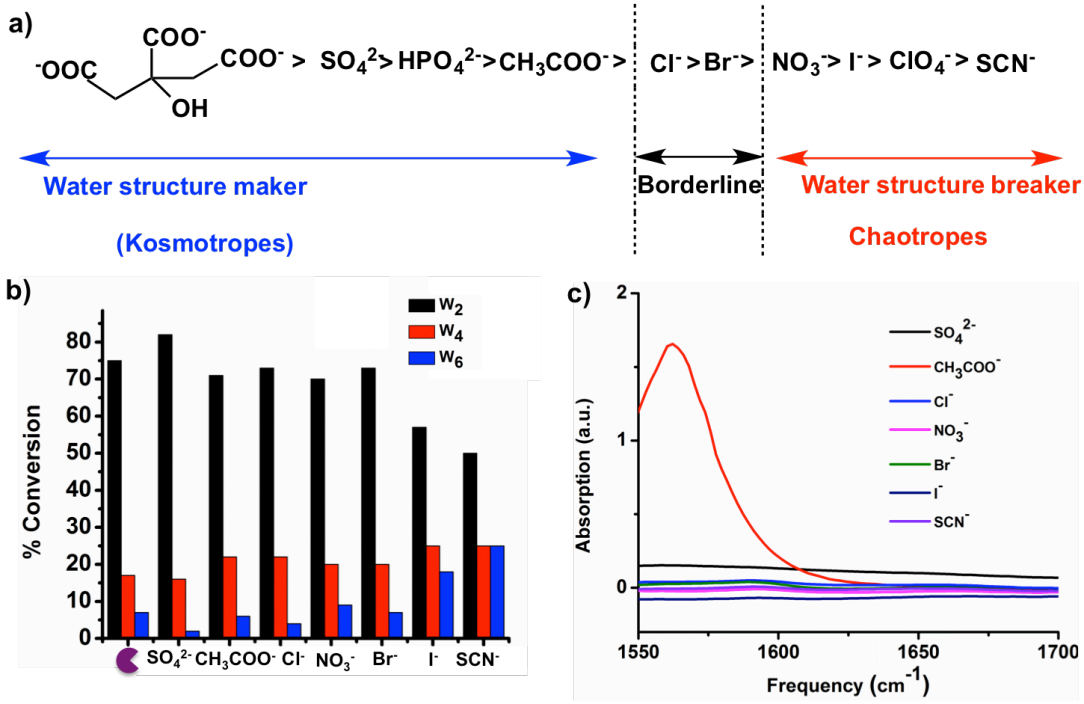

Figure 6.8 a) Hofmeister salts from "kosmotropes" (structure makers) to "chaotropes" (structure breakers)**, b)** Histogram of the conversion of $\mathbf{W_4}$ and $\mathbf{W_6}$ upon the addition of 1M of different salts (Na_2SO_4, $C_2H_3NaO_2$, NaCl, $NaNO_3$, NaBr, NaI, NaSCN), in 100 mM sodium phosphate buffer pH 8 and **c)** FT-IR spectrum upon the addition of 1M of different salts.

There were no significant differences in the signal intensities for the hydrogen bonding network upon the addition of different salts using FT-IR spectroscopy, suggesting hydrogen bonding efficiency is substantially unaffected by the presence of these inorganic salts, in agreement with our previous work,[161] where the addition of salts mainly affected the arrangement of the fluorophores and the supramolecular order of the building blocks (**Figure 6.8c**). As expected for sodium acetate an intense peak for the carboxylate peak was assigned at 1580 cm^{-1}. In Appendix (**Figure 14**), the FT-IR spectrum upon the adition of different salts is available excluding sodium acetate for a better comparison (carboxylate peak).

6.3.5 Effect of solvent on library distribution

Having established the effect of salts on library distribution, we expected changes in the solvent environment to direct the formation and furthermore amplification of the tryptophan-based oligomers ($\mathbf{W_4}$, $\mathbf{W_6}$), as it might have a dramatic impact on supramolecular interactions. Furthermore, solvent composition has also been reported to influence molecular self-assembly, through an interplay of H-bonding and hydrophobic interactions.[162] Nonetheless, in our system solvent environment may affect not only the formation of different peptide species, but also enzyme conformation and activity. Conveniently, thermolysin was previously shown to remain active in amide hydrolysis and condensation in a variety of solvent environments.[163] In addition, the ratio of the co-solvent system was found to be important for the activity, as in almost equal mixture (60-40 or 50-50) a deactivation of the enzyme was observed.[163] Thus, in order to selectively amplify $\mathbf{W_4}$ or $\mathbf{W_6}$, the library was exposed to a co-solvent system using either 10 or 80% organic media-acetonitrile (ACN) or tetrahydrofuran (THF) in phosphate buffer.

Notably, the presence of 10% THF did not alter the distribution of the library members, as **W_4** was formed in 14% yield, while **W_6** yield 5%, similar to the phosphate buffer environment after 4 days of the reaction. Replacing THF with ACN (10%), a slight increase of **W_4** was observed at 22%, while **W_6** was formed in a low yield (<3%). An increase of the organic ratio to 80% THF did not result in the formation of any tryptophan oligomers (**W_4, W_6**), while high percentage of ACN (80%) revealed the formation of **W_4** in low yield (<10%) after 4 days. The conversion yields remained unchanged up to 15 days of the reaction.

The addition of salt in the presence of 80% ACN gave rise to a significant enhancement of **W_4**. More specifically, in the presence of 1M NaCl, a dramatic enhancement in the formation of the tetrameric product was identified, as **W_4** reached the highest yield conversion of 70% after 4 days, while **W_6** was not observed at all in the system (**Figure 6.10)**. Peptide oligomerisation was not observed in 80% THF with different salts (Appendix, **Figure 15a**). It is worth mentioning that in the presence of other salts (sodium sulfate, acetate, nitrate, bromide, iodide) the percentage of **W_4** was never higher than 20% (Appendix, **Figure 15b).** Overall, these observations suggest that the approach of cooperative effects (organic solvent in the presence of anions) may be used to favour the formation and enhancement of peptide products in a DPL, however at this stage, is hard to fully rationalise and explain the cooperative effects of salts and solvents using biocatalytic self-assembly.

The enhancement of the conversion yields for tryptophan oligomers coincided with nanostructure formation observed using AFM (**Figure 6.11a-d)**. Initially, **W_2** formed large aggregates. After oligomerisation and assembly, spherical aggregates started to form as **W_4** (16%) and **W_6** (6%) were produced in the library in low yield. A

complete structural reconfiguration was observed in 80% ACN with 1M NaCl, where, $\mathbf{W_4}$ was found to be in the highest yield (70%).

Figure 6.10 a) Tryptophan-based dynamic peptide library, highlighting the

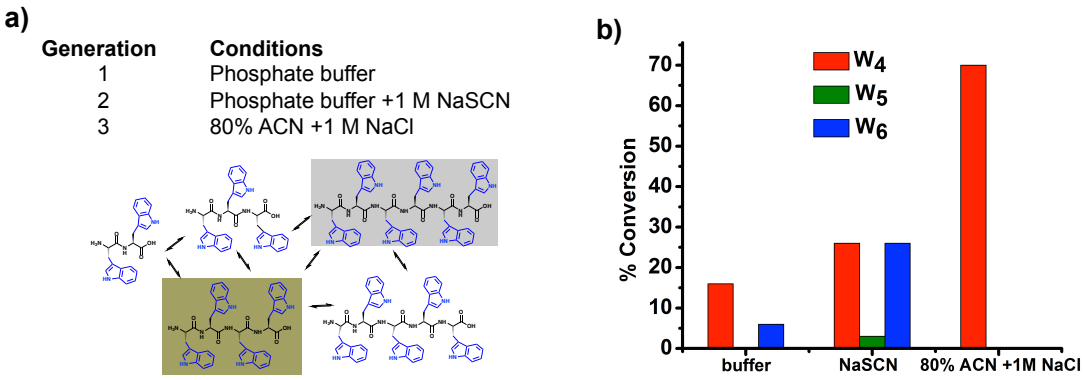

formation of $\mathbf{W_4}$ and $\mathbf{W_6}$, and **b)** HPLC conversions of tryptophan oligomers at different environmental conditions, where $\mathbf{W_4}$ may be significantly enhanced in 80% ACN with 1M NaCl.

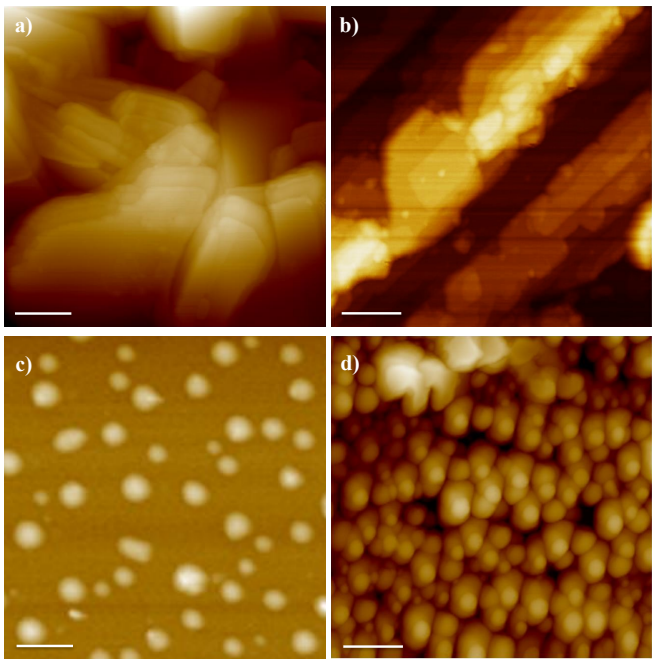

Figure 6.11 AFM images **a**) before, **b**) after the enzyme addition, **c**) in the presence of 1M sodium thiocynate (NaSCN) in phosphate buffer and **d**) in the presence of 1M sodium chloride (NaCl) in 80% ACN for $\mathbf{W_2}$ library, scale bar 500 nm.

6.3.6 Dynamic Peptide Libraries (DPLs).

Having demonstrated that $\mathbf{F_2}$ reconfigures to predominantly $\mathbf{F_6}$ in aqueous buffer, while $\mathbf{L_2}$ forms a mixture of structures, we then investigated whether competing dipeptides could form interesting structures. The mixing of dipeptide building blocks may open the door for the formation of heterogeneous sequence control (in length and in chemical composition). We also investigated whether environmental conditions could be used to control the outcome of the competition, as previously observed for the dramatic amplification of $\mathbf{W_4}$ (80% ACN with NaCl), thus producing components, which display different morphologies depending on their environmental response, mainly by interplaying with H-bonding or hydrophobic interactions (**Scheme 6.1**). The approach would allow for sequence optimization to match specific conditions.

Thus, starting from an equal mixture of $\mathbf{F_2}$ and $\mathbf{L_2}$ (**Figure 6.12a**) (using 15 mM each of the dipeptides), in the presence of thermolysin, in aqueous media (100 mM sodium phosphate buffer pH 8), a number of peptide oligomers were observed. The percentage of the peptide oligomers formed in the DPL was found to be in low abundance at the concentrations used (for each dipeptide half of that used in the single component experiments). The highest yield conversion was identified after 2 days for $\mathbf{F_4}$ (5%) and $\mathbf{L_6}$ (4%), followed by 2% of $\mathbf{F_6}$ and $\mathbf{L_4}$ respectively (**Figure 6.12b**). It is worth mentioning that the relative distribution of the peptides formed remained unchanged even after 15 days of the reaction. A thermodynamically stable product (self-assembled state) was not revealed in this case, which may be attributed to a concentration effect or to a disruption of the self-assembly of the mixture of the

dipeptides in the library.[164] Additionally using TEM, there was no nanostructural reconfiguration observed before and after the enzyme addition (**Figure 6.12c**).

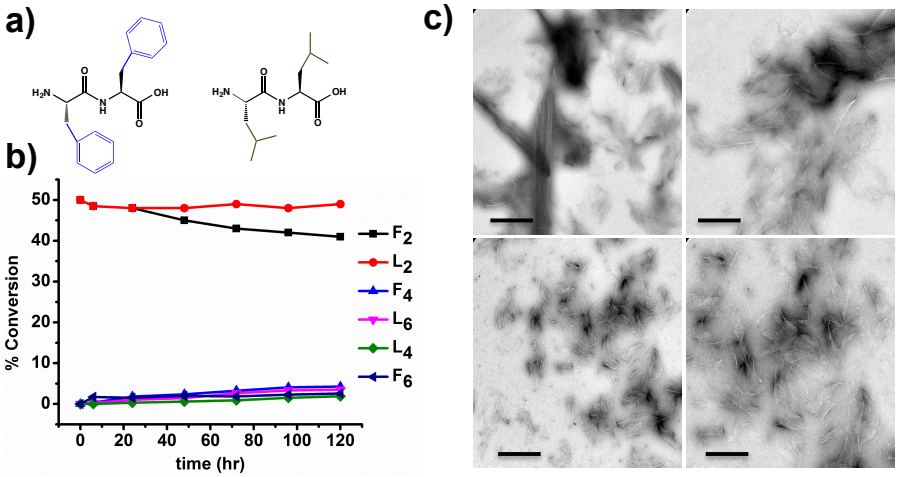

Figure 6.12 a) Chemical structures of the library members **b)** HPLC profile of oligomer distribution after thermolysin addition and **c)** TEM images before and after biocatalytic oligomerisation at different time points, scale bar 500 nm.

6.3.7 Environmental response of Dynamic Peptide Libraries (DPLs).

A DPL where a number of different molecular species are formed but only in low yield opens up opportunities to interplay with the environmental conditions and supramolecular interactions in order to enhance their formation, which may result in the discovery of functional nanostructures for specific conditions, e.g., a "*searchable*" DPL. There are various triggers to affect the formation of different products in a DPL and in previous Sections (**6.3.4, 6.3.5**), the effect of salts and solvents on the distribution of the tryptophan oligomers was demonstrated, leading finally to the discovery of $\mathbf{W_4}$ (80% in ACN with NaCl), accompanied with the formation of spherical aggregates.

In the $\mathbf{F_2/L_2}$ library, the addition of different anions (SO_4^{2-}, CH_3COO^-, Cl^-, Br^-, I^-), did not result in a noticeable change of the relative distribution of the peptides

formed, as previously observed for the tryptophan libraries. Subsequently, the DPL experiments were firstly performed in 10% acetonitrile (ACN), where a reduction of hydrophobic effect is expected, with enhancement of hydrogen-bonding capacity. This system is referred to as **generation 2.1**. Notably, the formation of the peptide products were dramatically enhanced, reaching final yield conversions after 3 days, with the highest yield conversion to be observed for $\mathbf{F_6}$ (≈ 26%), ten times higher than the initial $\mathbf{F_2/L_2}$ experiment (phosphate buffer, 100 mM). The reactions yields were furthermore increasing to 11% for $\mathbf{F_4}$ and 10% for $\mathbf{L_6}$ respectively. $\mathbf{L_2}$ was consumed in a percentage of 39%, while $\mathbf{F_2}$ was almost at ≈15% yield. The conversion yields remain unchanged after 20 days (**Figure 6.13b**).

The existence and outcome of competition to be dictated by solvent environment, prompted us to investigate the DPL behaviour in a different solvent. Replacing ACN with tetrathydrofuran (THF), an enhancement of hydrophobic interactions is expected, accompanied by relatively lower hydrogen bonding capacity compared to acetonitrile. Notably, the hexameric product of phenylalanine ($\mathbf{F_6}$) was the major product present in the system after 2 days, with also traces of $\mathbf{F_4}$ and $\mathbf{L_6}$ (<1%). $\mathbf{L_2}$ was found in a percentage of 48%, while $\mathbf{F_2}$ was almost at ≈20% yield**.** The percentage of $\mathbf{F_6}$ in 10% THF found to be about 30% after 7 days (**generation 2.2**). The conversion yields did not change over time (20 days). As a result of changing the environment, by adding a hydrophobic solvent to water, the peptide analogues with lower length ($\mathbf{L_4}$**,** $\mathbf{F_4}$) may not be stabilized, giving rise to a significantly high conversion for the more hydrophobic peptide analogue $\mathbf{F_6}$**,** which appeared to be the thermodynamically stable self-assembled component in this environment. As

previously observed for the tryptophan libraries, at near-equal amounts of the co-solvent system, (50-50 or 60-40%) there was no product formed in the library.

The DPL approach also works at a much higher solvent concentration (80%) where the hydrophobic effect is clearly diminished, the peptides become more soluble, and H-bonding interactions are enhanced.

Under these conditions, a different pattern emerges. In 80% ACN (**generation 3.1)**, the formation of the tetrapeptide (**F_2L_2)** was observed in a percentage of 12%, while in similar percentage (≈11%) **L_4** was formed after 2 days of the reaction. Traces of **F_4** and **F_6** (<2%) were also found (**generation 3.1**). **L_2** was consumed in a percentage of 31%, while **F_2** was almost at ≈44% yield**.** Subsequently, changing the environment from 80% ACN to 80% THF (**generation 3.2)**, the percentage of the tetrapeptide (**F_2L_2**) was increased to 16%, while the peptide oligomers with lower length presented in the library were not formed (only **L_4** was observed in a percentage of 1%) (**generation 3.2**). In this environment, the dipeptide precursors dominated in the system as they found to be a in a percentage of ≈42% each. As describer earlier, the addition of salts in aqueous media did not change the distribution of the peptide oligomers formed in the DPL. Nonetheless, a combination of environmental triggers (salt and solvents) had a dramatic impact on the formation and yield of the products observed. Remarkably, the presence of 1M sodium sulfate (Na_2SO_4) in 80% ACN slightly enhance the formation of **F_2L_2** (18%), while there is a reformation of **F_6**, **L_4**, **L_6** observed in the library **(generation 4.1**). Interestingly, at 80% THF in the presence of 1M sodium sulfate (Na_2SO_4), the highest yield conversion (60%) for **F_2L_2** was noticed after 3 days of 60%. **L_4** was also presented in

the library but in low yield (<5%) (**generation 4.2**). $\mathbf{F_2}$ was found to be in a percentage of 20%, while $\mathbf{L_2}$ at 15%.

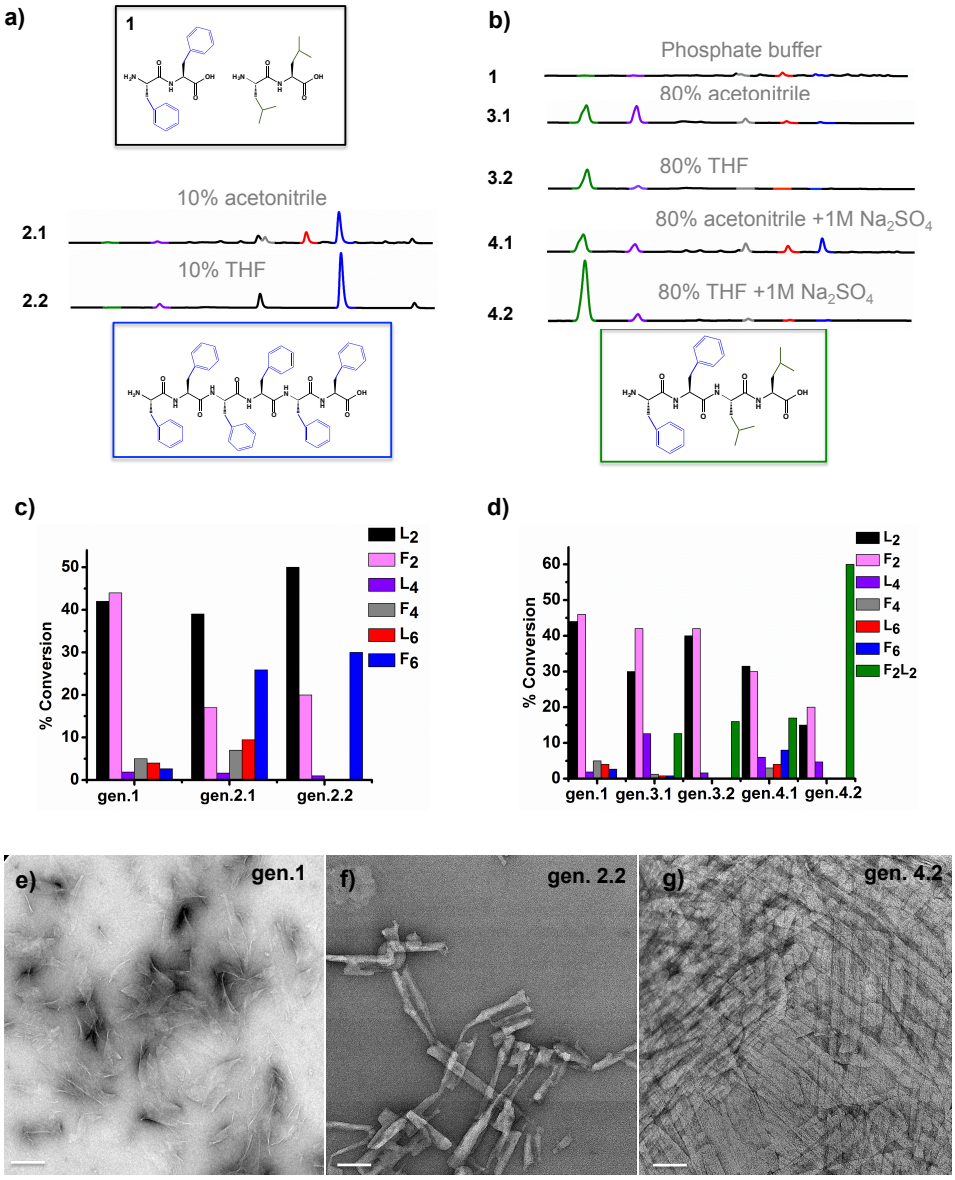

Figure 6.13 a) HPLC profiles of $\mathbf{F_2}$/$\mathbf{L_2}$ library at different environmental conditions, **b, c)** Histograms of % conversion yields of different peptide species formed in the DPL of 15 mM each of diphenylalanine ($\mathbf{F_2}$) and dileucine ($\mathbf{L_2}$) in the presence of 1 mg of thermolysin pH 8 at different environmental conditions and**)** TEM images of the library in **e)** phosphate buffer, **f)** 10% THF and **g)** 80% THF with 1M sodium sulfate (Na_2SO_4), scale bar 500 nm.

Aditional histograms with conversion yields for the dipeptide libraries (**F_2/L_2**) are available in the Appendix (**Figure 16**). Nanostructure formation was visualised in different generations using TEM. Initially, in phosphate buffer, sheet-like structures were identified, where the dipeptide precursors were found to remain in a high yield (≈40% each) (**Figure 6.13e**). Subsequently, 10% THF led to the formation of rod like assemblies, where the hexamer of phenylalanine was in a high conversion yield (30%). After increasing the percentage of organic solvent to 80%, a fibrillar network was observed, leading finally to the formation of multilayer tape-like assemblies upon the addition of 1M sodium sulfate (Na_2SO_4), where the tetrapeptide (**F_2L_2**) was found to be in a percentage of 60%, while **L_2** was remained at 15% and **F_2** at 20% respectively (**Figure 6.13g**). From the above observations, is not possible to say with certainty if these assemblies represent descrete or co-assembled nanostructures, however, from the HPLC profiles is clear that according to the environment, different peptide species outcompete others.

Additive experiments (80% of ACN or THF in the presence of 1M of different salts-sodium acetate, sodium chloride, magnesium chloride) were further investigated, with the relative distribution of the peptide oligomers shown in Appendix (**Figure 17**).

6.3.8 Supramolecular interactions in the searchable DPLs.

To acquire more insights at the supramolecular level, the peptide libraries were characterized by spectroscopic methods. Hydrogen-bonding type interactions were identified using FT-IR spectroscopy. Initially, prior to enzyme addition two peaks were observed for the mixture of **F_2/L_2** in aqueous media, one at 1623 cm^{-1}, corresponding to intramolecular hydrogen bonding between amide modes and a

second peak at 1680 cm^{-1}, which may be attributed to a less ordered hydrogen-bonding pattern.[12] A broad peak at 1588 cm^{-1} may be assigned to the ionized terminal of the carboxylate groups. In the presence of 10% THF the peak at 1623 cm^{-1}, was slightly enhanced, suggesting a more ordered hydrogen-bonding network. A significant enhancement of the FT-IR signal at 1623 cm^{-1} was detected as the peptide library was exposed to 10% ACN, where the formation of peptide species is driven more by hydrogen bonding type interactions (**L_4, F_4**) (**Figure 6.14a**). Remarkable differences in supramolecular interactions were identified as the concentration of the organic solvent was increased, where the peptide became more soluble. As **F_2L_2** was formed in the library at 80% ACN, the hydrogen bonding network became less ordered, as the peak at 1623 cm^{-1} was lost, while the peak at 1680 cm^{-1} remained. Furthermore, as the environment was adopted to less polar conditions at 80% THF, both of the peaks, previously observed for the conformation of the peptide backbones were absent, highlighting the importance of the environment on supramolecular interactions and self-assembly of the peptide libraries (**Figure 6.14b**). Notably, in the presence of 1M Na_2SO_4 in 80% THF, a weak peak at 1623 cm^{-1} was reformed, that is in the conditions where **F_2L_2** was formed at the highest yield.

Circular Dichroism (CD) spectroscopy was used to further investigate the chiral supramolecular organization of the building blocks in peptide libraries. A weak peak at 218 nm was identified for the **F_2/L_2** mixture in aqueous media, prior to enzyme addition. A continuous enhancement of the CD signal was detected in 10% THF and ACN respectively, suggesting enrichment of supramolecular chirality, as the conversion yield for the peptide products was significantly enhanced in these conditions (**Figure 6.14c**).

Continuous enhancement of the CD signal (225 nm) was observed at higher concentrations of acetonitrile, involving a more chiral stacking of the phenylalanine amino acid residues. The supramolecular chirality was lost when replacing ACN with THF (80% THF) (**Figure 6.14d**).

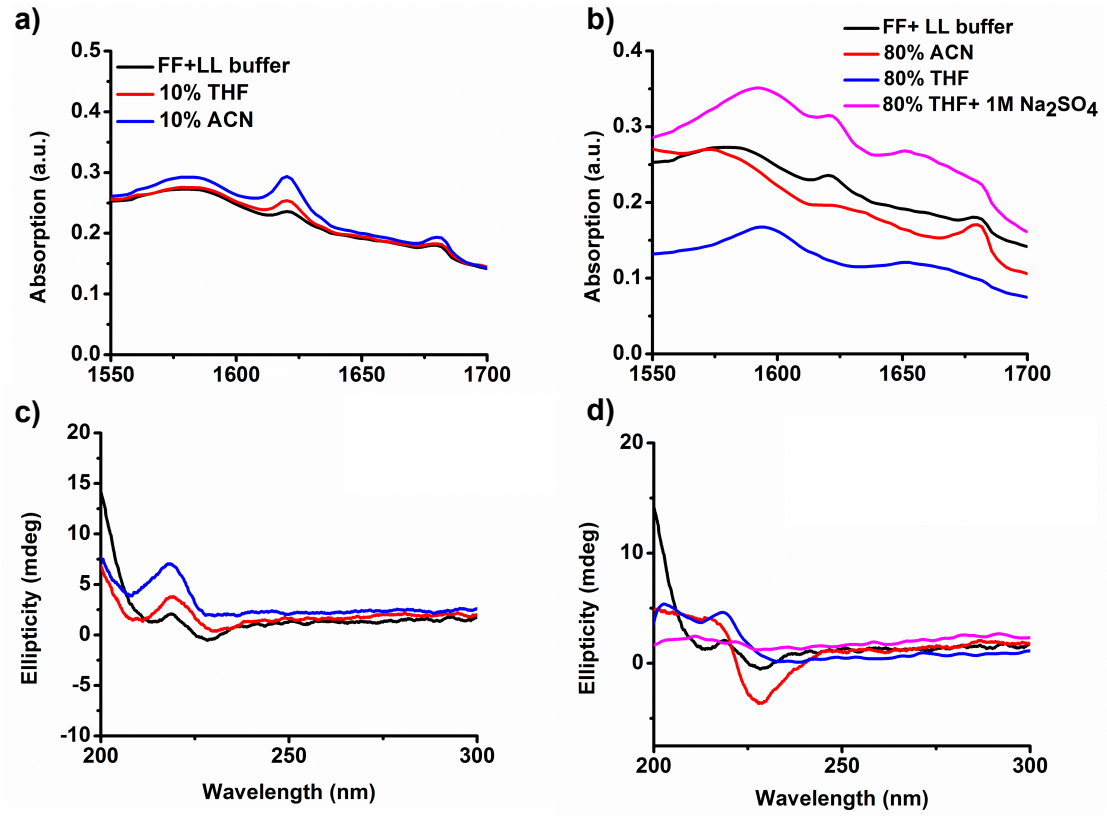

Figure 6.14 a, b) FT-IR and **c, d)** CD spectra **of** 15 mM of diphenylalanine (**F_2**) and 15 mM of dileucine (**L_2**) in the presence of 1 mg of thermolysin pH 8 at different environmental conditions.

6.3.9 Three-component mixture on dynamic peptide libraries (F_2, L_2, W_2)

The existence and the outcome of competition through environmental triggers on **F_2/L_2** library, prompted us to investigate the effect of the environment in a more complex library, consisting of three dipeptide precursors (**F_2, L_2, W_2**), with the aim of following the same pathway to discover nanostructures (**Figure 6.15a**). An equal concentration of three dipeptides (10 mM each) was first dissolved in phosphate

buffer. HPLC analysis of the library revealed the formation of the tetrapeptide (**F_2L_2**) and the tetramer of tryptophan (**W_4**) in low yield (3% and 5% respectively). **F_2** and **L_2** were remained at 31.5% each, while **W_2** in a percentage of 29%. Notably, upon exposure of the library to 80% ACN, a new library pattern emerged. The tetrapeptide (**W_2L_2**, 5%) and the hexapeptide (**W_2L_4**, 7%**)** were formed, however the dipeptide precursors remain in high yield. Traces of **L_4**, **F_4** and **F_6** were also found in the system. Furthermore, **F_2L_2**, was significantly amplified (23%) in 80% THF with 1M Na_2SO_4, whereas the addition of 1M NaCl in the same percentage of THF, selectively enhanced the formation of **W_2L_2** (40%). In these environments, the dipeptide precursors were found at **L_2**≈13%, **F_2**≈20%, **W_2**≈28% and 5%, 23,5%, 13% respectively. Replacing THF with ACN in the presence of sodium sulfate (Na_2SO_4), the hexapeptide (**W_2L_4**) was found in high yield (≈20%). An equal formation of **W_4** and **W_2L_2** (≈13%) was also observed. The dipeptide precursors were found at **L_2**≈18%, **F_2**≈21%, **W_2**≈7%. **W_4** was dramatically enhanced (70%) in the presence of 1M NaCl (**Figure 6.15a-d)**. Atomic Force Microscopy (AFM) images revealed shape transitions in the libraries through the additive experiments. Initially, ring-like structures were found for the mixture in aqueous media (**Figure 6.15d**). Fusion and further aggregation was observed in 80% THF. Large aggregates were observed in the presence of 1M Na_2SO_4, in 80% THF. Finally, micellar aggregates were revealed in the presence of 80% ACN with 1M NaCl, corresponding to **W_4** **(Figure 6.15g**). As mentioned before, is not possible to say with certainty if the structures formed represent descrete or co-assembled nanostructures, however, from the HPLC profiles is clear that according to the environment, different peptide species outcompete others.

Aditional histograms for repeating experiment with conversion yields and the mass spectra for the dipeptide libraries ($\mathbf{F_2/L_2/W_2}$) are available in the Appendix (**Figure 18, 19**).

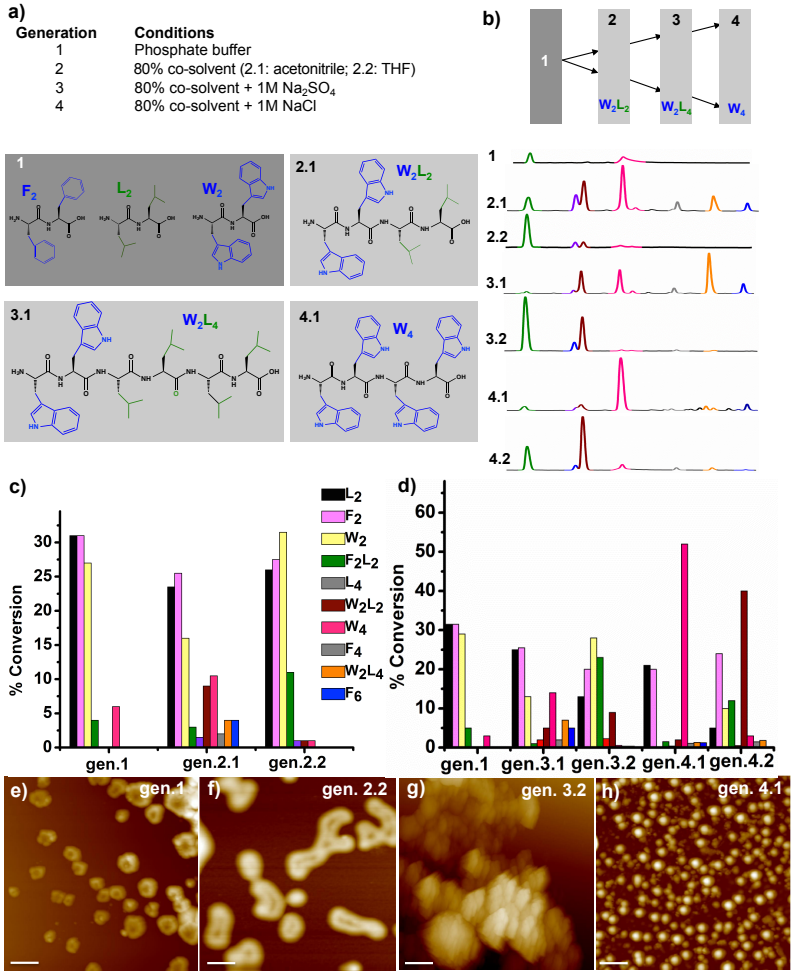

Figure 6.15 a) HPLC of three component dipeptide mixture of 10 mM diphenylalanine ($\mathbf{F_2}$), 10 mM dileucine ($\mathbf{L_2}$) and 10 mM ditryptophan ($\mathbf{W_2}$) in the presence of 1 mg of thermolysin at pH 8 with the conditions set to influence the formation of different peptide species (generations), **b, c)** Histograms of % conversion yields of different peptide species formed in the DPL at different environmental conditions and **d-g**) AFM images of the library in phosphate buffer, 80% THF, 80% THF with 1M sodium sulfate (Na_2SO_4) and 80% ACN with 1M sodium chloride (NaCl), scale bar 500 nm.

6.3.10 Shape control comparing biocatalytic and chemical synthesized assemblies

The observations of different supramolecular nanostructures and interactions in the peptide libraries at different environmental conditions prompted us to investigate a direct comparison between chemically and enzymatically driven peptide synthesis, with the aim of achieving shape control. Thus, **F_6**, **F_2L_2** and **W_4** were chemically synthesized. Two heat-cool cycles (90^0C for 5 minutes) were applied in order to enhance the solubility of the chemically synthesized **F_6** and to ensure thermodynamic stability, avoiding the formation of kinetic aggregates. Similar hydrogen-bonding pattern was revealed for the chemical version of **F_6**, as the FT-IR spectrum in aqueous media contained a peak at 1625 cm^{-1}, close to that observed for the enzymatic one (1623 cm^{-1}) (**Figure 6.16a)**. However, there were significant differences in supramolecular chirality. More specifically, a weak CD signal was observed, remarkably different from the supramolecular chirality profile of the biocatalytic synthesis of **F_6** (peak at 230 nm) (**Figure 6.16d)**. The formation of small fibrillar assemblies was observed using AFM and Cryo-TEM in agreement with the fibrillar network formed for **F_6** *via* biocatalytic self-assembly (**Figure 6.16g,j)**.

Furthermore, similar conformation for the peptide backbones and chiral organization of the building blocks was revealed for the enzymatic and chemical version of **F_2L_2** **(Figure 6.17 b, e)**. The spectroscopic evidence coincides with microscopic results, where flat tape-like structures were observed in phosphate buffer (**Figure 6.16h,k)**. Similarly, **W_4** self-assembled into spherical aggregates, showing an identical, limited hydrogen-bonding network and supramolecular chirality (slightly enhanced CD signal for the chemically synthesized **W_4**) (**Figure 6.16c-l)**. Overall, these observations suggest that shape control may be attained, comparing biocatalytic and

chemical synthesis of the peptide-based nanomaterials, which is highly associated with supramolecular interactions, as this may be achieved through different supramolecular pathways and application of external stiuli (temperature) to ensure thermodynamic stability, avoiding kinetically trapped supramolecular aggregates, resulting in the discovery of adaptive functional nanostructures. Aditional Cryo-TEM images are available in the Appendix (**Figure 20**).

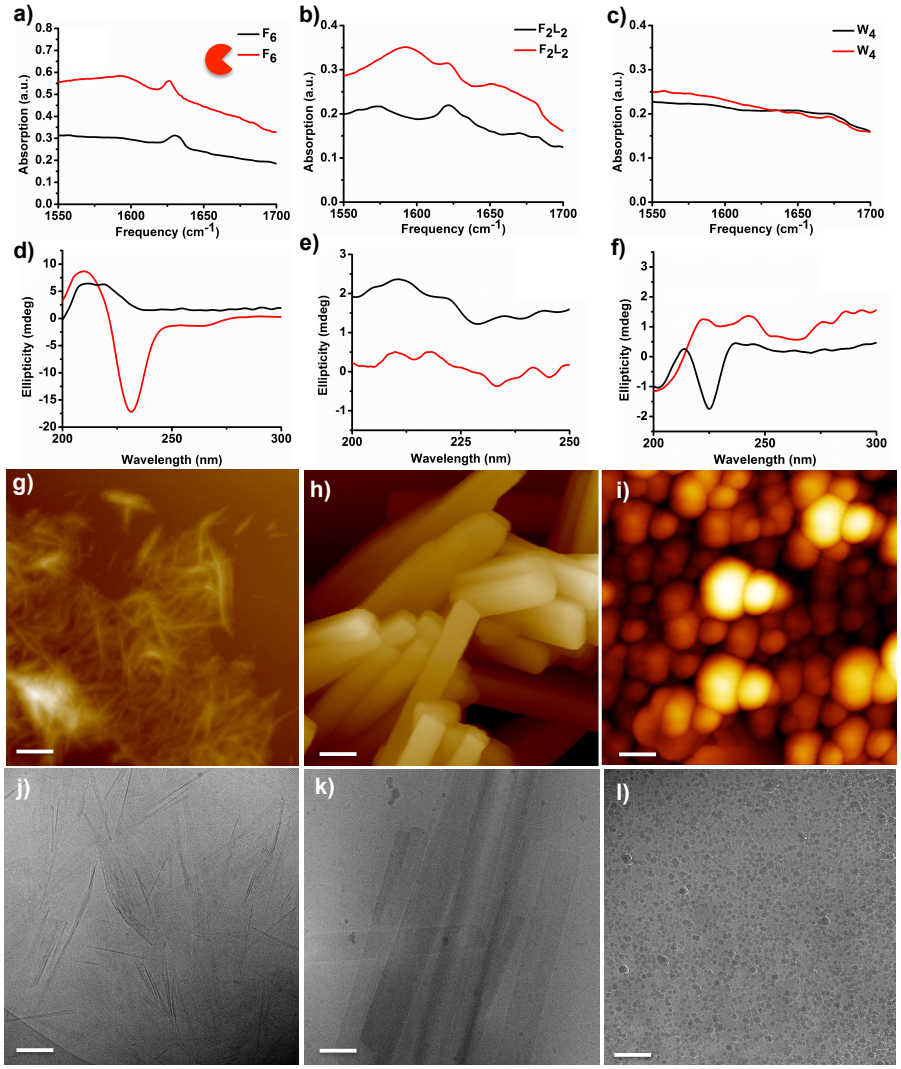

Figure 6.16 FT-IR and CD spectra of chemically and enzymatically made **a, d) F_6, b, e) F_2L_2, c, f) W_4,** AFM and Cryo-TEM images of chemically synthesized **g, j) F_6, h, k) F_2L_2 and i, l) W_4**, scale bar 500 nm.

In order to furthermore investigate the molecular association and interactions that drive the assembly of the chemically synthesized peptides, that were significantly amplified in the dynamic peptide libraries under different condiditons using biocatalytic self-assembly, WAXS diffraction patterns were obtained. For **W_4** there was no peak associated with β-sheet spacing, however, there were two peaks observed (3.7, 3.8Å), for the stacking of the tryptophan amino acid residues, highlighting ithe fact that its formation is driven by the hydrophobic effect and to a lesser extent from hydrogen bonding interactions. Dismilarly to **W_4**, the WAXS patern of **F_6** and **F_2L_2** exhibited a peak at 4.8Å, associated with β-sheet like interactions, in aggrement with the FT-IR findings (**Figure 6.17**). Peaks for stacking interactions were also observed.

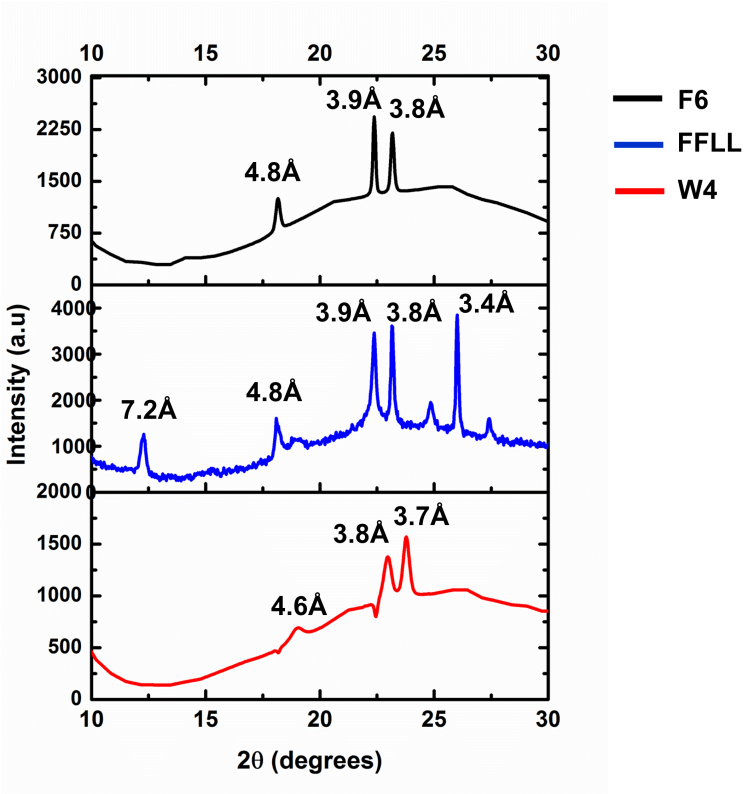

Figure 6.17 WAXS data of dried sample in phosphate buffer pH 8 measured after 24 h of **F_6**, **F_2L_2** and **W_4**.

6.4 Conclusion

In summary, we demonstrated the use of thermodynamically driven biocatalytic self-assembly to trigger peptide oligomerization from simple dipeptide building blocks. To achieve this, we identified new minimalistic self-assembling peptides, providing sequence control of shape. We show that these systems demonstrate oligomer selection (mainly tetra- and hexamers) with the length of the final peptide component to be dictated by peptide sequence and self-assembly propensity, as the highest was identified for diphenylalanine **($F_2 \rightarrow F_6$),** while for dileucine **($L_2 \rightarrow L_4/L_6$)** and ditryptophan **($W_2 \rightarrow W_4/W_6$)**, peptide components with lower length were observed in the system. Furthermore, we demonstrated differential component selection, by varying the environmental conditions (salts, solvents,) in DPLs, suggesting that environmental triggers have a dramatic impact on the existence and outcome of competition. Finally, shape selection and control through a direct comparison between chemically and biocatalytically driven formation of different peptides is demonstrated, suggesting that this concept may be used as an alternative for resynthesizing fascinating molecules. This work provides a step towards a better understanding of structural adaption, response and reconfiguration and may open up new opportunities in the discovery of novel adaptive nanomaterials.

7. Biocatalytic pathway selection in transient tripeptide nanostructures*

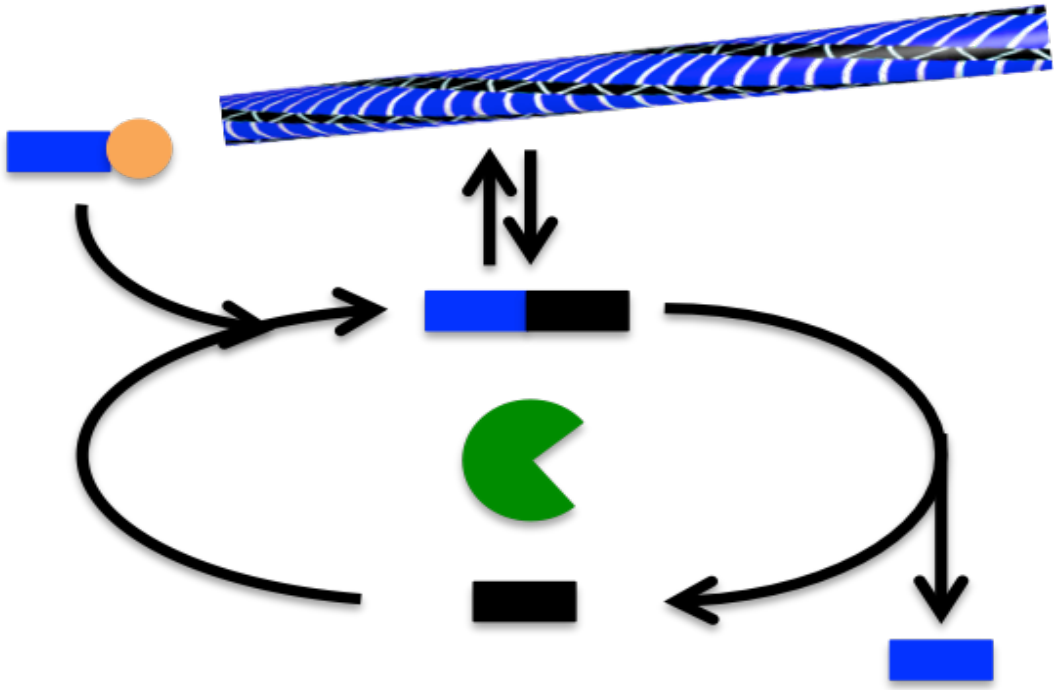

Objectives

The key research objectives of this chapter are to:

i) Demonstrate a simple mimic of a more complex biological system that displays transient, sequence dependent formation of supramolecular nanostructures based on biocatalytic formation and hydrolysis of self-assembling tripeptides.

ii) Investigate a biocatalytic pathway selection, where the kinetics and consequent lifetime of transient nanostructures formed can be controlled by peptide sequence.

iii) Investigate a direct competition between nucleophiles for kinetically controlled peptide libraries.

* This work was published in part as: C. G. Pappas, I. R. Sasselli, R. V. Ulijn, *Angew. Chem. Int. Ed.*, 2015, **74**, 119-8123.

C.G.P. and R.V.U. conceived, designed the experiments, analysed the data and wrote the paper. I.R.S. performed the FT-IR experiments.

7.1 Introduction

Living systems are exceptionally capable of altering their structures in response to changing situations, largely through molecular assembly and dis-assembly via competing catalytic pathways under the influence of chemical fuels. There is tremendous interest in developing man-made analogues of such systems, which provide insights into the workings of biology's remarkable ability to adapt to changing environments and may find use in future adaptive nanotechnologies.[1-7] Dynamic processes in living systems are regulated by balancing thermodynamic and kinetic aspects. The rapid responses required for biological survival are achieved through catalytic amplification, which enables dynamic change under otherwise constant conditions. Indeed, enzymes are increasingly used to activate or deactivate a variety of functions in designed, peptide based nanostructures, including self-assembly.[9] Furthermore, nature's self-assembly systems operate away-from-equlibrium, facilitating 'unfavorable' reactions by coupling them to hydrolysis of a high-energy molecular fuel. Most existing laboratory-based self-assembly processes[16, 149,150,165] are designed with thermodynamics, rather than kinetics, in mind. Changes in environmental conditions such as temperature, ionic strength, solvent and pH result in thermodynamically driven self-assembly. In particular for supramolecular gels,[136,166,167] equilibrium is not always reached due to the formation of kinetically trapped aggregates and consequently the self-assembly route is crucial in determining the final supramolecular architecture. Kinetics may also be controlled by taking advantage of catalytic production of self-assembly building blocks, as demonstrated using enzymatic[73] and chemical catalysis.[72] The first example of a chemically fuelled, non-equilibrium supramolecular system was demonstrated by Boekhoven et al., who showed that transient hydrogelation may be achieved by

catalytic esterification (to form a gelator) and competing, thermodynamically favored hydrolysis of the ester group.[77] We recently demonstrated chemically fuelled biocatalytic formation of peptide nanofibers which display dynamic instability based on transient formation (fuelled by ester hydrolysis) and degradation of an aromatic dipeptide amphiphile.[78] Transient self-assembling nanostructures have also been achieved by controlled protonation and consequent dis-assembly, using dynamically controlled pH gradients (see section **2.5**).[168]

Sequence dependent function may be found even in very short peptide sequences.[11-14,169] Thus, a system where different peptides are formed through competing pathways provides interesting opportunities for nanostructures with adaptive functions. Here, we demonstrate peptide sequence dependent pathway selection in chemically fuelled biocatalytic self-assembly of tripeptides. We show that these systems demonstrate transience, with the lifetime of the nanostructures formed dictated by peptide sequence (selection of the nucleophile). We stress that the approach used in this chapter is conceptually different from the previous (**Chapters 4, 5**) on equilibrium-driven enzymatic self-assembly[62,67,135] where thermodynamic stabilization of the peptide product drives the reaction, with the equilibrium situation represents the assembled state, - *i.e.*, equilibrium driven formation of peptide nanostructures. In the current approach we deliberately focus on peptides that do not assemble at equilibrium, - *i.e.*, we operate them under conditions where self-assembly is not favoured. This is key to achieving transience,[77,78] as demonstrated previously, nanostructure formation should be unfavourable at equilibrium.

7.2 Materials and Methods

Aspartame and chymotrypsin were purchased from Sigma-Aldrich UK and the amino acid nucleophiles form Bachem.

7.2.1 Sample preparation

20 mM of aspartame (DF-OMe) and 40 mM of the amino acid amide (Phe-NH_2, Tyr-NH_2, Trp-NH_2, Val-NH_2, Leu-NH_2, Ser-NH_2, Thr-NH_2) were dissolved in 1 ml of 100 mM sodium phosphate buffer pH 8 in the presence of 1 mg of chymotrypsin. The mixture was gently vortexed for 30s and sonicated for 70s in order to obtain a homogenous solution. Gelation was observed in the sonication bath for Phe-NH_2, Tyr-NH_2. For the competition experiments we used 20 mM of aspartame and 40 mM of the nucleophiles (Phe-NH_2 and Tyr-NH_2) in the presence of 1 mg of α-chymotrypsin.

7.2.2 HPLC

A Dionex P780 HPLC system equipped with a Macherey-Nagel C18 column of 270 mm length, 4.7 mm internal diameter and 7 mm particle size was used to quantify conversions to peptide derivatives. For the preparation of the HPLC samples 20 μl of the sample (gel or solution) was diluted to 1 ml mixture of acetonitrile:water (50:50) in the presence of 0.01% trifluoroacetic acid. The relative areas under the peaks were used to identify the percentage of the products. All the chromatographs were monitored at 214, 225 and 265 nm. The ratio of the areas observed at 265 nm (monitoring aromatics) and 225 nm (amides) for tripeptide to dipeptide was 0.97:1 for DFF/DF and 0.95:1 for DFY/DF. The conversions were determined by the ratio of areas and corrected for these ratios. Data shown are for 225 nm.

7.2.3 Infrared Spectroscopy

For FT-IR experiments see Section **3.2.9**.

7.2.4 TEM

Carbon-coated copper grids (200 mesh) were glow discharged in air for 30 s. The support film was touched onto the gel surface for 3s and blotted down using filter paper. Negative stain (20 ml, 1% aqueous methylamine vanadate (Nanovan; Nanoprobes) was applied and the mixture was blotted again using filter paper to remove excess. The dried specimens were then imaged using a LEO 912 energy filtering transmission electron microscope operating at 120kV fitted with 14 bit/2 K Proscan CCD camera.

7.2.5 Diffusion Ordered NMR Spectroscopy (DOSY)

Samples were prepared in sodium phosphate buffer pH 8 in D_2O at 10 mM peptide concentration as a compromise between solubility and NMR signal intensity. DOSY spectra were acquired at 700 MHz using a Bruker Avance 700 at 298 K. The eddy current delay (Te) was set to 7 ms. The diffusion time was adjusted to 100 ms. The duration of the pulse field gradient, δg, was optimized in order to obtain 7% residual signal with the maximum gradient strength with the resulting value of 3.7 ms.

7.3 Results and Discussion

7.3.1 Design of the transient supramolecular system

In order to produce transient structures, a "poor assembler" is required, necessitating a balance of attractive and repulsive forces within one molecule. In addition, the peptide should be a good substrate for the enzymatic reaction. We chose α-chymotrypsin, which has previously been used in biocatalytic self-assembly,[78] and has a well-documented preference for aromatic residues at the C-terminus. Conveniently, the artificial sweetener aspartame, a dipeptide methyl ester (DF-OMe), used as a sugar substitute in some foods and beverages,[170,171] is a potential substrate for α-chymotrypsin that also provides phenylalanine (F) in position two to ensure the peptides have a propensity to aggregate and a conflicting aspartic acid (D) at the N-terminus position. Aspartame provides a low cost, water-soluble activated precursor for formation of transient nanostructures. The third amino acid is used to regulate the properties of the material formed, by using a range of amino acid amides (**Scheme 7.1**) to form DFX-NH_2. It is anticipated that transient supramolecular architecture and hydrogel formation arises from aromatic-stacking interactions between the aromatic amino acid residues and hydrogen bonding between the tripeptide backbones.[12,52,108]

Thus, starting from aspartame (**1***) and a range of amino acid (X = W, Y, F, L, V, S or T) amides with α-chymotrypsin[78] as the catalyst, a range of potential tripeptide amides may be formed (DFX-NH_2). The forward reaction, resulting in peptide formation (**1***→**2**, **Scheme 7.1**) was enabled by α-chymotrypsin-catalyzed trans-acylation.[74,172] Provided that self-assembly is thermodynamically unfavored under the conditions used, this should lead to transient existence of **2**, which is

subsequently hydrolyzed to **1** (**Scheme 7.1**). It should be noted that transient supramolecular structures would only exist if the amide bond formation (**1***→**2**) is faster than ester hydrolysis (**1***→**1**) and amide hydrolysis (**2**→**1**) is slow.

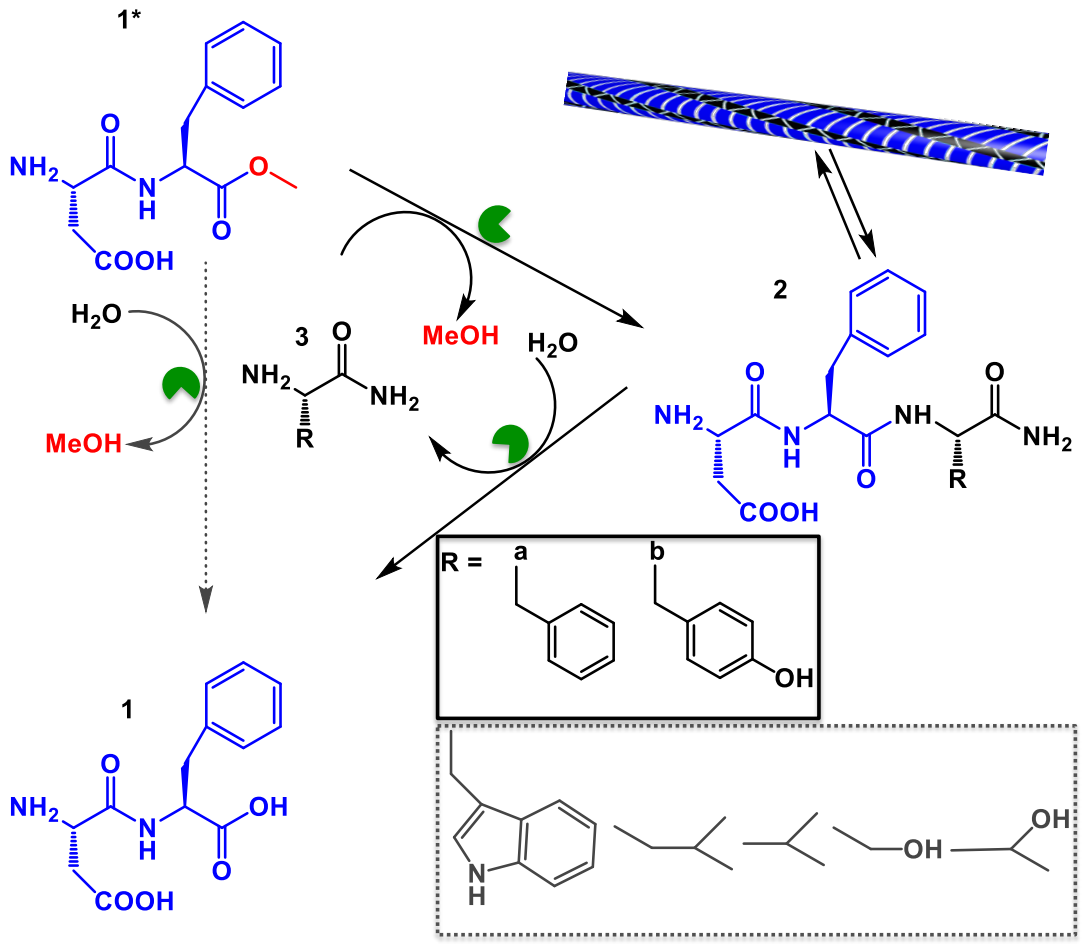

Scheme 7.1 Sequence controlled pathway selection in transient biocatalytic self-assembly from a dipeptide precursor (aspartame) with different amino acid nucleophile amides in presence of α-chymotrypsin.

7.3.2 Chemical design dictates the kinetics of the reaction and consequent lifetime of the nanostructures formed.

Remarkably, we observed a substantial difference in pathway selection depending on the choice of amino acid amide nucleophile. In the presence of W, L, V, S and T no trans-acylation was observed. Instead, hydrolysis (**1*→1)** occured within 30 minutes. Using high-performance liquid chromatography (HPLC), **2** was not observed, indicating its transient existence was either of very short duration and immediately hydrolyzed or not occurring at all. This is unexpected because in previous work, it has been shown that a variety of amino acid amides (L, V, S) may be used as nucleophiles with high yielding (70-80%) in chymotrypsin catalyzed peptide synthesis via trans-acylation,[172] although in that work the polymeric peptide product was thermodynamically stable, and the **2→1** reaction was not favored.

By contrast, peptide formation and self-assembly was obtained when using F-NH_2 (**3a**) or Y-NH_2 (**3b**). We observed instant hydrogel formation after gently vortexing and sonicating (gelation was observed inside the sonication bath). It is noteworthy that without sonication (only vortexing) of the precursor solution, gelation was observed after 7 minutes, indicating that ultrasonic energy enhances the kinetics of the system. No gelation was observed without the addition of α-chymotrypsin into the system. Digital photos of macroscopic transitions are available in **Figure 7.1**. Monitoring the DF-OMe/F-NH_2 reaction by HPLC, it was identified that the tripeptide product (**2a**) reached the highest yield conversion during 30 minutes. Gradually, the peptide hydrolyzed, giving rise to the formation of DF (**1**), while after 72 hours the percentage of **2a** was found to be around 10% (**Figure 7.2a**), which represents the equilibrium conversion for DFF-NH_2 (which is clearly below the

critical gelation concentration). Replacing phenylalanine (F-NH_2, **3a**) to tyrosine amide (Y-NH_2, **3b**), we observed that the lifetime of the gel could be reduced significantly, from 24 to 4 hours. HPLC analysis of the reaction revealed that DFY-NH_2 (**2b**) reached a complete conversion after 30 minutes. After 2 hours, the tripeptide was reduced to 40% and it completely disappeared after 10 hours (**Figure 7.2b**), showing that this peptide has a lower self-assembly propensity compared to DFF-NH_2. It should be noted that by using mass spectroscopy we observed the formation of the dimeric product (DFDF, 541.83) as well as some diketopiperazine (DKP, 263.1131) present in the starting material however only in low abundance. The HPLC chromatographs and mass spectra of all the reactions at different time points are available in the Appendix (**Figure 21-28**). Additional time dependent repeating HPLC experiments for the transient systems are available in Appendix (**Figure 29**).

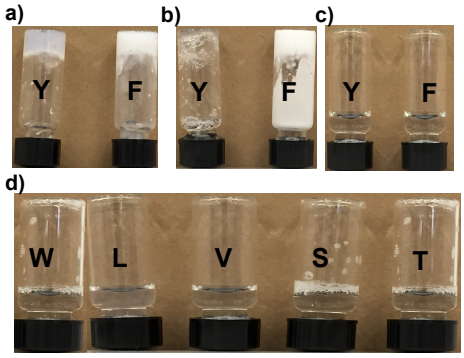

Figure 7.1 Digital photos of the samples containing 20 mM of aspartame, 40 mM of F-NH_2 or Y-NH_2 and 1 mg chymotrypsin in 1 ml sodium phosphate buffer (100 mM pH 8) **a)** with and **b)** without ultrasonic exposure, **c)** Samples (solutions) containing 20 mM of aspartame, 40 mM of F-NH_2 or Y-NH_2 without the addition of chymotrypsin and **d)** samples (solutions) containing 20 mM of aspartame, 40 mM of other nucleophile amides (W, L, V, S, T) and 1 mg chymotrypsin in 1 ml sodium phosphate buffer (100 mM pH 8).

These results indicate that sequence-specific interactions played a major role for the formation of the transient product and may be used to achieve a pathway switch. We propose that the relatively long lifetime nanofibers observed for **2a** and **2b** are potentially less prone to enzymatic hydrolysis in their assembled state (i.e. delaying **2→1**).

In order to further investigate the temporary formation and degradation of the peptide nanostructures, Transmission Electron Microscopy (TEM) was used at different time points. **Figure 7.2c,e** shows the precursor **1**. In the case of DFF-NH_2, early stage TEM images show an entangled fibrillar network. The length of the fibers was found to be <7 μm (**Figure 7.2d**). After 7 hours considerable shortening of fibers was observed (**Figure 7.2e**). At this stage, **2a** remained in the gel phase due to the presence of 70% of the tripeptide. After 48 hours we noticed further shortened fibers of approximately 1-2 μm in length (**Figure 7.2f**), where the concentration of the tripeptide was found to be around 20%. Finally after 72 hours, at a conversion of ~10%, short fibers remained visible (**Figure 7.2g**). The formation and shortening of the supramolecular architecture provides strong evidence of a dynamically unstable system.

TEM was also used to probe the structural changes at the microscopic level in the case of DFY-NH_2 (**2b**). Initially, TEM revealed an entangled fibrillar network of approximately 7-8 μm of length. After 4 hours the fibers broke down to about 3 μm as the tripeptide remained in the gel phase of a concentration 30%. After 8 hours further shortening of fibers was observed and after 24 hours spherical aggregates were formed (**Figure 7.2h-l**) corresponding to the complete hydrolysis, suggesting that they represent DF.

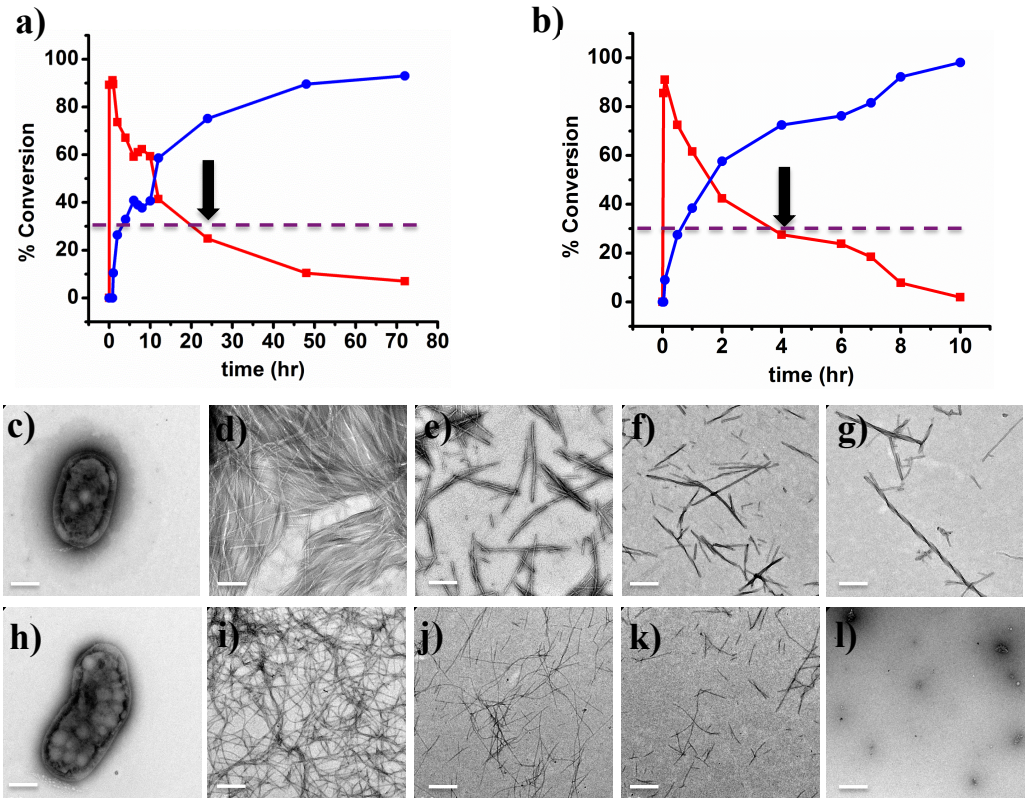

Figure 7.2 a,b) HPLC analysis of **2a** and **2b** product formation and degradation with the red line representing DFF-NH_2 or DFY-NH_2 and the blue line representing DF. The black arrow represents the gel-to-sol transition and the dotted purple line the critical aggregation concentration. **c-g)** TEM pictures of aspartame (**1**) and **2a** tripeptide product after 0.08, 7, 48 and 72 hours respectively and **h-l)** TEM pictures of **1** and **2b** tripeptide after 0.08, 4, 8 and 24 hours respectively, scale bar 500 nm.

The transient supramolecular reconfiguration and gelation could be repeated up to three cycles, however the conversion to transient tripeptide product (**2a)** reduced to 70 and 30% respectively, while for **2b** reduced to 27 and 10%, which was most likely related to the accumulation of DF in the system, which is the competitive reaction (waste product). Microfluidic devices would be of a great importance to constantly refuel the syetems and keep the transient products in high yield (**Figure 7.3a,b**).

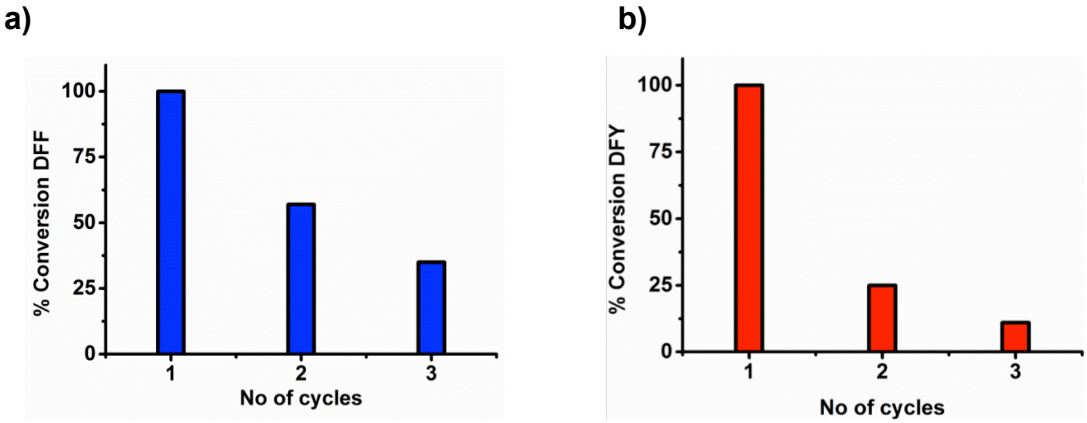

Figure 7.3 HPLC graph showing refuelling experiment for **a)** DFF-NH_2 and **b)** DFY-NH_2 tripeptide after the addition of 1 equivalent of aspartame (20 mM) after 24 hours.

7.3.3 Transient supramolecular interactions

In order to probe insights into the temporary supramolecular interactions we used FT-IR to follow the transient β-sheet-like arrangement of the amide groups.[12] No hydrogen bonding type interactions were found for **1*** in the amide region indicating that the structures observed by TEM are dis-organized aggregates. Upon trans-acylation and assembly for **2a,** a strong peak at 1648 cm^{-1} was identified, suggesting hydrogen-bonded network with limited long-range order.[173] Additionally, a peak

assigned to the carboxylate group of the side chain of aspartic acid was found at 1688 cm^{-1}.

Gradually, after 7 hours, the peak at 1648 cm^{-1} was disrupted and after 72 hours was lost (**Figure 7.4a**), with the spectrum containing a small contribution to higher wavenumber of the 1688 cm^{-1} band compared to the aspartame spectrum. In contrast, FT-IR analysis of **2b** revealed a strong peak at 1624 cm^{-1}, suggesting formation of more ordered hydrogen bonding type interactions between the tripeptides. Additionally, a peak appears at 1647 cm^{-1}, as previously observed for **2a**. After 4 hours, the intensity of the peak for the β-sheet like arrangement was reduced, with the peak disappearing after 24 hours (**Figure 7.4b**). The FT-IR spectrum of 1mg/ml of α-chymotrypsin as a control experiment shows a very weak peak at 1624 cm^{-1} for hydrogen bonding type interactions.

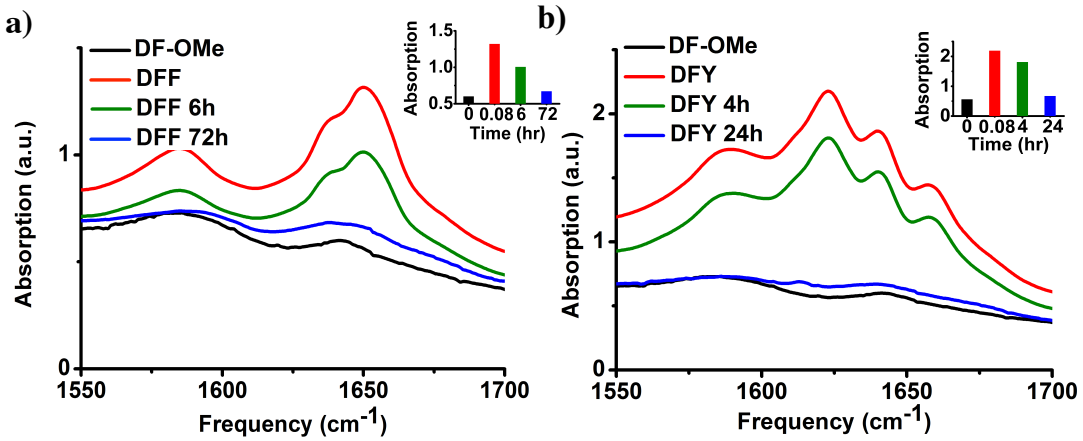

Figure 7.4 a-b) FT-IR spectra in D_2O of 20 mM of aspartame (**1**) in 100 mM sodium phosphate buffer pH 8 and **2a** and **2b** respectively at different time points. Inset graphs represent plots of the absorption values at 1648 cm^{-1} and 1624 cm^{-1} for **2a** and **2b** respectively.

To further investigate transient supramolecular reconfiguration and assembly we used Diffusion Ordered NMR Spectroscopy (DOSY NMR), which was not possible in the case of **2a** due to formation of some insoluble material. Following the reaction, it was revealed that the hydrodynamic radius of the molecule became bigger as the diffusion for **2b** reduced ($5x10^{-10}$ m^2s^{-1}). The diffusion constant was then increasing, as the amide hydrolysis appeared and was found to be close to that of the starting material (~6 $x10^{-10}$ m^2s^{-1}) (**Figure 7.5**).

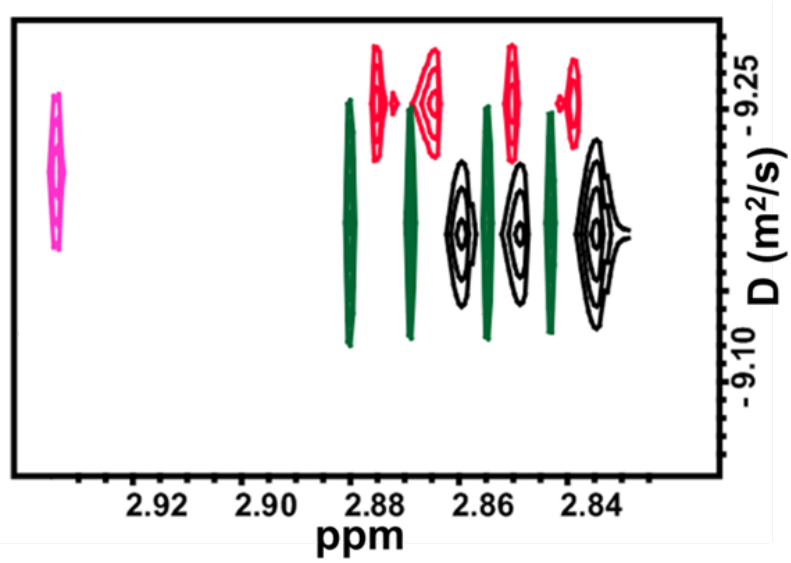

Figure 7.5 DOSY NMR spectra at 298K of 20 mM of aspartame (pink) and **2b** formation (red) and degradation (green after 8 hours and black after 24 hours) in D_2O pH 8.

7.3.4 Competitive transient biocatalytic self-assembly

The structural differences on supramolecular self-assembly and the control of the kinetics by chemical design prompted us to investigate a direct competition experiment between the nucleophiles (**3a, 3b**) in the presence of the enzyme catalyst and the acyl donor.

We used 20 mM of aspartame and 40 mM of the nucleophiles (20 mM of each nucleophiles) in the presence of 1 mg of α-chymotrypsin. As shown in **Figure 7.6a**, after 1 hour of the competitive reaction, **2b** was formed preferentially in a yield conversion of 70%, with 30% of **2a**. Gradually, both of the tripeptides started to break down and after 48 hours the concentration of **2b** was found to be 20%, while **2a** almost disappeared (~3%).

FT-IR spectrum of the competition experiments revealed a peak at 1624 cm^{-1}, which was previously observed for **2b** (**Figure 7.6b**). TEM experiments revealed sequential fiber formation and degradation (**Figure 7.6c-f**) with the fibers looking thin and less twisted close to the fibrillar nature of **2b**. It is not possible to say with certainty whether **2a** and **2b** form co-assembled or discrete structures. The remarkably similar degradation profile for both suggests that degradation mechanisms are linked. However, it is clear from our results that **2b** is preferentially formed as it reaches a higher yield, so in terms of molecular composition it outcompetes **2a**. These data therefore suggest that kinetic (rather than thermodynamic[62,67,135]) selection of nanostructures occurs. Histograms with the fibrillar length distribution for all the TEM experiments can be found at **Figure 7.7**. Additional TEM images for fibrillar formation and degradation in the case of **2a**, **2b** and for the competition experiments are available in **Figure 7.8**.

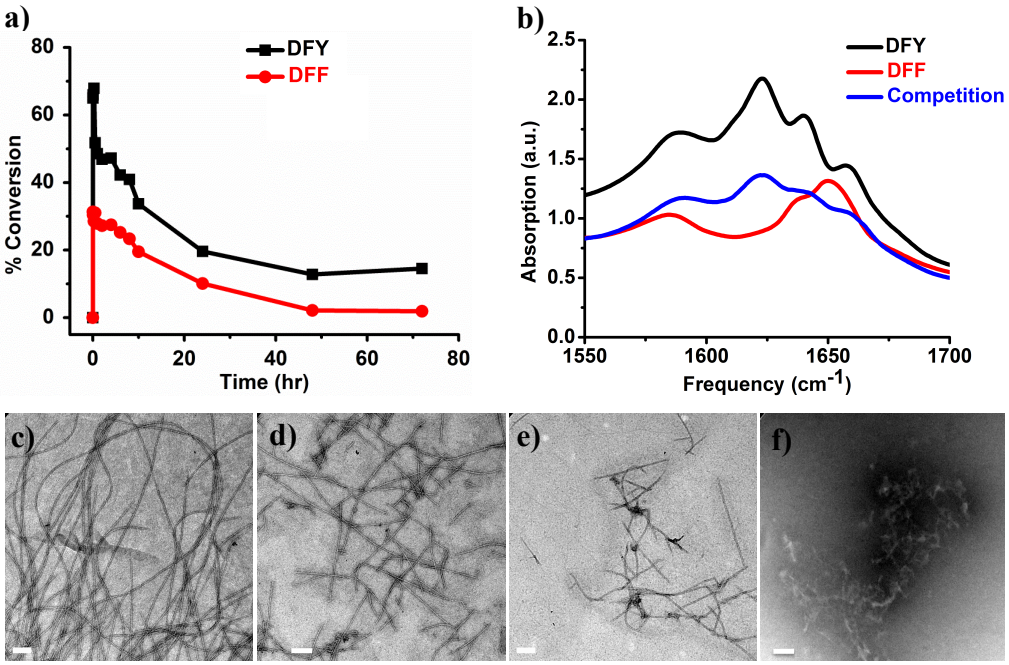

Figure 7.6 a) HPLC of the competition experiment between **2a** and **2b** in phosphate buffer pH 8 b) FT-IR of **2a**, **2b** and mixture after 0.08 hours (gel formation), and **c-f)** TEM images of the mixture after 0.08, 4, 24 and 72 hours respectively, scale bar 500 nm.

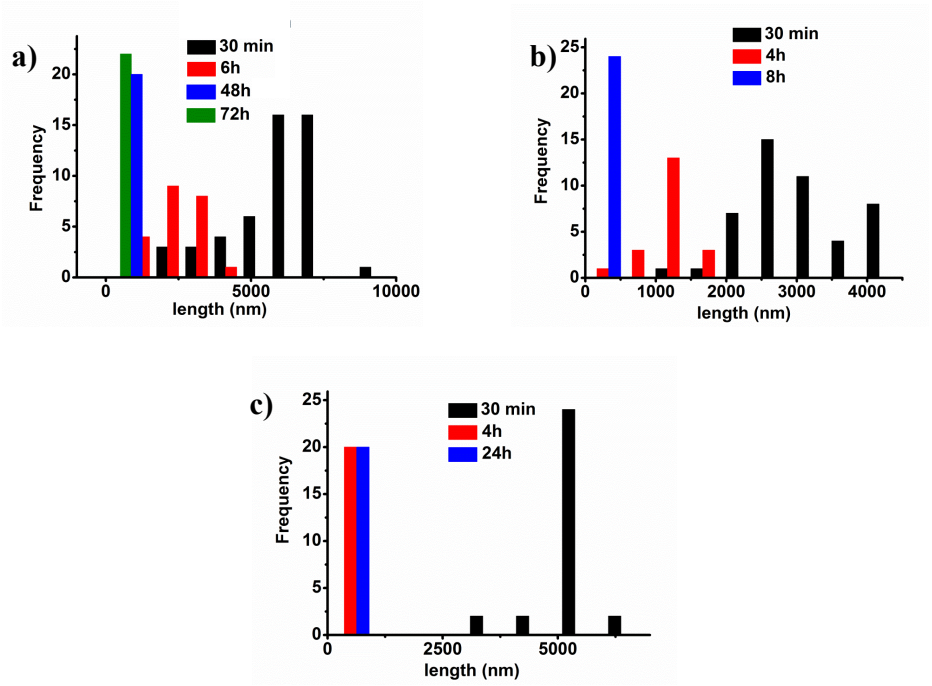

Figure 7.7 Histograms of the fibrillar length distribution of **a) 2a**, **b) 2b** and **c**) on the competition experiment at different time points.

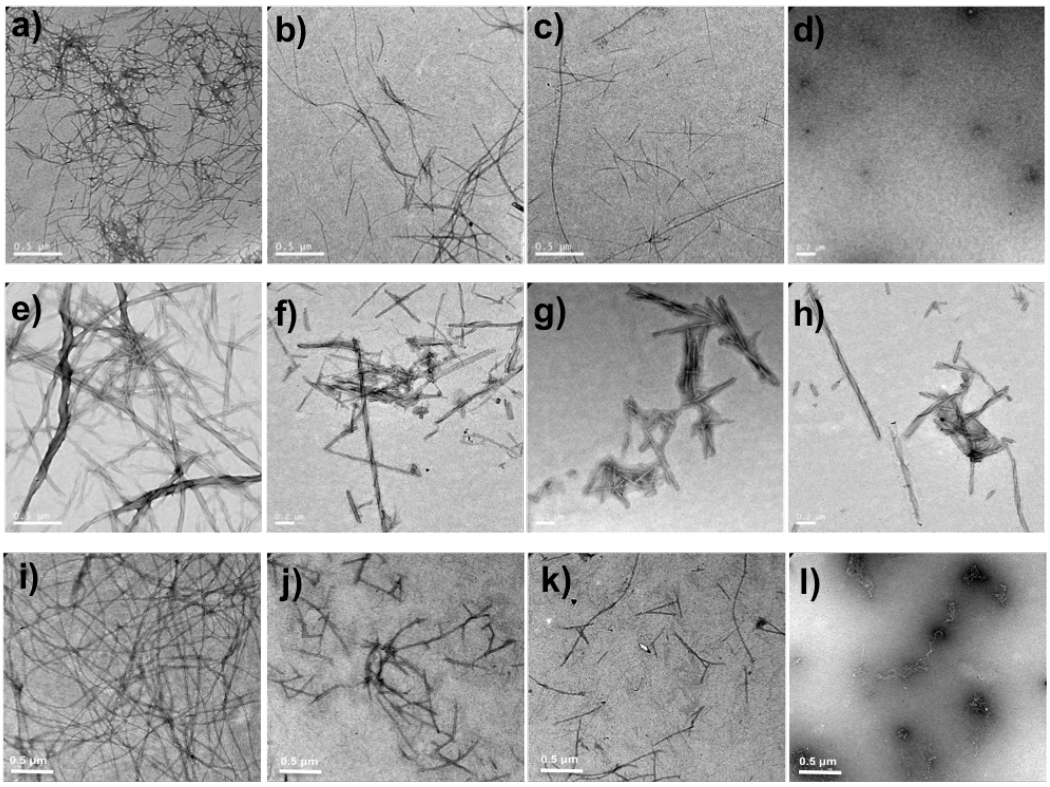

Figure 7.8 Additional TEM images of fiber formation and degradation for **a-d) 2b e-h) 2a** and **i-l)** for the competition experiments.

7.4 Conclusion

In summary, we have demonstrated sequence dependent pathway selection in *non-equilibrium* biocatalytic assembly, driven by the hydrolysis of the methyl ester of the sweetener aspartame, to drive the reaction. These dynamically unstable systems could be refuelled several times by addition of aspartame. In direct competition between F-NH_2 and Y-NH_2, the kinetically preferred product (DFY-NH_2) rather than the most stable product (DFF-NH_2) dominates, demonstrating kinetic, rather than thermodynamic selection of nanostructures. We demonstrate control of the kinetics and consequent lifetime of the nanostructures formed by chemical design. In future, time dependent rheological experiments in order to follow the whole process of tripeptide formation (gel state) and gradually hydrolysis (solution state) will be very insightful. Taking into consideration the different kinetic profiles for the nucleophiles used, these experiments may give a better understanding regarding the role of the mechanical properties in non-equilibrium transient peptide self-assembling systems. The work provides a step toward a better understanding of structural adaption in biological systems and opens up new opportunities to create supramolecular systems for non-equilibrium motility and shape control.

8. Directing peptide self-assembly using sound waves

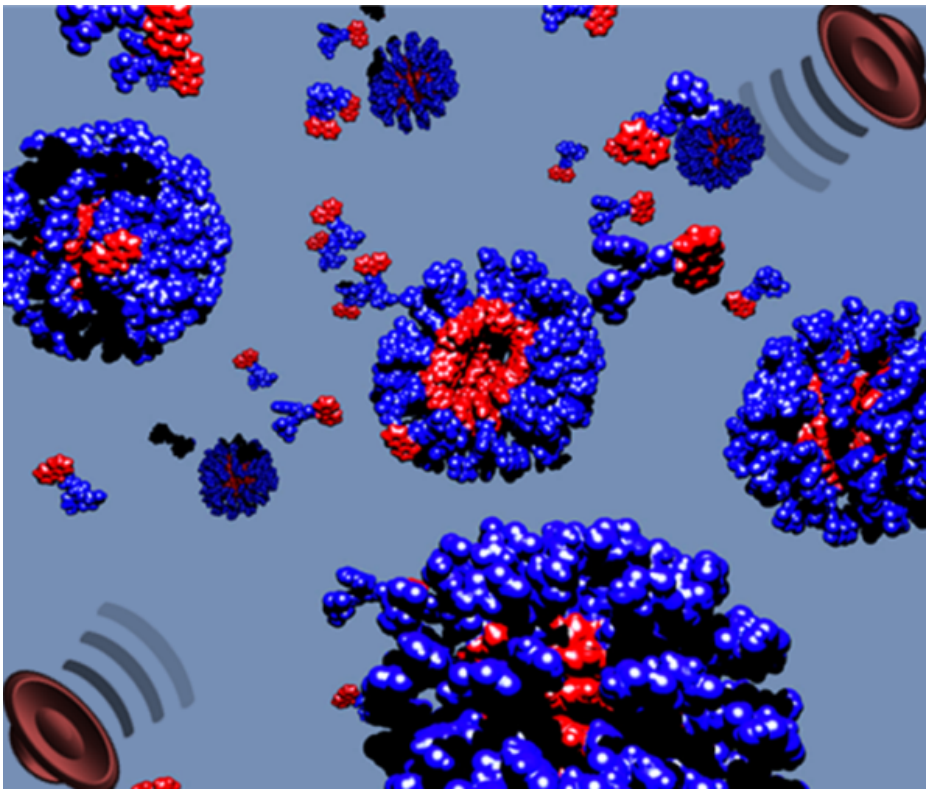

"*Project in collaboration with University of West of Scotland, Stuart Reid (Reader) and Peter Childs (PhD)*".

Objectives

The key research objectives of this chapter are to:

i. Demonstrate the effect of audible sound waves (<20,000 Hz) on molecular self-assembly.

ii. Investigate the effect of audible sound waves on supramolecular interactions (hydrophobic and H- bonding) that drive the assembly of aromatic dipeptide amphiphiles.

iii. Compare the effect of acoustic vibrations with thermal heating, interplaying with two different stimuli in order to lock/unlock suprmolecular states.

8.1 Introduction

Sound is a mechanical wave, a vibration that can be transmitted through a medium (air, water, organic phases) with different range of frequencies. Sound that is perceptible by humans has frequencies from about 20-20,000 Hz. Frequencies higher than 20,000 Hz, which is the limit of human hearing range, belong to ultrasonic region (see Section **2.3**). There is a widespread but rather unscientific view that the human body responds to low frequency mechanical vibrations, particularly those found in music and in massage more generally. It is increasingly clear, that cells are highly sensitive to a multitude of physical and mechanical cues presented by their environment.[174] However, the mechanism by which pressure waves affect biological processes remains questionable. It seems reasonable that effects on supramolecular interactions are of importance in this context.

Molecular self-assembly[175-185] can be directed using a variety of stimuli. Ultrasonic vibrations (>20,000 Hz) are commonly used to disrupt intermolecular interactions, to solubilize molecules and to disperse particles.[105] In addition, there are examples where ultrasound is used as an external stimulus to control self-assembly, which were discussed in detail earlier in the literature review (see Section **2.3**).[53-55] These studies involve high energy pressure waves with high frequencies (>20,000 Hz). Upon ultrasound exposure, supramolecular reconfiguration is observed mainly in organic media, with a few reports published to date in aqueous media.[58] While exact mechanisms are not completely understood, sonication time, cavitation and temperature are key factors in this process. In 2010, Tsuda and coworkers reported on the design of a supramolecular nanofibre that in chloroform becomes preferentially aligned to the propagation direction of *audible sound*,[59,60] indicating

that specific audible sound range frequency (100-500 Hz) may be used to influence supramolecular organisation. To date, there is no report of supramolecular (re)-arrangement upon audible sound exposure in aqueous media. The use of aqueous vibrations could become useful in supramolecular chemistry and even biology, by investigating the effect of low energy frequencies on supramolecular interactions and even cells responses.

It is the objective of this study to i) systematically investigate the role of pressure waves on molecular self-assembly ii) investigate the effect of pressure waves on supramolecular interactions (hydrophobic and H- bonding) that drive the assembly of aromatic dipeptide amphiphiles and iii) compare the effect of acoustic vibrations with thermal heating, interplaying with two different stimuli in order to lock/unlock supramolecular states.

Herein, we report on the effect of audible sound (100-1000 Hz) on an aromatic dipeptide amphiphile (Fmoc-YD-OH) in aqueous solution, which could undergo supramolecular reorganization to form bigger in size aggregates, as evidenced using fluorescence, FT-IR, DLS, DOSY NMR, AFM and TEM microscopy.

8.2 Materials and Methods

8.2.1 Fluorescence spectroscopy

Fluorescence emission spectra were measured on a Jasco FP-6500 spectrofluorometer with light measured orthogonally to the excitation light, with excitation at 280 nm and an emission data range between 300 and 600 nm.

8.2.2 Atomic force microscopy (AFM)

For AFM experiments see Section **6.2.5**.

8.2.3 Transmission Electron Microscopy (TEM)

For TEM experiment see Section **3.2.4**.

8.2.4 Dynamic light scattering (DLS)

30 mg of the dipeptide was dissolved in 3 ml phosphate buffer (100 mM) in pH 8 and filtered with a 0.45 mm Anotop filter. The samples were treated with sound for 60 min and transferred to borosilicate glass cuvettes for scattering measurements. DLS experiments were carried out using a 3D LS spectrometer (LS instruments) using vertically polarized He–Ne laser light (25 mW, with a wavelength of 632.8 nm) with an avalanche photodiode detector at a scattering angle of 90^0.

8.2.5 Diffusion Ordered NMR Spectroscopy (DOSY)

For DOSY experiments see Section **7.2.5**.

8.3 Results

8.3.1 Spectroscopic evidence of the effect of sound on molecular self-assembly

We synthesized the aromatic dipeptide amphiphile Fmoc-YD-OH (**Figure 1a,** Appendix **Figure 30**) with the expectation that sound waves may affect the relative importance of hydrophobic/stacking interactions among the aromatics and H-bonding type interactions between the dipeptide backbones. In order to investigate the effect of sound waves, we used a small portable speaker (X-Mi X Mini II 2nd Generation Capsule iPhone), which was connected with a smart phone (iPhone 5) (**Figure 8.1b)**. The audible sound frequencies (100-1000 Hz) were provided by an Apple application called Tune Generator. The phone calibration was achieved using a laser calibrator indicating highly accurate frequencies (**Figure 8.1c,** Appendix**, Figure 31, 32)**.

In order to acquire insights into the supramolecular reorganization induced by pressure waves, we used a variety of spectroscopic techniques. 20 mM of the dipeptide was dissolved in 100 mM phosphate buffer at pH 8, forming macroscopically a transparent solution. We used an optical cuvette, which contained 1 ml phosphate buffer pH 8 of the Fmoc-dipeptide (0.02 M). The portable speaker was located inside in the fluorometer instrument and was fixed 2 cm above the cuvette. The distance of the speaker to the cuvette was fixed in order to avoid the vibrational effect of the speaker to the cuvette, causing possibly different mechanical effects. The Fluorescence emission spectra (**Figure 8.2a**) principally monitored the emission of the fluorenyl moieties, and in this case displayed two characteristic peaks, a narrow band at 320 nm (monomeric state) and a relatively broad, red-shifted structure displaying maximum at 380 nm (excimeric state), which was previously

assigned to micellar formation.[123] Exposing the Fmoc-dipeptide to different frequencies ranging from 100-1,000 Hz for 60 minutes, a different response was observed. The fluorescence intensity for both the characteristic peaks (320 and 380 nm) decreased, as the frequency was increased. More specifically, in the highest frequency (1,000 Hz), the fluorescence intensity was decreased from 710 to 525 a.u. (320 nm peak) and from 310 to 200 a.u. (380 nm peak) respectively (**Figure 8.2a**). These observations suggested that the fluorophores are aggregating, promoting supramolecular aggregation, arised from liquid vibrations.

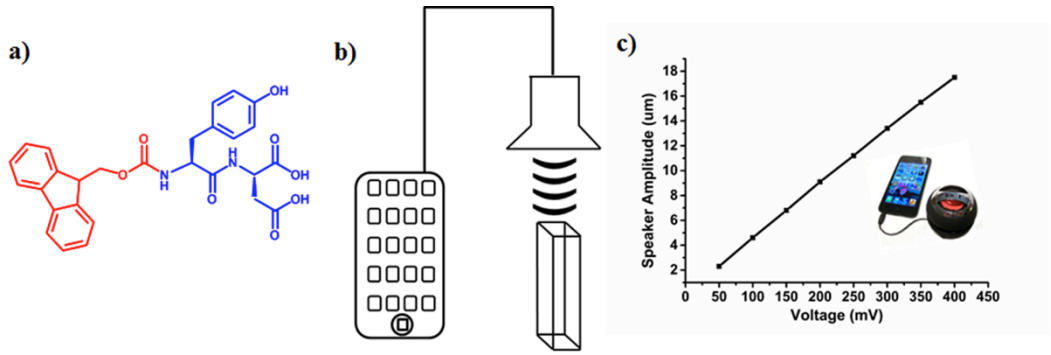

Figure 8.1 a) Chemical structure of the audible sound-responsive Fmoc-dipeptide **b)** Experimental set up **c)** Plot of the speaker amplitude *versus* the voltage in 1,000 Hz.

To further support the above observations of supramolecular aggregation, Dynamic Light Scattering (DLS) experiments were performed. DLS analysis of the Fmoc-dipeptide in phosphate buffer pH 8 (0.02M) revealed that the solution contained self-assembled nano-objects with an average hydrodynamic radius of 670 nm. Filtering of the solution, led to the formation of monodisperse system, showed an average hydrodynamic radius of 60 nm. Exposing the solution to sound waves of different frequencies (100, 250, 500, 1,000 Hz) for 60 minutes, the hydrodynamic radius increased from 60 to 80, 90, 100, 120 nm respectively (**Figure 8.2b**). Notably, the

size of the aggregates before audible sound exposure and upon 1,000 Hz doubles in size, indicating that in higher frequencies, sound promotes formation of larger aggregates.

FT-IR spectroscopy was also used in order to investigate the effect of sound vibrations on H-bonding interactions. The FT-IR spectrum of the dipeptide prior to sound exposure, revealed two characteristic peaks, one at 1580 cm^{-1}, assigned to the carboxylate groups and a second at 1680 cm^{-1} for the stacked carbamate. There was not a remarkable difference on the FT-IR spectrum after sound exposure (from 100-500 Hz). However, in the highest frequency of 1,000 Hz, the carbamate (1680 cm^{-1}) and the carboxylate peak (1580 cm^{-1}) showed a noticeable difference (**Figure 8.2c**), as an enhancement for the intensity was observed. Overall, the spectroscopic results suggested that audible sound frequencies (<1,000 Hz) modulate supramolecular aggregation of aromatic peptide amphiphiles, by affecting in particular hydrophobic and to a smaller extent H-bonding type interactions.

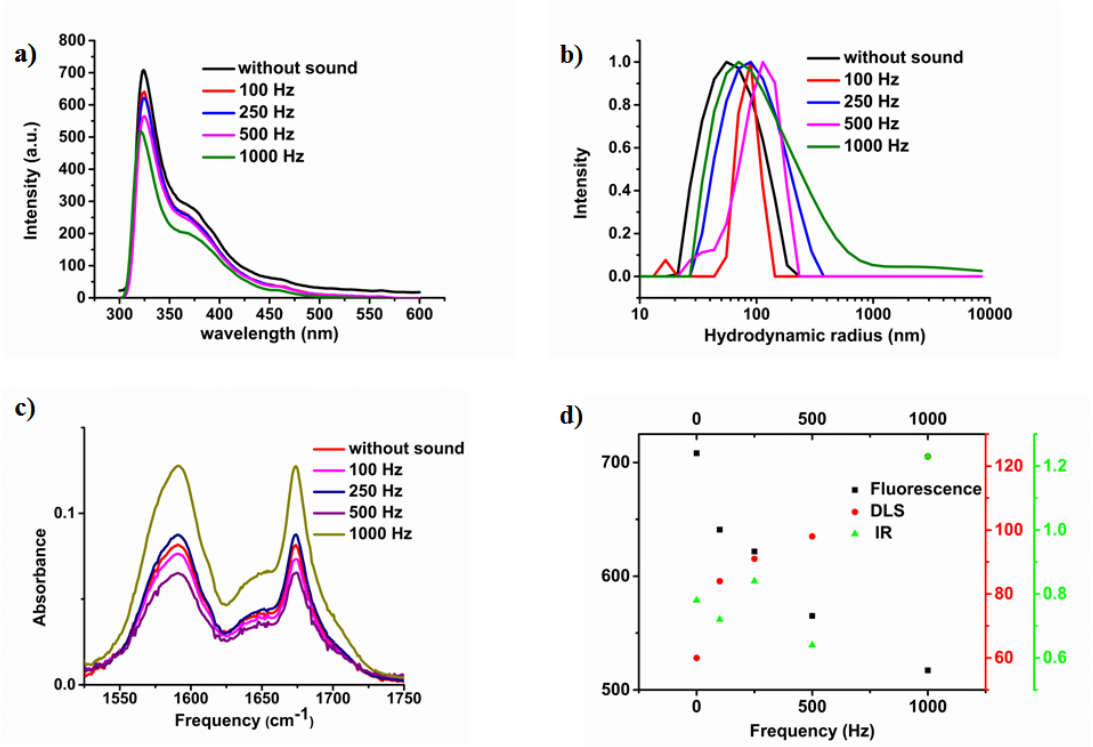

Figure 8.2 a) Fluorescence emission spectrum (excitation 280 nm) **b)** DLS data **c)** FT-IR absorbance spectrum without sound and after sound exposure at 100, 250, 500 and 1,000 Hz for 60 minutes and **d)** Plot of fluorescence intensity, FT-IR absorbance and hydrodynamic radius *versus* the selected frequencies.

Diffusion Ordered NMR Spectroscopy (DOSY) was used to further investigate the supramolecular aggregation in solution.[12] The diffusion coefficient of 20 mM of the Fmoc-dipeptide in phosphate buffer at pH 8 was found about 2.98 $x10^{-10}$ m^2/s. Exposing the dipeptide in pressure waves (1,000 Hz) for 60 minutes, we identified a difference in chemical shift mainly for the aromatic protons of the Fmoc group and the Hα protons of the dipeptide. The change of the chemical shift is evidence of the change of the environment and the molecular interactions. Indeed, the diffusion coefficient of the Fmoc-dipeptide after sound exposure was decreased (2.72 $x10^{-10}$ m^2/s), indicating that the hydrodynamic radius of the aggregates becomes larger, as derived from Stokes-Einstein equation (**Figure 8.3**).

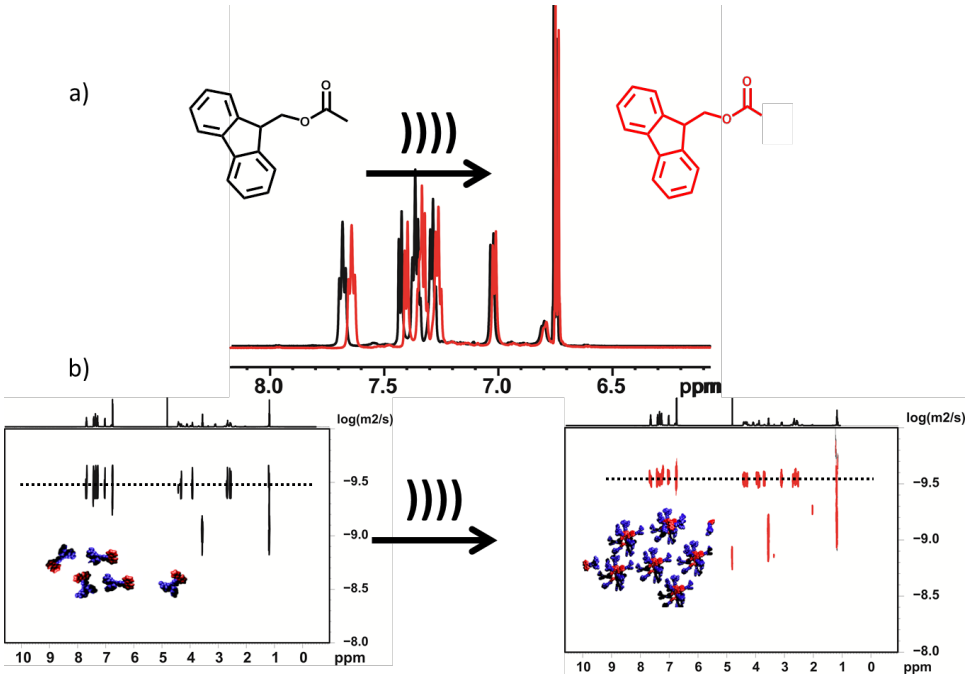

Figure 8.3 a) Overlay of ^{1}H NMR spectra of the selected aromatic region before (black) and after sound exposure (red) in 1,000 Hz for 60 minutes and **b)** DOSY NMR spectrum of the Fmoc-dipeptide before and after sound exposure at 298K.

8.3.2 Microscopic visualization of sound induced bigger in size aggregates

Analysis by Transmission Electron Microscopy (TEM) and Atomic Force Microscopy (AFM) (**Figure 8.4**) indicated that the nanometre - to micrometer aggregating self-assembled structure was directed audible sound waves. The Fmoc-dipeptide in phosphate buffer prior to sound exposure self-assemble into spherical aggregates, confirming the spectroscopic evidence (**Figure 8.3a,f**). In 1,000 Hz, (**Figure 8.3e,j**) the size of the aggregates was close to micrometre range (980 nm), showing the formation of spherical clusters. All the samples for the microscopy experiments were unfiltered.

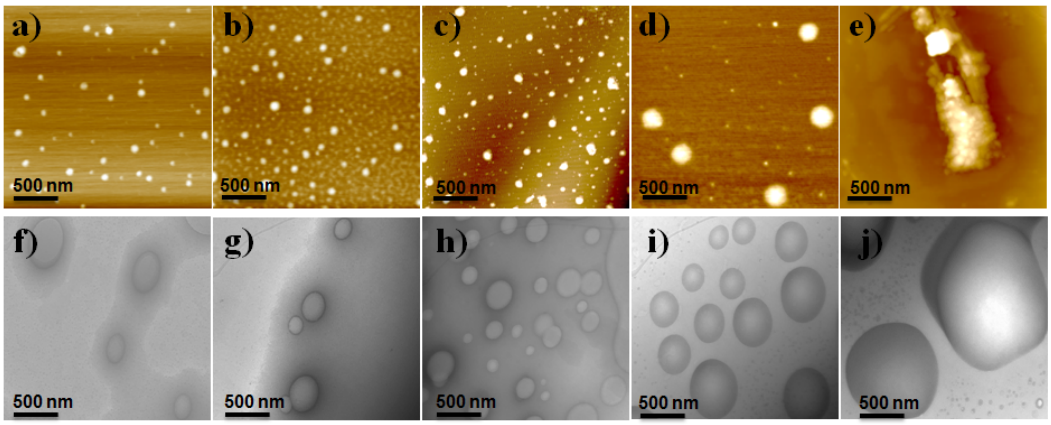

Figure 8.4 Microscopic visualisation of sound induced aggregation on Fmoc-protected dipeptide (Fmoc-YD-OH). **a-e)** AFM (Atomic Force Microscopy) and **f-j**) TEM (Transmission Electron Microscopy) images of Fmoc-Y-D-OH before **a, f**) and after sound exposure of different frequencies 100 Hz **b, g)**, 250 Hz **c, h)**, 500 Hz **d, i)** and 1,000 Hz **e, j)**.

8.3.3 Unlocking the supramolecular aggregation using temperature

Notably, when the sound was switched off, the fluorescence intensity was stable overnight as measured using fluorescence spectroscopy (available fluorescence spectar and histograms are available on the Appendix, **Figure 33**). Audible sound waves as an external stimulus offered into the system the appropriate energy and enable access to local minima. In order to test if the aggregated state represents local minima, increased temperature was introduced. As it shown in **Figure 8.5a**, monitoring the fluorescence spectrum of 20 mM of the Fmoc-dipeptide in buffer at pH 8 in 50^0C, the micellar peak at 380 nm disappeared and the structure was completely disassembled. The structure can be reorganized as the system was cooled down at room temperature, reverting back to the initial state.

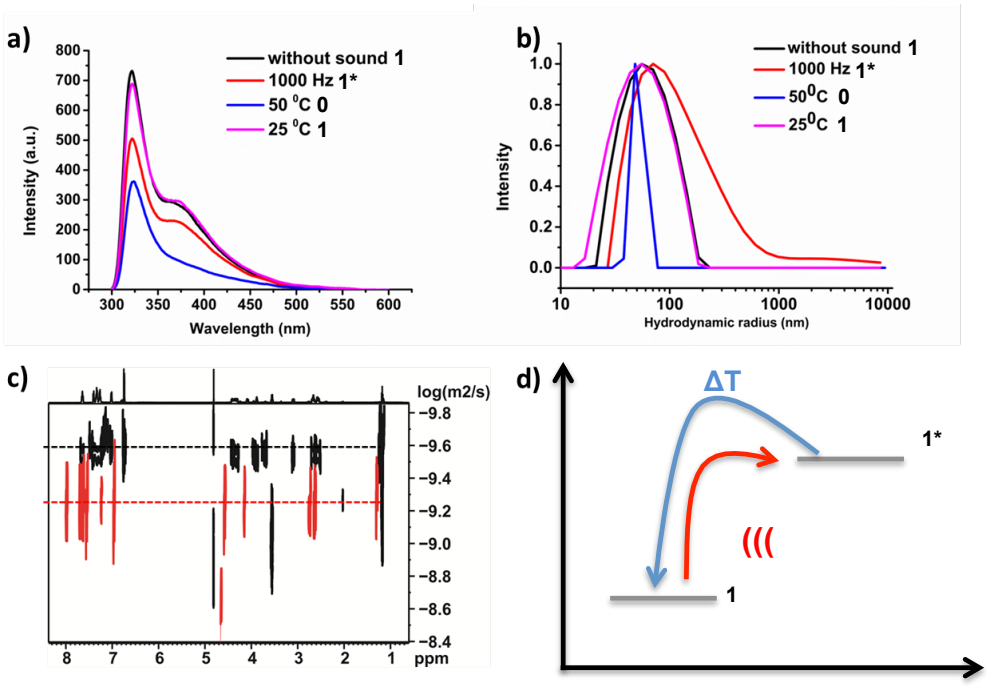

Figure 8.5 a) Fluorescence emission spectrum showing the effect of audible sound (1,000 Hz) and temperature on molecular self-assembly, **b)** Size distribution of spherical aggregates upon sound exposure (1,000 Hz) and in high temperature, **c)** Overlay of the DOSY NMR spectra in the highest frequency (1,000 Hz-black line) and in high temperature (red line), showing completely disassembled system, and **d)** Schematic representation of the effect of external stimuli (audible sound, temperature) on the molecular self-assembly.

The interplay between sound waves and temperature for structure reversibility was further confirmed using Dynamic Light Scattering (DLS) experiments. The hydrodynamic radius of the molecule was identified close to 50 nm in high temperature, whereas in 1,000 Hz was found around 120 nm. Additionally, DOSY NMR revealed that in high temperature the diffusion coefficient of the Fmoc-dipeptide was found around $5x10^{-10}$ m^2/s, whereas after sound exposure was $2.7x10^{-10}$ m^2/s.

8.4 Conclusion

We have demonstrated that upon audible sound exposure (100-1,000 Hz) the spherical aggregates of the aromatic dipeptide amphiphile Fmoc-YD-OH underwent supramolecular reorganization to from larger aggregates. Using a variety of spectroscopic and microscopic techniques, we observed that the dipeptide showed different acoustic response in different frequencies. Audible sound waves gave rise to a local increase of acoustic pressure, resulting also in a local increase of temperature causing supramolecular (re)-organisation of nanostructures. Compared to the ultrasonic (80,000 Hz) responsive systems that were developed in **Chapters 3** and **4**, where the cavitation phenomenon (formation of bubbles - high temperaure) had a great impact on the supramolecular transitions observed, in this **Chapter** the use of lower energy frequency oscillating pressure waves resulted in the formation of larger aggregates.

The results provide a first step towards rational use of audible sound to control and direct molecular self-assembly. In addition, this would open up opportunities to provide greater objectivity in this area, by manipulating frequencies in a highly controlled manner and observing molecular responses. In this way, we would have a potential route to investigation of many aspects of the reactions of biomolecular assemblies and cells to vibration with potential revolutionary consequences for health care and origin of life studies.

9. Conclusion and Future research

9.1 Conclusion

The biological world consists of a variety of self-organized assemblies. The complexity of biological structures arises from chemical diversity of building blocks dynamically interacting through a balance between thermodynamic and kinetic aspects. It is still challenging for chemists to design supramolecular systems that can adapt, respond, change and reconfigure according to the environmental changes, by interplaying between thermodynamic or transient (kinetic) supramolecular pathways. The objective of this research was to design minimal supramolecular systems, inspired by more complex biological machinery that can be directed by specific supramolcular routes and stimuli.

In particular, it focused on the effect of ultrasound (**80 KHz**) on molecular self-assembly, showing anisotropic changes on tripeptide arrangement (**Chapter 3**) or transiently driven supramolecular reconfigurations (**Chapter 4)**. This was achieved by using tripeptide hydrogels or organogels by varying the amino acid stereochemistry (D-L-L) in the N-terminus of the peptide sequence used. Exposure to ultrasound resulted in highly oriented tripeptide **gel** nanostructures (nanofibres, nanotubes), accompanied with significant enhancement of supramolecular chirality, and hydrogen bonding type interactions, depending on the peptide sequence and solvent environment (**Chapter 3)**.

The first example of using ultrasound to transiently control supramolecular self-assembly was reported in **Chapter 4**. This was demonstrated by using two clearly similar in structure aromatic dipeptide amphiphiles, with different electron density properties and thermal behaviour, giving rise to an altered relative contribution of aromatic and hydrogen bonding type interactions. Ultrasonic energy was used in this

case to achieve transient reorganization of supramolecular nanostructures (fibres to spherical aggregates or tapes to twisted fibres), which revert back to the original state when sound is switched off, providing a step towards a rational use of ultrasound to fuel transient energy dissipating supramolecular systems.

Thermodynamic and kinetic pathways on molecular self-assembly were also investigated *via* another trigger. Biocatalytic self-assembly is an attractive tool to direct supramolecular systems. As shown in **Chapter 5,** thermodynamically driven biocatalytically self-assembly can be used to design tunable nanostructures by simply regulating the electronic properties of phenylalanine, with electron donating or withdrawing groups. Thermodynamically driven biocatalytic self-assembly was further used to trigger peptide oligomerisations from simple dipeptide building blocks, resulting in nanostructure reconfiguration and sequence selection (**Chapter 6**). A reversible system of this type operated under thermodynamic control, with the formation of different peptide species, opens up opportunities for dynamic peptide libraries (DPLs). Differential component selection was identified upon mixing dipeptides in the presence of thermolysin. This observation was further investigated by operating the DPL experiments in different conditions, such as salts, solvents or combination of them. Interestingly, the additive experiments led to a remarkable enhancement of the conversions of the species formed, resulting in thermodynamically stable supramolecular networks. A number of new nanostructures were discovered.

In contrast with thermodynamically stable biocatalytic reconfigurations, a *non-equilibrium* transient supramolecular system is described in **Chapter 7**. In this case, structural adaption is achieved based on biocatalytic formation and hydrolysis of

self-assembling tripeptides, which catalyzed by chymotrypsin. The peptide sequence dictates the kinetics of the reaction and the consequent lifetime of the nanostructures formed. In the final Chapter of this thesis (**Chapter 8**), it was demonstrated the use of audible sound frequencies (<1,000 Hz) to trigger supramolecular aggregation of aromatic dipeptide amphiphiles, giving insights on the effect of pressure waves on supramolecular interactions.

9.2 Future Research

The conclusions drawn from this thesis have opened up substantial opportunities for further research. This section acknowledges the required improvements and set up a research agenda for future research. Having established the effect of high oscillating pressure waves on molecular self-assembly, the next obvious step is to investigate the effect of different frequencies and (ultra)-sound energies on the fabrication of nanomaterials, which may have applications in acoustics. Furthermore, from the last chapter of this thesis (**Chapter 8**), it was demonstrated that lower energy frequencies (audible sound frequencies, <1,000 Hz) might be used to affect molecular self-assembly. It will be interesting to take this a step further and investigate the effects on biological assemblies. For example, influence stem cells differentiation using aqueous vibrations will be of a great importance, as it is increasingly clear that cells are highly sensitive to a multitude of physical and mechanical cues presented by their environment, making sound a potential therapeutic tool for targeting different diseases.

Moreover, there is a significant effort from researchers to design and direct transient chemically fuelled self-assembling systems. There is a tremendous interest in developing man made analogues of such supramolecular systems, which provide

insights into the workings of biology's remarkable ability to adapt to changing environments. A continuous refueling of these systems with constant chemical energy still remains a challenge. Biocatalytic routes in combination with microfluidic devices are required to achieve *in situ* reactivation.

The combination of oscillating pressure waves to trigger directionality and alignment of peptide nanostructures (**Chapter 3**) with the use of enzymes to trigger biocatalytic transience on supramolecular systems (**Chapter 7**) might be a useful future research direction. It is known that the majority of bilayer vesicular structures produced from phospholipids formed hastily under certain conditions however is generally temporary biological machinery that rapidly reconfigure to the more stable hydrated crystals or other molecular shapes. The environment (conditions of formation), dictates the shape and size of the vesicles. It is challenging to perform transient biocatalytic reactions (minimalistic peptide self-assembly and enzymes) in the presence of lipid bilayers in order to investigate their effect on the kinetics of the reaction and the nanostructures formed. The oscillating pressure waves may be applied to direct and control the shape, the size and fusion of these supramolecular systems. "Transient morphogenesis" will be of great interest to mimic more complex biological processes and will probably give us a better understanding of fundamental processes in developmental biology.

Finally, Dynamic combinatorial libraries (DCLs) are prominent tools in chemists' hands for discovering the "unpredicted" and have given rise to the fabrication of many interesting molecules with emergent supramolecular properties. An example of purely peptidic libraries exchanging amide bonds has been reported in **Chapter 6**. It was shown that aromatic (**F_2, W_2**) and hydrophobic dipeptides (**L_2**) could be used to

trigger peptide oligomerisations, with the yields and the selection of the most thermodynamically stable supramolecular component to be dictated by the environment, such as salts and solvents. The screening of the whole sequence space of dipeptide sequences will be important, in order to investigate the behaviour of hydrophilic (**FS, FT, FQ**) or charged dipeptide sequences (**FD, FK, FR, FE**) on biocatalytic self- and co-assembly, which will probably give unexpected supramolecular architectures and properties. Replacing the enzyme with minimal peptide catalysts and design Dynamic Peptide Libraries (DPLs) using peptides to form and break other amide bonds will be tremendously interesting. This pathway will give a better understanding in the way that molecules form, adapt, respond and reconfigure according to the environment, as the advent of Darwinian evolution required the emergence of molecular mechanisms for the variation of the fitness.

Appendix

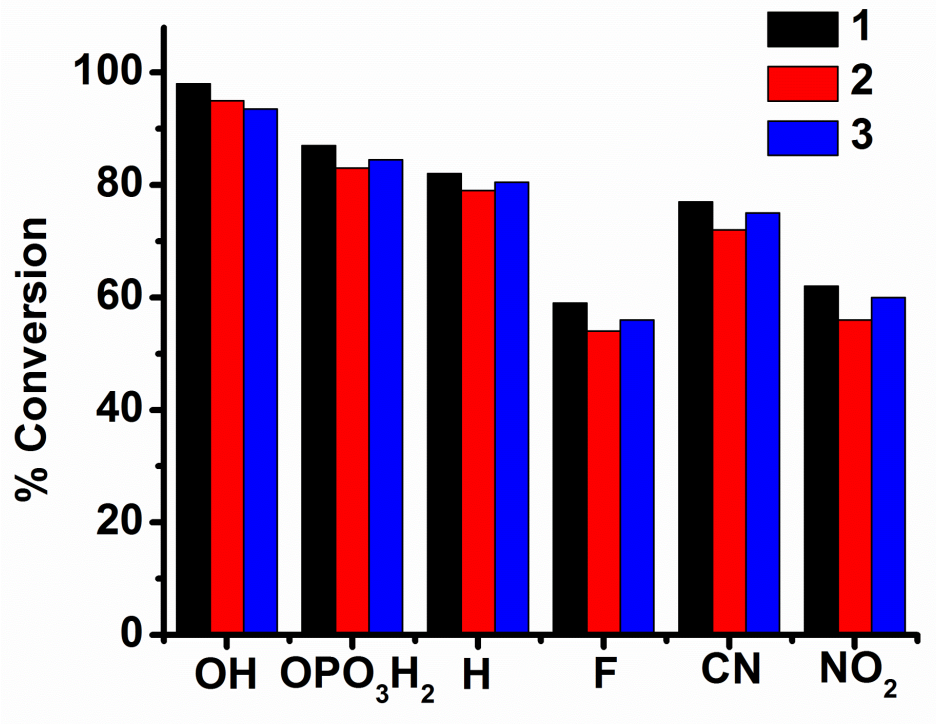

Figure 1 Histograms of HPLC conversion yield of the aromatic dipeptide amphiphiles Fmoc-Phe(4-X)-Phe-NH_2 for three repeating experiments after 24 hours of thermolysin addition.

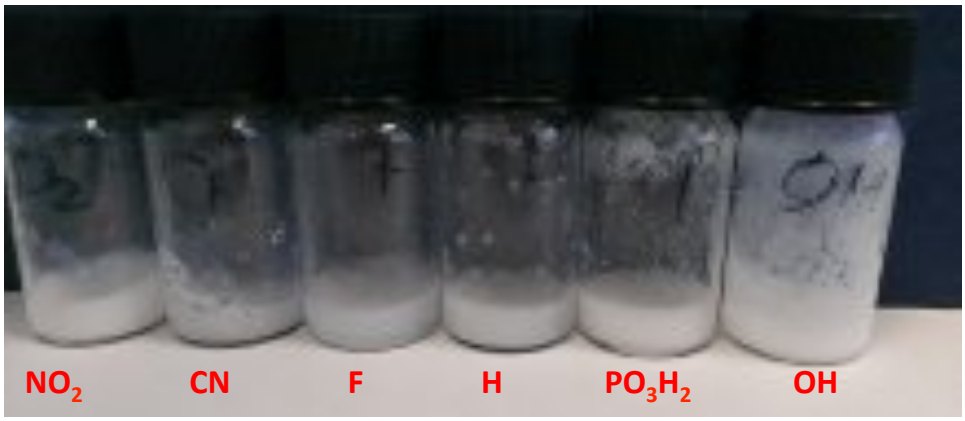

Figure 2 Macroscopically observed samples with different electronic substituents (Fmoc-Phe(4-X)-Phe-NH_2) after thermolysin adittion.

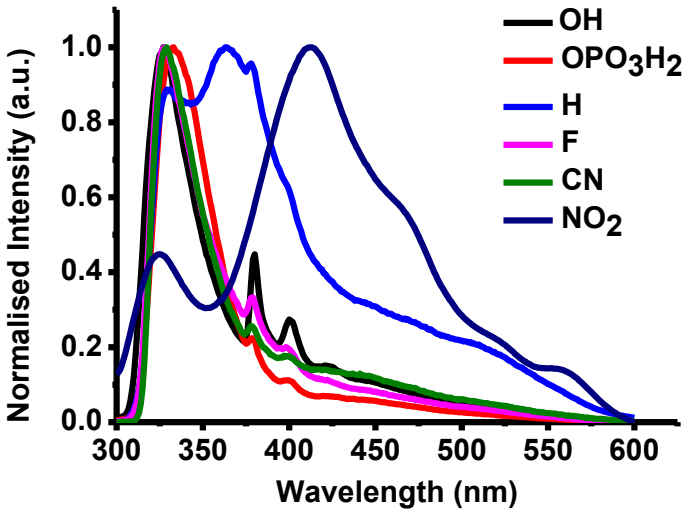

Figure 3 Fluorescence emission spectrum of Fmoc-Phe(4-X)-Phe-NH_2 dipeptide derivatives after 24 hours of thermolysin addition.

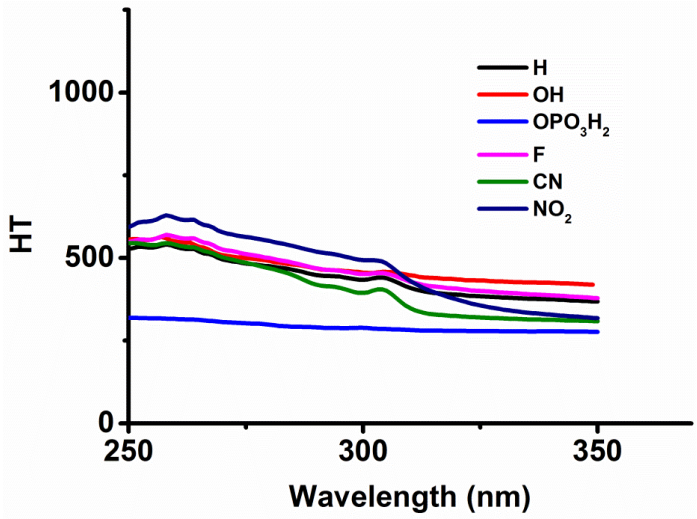

Figure 4 HT values for the CD experiments.

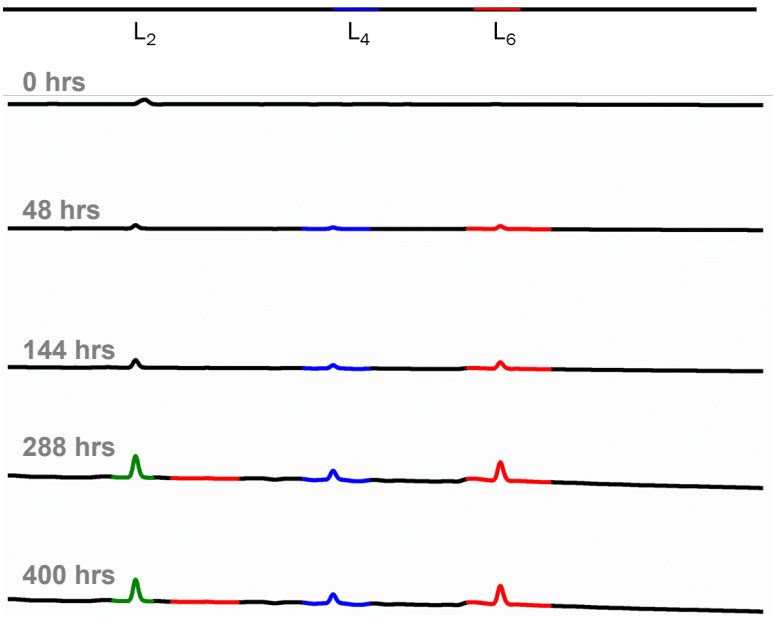

Figure 5 HPLC profile of 30 mM **L_2** prior to and after the addition of 1 mg thermolysin in 100 mM phosphate buffer pH 8 at different time points of the reaction.

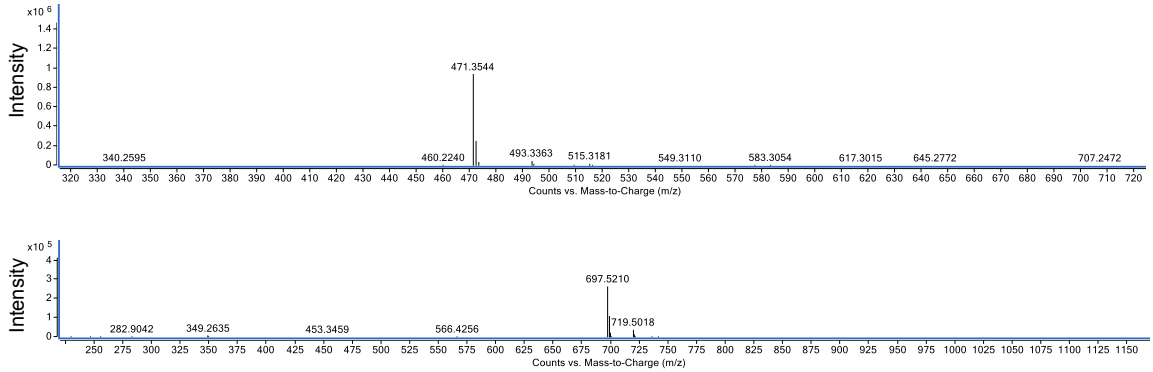

Figure 6 Mass spectra of **a L_4** and **b L_6** after the addition of 1 mg.mL^{-1} thermolysin.

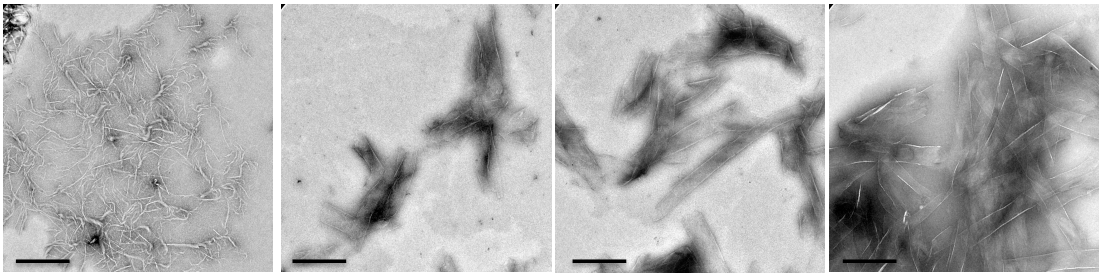

Figure 7 TEM images of $\mathbf{L_2}$ prior to and after the enzyme addition after 1, 3 and 8 days of the reaction, scale bar 500 nm.

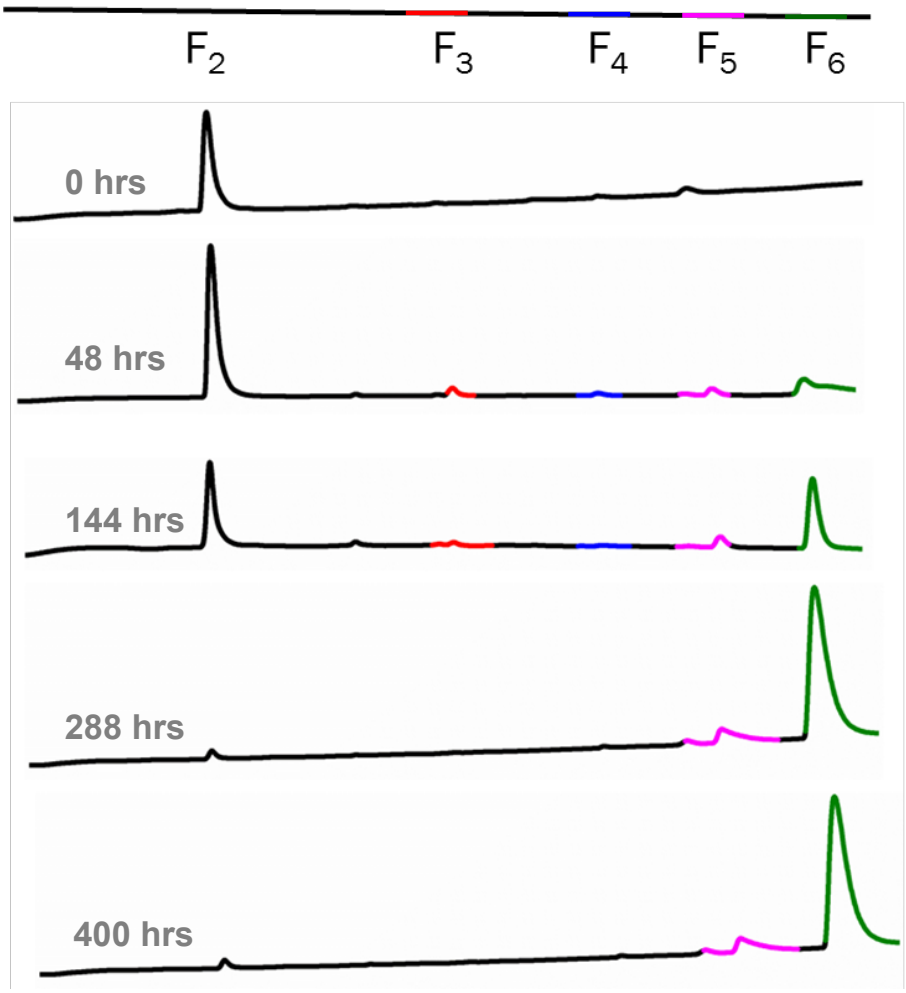

Figure 8 HPLC profile of 30 mM $\mathbf{F_2}$ prior to and after the addition of 1 mg thermolysin in 100 mM phosphate buffer pH 8 at different time points of the reaction.

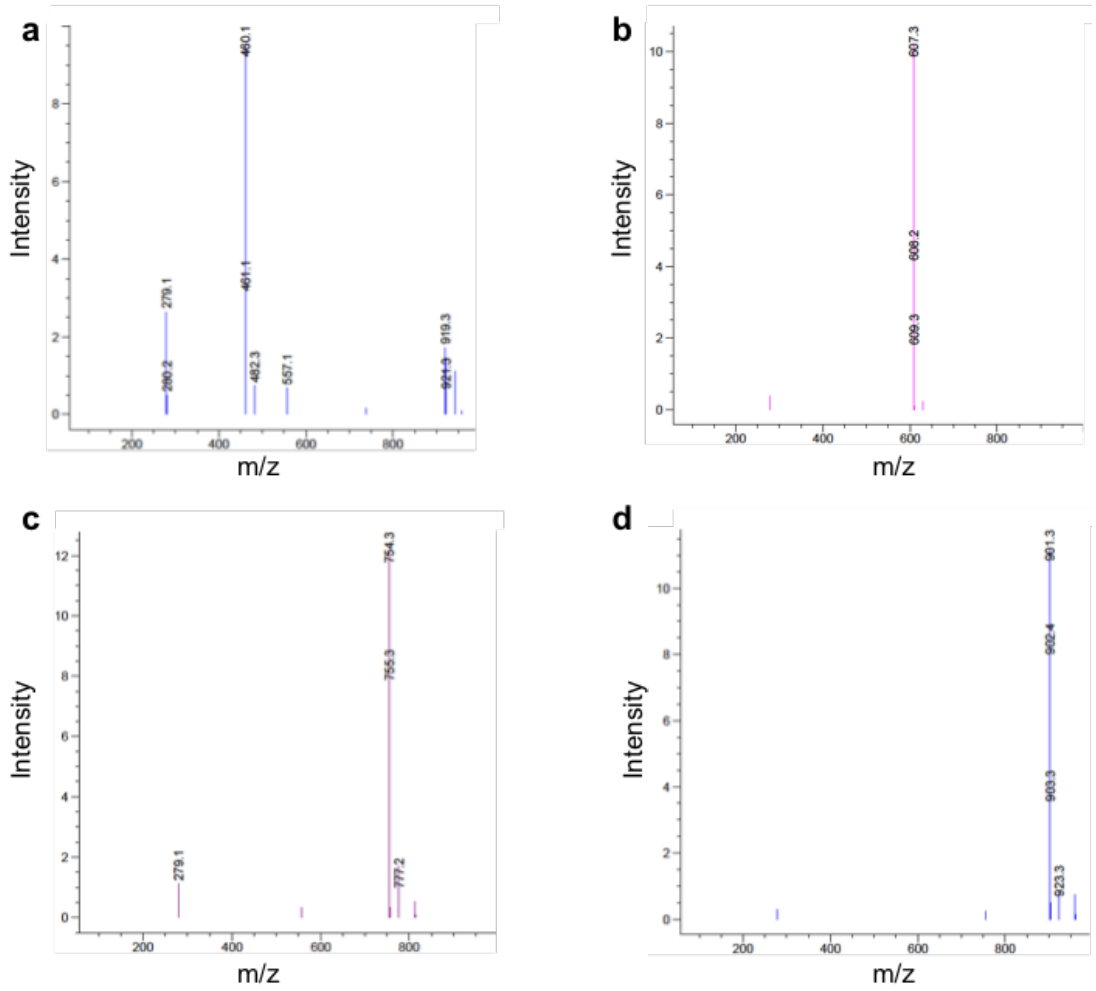

Figure 9 Mass spectra of the formation of phenylalnine oligomers in the $\mathbf{F_2}$ library after the addition of 1 mg thermolysin **a), $\mathbf{F_3}$, b), $\mathbf{F_4}$ c), $\mathbf{F_5}$ and d) $\mathbf{F_6}$.

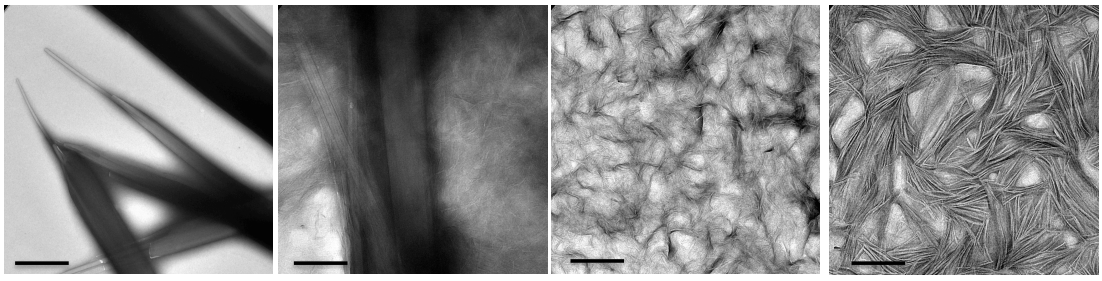

Figure 10 TEM images of $\mathbf{F_2}$ prior to and after the enzyme addition after 1, 4 and 12 days of the reaction, scale bar 500 nm.

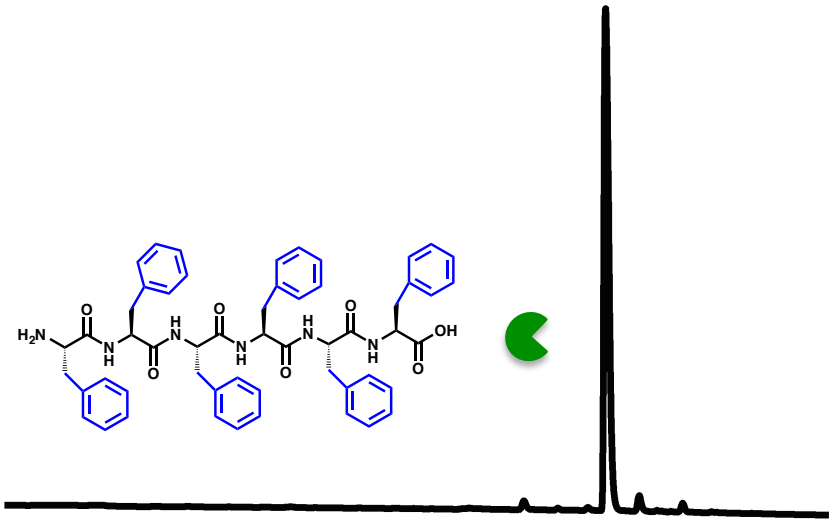

Figure 11 HPLC profile of 30 mM of $\mathbf{F_6}$ in phosphate buffer 100 mM pH 8 upon the addition of 1mg/ml thermolysin after 12 days of the reaction.

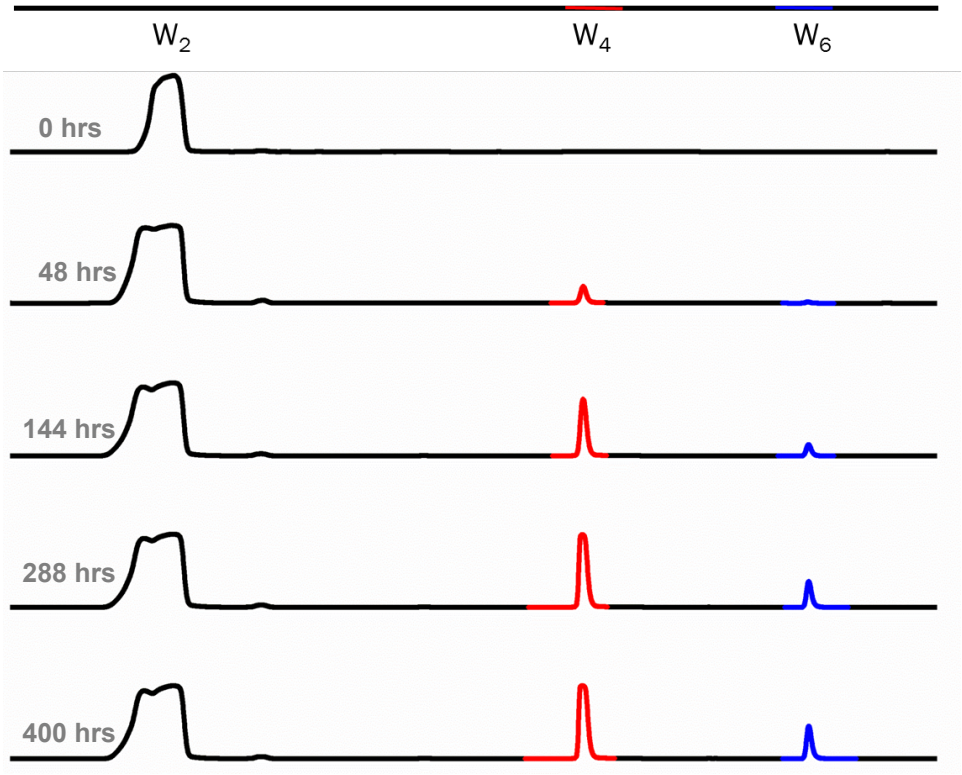

Figure 12 HPLC profile of 30 mM $\mathbf{W_2}$ prior to and after the addition of 1 mg thermolysin in 100 mM phosphate buffer pH 8 at different time points of the reaction.

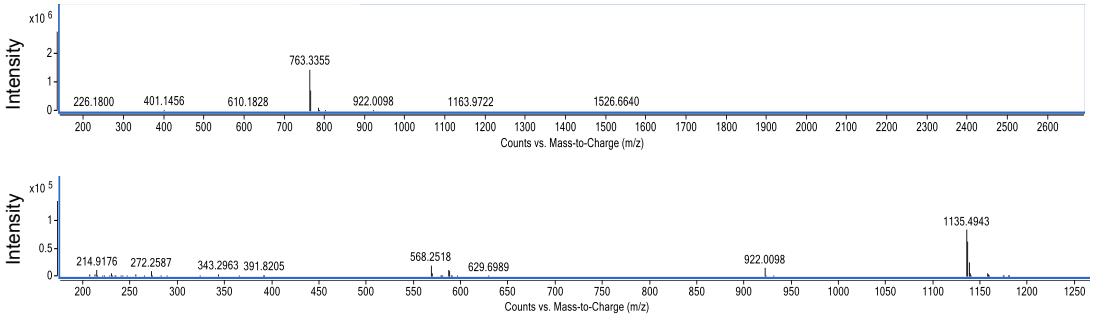

Figure 13 Mass spectra of $\mathbf{W_4}$ and $\mathbf{W_6}$ after the addition of 1 mg thermolysin.

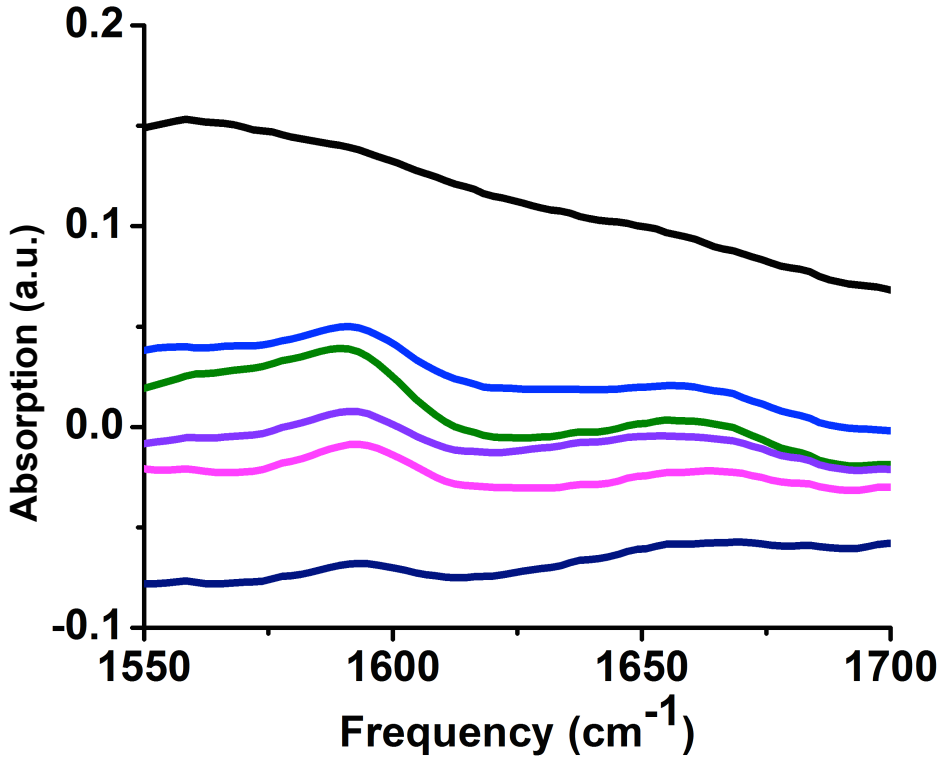

Figure 14 FT-IR spectra of 30 mM $\mathbf{W_2}$ after the addition of 1 mg thermolysin in the presence of 1M sodium salts, excluding sodium cetate for a better comparison (carboxylate peak at 1580 cm^{-1}).

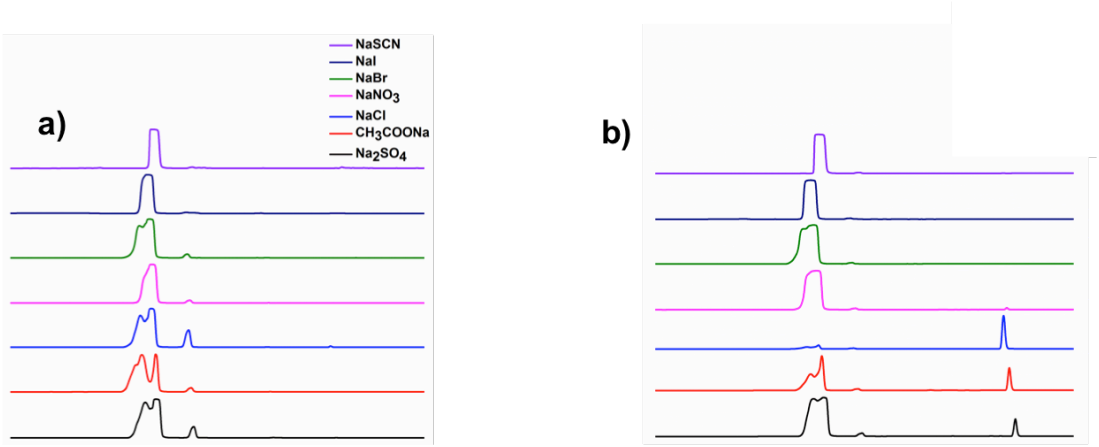

Figure 15 HPLC profiles of 30 mM W_2 upon the addition of 1 mg thermolysin with different salts in a) 80% THF and b) 80% ACN.

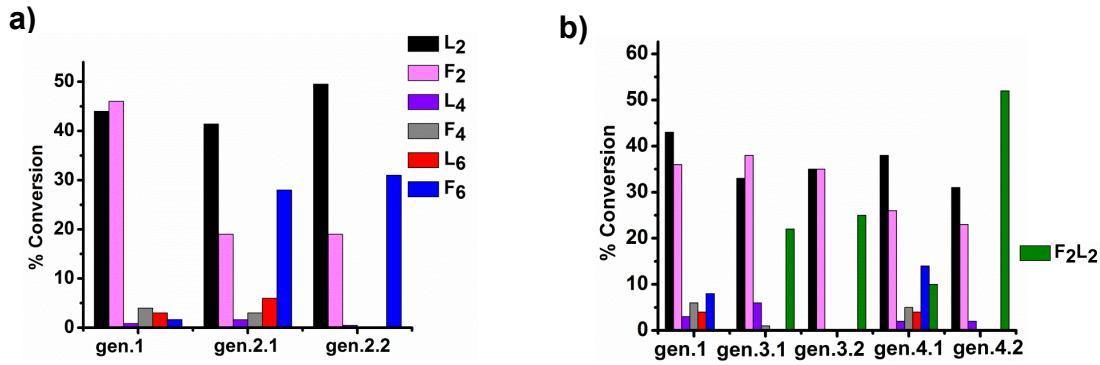

Figure 16 Histograms of the conversion yields of different peptide species fromed in the DPLs of 15 mM each of diphenylalanine (**F_2**) and dileucine (**L_2**) in the presence of 1 mg thermolysin pH 8 at different environmental conditions.

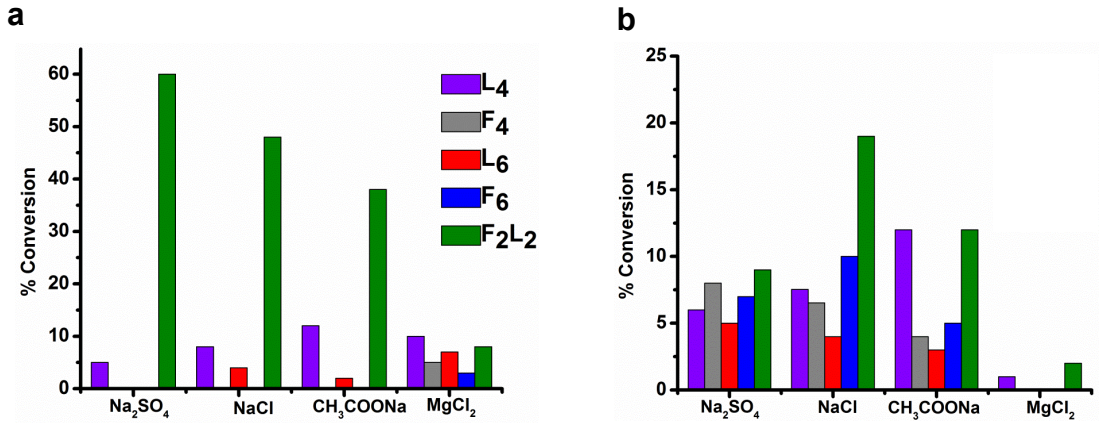

Figure 17 Histograms of % conversion yields of 15 mM **F_2** and 15 mM **L_2** in a 80% THF and b 80% ACN upon the addition of 1M different salts.

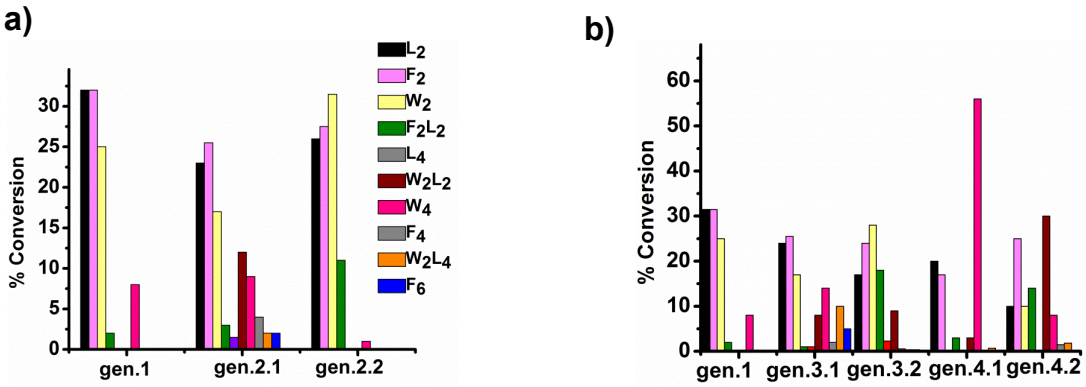

Figure 18 Histograms of the conversion yields of different peptide species fromed in the DPLs of 10 mM each of diphenylalanine (**F_2**), dileucine (**L_2**) and ditryptophan (**W_2**) in the presence of 1 mg thermolysin pH 8 at different environmental conditions.

Figure 19 Mass spectra of the formation of **a**) **F_2L_2** in 80% THF with 1M Na_2SO_4 of 15 mM **F_2** and 15 mM **L_2**, **b)** W_2L_2, **c**) W_2L_4 in 80% ACN of 10 mM **F_2** 10 mM **L_2** and 10 mM **W_2** upon the addition of 1 mg thermolysin.

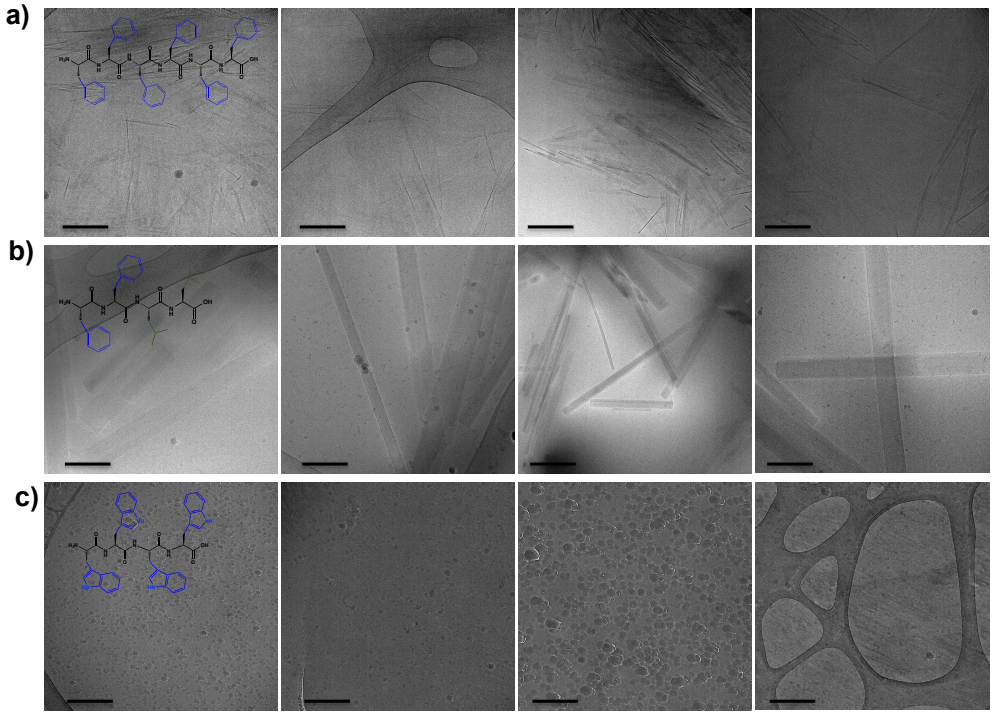

Figure 20 Cryo-TEM images of chemically synthesized **a)** $\mathbf{F_6}$, **b)** $\mathbf{F_2L_2}$ and **c**) $\mathbf{W_4}$ assembled in phosphate buffer 100 mM pH 8, scale bar 500 nm.

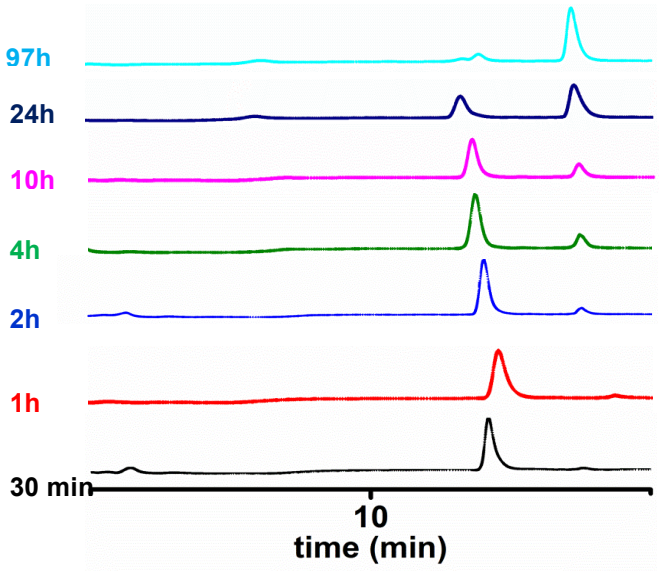

Figure 21 HPLC chromatograph of 20 mM of aspartame with 40 mM of H-Phe-NH_2 in the presence of 1 mg of chymotrypsin. The chromatographs are monitored at 225 nm.

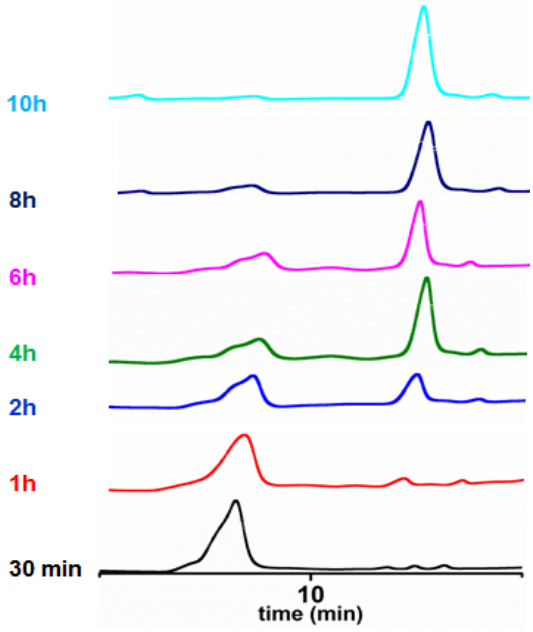

Figure 22 HPLC chromatograph of 20 mM of aspartame with 40 mM of H-Tyr-NH_2 in the presence of 1 mg of chymotrypsin. The chromatographs are monitored at 225 nm.

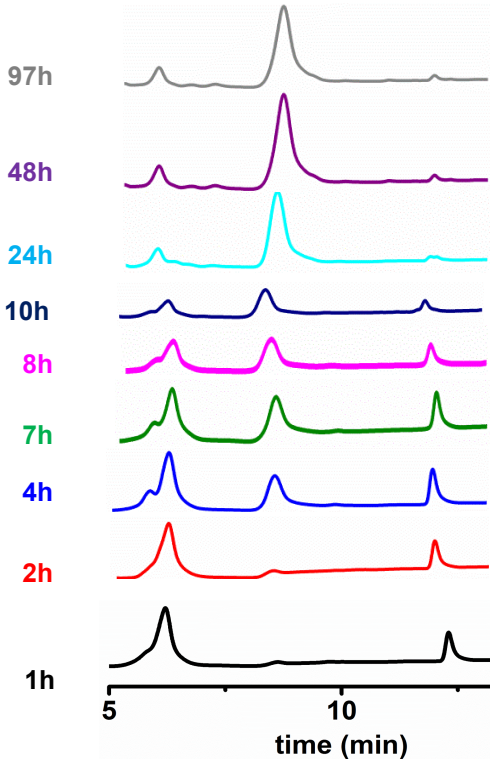

Figure 23 HPLC chromatograph of 20 mM of aspartame with 20 mM of H-Phe-NH_2 and 20 mM of H-Tyr-NH_2 in the presence of 1 mg of chymotrypsin. The chromatographs are monitored at 225 nm.

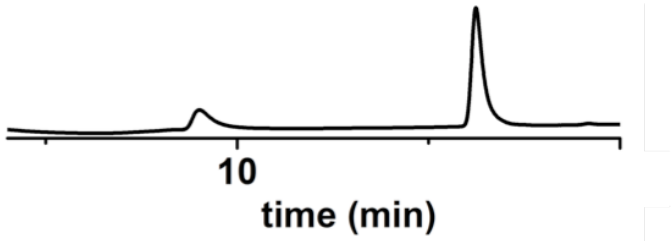

Figure 24 Representative HPLC chromatograph of 20 mM of aspartame with 40 mM of different amino acid amides (W, L,V, S, T) in the presence of 1 mg of chymotrypsin after 30 minutes of the reaction.

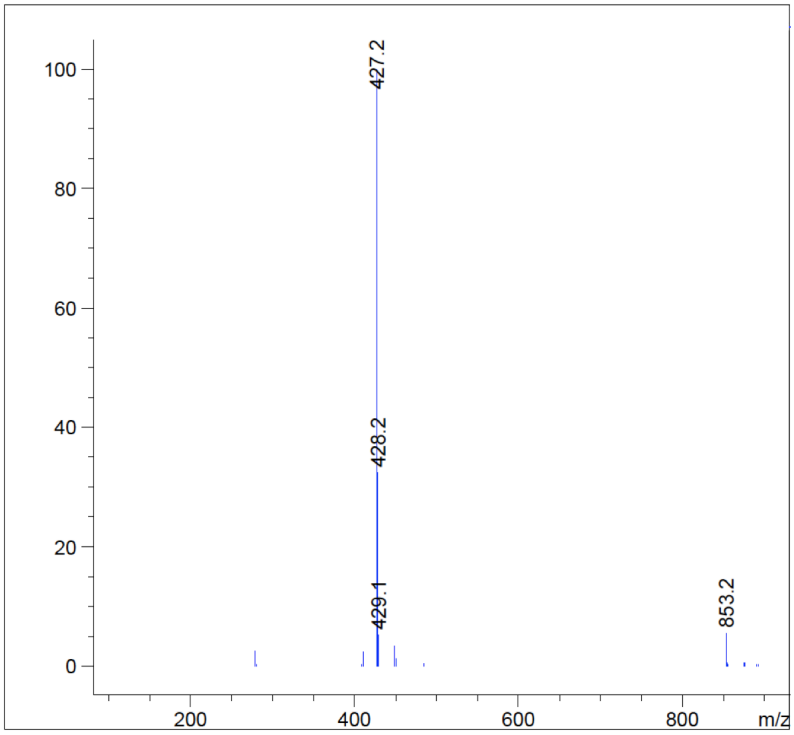

Figure 25 Mass spectrum of 20 mM of aspartame with 40 mM of H-Phe-NH_2 in the presence of 1 mg of chymotrypsin at 30 minutes of the reaction.

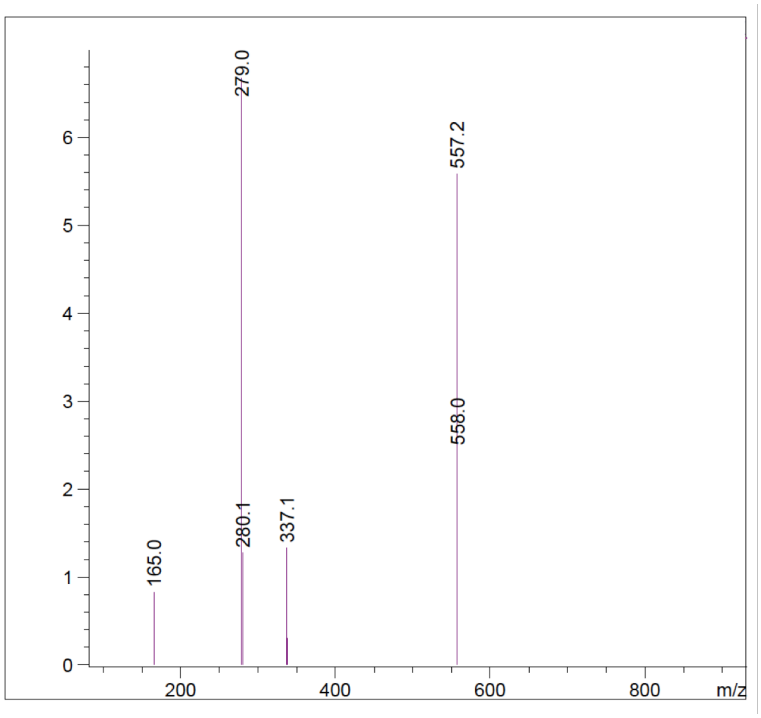

Figure 26 Mass spectrum of 20 mM of aspartame with 40 mM of H-Phe-NH_2 in the presence of 1 mg of chymotrypsin at 3 days of the reaction.

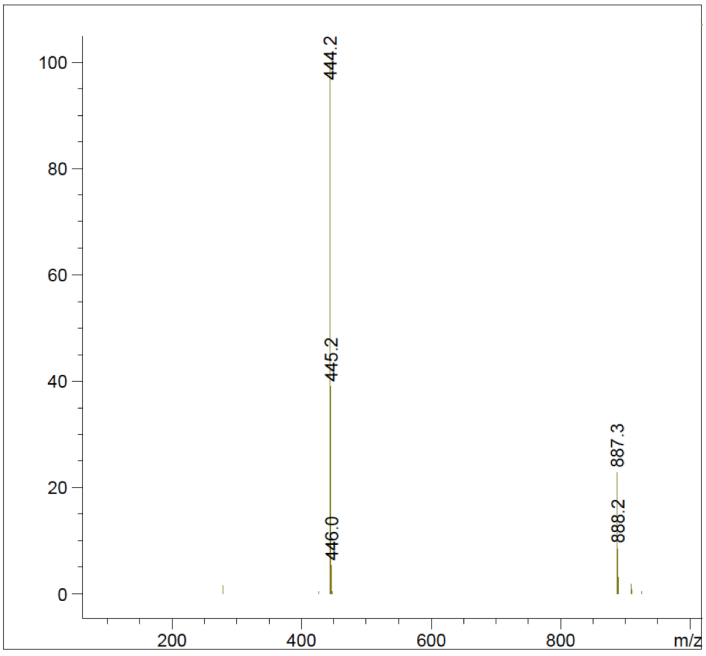

Figure 27 Mass spectrum of 20 mM of aspartame with 40 mM of H-Tyr-NH_2 in the presence of 1 mg of chymotrypsin at 30 minutes of the reaction.

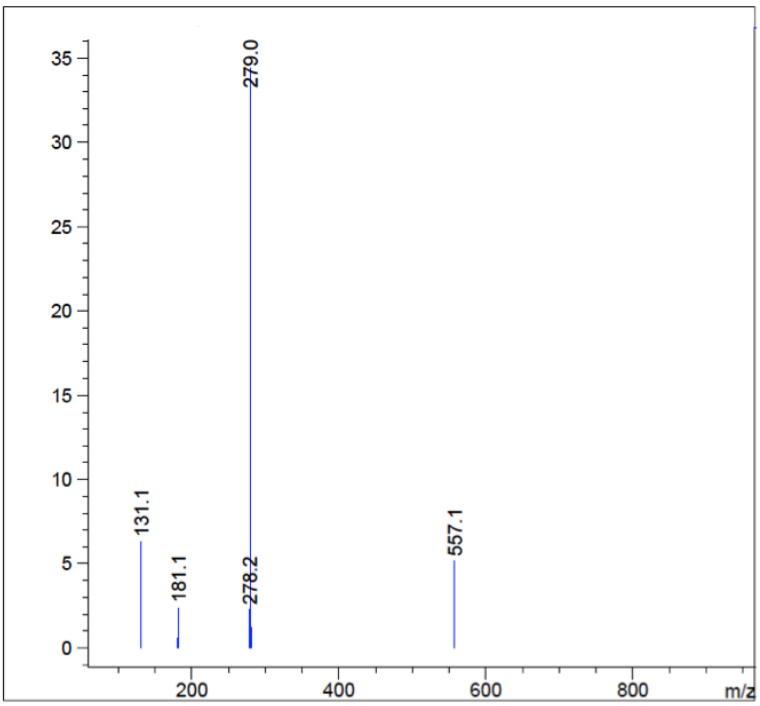

Figure 28 Mass spectrum of 20 mM of aspartame with 40 mM of H-Tyr-NH_2 in the presence of 1 mg of chymotrypsin at 10 hours of the reaction.

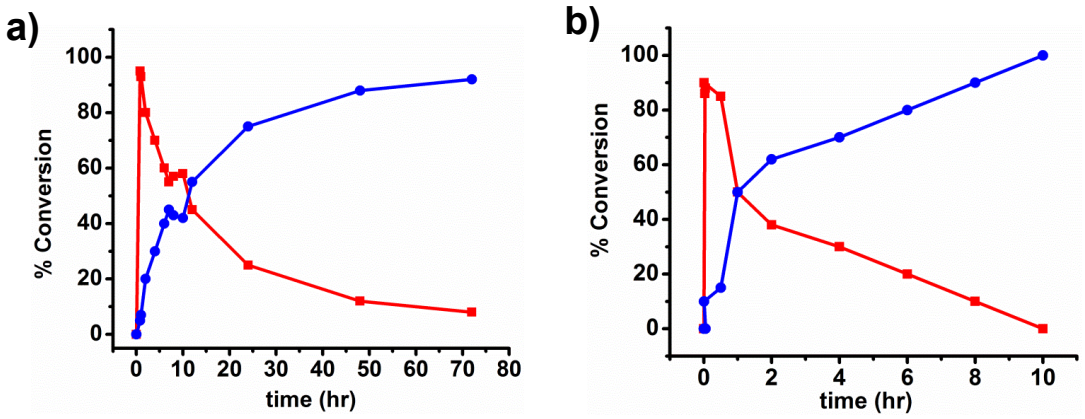

Figure 29 HPLC profiles of **a)** DFF-NH_2 and **b)** DFY-NH_2 formation and degradation over time.

Synthesis of Fmoc-YD-OH

Fmoc-Tyr(tBu)-OH, H-Asp(tBu)-OtBu.HCl and HBTU were dissolved in anhydrous dimethylformamide (~15 ml) and DIPEA was added. The reaction mixture was left to stir for twenty four hours. Product was precipitated out by addition of saturated sodium bicarbonate solution (~30 mL) and extracted into ethyl acetate (~50 mL). The mixture was washed with equal volumes of saturated brine, 1M hydrochloric acid and brine again. The resulting organic layer was dried by anhydrous magnesium sulphate and the ethyl acetate was removed by evaporation in vacuo. The resulting solid was then purified by column chromatography using 2.5 % methanol in dichloromethane as eluent. Fractions were tested using TLC using UV (254 nm) light to visualise spots. Fractions containing the compound were combined and solvent removed in vacuo. The removal of the t-Bu and protecting groups was carried out by dissolving the sample in dichloromethane and adding 10 mL of trifluoroacetic acid. The reaction mixture was stirred for 24 hours. The dichloromethane was removed by evaporation in vacuo. The TFA was removed by complexing with toluene (~10 mL) and THF (~2 mL) and solvent removed by evaporation in vacuo (carried out in triplicate). The resulting solid was washed 6 times with cold diethyl ether and the product dried under vacuum.

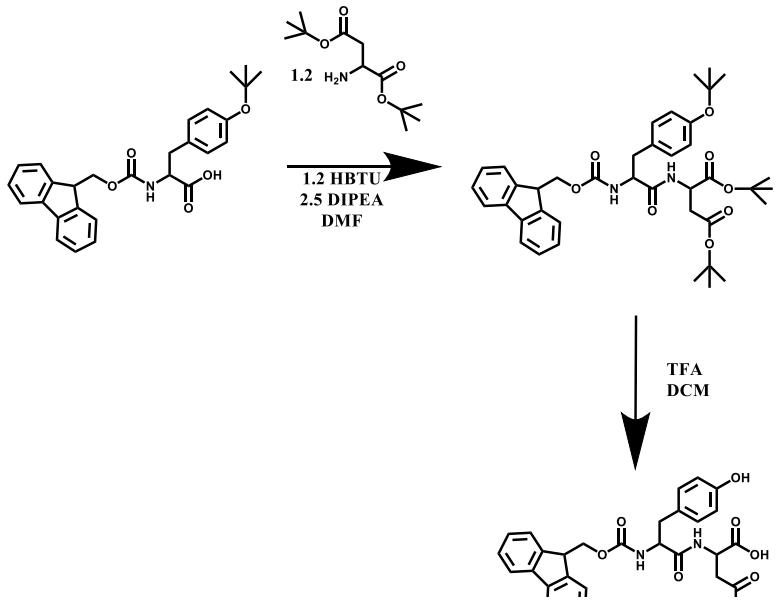

Characterization of the aromatic peptide amphiphile (Fmoc-YD)

Purity by HPLC (300 nm) = 98.79 %. δH (DMSO, 500 MHz): 12.7 (1H, s, OH), 12.4 (1H, s, OH), 9.1 (1H, s, Tyr OH), 8.34 – 8.32 (1H, d, J = 8 Hz), 7.88 – 7.87 (2H, d, J = 7.5 Hz, 2 fluorenyl Ar-CH), 7.65 – 7.61 (2H, m, 2 fluorenyl Ar-CH), 7.53 – 7.51 (1H, d, J = 9 Hz, Asp-NH), 7.43 – 7.39 (2H, m, 2 fluorenyl Ar-CH), 7.34 – 7.28 (2H, m, 2 fluorenyl Ar-CH), 7.10 – 7.09 (2H, d, j = 8.3 Hz, 2 Tyr Ar-CH), 6.64 – 6.62 (2H, d, J = 8.35 Hz, 2 Tyr Ar-CH), 4.57 – 4.55 (1H, m, Tyr CαH), 4.19 – 4.10 (4H, m, fluorenyl CH, fluorenyl CH_2 and Asp CαH), 2.92 – 2.91 (1H, m, Tyr CH), 2.73 – 2.71 (3H, m, 1Tyr CH, 2 Asp CH). δC (DMSO, 500 MHz): 172 (1C, Asp side chain C=O), 172 (2C, 1 Asp C=O and Tyr side chain C=O), 155.7 (2C, 1 Tyr Cq and 1 fluorenyl C=O), 128.1 (1C, Cq Tyr), 114.8 (1C, Tyr ArCH), 120.4 (1C, fluorenyl ArCH), 125.3 (1C, fluorenyl ArCH), 127 (1C, fluorenyl ArCH), 127.5 (1C, fluorenyl ArCH), 130.1 (1C, Tyr ArCH), 140.6 (1C, fluorenyl Cq), 143 (1C, fluorenyl Cq), 65.6 (1C, fluorenyl CH2), 56.2 (1C, Tyr Cα), 48.6 (1C, Asp Cα), 46 (1C, fluorenyl CH), 36.7 (1C, Tyr CH2), 35.9 Asp side chain CH_2). MS (ES+): m/z 519.2, [M + H]+.

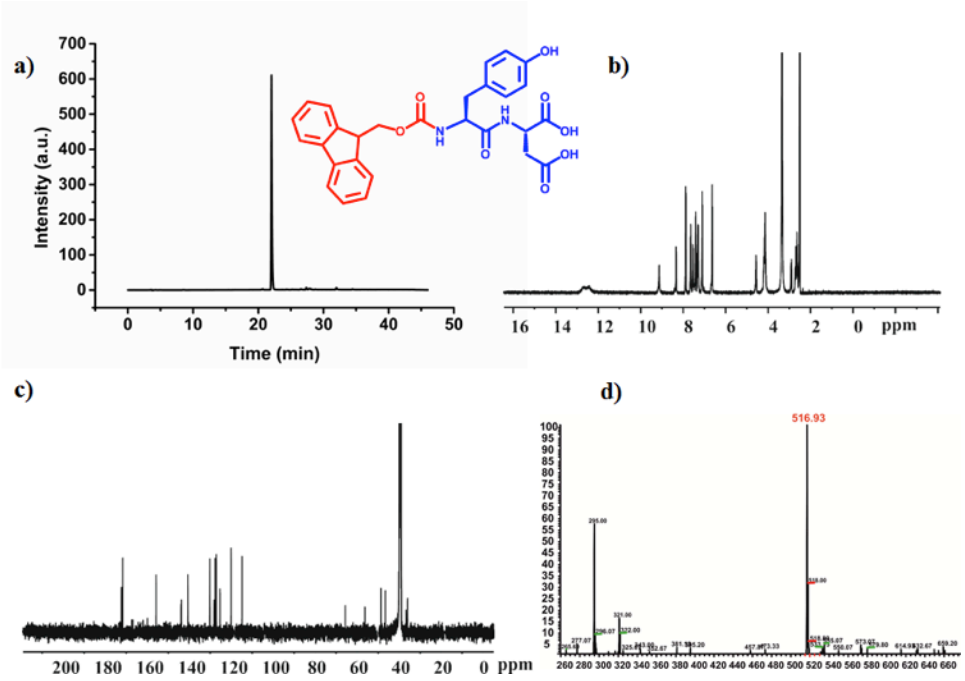

Figure 30 a) HPLC of the purified peptide **b)** ^{1}H NMR spectrum of the Fmoc-dipeptide in DMSO-d_6 **c)** ^{13}C NMR of the dipeptide in DMSO-d_6 and **d)** Mass spectrum of the Fmoc-dipeptide.

Figure 31 Experimental set-up, showing the speaker connected with an iphone 5 and inside the fluorimeter (2 cm above the fluorescence cuvette) to provide liquid vibrations.

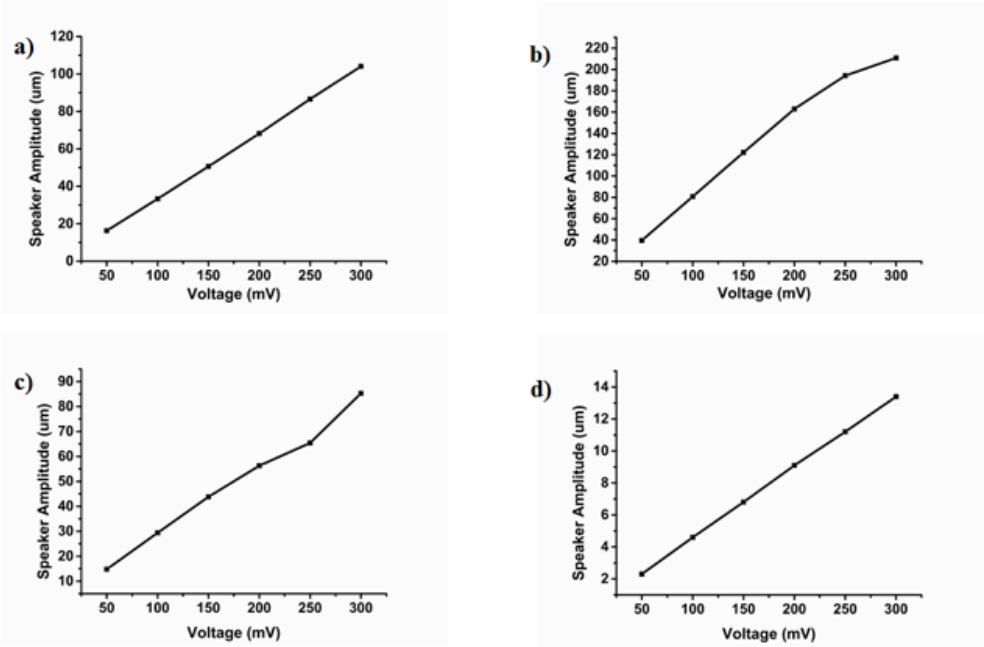

Figure 32 Speaker calibration in the selected frequencies of **a)** 100 **b)** 250 **c)** 500 and **d)** 1,000 Hz.

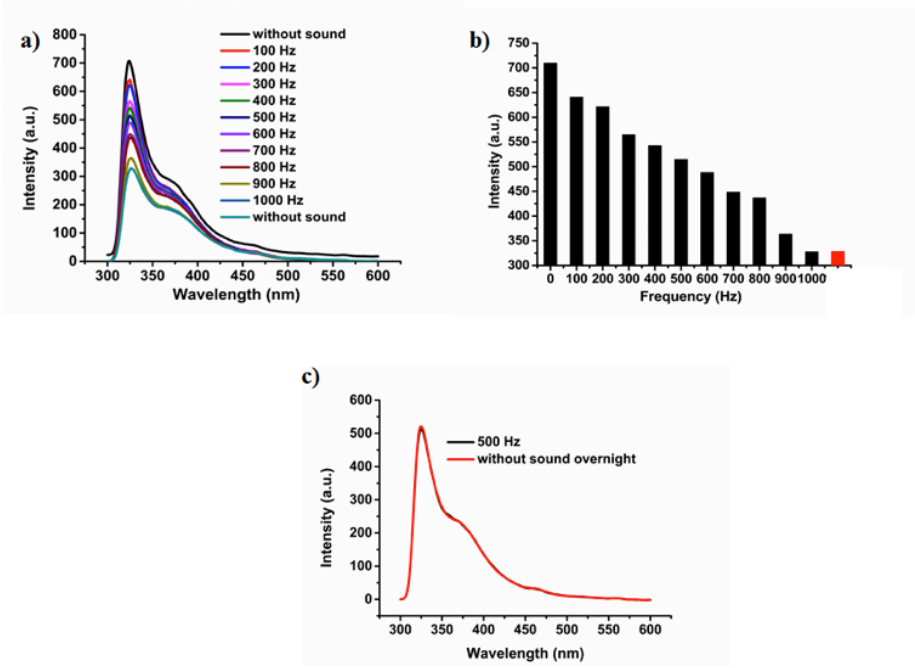

Figure 32 a) Fluorescence emission spectrum of the Fmoc-dipeptide exposing into different frequencies **b)** Histogram of the fluorescence intensity of the monomeric state (324 nm) *versus* the frequency, highlighted with red colour the bar for switching the sound off overnight and **c)** Fluorescence emission spectrum of the Fmoc-dipeptide in 500 Hz and without sound overnight.

References

1. S.C. Warren, O. Guney-Altay, B. A. Grzybowski, *J. Phys. Chem. Lett*., 2012, **3**, 2103-2111.

2. S. Mann, *Angew. Chem. Int. Ed*., 2013, **72**, 177-172.

3. S. N. Semenov, A. J. Markvoort, T. F. de Greef, W. T. Huck, *Angew. Chem. Int. Ed.*, 2014, **73**, 8077-8079.

4. J. Li, P. Nowak, S. Otto, *J. Am. Chem. Soc.,* 2013, **137**, 9222-9239.

5. A. Grinthal, J. Aizenberg, *Chem.Soc. Rev.*, 2013, **42**, 7072-7087.

6. J. M. P. Gutierrez, T.Hinkley, J. W.Taylor, K. Yanev, L. Cronin, *Nat. Commun.*, 2014, **7**, 7771-7779.

7. S. N. Semenov, A. S. Y. Wong, R. M. van der Made, S. G. J. Postma, J. Groen, H. W. H. van Roekel, T. F. A. de Greef, W.T. Huck, *Nat. chem.*, 2017, **7**, 170-177.

8. G. Cravotto and P. Cintas, *Chem. Soc. Rev.*, 2009, **38**, 2684-2697.

9. Y. Kuang, J. F. Shi, J. Li, D. Yuan, K. A. Alberti, Q. B. Xu, B. Xu, *Angew. Chem. Int. Ed.*, 2014, **73**, 8104-8107.

10. Q.G. Wang, Z. M. Yang, X. Q. Zhang, X. D. Xiao, C. K. Chang, B. Xu, *Angew. Chem. Int. Ed.*, 2007, **47**, 4287-4289.

11. C. M. Rufo, Y. S. Moroz, O.V. Moroz, J. Stöhr, T. A. Smith, X. Hu, W. F. DeGrado, I. V. Korendovych, *Nat. Chem.*, 2014, **7**, 303-309.

12. P. M. J. W. Frederix, G. Scott, Y. Abul-haija, D. Kalafatovic, C.G. Pappas, N. Javid, N. Hunt, R.V. Ulijn, T. Tuttle, *Nat. Chem.*, 2014, **7**, 30-37.

13. M. Reches, E. Gazit, *Science,* 2003, **300**, 727-727.

14. J. M. Slocika, R. R. Naik, *Chem. Soc. Rev.*, 2010, **39**, 3474-3473.

15. G. M. Whitesides and B. Grzybowski, *Science*, 2002, **295**, 2418- 2421.

16. T. Aida, E. W. Meijer, and S. I. Stupp, *Science*, 2012, **335**, 813-817.

17. G. Fichman and E. Gazit, *Acta biomaterialia*, 2014, **10**, 1671-1682.

18. L. A. Estroff and A. D. Hamilton, *Chem. Rev.,* 2004, **104**, 1201-1217.

19. J. E. Gough, A. Saiani and A. F. Miller, *Bionspired, Biomimetic and Biomaterials*, 2012, **1**, 4-12.

20. A. L. Boyle, D. N. Woolfson, *Chem. Soc. Rev.*, 2011, **40**, 4295-4306.

21. I. W. Hamley, *Angew. Chem. Int. Ed.*, 2014, **53**, 6866-6881.

22. R. J. Williams, R. J. Mart and R. V. Ulijn, *Biopolymers*, 2010, **94**, 107-117.

23. S. Boothroyd, A. Saiani and A. F. Miller, *Macromol. Symp.*, 2008, **273**, 139-145.

24. E. Gazit, *Chem. Soc. Rev.*, 2007, **36**, 1263-1269.

25. S. Fleming, R. V. Ulijn, *Chem. Soc. Rev.*, 2014, **43**, 8150-8177.

26. S. Fleming, S. Debnath, P. W. J. M. Frederix, T. Tuttle and R. V. Ulijn, *Chem. Commun.*, 2013, **49**, 10587-10589.

27. R. Vegners, I. Shestakova, I. Kalvinsh, R. M. Ezzell and P. A. Janmey, *J. Pept. Sci.*, 1995, **1**, 371-378.

28. V. Castelletto, G. Cheng, B. W. Greenland, I. W. Hamley and P. J. F. Harris, *Langmuir*, 2011, **27**, 2980-2988.

29. Y. Zou, K. Razmkhah, N. P. Chmel, I. W. Hamley and A. Rodger, *RSC Adv.*, 2013, **3**, 10854-10858.

30. H. Zhang, H. Wang, G. Xu and S. Yuan, *Colloids Surf.*, A, 2013, **417**, 217-223.

31. Y. Zhang, Z. Yang, F. Yuan, H. Gu, P. Gao and B. Xu, *J. Am. Chem. Soc.*, 2004, **126**, 15028-15029.

32. Y. Kuang and B. Xu, *Angew. Chem., Int. Ed.*, 2013, **52**, 6944-6948.

33. J. K. Sahoo, S. K. M. Nalluri, N. Javid, H. Webb and R. V. Ulijn, *Chem. Commun.*, 2014, **50**, 5462-5464.

34. B. Adhikari, J. Nanda and A. Banerjee, *Soft Matter*, 2011, **7**, 8913-8922.

35. S. Sutton, N. L.Campbell, A. I. Cooper, M.Kirkland, W. J. Frith and D. J. Adams, *Langmuir*, 2009, **25**, 10285-10291.

36. C. G. Pappas, Y. M. Abul-Haija, A. Flack, P.W. J. M. Frederix and R. V. Ulijn, *Chem. Commun.*, 2014, **50**, 10630-10633.

37. M. Hughes, H. Xu, P. W. J. M. Frederix, A. M. Smith, N. T. Hunt, T. Tuttle, I. A. Kinloch and R. V. Ulijn, *Soft Matter*, 2011, **7**, 10032-10038.

38. M. Hughes, P. W. J. M. Frederix, J. Raeburn, L. S. Birchall, J. Sadownik, F. C. Coomer, I.-H. Lin, E. J. Cussen, N. T. Hunt, T. Tuttle, S. J. Webb, D. J. Adams and R. V. Ulijn, *Soft Matter*, 2012, **8**, 5595-5602.

39. S. Zhang, T. Holmes, C. Lockshin, A. Rich, *Proc. Natl. Acad. Sci. USA*, 1993, 90, 3334-3338.

40. M. R. Ghadiri, J. R. Granja, R. A. Milligan, D. E. McRee, N. Khazanovich, *Nature,* 1993*,* **366**, 324-327.

41. T. O. Mason, D. Y. Chirgadze, A. Levin, L. Adler-Abramovich, E. Gazit, T. P. J. Knowles, and A. K. Buell, *ACS Nano*, 2014, **8**, 1243-1253.

42. L. Adler-Abramovich and E. Gazit, *Chem. Soc. Rev.*, 2015, **43**, 6881-6893.

43. X. Yan, P. Zhua and J. Li, *Chem. Soc. Rev.*, 2010, **39**, 1877-1890.

44. N. Amdursky, , M. Molotskii, E. Gazit, G. Rosenman, *J. Am. Chem Soc.*, 2010, **132**, 15632-15636.

45. N. Sanchez-de Groot, T. Parella, F. Aviles, J. Vendrell, and S. Ventura, *Biophys. J.*, 2007, **92**, 1732-1741.

46. P. W. J. M. Frederix, R. V. Ulijn, N. T. Hunt and T. Tuttle, *J. Phys. Chem. Lett*., 2011, **2**, 2380-2384.

47. M. Gorleroa, R. Wieczoreka, K. Adamalac, A. Giorgid, M. E. Schininàd, P. Stanoa, P.L.Luisia, *FEBS Letters*, 2009, **583**, 153-156.

48. M. Reches and E. Gazit, *Nano Lett.*, 2004, **4**, 581-585.

49. P. Tamamis, L. Adler-Abramovich, M. Reches, K. Marshall, P. Sikorski, L. Serpell, E. Gazit and G. Archontis, *Biophys. J.*, 2009, **96**, 5020-5029.

50. C. Guo, Y. Luo, R. Zhou and G.Wei, *Nanoscale,* 2014**, 6**, 2800-2811.

51. P. Moitra, K. Kumar, P. Kondaiah and S. Bhattacharya, *Angew. Chem. Int. Ed*., 2014, **53**, 1113-1117.

52. S. Marchesan, C. D. Easton, F. Kushkaki, L. Waddington, P. G. Hartley, *Chem. Commun.*, 2012, **48**, 2195-2197.

53. T. Naota and H. Koori, *J. Am. Chem. Soc.*, 2005, **127**, 9324-9325.

54. K. Isozaki, H. Takaya and T. Naota, *Angew. Chem., Int. Ed.*, 2007, **46**, 2855-2860.

55. D. Bardelang, F. Camerel, J. C. Margeson, D. M. Leek, M. Schmutz, M. B. Zaman, K. Yu, D. V. Soldatov, R. Ziessel, C. I. Ratcliffe and J. A. Ripmeester, *J. Am. Chem. Soc.*, 2008, **130**, 3313-3315.

56. Y. Wang, C. Zhan, H. Fu, X. Li, X. Sheng, Y. Zhao, D. Xiao, Y. Ma, J. S. Ma and J. Yao, *Langmuir*, 2008, **24**, 7635-7638.

57. D. Ke, C. Zhan, A. D. Li and J. Yao, *Angew. Chem. Int. Ed.*, 2011, **50**, 3715-3719.

58. S. F. Pan, S. Luo, S. Li, Y. S. Lai, Y. Y. Geng, B. He and Z. W. Gu, *Chem. Commun.*, 2013, **49**, 8045-8047.

59. A. Tsuda, Y. Nagamine, R. Watanabe, Y. Nagatani, N. Ishii and T. Aida, *Nat. chem.*, 2010, **2**, 977-983.

60. R. Miura, Y. Ando, Y. Hotta, Y. Nagatani, and A. Tsuda, *Chem. Plus. Chem.,* 2014, **79**, 516-523.

61. E. Mattia and S. Otto, *Nat. Nanotechnol*., 2015, **10**, 111-119.

62. R. J. Williams, A. M. Smith, R. Collins, N. Hodson, A. K. Das, R. V. Ulijn, *Nat. Nanotechnol.*, 2009, **4**, 19-24.

63. T. F. A. de Greef and E. W. Meijer, *Nature*, 2008, **453**, 171-173.

64. J. Boekhoven, W. E. Hendriksen, G. J. M. Koper, R. Eelkema, J. H. van Esch, *Science*, 2015, **349**, 1075-1079.

65. S. Boothroyd, A. F. Miller and A. Saiani, *Faraday Discuss.*, 2013, **166**, 195-207.

66. S. Toledano, R. J. Williams, V. Jayawarna and R. V. Ulijn, *J. Am. Chem. Soc.*, 2006, **128**, 1070-1071.

67. S. K. Nalluri, C. Berdugo, N. Javid, P. W. Frederix, R. V. Ulijn, *Angew. Chem. Int. Ed.*, 2014, **63**, 6882-6887.

68. J. B. Guilbaud, E. Vey, S. Boothroyd, A. M. Smith, R.V. Ulijn, A. Saiani and A. F. Miller, *Langmuir*, 2010, **26**, 11297-11303.

69. J. B. Guilbaud, C. Rochas, A. F. Miller and A. Saiani, *Biomacromolecules*, 2013, **14**, 1403-1411.

70. L. Szkolar, J. B. Guilbaud, A. F. Miller, J. E. Gough and A. Saiani, *J. Pept. Sci.*, 2014, **20**, 578-584.

71. J. M Berg, J. L Tymoczko, L. Stryer. *5th Edition Biochemistry*, New York, 2002.

72. J. Boekhoven, J. M. Poolman, C. Maity, F. Li, L. van der Mee, C.B. Minkenberg, E. Mendes, J. H. van Esch, R. Eelkema, *Nat. chem.*, 2013, **5**, 433-437.

73. A. R. Hirst, S. Roy, M. Arora, A. K. Das, N. Hodson, P. Murray, S. Marshall, N. Javid, J. Sefcik, J. Boekhoven, J. H. van Esch, S. Santabarbara, N. T. Hunt and R. V. Ulijn, *Nat. chem.*, 2010, **2**, 1089-1094.

74. X. Qin, W. Xie, S. Tian, J. Cai, H. Yuan, Z. Yu, G. L. Butterfoss, A. C. Khuong and R. A. Gross, *Chem. Commun.*, 2013, **49**, 4839-4841.

75. J. M. Carnall, C. A. Waudby, A. M. Belenguer, M. C. Stuart, J. J. Peyralans and S. Otto, *Science*, 2010, **327**, 1502-1506.

76. G. Leonetti and S. Otto, *J. Am. Chem. Soc.*, 2015, **137**, 2067-2072.

77. G. J. Boekhoven, A. M. Brizard, K. N. Kowlgi, G. J. Koper, R. Eelkema, J. H. van Esch, *Angew. Chem. Int. Ed.*, 2010, **49**, 4826-4828.

78. S. Debnath, S. Roy, R. V. Ulijn, *J. Am. Chem. Soc.*, 2013, **136**, 16789-16792.

79. T. Heuser, E. Weyandt and A. Walther, *Angew. Chem., Int. Ed*, 2015, **54**, 1-6.

80. G.Ragazzon, M. Baroncini, S. Silvi, M.Venturi and A.Credi, *Nat. Nanotechnol.*, 2015, **10**, 70-75.

81. S. Bai, C. G. Pappas, S. Debnath, P. W. J. M. Frederix, J. Leckie, S. Fleming, R. V. Ulijn, *ACS Nano*, 2014, **8**, 7005-7013.

82. A. W. Feinberg, A. Feigel, S. S. Shevkoplyas, S. Sheehy, G. M. Whitesides, K. K. Parker, *Science*, 2007, **317**, 1366-1370.

83. A. Merzlyak, S. Indrakanti, S. W. Lee, *Nano Lett.*, 2009, **9**, 846-852.

84. C. J. Bettinger, R. Langer, J. T. Borenstein, *Angew. Chem. Int. Ed.*, 2009, **48**, 5406-5415.

85. R. Nelson, M. R. Sawaya, M. Balbirnie, A. Ø. Madsen, C. Riekel, R. Grothe, D. Eisenberg, *Nature*, 2005, **435**, 773-778.

86. C. M. Dobson, *Nature*, 2003, **426**, 884-890.

87. S. W. Choi, W. S. Kang, J. H. Lee, C. K. Najeeb, H. S. Chun, J. H. Kim, *Langmuir*, 2010, **26**, 15680-15685.

88. B. H. Kim, D. O. Shin, S. J. Jeong, C. M. Koo, S. C. Jeon, W. J. Hwang, S. Lee, M. G. Lee, S. O. Kim, *Adv. Mater.*, 2008, **20**, 2303-2307.

89. D. Kohler, M. Schneider, M. Kruger, C. M. Lehr, H. Moehwald, D. Y. Wang, *Adv. Mater.*, 2011, **23**, 1376-1379.

90. M. Reches, E. Gazit, *Nature Nanotech.*, 2006, **1**, 195-200.

91. M. C. Vasudev, H. Koerner, K. M. Singh, B. P. Partlow, D. L. Kaplan, E. Gazit, T. J. Bunning, R. R. Naik, *Biomacromolecules*, 2014, **15**, 533-540.

92. B. R. Cao, Y. Zhu, L. Wang, C. B. Mao, *Angew. Chem. Int. Ed.*, 2013, **53**, 11750-11754.

93. R. J. A. Hill, V. L. Sedman, S. Allen, P. M. Williams, M. Paoli, L. Adler-Abramovich, E. Gazit, L. Eaves, S. J. B. Tendler, *Adv. Mater.* 2007, **19**, 4474-4479.

94. S. M. Zhang, M. A. Greenfield, A. Mata, L. C. Palmer, R. Bitton, J. R. Mantei, C. Aparicio, M. O. de la Cruz, S. I. Stupp, *Nat. Mater.*, 2010, **9**, 594-601.

95. X. H. Yan, J. B. Li, H. Möhwald, *Adv. Mater.*, 2011, **23**, 2796-2801.

96. X. Yan, Y. Su, J. Li, J. Früh, H. Möhwald, *Angew. Chem. Int. Ed.*, 2011, **50**, 11186-11191.

97. J. Zhou, X. Du, Y. Gao, J. Shi, B. Xu, *J. Am. Chem. Soc.*, 2014, **136**, 2970-2973.

98. B. D. Wall, S. R. Diegelmann, S. Zhang, T. J. Dawidczyk, W. L. Wilson, H. E. Katz, H. Q. Mao and J. D. Tovar, *Adv. Mater.*, 2011, **23**, 5009-5014.

99. M. Wallace, A. Z. Cardoso, W. J. Frith, J. A. Iggo, D. J. Adams, *Chem. Eur. J.*, 2014, **20**, 16484-16487.

100. M. Reches and E. Gazit, *Nat. Nanotechnol.*, 2006, **1**, 195-200.

101. A. M. Hung, S. I. Stupp, *Langmuir*, 2009, **25**, 7084-7089.

102. N. Komiya, T. Muraoka, M. Iida, M. Miyanaga, K. Takahashi, T. Naota, *J. Am. Chem. Soc*. 2011, **133**, 16054-16061.

103. L. Sambri, F. Cucinotta, G. De Paoli, S. Stagni, L. De Cola, *New J. Chem.*, 2010, **34**, 2093-2096.

104. A. Kotal, T. K. Paira, S. Banerjee, T. K. Mandal, *Langmuir*, 2010, **26**, 6576-6582.

105. G. Cravotto, E. C. Gaudino, P. Cintas, *Chem. Soc. Rev.*, 2013, **42**, 7521-7534.

106. D. Ke, C. Zhan, X. Li, X. Wang, Y. Zeng, J. Yao, *J. Colloid Interface Sci.*, 2009, **337**, 54-60.

107. C. G. Pappas, T. Mutasa, P. W. J. M. Frederix, S. Fleming, S. Bai, S. Debnath, S. M. Kelly, A. Gachagan, Rein V. Ulijn, *Mater. Horiz.*, 2015, **2**, 198-202.

108. S. Marchesan, C. D. Easton, K. E. Styan, L. Waddington, F. Kushkaki, L. Goodall, K. M. McLean, J. S. Forsythe, P. G. Hartley, *Nanoscale*, 2014, **6**, 5172-5180.

109. R. Adachi, K. Yamaguchi, H. Yagi, K. Sakurai, H. Naiki, Y. Goto, J. Bio. Chem., 2007, 282, 8978–8983; T. R. Dafforn, J. Rajendra, D. J. Halsall, L. C. Serpell, A. Rodger, *Biophys. J.*, 2004, **86**, 404-410.

110. S. Fleming, P. W. J. M. Frederix, I. Ramos-Sasselli, N. Hunt, R. V. Ulijn, T. Tuttle, *Langmuir*, 2013, **29**, 9510-9515.

111. P. Jonkheijm, P. van der Schoot, A. P. Schenning and E. W. Meijer, *Science*, 2006, **313**, 80-83.

112. G. O. Lloyd and J. W. Steed, *Nat. chem.*, 2009, **1**, 437-442.

113. X. Yu, L. Chen, M. Zhang and T. Yi, *Chem. Soc. Rev.*, 2014, **43**, 5346-5371.

114. S. Zhang, S. Yang, J. Lan, Y. Tang, Y. Xue and J. You, *J. Am. Chem. Soc.*, 2009, **131**, 1689-1691.

115. D. W. Balkenende, S. Coulibaly, S. Balog, Y. C. Simon, G. L. Fiore and C. Weder, *J. Am. Chem. Soc.*, 2014, **136**, 10493-10498.

116. L. C. Palmer and S. I. Stupp, *Acc. Chem. Res.*, 2008, **41**, 1674-1684.

117. S. Zhang, *Nat. biotech.*, 2003, **21**, 1171-1178.

118. H. Yokoi, T. Kinoshita, S. Zhang, *Proc. Natl. Acad. Sci.*, 2005, **102**, 8414-8419.

119. H. Okumura and S. G. Itoh, *J. Am. Chem. Soc.*, 2014, **136**, 10549-10552.

120. C. Tang, R. V. Ulijn and A. Saiani, *Langmuir*, 2011, **27**, 14438-14449.

121. C. Tang, R. V. Ulijn and A. Saiani, *The European physical journal*, 2013, **36**, 111.

122. J. Raeburn, B. Alston, J. Kroeger, T. O. McDonald, J. R. Howse, P. J. Cameron and D. J. Adams, *Mater. Horiz.*, 2014, **1**, 241-246.

123. J. W. Sadownik, J. Leckie and R. V. Ulijn, *Chem. Commun.*, 2011, **47**, 728-730.

124. J. M. Lehn, *Science*, 2002, **295**, 2400-2403.

125. A. R. Hirst, B. Escuder, J. F. Miravet and D. K. Smith, *Angew. Chem. Int. Ed.*, 2008, **47**, 8002-8018.

126. E. Busseron, Y. Ruff, E. Moulin and N. Giuseppone, *Nanoscale*, 2013, **5**, 7098-7140.

127. R. V. Ulijn and A. M. Smith, Chem. Soc. Rev., 2008, **37**, 664-675.

128. D. J. Adams, L. M. Mullen, M. Berta, L. Chen and W. J. Frith, *Soft Matter*, 2010, **6**, 1971-1980.

129. Z. Yang, G. Liang, Z. Guo and B. Xu, *Angew. Chem. Int. Ed.*, 2007, **46**, 8216-8219.

130. J. M. Spruell and C. J. Hawker, *Chem. Sci.*, 2011, **2**, 18-26.

131. M. Zelzer, S. J. Todd, A. R. Hirst, T. O. McDonald and R. V. Ulijn, *Biomat. Sci.*, 2013, **1**, 11-39.

132. S. Winkler, D. Wilson and D. Kaplan, *Biochemistry*, 2000, **39**, 12739-12746.

133. B. H. Hu and P. B. Messersmith, *J. Am. Chem. Soc.*, 2003, **125**, 14298-14299.

134. L. Chronopoulou, S. Lorenzoni, G. Masci, M. Dentini, A. R. Togna, G. Togna, F. Bordi and C. Palocci, *Soft Matter*, 2010, **6**, 2525-2532.

135. S. K. M. Nalluri and R. V. Ulijn, *Chem. Sci.*, 2013, **4**, 3699-3705.

136. J. Raeburn, A. Z. Cardoso and D. J. Adams, *Chem. Soc. Rev.*, 2013, **42**, 5143-5156.

137. K. M. Eckes, X. Mu, M. A. Ruehle, P. Ren and L. J. Suggs, *Langmuir*, 2014, **30**, 5287-5296.

138. D. M. Ryan, T. M. Doran, S. B. Anderson and B. L. Nilsson, *Langmuir*, 2011, **27**, 4029-4039.

139. D. M. Ryan, S. B. Anderson and B. L. Nilsson, *Soft Matter*, 2010, **6**, 3220-3231.

140. M. Reches and E. Gazit, *Physical biology*, 2006, **3**, 10-19.

141. V. Z. Poenitzsch, D. C. Winters, H. Xie, G. R. Dieckmann, A. B. Dalton and I. H. Musselman, *J. Am. Chem. Soc.*, 2007, **129**, 14724-14732.

142. A. A. Profit, V. Felsen, J. Chinwong, E.-R. E. Mojica and R. Z. B. Desamero, *Proteins: Structure, Function, and Bioinformatics*, 2013, **81**, 690-703.

143. C. Hansch, A. Leo and R. W. Taft, *Chem. Rev.*, 1991, **91**, 165-195.

144. Y. M. Abul-Haija, S. Roy, P. W. J. M. Frederix, N. Javid, V. Jayawarna and R. V. Ulijn, *Small*, 2014, **10**, 973-979.

145. K. Thornton, A. M. Smith, C. L. R. Merry and R. V. Ulijn, *Biochem. Soc. Trans.* 2009, **37**, 660-664.

146. K. Thornton, Y. M. Abul-Haija, N. Hodson and R. V. Ulijn, *Soft Matter*, 2013, **9**, 9430-9439.

147. A. Mahler, M. Reches, M. Rechter, S. Cohen and E. Gazit, *Adv. Mater.*, 2006, **18**, 1365-1370.

148. V. Jayawarna, M. Ali, T. A. Jowitt, A. F. Miller, A. Saiani, J. E. Gough and R. V. Ulijn, *Adv. Mater*, 2006, **18,** 611-614.

149. J. M. Lehn, *Science* 1993, **270**, 1772-1773.

150. R. M. Capito, H. S. Azevedo, Y. S. Velichko, A. Mata, S. I. Stupp, *Science*, 2008, **319**, 1812-1817.

151. K. Adamala and J. W. Szostak, *Nat. Chem.*, 2013, **5**, 495-501.

152. F. B. L. Cougnon and J. K. M. Sanders, *Acc. Chem. Res.,* 2012**, 45**, 2211-2221.

153. J. M. Lehn, *Top. Curr. Chem.*, 2011, **322**, 1-32.

154. J. M. Lehn, *Chem. Soc. Rev.*, 2007, **36**, 151-160.

155. S. Otto, R. L. E. Furlan, J. K. M. Sanders, *Science*, 2002, **297**, 590-593.

156. E. Moulin, G. Cormos, N. Giuseppone, *Chem. Soc. Rev.*, 2012, **41**, 1031-1049.

157. N. Ponnuswamy, F. B. L. Cougnon, J. M. Clough, G. D. Pantos and J. K. M. Sanders, *Science*, 2012, **338**, 783-785.

158. J. Atcher, A. Moure, J.Bujons and I. Alfonso, *Chem. Eur. J.*, 2015, **21**, 6869-6878.

159. J. Akerlund, S. Harmeier, J. Pumphrey, D. C. Timm and J. I. Brand, *J. of Applied Pol. Science*, 2000, **78**, 2213-2218.

160. F. Hofmeister, *Arch. Exp. Pathol. Pharmakol*., 1888, **24**, 247.

161. S. Roy, N. Javid, P.W.J.M. Frederix, D.A. Lamprou, A.J. Urquhart, N.T. Hunt, P.J. Halling and R.V. Ulijn, *Chem. Eur. J.*, 2012, **18**, 11723-11731.

162. P. A. Korevaar, C. J. Newcomb, E. W. Meijer, and S. I. Stupp, *J. Am. Chem. Soc.*, 2014, **136**, 8540-8543.

163. R.V. Ulijn, L. De Martin, L. Gardossi, A.E.M. Janssen, B.D. Moore and P.J. Halling. *Biotechnol. Bioeng*., 2002, **80**, 509-515.

164. S. Fleming, S. Debnath, P. W. J. M. Frederix, N. T. Hunt and R. V. Ulijn, *Biomacromolecules*, 2014, **15**, 1171-1184.

165. G. M. Whitesides, M. Boncheva, *Proc. Natl Acad. Sci. USA*, 2002, **99**, 4769-4774.

166. W. Edwards, D. K. Smith, *J. Am. Chem. Soc.*, 2013, **136**, 6911-6920.

167. P. Terech, R. G. Weiss, *Chem. Rev*., 1997, **97**, 3133-3160.

168.T. Heuser, A. K. Steppert, C. Molano Lopez, B. Zhu, A. Walther, *Nano Letters*, 2014, DOI: 10.1021/nl7039707.

169. J. Naskar, G. Palui, A. Banerjee, *J. Phys. Chem. B*, 2009, **113**, 11787-11792.

170. R. H. Mazur *Physiology and Biochemistry* (L. D. Stegink and L. J. Filer Jr., Eds.), 1974, 3-9.

171. J. Suez, T. Korem, D. Zeevi, G. Zilberman-Schapira, C. A. Thaiss, O. Maza, D. Israeli, N. Zmora, S. Gilad, A. Weinberger, Y. Kuperman, A. Harmelin, I. Kolodkin-Gal, H. Shapiro, Z. Halpern, E. Segal, E. Elinav, *Nature*, 2014, **684**, 181-186.

172. J. Fastrez, A. R. Fersht*, Biochemistry*, 1973, **12**, 2027-2034.

173. A. Barth, C. Zscherp, *Quarterly Reviews of Biophysics*, 2002, **37**, 4, 369-430.

174. H. Nikukar, S. P. Reid, M. Tsimbouri, M.O. Riehle, A. S. G. Curtis and M. J. Dalby, *ACS Nano*, 2013, **7**, 2758-2767.

175. M. J. Webber, E. A. Appel, E. W. Meijer and R. Langer, *Nat. Mater.*, 2015, 15, 13-26.

176. F. Tantakitti, J. Boekhoven, X. Wang, R. V. Kazantsev, T. Yu, J. Li, E. Zhuang, R. Zandi, J. H. Ortony, C. J. Newcomb, L. C. Palmer, G. S. Shekhawat, M. O. de la Cruz, G. C. Schatz and S. I. Stupp, *Nat. Mater.*, 2016, DOI: 10.1038/nmat4538.

177. G. A. Silva, C. Czeisler, K. L. Niece, E. Beniash, D. A. Harrington, J. A. Kessler and S. I. Stupp, Science, 2004, 303, 1352-1355.

178. A. Aggeli, M. Bell, N. Boden, J. N. Keen, P. F. Knowles, T. C. McLeish, M. Pitkeathly and S. E. Radford, *Nature*, 1997, **386**, 259-262.

179. N. A. Peppas and R. Langer, *Science*, 1994, **263**, 1715-1720.

180. N. Huebsch and D. J. Mooney, *Nature*, 2009, **462**, 426-432.

181. E. A. Appel, J. del Barrio, X. J. Loh and O. A. Scherman, *Chem. Soc. Rev.*, 2012, **41**, 6195-6214.

182. R. Dong, Y. Zhou, X. Huang, X. Zhu, Y. Lu and J. Shen, *Adv. Mater.*, 2015, **27**, 498-526.

183. A. Aggeli, I. A. Nyrkova, M. Bell, R. Harding, L. Carrick, T. C. McLeish, A. N. Semenov and N. Boden, *Proc Natl Acad Sci U S A*, 2001, **98**, 11857-11862.

184. J. P. Schneider, D. J. Pochan, B. Ozbas, K. Rajagopal, L. Pakstis and J. Kretsinger, *J. Am. Chem. Soc.*, 2002, **124**, 15030-15037.

185. V. Gauba and J. D. Hartgerink, *J. Am. Chem. Soc.*, 2007, **129**, 2683-2690.